ABSTRACT

BANG, YOUNGSUK. Hybrid Reduced Order Modeling Algorithms for Reactor Physics Calculations. (Under the direction of Hany S. Abdel-Khalik).

Reduced order modeling (ROM) has been recognized as an indispensable approach when the engineering analysis requires many executions of high fidelity simulation codes. Examples of such engineering analyses in nuclear reactor core calculations, representing the focus of this dissertation, include the functionalization of the homogenized few-group cross-sections in terms of the various core conditions, e.g. burn-up, fuel enrichment, temperature, etc. This is done via assembly calculations which are executed many times to generate the required functionalization for use in the downstream core calculations. Other examples are sensitivity analysis used to determine important core attribute variations due to input parameter variations, and uncertainty quantification employed to estimate core attribute uncertainties originating from input parameter uncertainties.

ROM constructs a surrogate model with quantifiable accuracy which can replace the original code for subsequent engineering analysis calculations. This is achieved by reducing the effective dimensionality of the input parameter, the state variable, or the output response spaces, by projection onto the so-called active subspaces. Confining the variations to the active subspace allows one to construct an ROM model of reduced complexity which can be solved more efficiently. This dissertation introduces a new algorithm to render reduction with the reduction errors bounded based on a user-defined error tolerance which represents the main challenge of existing ROM techniques. Bounding the error is the key to ensuring that the constructed ROM models are robust for all possible applications. Providing such error

www.manaraa.com

bounds represents one of the algorithmic contributions of this dissertation to the ROM state-of-the-art.

Recognizing that ROM techniques have been developed to render reduction at different levels, e.g. the input parameter space, the state space, and the response space, this dissertation offers a set of novel hybrid ROM algorithms which can be readily integrated into existing methods and offer higher computational efficiency and defendable accuracy of the reduced models. For example, the snapshots ROM algorithm is hybridized with the range finding algorithm to render reduction in the state space, e.g. the flux in reactor calculations. In another implementation, the perturbation theory used to calculate first order derivatives of responses with respect to parameters is hybridized with a forward sensitivity analysis approach to render reduction in the parameter space. Reduction at the state and parameter spaces can be combined to render further reduction at the interface between different physics codes in a multi-physics model with the accuracy quantified in a similar manner to the single physics case.

Although the proposed algorithms are generic in nature, we focus here on radiation transport models used in support of the design and analysis of nuclear reactor cores. In particular, we focus on replacing the traditional assembly calculations by ROM models to facilitate the generation of homogenized cross-sections for downstream core calculations. The implication is that assembly calculations could be done instantaneously therefore precluding the need for the expensive evaluation of the few-group cross-sections for all possible core conditions. Given the generic natures of the algorithms, we make an effort to introduce the material in a general form to allow non-nuclear engineers to benefit from this work.

www.manaraa.com

© Copyright 2012 by Youngsuk Bang

All Rights Reserved

www.manaraa.com

Hybrid Reduced Order Modeling Algorithms for Reactor Physics Calculations

by
Youngsuk Bang

A dissertation submitted to the Graduate Faculty of
North Carolina State University
in partial fulfillment of the
requirements for the degree of
Doctor of Philosophy

Nuclear Engineering

Raleigh, North Carolina

2012

APPROVED BY:

Dr. Hany S. Abdel-Khalik Committee Chair	Dr. Dmitriy Y. Anistratov
Dr. Ilse C.F. Ipsen	Dr. Matthew A. Jessee

www.manaraa.com

DEDICATION

The LORD is my strength and my song, and he has become my salvation;

this is my God, and I will praise him, my father's God, and I will exalt him.

(Exodus 15:2)

I dedicate this dissertation to my family, especially ...

to my Wife, HeeYeon for her patience and understanding;

to Dad and Mom for their support and encouragement;

to my Son, SeungHyun for all joys he brings to me.

www.manaraa.com

BIOGRAPHY

Youngsuk Bang was born in Seoul, Korea on November, 1980 . He received his B.S. and M.S degrees in nuclear engineering from Seoul National University in Korea in 2004 and 2006, respectively. He spent the following three years working at FNC technology, Co. and the Research Institute Energy and Resources at Seoul National University. In the fall of 2009, he started pursuing a Ph.D. degree in the Department of Nuclear Engineering at North Carolina State University (NCSU) in the United States. Youngsuk is married to HeeYeon in 2007, and has one son, SeungHyun, born in 2011.

www.manaraa.com

ACKNOWLEDGMENTS

I would like to express my gratitude to my thesis advisor, Dr. Abdel-Khalik, for his support and guidance throughout my graduate studies at NCSU. I appreciate the opportunities he provided. I am grateful to my committee members for their insightful and critical comments; to Dr. Ipsen. It was amazing that during enjoying the classes provided with her generous smile, I could learn the really necessary things at the perfectly right moments; to Dr. Anistratov. Through his classes, I could build my background on reactor physics calculations and feel confident in dealing with the problems; to Dr. Jessee. I could learn many things from his dissertation. Including my summer internship at Oak Ridge National Laboratory, I owe a debt of gratitude to him for helping me from setting up the model inputs to analyzing the simulation results.

I would like to offer my sincere thanks to Dr. Mertyurek. Through discussing with him, I could learn a lot of things about the realistic calculations and reassure the key points of this research. If it were not his help, this project could not finished on schedule. I would also like to thank to Dr. Kang-Seok Kim and Dr. Seok-Ho Kim for insightful discussions and their prayers for my family during my internship.

I owe a great deal to Hermine and Ganga for their administrative supports. With their extra care for my crunch-time matters, I could focus on my study and make things done without a difficulty. Special gratitude is also extended to my dear colleagues; Jason, Shota, Bassam, Abdo, Zeyun, Qiong, Congjian, Chris, Richard, Ahmad, Apil, Dr. Kyoung Ook Lee, Dr. Jae Seok Heo, Dr. Cyrus Proctor.

www.manaraa.com

My heartfelt appreciation goes to Dr. Chang Hyun Chung for his guidance. I am grateful to Dr. Byung Chul Lee and all members of FNC Technology, Co. for their continuous support. I am also grateful to Dr. Chang Kyu Park for his timely advice. I would like to thank to Dr. Sung-Kyun Zee for his advice and encouragement. I have greatly appreciated to President Chun-Kil Oh for his heartwarming hospitality and encouragement.

Last but not least, I would like to thank to my parents and parents-in-law for their continuous prayers and for always believing in me. Their wise advice keep awake my mind and encourage me to overcome my weakness. I am deeply indebted to my younger brother for my absence in his important moments. I've dedicated this dissertation to my wife HeeYeon for her love and unwavering support.

www.manaraa.com

TABLE OF CONTENTS

www.manaraa.com

www.manaraa.com

www.manaraa.com

www.manaraa.com

LIST OF TABLES

www.manaraa.com

www.manaraa.com

LIST OF FIGURES

www.manaraa.com

www.manaraa.com

www.manaraa.com

www.manaraa.com

www.manaraa.com

www.manaraa.com

CHAPTER 1. INTRODUCTION

Predictive science which refers to *the application of computational models to the study and the prediction of physical or engineering systems* has emerged as a powerful and an indispensable tool for resolving scientific and engineering problems. As the physical understanding and scientific theories are deepened, more details are added to the models in order to provide more accurate predictions. Nevertheless, the computational cost in terms of storage requirements and execution time also increases due to the increased modeling details, i.e., higher dimensional models. Therefore, the added benefit of high-fidelity prediction may not be fully realized due to the overwhelming computational requirements. In routine engineering calculations where the turnaround time for simulation must be fast, high premium is placed on the computational efficiency. Interestingly, the fidelity is sometimes sacrificed in order to improve the efficiency of the calculations, especially when many executions of the models are required to complete certain engineering-oriented studies such as design optimization, sensitivity analysis, and uncertainty quantification.

Reactor physics, the main focus of this dissertation, is the key element of the reactor core analysis wherein the radiation transport and interactions with the reactor materials, e.g., fuel, coolant, and structural materials, are modeled via the Boltzmann equation. Given the huge level of heterogeneity deliberately introduced in the design for safety and economic reasons; and the complexity of cross-sections characterizing the interaction probabilities with reactor

www.manaraa.com

materials, one must rely on numerical methods and homogenization techniques to render predictions of reactor behavior in practical computational times. Numerical methods are needed since analytical solutions are available only for few over-simplified cases, e.g. a bare homogeneous slab reactor. Homogenization techniques are essential to reduce the effective model's dimensionality. More details on typical dimensions are given later in the text. For the moment, it suffices to say that there currently exists no detailed simulation of the entire reactor core with all the geometry details resolved and the various physics coupling incorporated that can be used on a routine basis for engineering design, analysis, and regulatory purposes.

Homogenization techniques achieve dimensionality reduction by dividing the computational phase space (energy, angle, space, and time) into numerous sub-regions over which separate fast calculations can be performed. Physical insight is then used to connect the solutions obtained from the various sub-regions. Specifically, reactor physics calculations are split over three stages, pin cell calculations used to get a detailed description over energy with many energy groups but limited to a single fuel pin; assembly calculations expand the spatial domain to a 2-dimensional slice of a fuel assembly, called lattice, and compress the energy details to a few-group cross-section representation; and finally core calculations for the analysis of the whole core but now with all the energy and spatial details homogenized over the various fuel lattices.

Another modeling complication results from the interaction between the different physics affecting reactor behavior via the so-called feedback terms. For example, both thermal

www.manaraa.com

hydraulics analysis and material transmutation feedback effects must be taken into account. This follows as cross-sections are known to depend on both the temperature of the fuel and the various material isotopic densities which continuously vary over time due to irradiation-induced transmutations.

Despite these complexities, the prediction accuracy of reactor calculations have been continuously improving over the years mainly because of the expertise gleaned over the many years of operation. This resulted in fine-tuning and customizing the models to the specific reactor and fuel loading. As the reactors age however, the predictive accuracy of the models is expected to degrade. To address this, the US nuclear community has emphasized the need to use the recent advances in computer power to improve the fidelity of existing reactor methods. There are currently several projects around the country which support this initiative by building new software tools that incorporate more modeling details and make less simplifying assumptions in order to improve the fidelity of the models. While laudable, we believe without a capability to render these simulations in practical times similar to these currently employed by the industry, it is unlikely that the benefits of these new developments will be realized in practice.

At a first glance, the use of powerful computer to better model reactors appears to be a logical step forward. Under the surface however this initiative implies a marked depart from current design philosophy which primarily relies on experimental validation for design, operation, and regulation decision making. In the new initiative, the simulation assumes a leading role in the above processes. For this to be credible, the errors in the simulation must

www.manaraa.com

be rigorously quantified, understood, and ultimately reduced. This has solicited the need for uncertainty quantification, sensitivity analysis, and data assimilation techniques to achieve these goals. Performing these analyses with existing commercial codes is considered computationally intractable. The situation is expected to worsen with the new software development efforts expected to be much more complex and requiring longer execution times.

Difficulties from prohibitive computational requirements have been a well-known problem to many other engineering fields (e.g. fluid dynamics, structural mechanics, geophysics, etc.) and have been studied extensively. Two approaches can be considered; surrogate model and reduced order model[1]. The ***surrogate model*** (also called the meta-model, the data-based model, the information-driven model or the approximate model) is a low cost but fairly accurate alternative of the original model. The surrogate-based approach has been already proposed and applied by many researchers in several scientific areas to reduce the computational cost in the forward mode simulations for uncertainty quantification and design optimization. The ***reduced order modeling*** (also called model order reduction) generates a lower-dimensional model to approximate the original often high dimensional

[1] Different classifications have appeared in the literature [Eldred, et al. (2004), Liem (2007)], we however distinguish between reduced order modeling and surrogate model constructions are two different techniques. In our definition, reduced order modeling refers to a model that retains the original physics of the model but now expressed in terms of fewer degrees of freedom. Surrogate modeling however replaces the original model by another model picked to approximate the physics behavior but with no real relation to the physical process being modeled. For example, least-squares polynomial fitting represents an example of a surrogate modeling technique. Nodal methods however represent an example of reduced order modeling techniques.

www.manaraa.com

model. The reduction is possible via mathematical transformation between the original dimensions and fewer dimensions, referred to hereinafter as the active degrees of freedom. If the transformation is linear, it can be described by linear algebra projection operation onto an active subspace, considered to contain all active degrees of freedom. Due to the reduction in dimensionality, the system of equations can be solved with reduced computational cost, e.g. smaller number of arithmetic operations or memory/storage requirements.

These surrogate modeling techniques and reduced order modeling techniques have been successfully used in many scientific fields but rarely used in reactor physics problems mainly due to their limitations. For example, the surrogate modeling techniques have been only applied to the problems with small number of parameters (i.e. less than 20). The reason is that the unknown coefficients of a surrogate model increases super-linearly; thus, the computational cost, i.e. the number of code executions to generate the training sample sets would become rapidly impractical, which is often referred to as the ***curse of dimensionality***. For reduced order modeling techniques, the source code should be accessible for modification needed to implement the reduction algorithm, which could be difficult for complicated or legacy codes. Moreover, the unique features of the current reactor physics calculation procedures should be addressed to reliably extract the active degrees of freedom with a given computational budget and accuracy requirements in addition to implementation concerns (e.g. parallelism).

Sensitivity analysis, used widely in reactor physics community can be considered as a surrogate modeling technique, whereas response variations are approximated by a Taylor

www.manaraa.com

series expansion retaining as many terms as the derivatives afforded by sensitivity analysis. In most cases only first order derivatives can be afforded resulting in a linear surrogate model. In typical reactor core design, the variations of the input parameters are expected to give rise to nonlinear behavior; thus the first order sensitivity analysis results would not credibly estimate the output response variations. Though the theory and the algorithms for higher order sensitivity analysis have been well-established, their implementation has been recognized as impractical because the higher order derivatives are difficult to compute and again the computational cost increases super-linearly depending on the number of inputs.

We can also consider that the conventional reactor calculation procedure, i.e. two-step approach with homogenization and group collapsing for pin-cell, assembly and full core calculations (discussed in Chapter 2), as a physical-based hierarchical reduced order modeling. Note that by introducing the approximating and simplifying techniques, the one very large core calculation (which is not do-able) is divided into very many small (moderate) size calculations (which are do-able). Therefore, the reactor calculations requires a large number of code executions. For example, to conduct a fuel loading optimization for a real reactor, a code should be executed for assembly models with different material composition, temperature and conditions by more than 200,000 times.

The goal in this dissertation is ***to reduce the computational cost in utilizing the high-fidelity computer simulation tools for sensitivity analysis, uncertainty quantification and design optimization by employing the surrogate modeling techniques and reduced order modeling techniques based on the subspace methodologies***. One severe problem in applying

www.manaraa.com

the existing surrogate model techniques to reactor calculations is coming from the large number of input parameters (reaction cross sections), e.g., $10^5 \sim 10^6$ depending on the model configurations, which poses the constructing a surrogate model impractical due to curse of dimensionality. The motivation is that the dimensionality issue of the surrogate modeling techniques can be alleviated by incorporating the reduced order modeling techniques to reduce the number of input parameters. Once the reduced transformation of input parameters is conducted appropriately, the surrogate model can be constructed economically and engineering analysis can be performed more efficiently .

To achieve the objective, the dissertation involves the following three major research tasks:

1. **Developing a framework for the surrogate (reduced order) modeling management**. In order to replace the original full order model, the surrogate model should be accurate enough within a required level of accuracy. Note that two sources of errors should be considered, i.e. error introduced by reduced order modeling and by surrogate modeling. ***The metrics to measure the errors and the methods for validating the approximate model are studied***.
2. **Developing an efficient method for reduced order transformation**. This study is mainly focused on the reduced order modeling on input-level reduction to alleviate the curse of dimensionality in surrogate modeling. The main idea of the reduced order modeling is to extract the influential components with respect to a physical model or

www.manaraa.com

subsequent calculations. In addition to accuracy, the ease of implementation in practice is considered; the (semi-) ***automatization*** and ***parallelism***.

3. **Incorporating the reduced order model with existing surrogate modeling techniques.** With reduced order modeling, conventional analysis methods can be implemented more efficiently. Combining the reduced order model and surrogate model in higher order sensitivity analysis, uncertainty propagation and design optimization are investigated and novel algorithms are suggested by ***hybridizing*** methods to alleviate the curse of dimensionality.

This dissertation is organized as follows. In Chapter 2, the general overview of nuclear power plants and the conventional reactor calculation procedures are provided to introduce the challenges in the current methods for reactor physics problems and core design calculations and to motivate this work. In Chapter 3, the literatures for surrogate modeling techniques, reduced order modeling techniques and other related works are reviewed and the state-of-art techniques are summarized. The main developments for reduced order modeling are described in Chapter 4. Starting from the basic concept, the fundamental mechanism of reduction in state-level and input-level and the algorithm for orthonormal basis construction with random samples are elaborated. Moreover, for multi-physics problems in which the several codes are coupled, the intersection subspace approach is proposed to achieve the further dimensional reduction while minimizing the error due to reduced order modeling. Because it is critical to estimate the error due to reduced order modeling and surrogate modeling; thus the general framework for dimensionally reduced surrogate modeling and

www.manaraa.com

suggestions for error estimation and reduced order determination (i.e. size of active subspace) are provided in Chapter 4. In Chapter 5 ~ Chapter 9, the proposed hybrid reduced order modeling techniques are implemented to reactor physics calculations to investigate the feasibility and to explore its applicability. Especially, Chapter 5 utilizes the state-level reduction to build the reduced order adjoint system to estimate the state variables changes due to initial condition variations. In Chapter 6 and Chapter 7, the input-level reduction techniques are exploited to construct the surrogate models for second order approximation by Taylor series expansion (Chapter 6) and polynomial regression (Chapter 7), respectively. In Chapter 8 and Chapter 9, the intersection subspace approach is introduced into surrogate modeling for uncertainty propagation and design optimization, respectively. In Chapter 8, the intersection subspace is defined between uncertainties and sensitivities of input parameters and resulting basis is utilized to uncertainty propagation with the linear surrogate modeling and the nonlinear surrogate modeling. In Chapter 9, the intersection subspace is identified at the interface of serially coupled codes in reactor lattice model and applicability and reducibility are extensively examined for BWR and PWR assembly models. The conclusion is followed in Chapter 10. In **Figure 1-1**, the organization of this dissertation is depicted.

www.manaraa.com

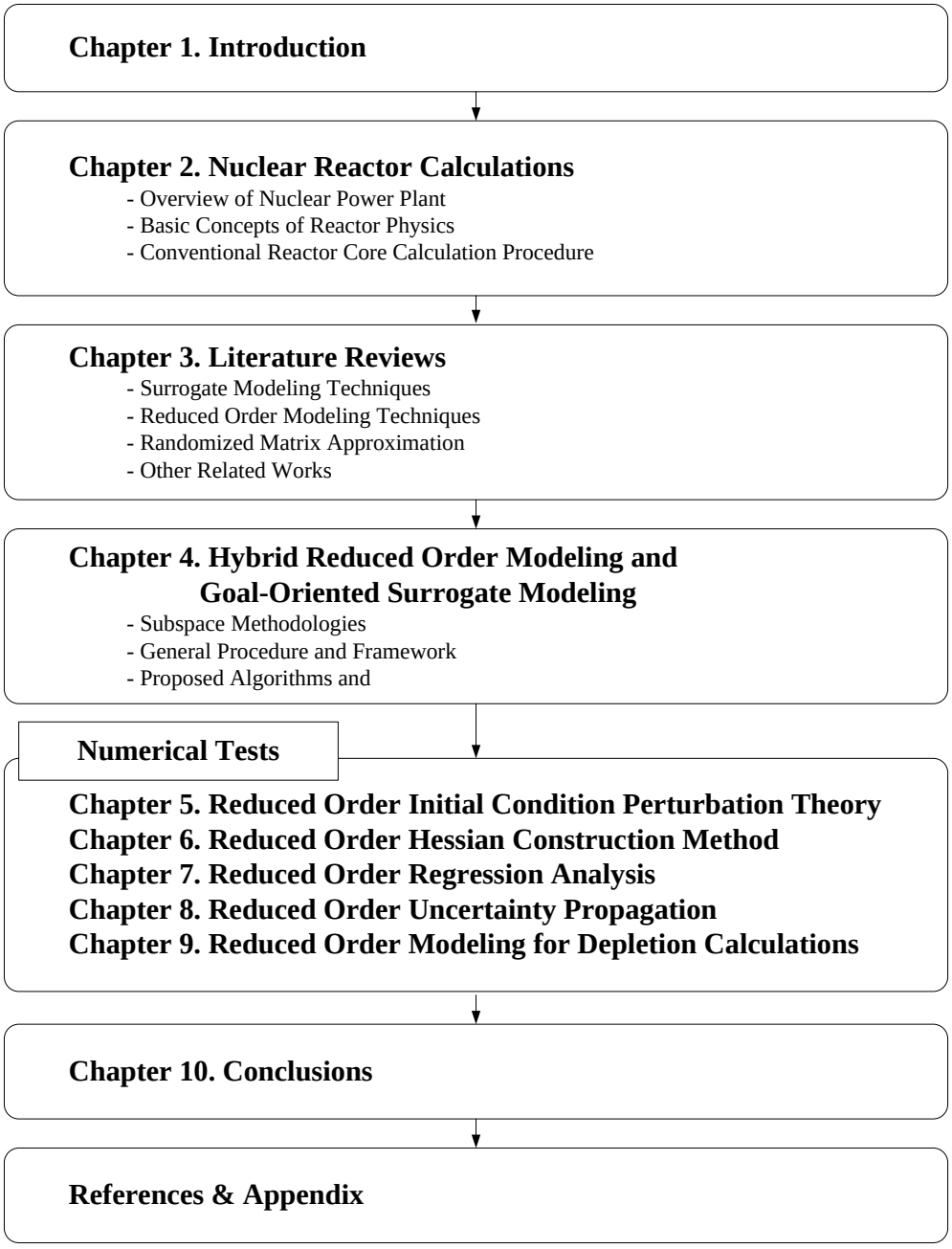

Figure 1-1. Organization of the Dissertation

www.manaraa.com

CHAPTER 2. NUCLEAR REACTOR CALCULATIONS

Nuclear power plant utilizes the fission energy as a heat source to produce steam and ultimately to generate the electrical power. In the fission reaction, neutrons play the key role, thus it is important to estimate the behavior and the distribution of the neutrons accurately to design and operate the reactor core safely and economically. In this chapter, the general description of the nuclear power plant and the conventional procedures used in reactor core calculations for design are briefly overviewed. First, the general description of the nuclear power plant configurations is provided. Next, the mathematical expressions of the neutron distribution calculations are described. After that, the conventional methods to calculate the full core power distribution are presented to motivate the topic of this dissertation.

2.1 Overview of Nuclear Power Plant

As a power plant, the nuclear power plant mainly consists of the reactor vessel (core), the coolant system, the steam generators and the turbines. The heat generated by the fission reaction in the reactor core is delivered by the coolant system to steam generators where the steam is produced which rotates the turbines to generate the electricity. Only considering the electricity generation, the nuclear power plant has the same design concept with other power plants utilizing the heat engine. However, the fission reaction which entails the production of

www.manaraa.com

hazardous radioactive materials makes the nuclear power plant to have unique design features.

The schematics of the pressurized water reactor (PWR) power plant and the boiling water reactor (BWR) are shown in **Figure 2-1** and **Figure 2-2**, respectively. For safety reasons, the coolant system is separated into isolated loops. For PWR, the water circulated in the primary loop, which is called the reactor coolant, removes the heat from the core and transfers it to the steam generators (SGs). After delivering the heat to the SGs, the reactor coolant is pumped back to the reactor core by the reactor coolant pumps (RCPs) to continue removing and transferring the heat from the core to the SGs. The water in the second loop, which is called feed water, is in vapor phase, i.e. steam, from SGs to condensers and is in liquid phase, i.e. water, from condensers to SGs. The steam produced in the steam generators rotates the turbines. Then, it is condensed to liquid phase in the condenser and pumped back to the SGs by the feedwater pumps continuously. The heat transfer between the primary loop and the second loop occurs through the steam generator tube walls in the SGs. The water in the third loop is called condensate which is from sea nearby or cooling tower and used to cool down the feedwater in the condenser. For BWR, the steam is produced in the reactor vessel, i.e. the primary loop is directly connected to the turbine system. As described above, each loop is isolated to prevent any radioactive material leakage to the environment. In addition, the reactor vessel, the SGs and the reactor coolant system are built inside of the containment building which has several safety features to protect the environment and the public due to the postulated accidents.

www.manaraa.com

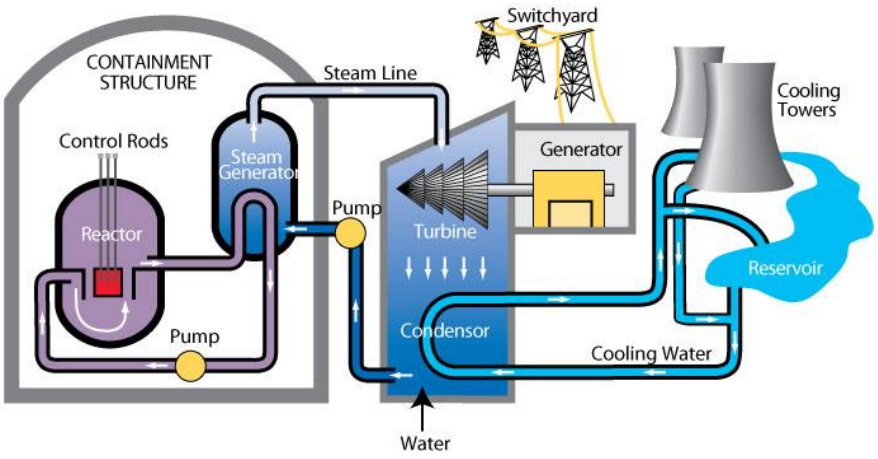

Figure 2-1. Schematic of Pressurized Water Reactor
(http://38.96.246.204/cneaf/nuclear/page/nuc_reactors/pwr.html)

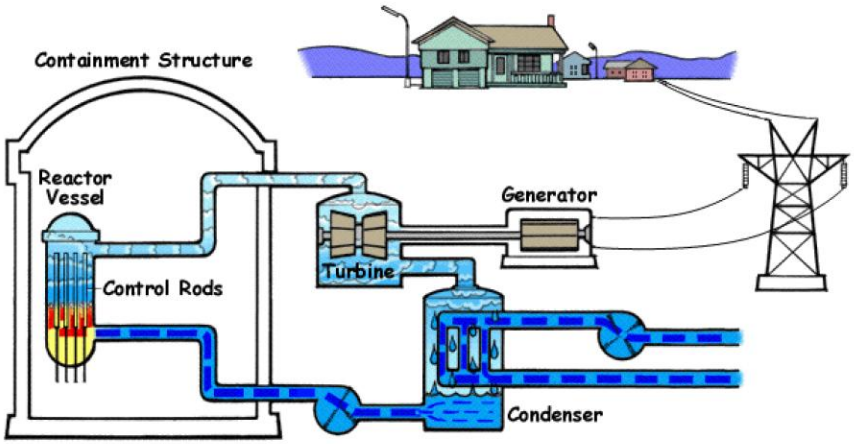

Figure 2-2. Schematic of Boiling Water Reactor
(www.ansn-jp.org/jneslibrary/npp2.pdf)

The general arrangement of the reactor vessel of PWR and BWR are shown in **Figure 2-3** and **Figure 2-4**, respectively. The reactor vessel mainly consists of fuel assemblies, reactor internals, control rod drive mechanisms (CRDMs) and instrumental detectors. The reactor internals support the core, maintain fuel alignment and CRDMs, limit fuel assembly, direct

www.manaraa.com

coolant flow past the fuel elements and the pressure vessel head, provide gamma and neutron shielding and provide guides for the in-core instrumentation. The CRDMs consist of a group of individual absorber rods which are used to control the reactivity of the core under the operating condition and to shutdown the reactor in accident conditions. Instrumentation is provided in and out of the core to monitor the nuclear, thermal-hydraulic and mechanical performance of the reactor and to provide inputs to automatic control functions. The fuel is loaded in the reactor core, which is comprised of an array of fuel assemblies which are similar in mechanical design, but different in fuel enrichment. Each fuel assembly consists of the fuel rods which contain fuel pellets as shown in **Figure 2-5**. Typically, a fuel assembly consists of a square array of 179 to 264 fuel rods, and 121 to 193 fuel assemblies are loaded into an individual reactor.

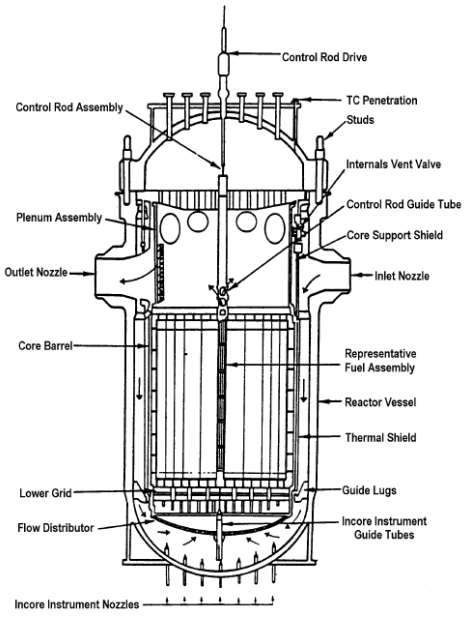

Figure 2-3. General Arrangement of PWR Reactor Vessel [Ivanov (1999)]

www.manaraa.com

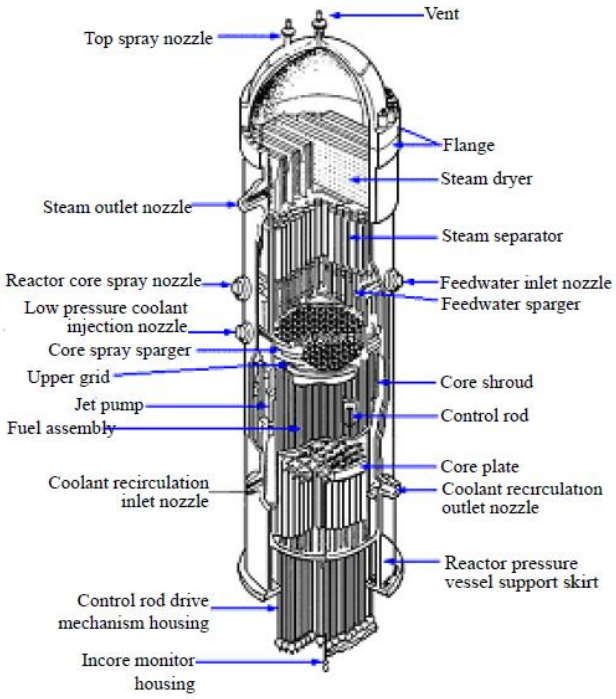

Figure 2-4. General Arrangement of BWR Reactor Vessel
(www.ansn-jp.org/jneslibrary/npp2.pdf)

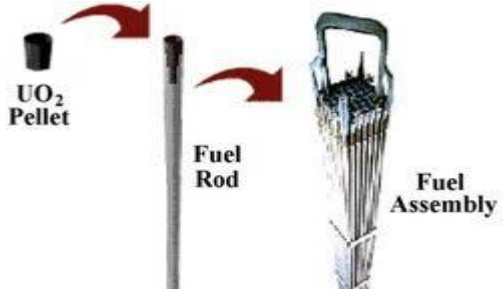

Figure 2-5. Diagram of Fuel Pellet, Fuel Rod and Nuclear Fuel Assembly
(http://www.nrc.gov/about-nrc/emerg-preparedness/images/fuel-pellet-assembly.jpg)

www.manaraa.com

2.2 Reactor Physics

The nuclear power plant utilizes the fission reaction to generate the heat. The energy produced in the fission reaction can be explained by Einstein's mass-energy equivalence [Lamarsh & Baratta (2001)]. When a heavy nucleus splits into two lighter nuclei, the mass defect occurs and this mass defect appears as kinetic energy in fission products and neutrons. To make the heavy nucleus fission, the neutron is used as an incident particle. As an example of such a reaction, consider a neutron incident upon a U-235 nucleus [Duderstadt & Hamilton (1976)]:

$$\text{neutron} + {}^{235}U \rightarrow \text{fission product} + \text{more neutrons} + \text{energy} \qquad (2.1)$$

Those kinetic energies in fission products would be converted into heat as they slow down by colliding with adjacent atoms. Note that as a result of the fission reaction, more neutrons are produced. Those newly produced neutrons may induce more fission reactions, which is called the ***fission chain reaction***. In thermal reactors, i.e. PWR and BWR, most of the fission reactions occur in the thermal energy region, therefore, the neutrons should be slowed down to induce the further reactions. During the slowing down process, the neutrons may be absorbed in non-fissionable material inside of the core or leak out from the system. In **Figure 2-6**, the schematic of a neutron life in reactor is depicted. In order to maintain the stable chain reaction, it is important to estimate the time varying neutron density and to design the core so that precisely one neutron from each fission reaction will induce another fission reaction. This can be expressed mathematically by defining ***multiplication factor*** k:

www.manaraa.com

$$k = \frac{\text{Rate of neutron production in reactor}}{\text{Rate of neutron loss in reactor}} \tag{2.2}$$

If $k = 1$, the number of neutrons would not be changed and hence the chain reaction will be time-independent, i.e. steady state. The system characterized by $k = 1$ is called ***critical***. If $k < 1$ or $k > 1$, the number of neutrons will decrease or increase, which are called subcritical or supercritical, respectively. The primary objective of nuclear reactor design and operation is maintaining the reactor core in the critical state.

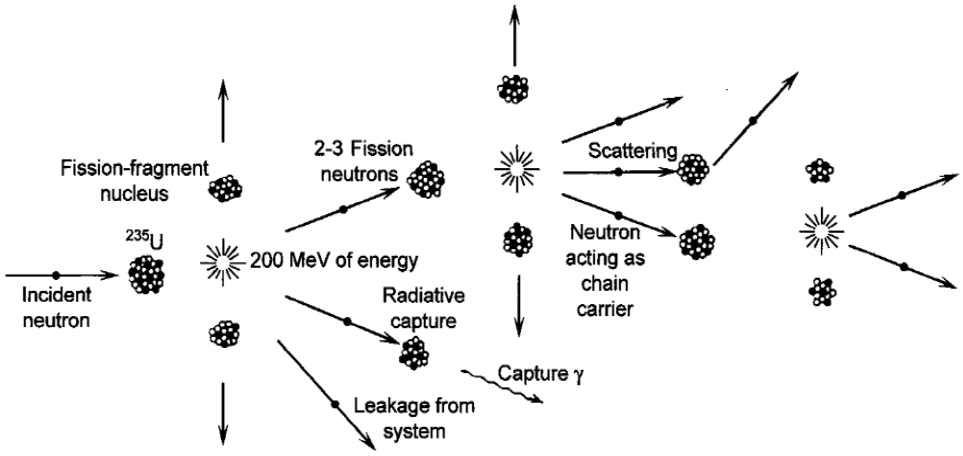

Figure 2-6. A Schematic of Neutrons Life in Fission Chain Reaction
[Duderstadt & Hamilton (1976), p.75]

Reactor physics deals with the determination of the neutron distribution in space, energy and time, which is established by the interaction of neutrons with the materials of the system under consideration [Stamm'ler & Abbate (1983)]. Define the angular neutron flux:

$$\psi\left(\vec{r},\vec{\Omega},E,t\right) = vn\left(\vec{r},\vec{\Omega},E,t\right) \tag{2.3}$$

www.manaraa.com

where $n\left(\vec{r},\vec{\Omega},E,t\right)d^3\vec{r}dEd\vec{\Omega}$ is the expected number of neutrons in $d^3\vec{r}$ about $\vec{r}$, energy dE about E, moving in direction $\vec{\Omega}$ in solid angle $d\vec{\Omega}$ at time t and v is a neutron velocity. Then, an angular interaction rate $\left[\text{No. of interaction}/\sec\right]$ can be defined by:

$$f\left(\vec{r},\vec{\Omega},E,t\right)=v\Sigma\left(\vec{r},\vec{\Omega},E\right)n\left(\vec{r},\vec{\Omega},E,t\right)=\Sigma\left(\vec{r},\vec{\Omega},E\right)\psi\left(\vec{r},\vec{\Omega},E,t\right) \tag{2.4}$$

The time rate of a neutron density change for an arbitrary volume V can be given by:

$$\frac{\partial}{\partial t}\left[\int_V n\left(\vec{r},\vec{\Omega},E,t\right)d^3\vec{r}\right]dEd\vec{\Omega}=\text{gain rate in } V\text{- loss rate from } V \tag{2.5}$$

Considering the gain and loss mechanisms, the neutron distribution can be expressed mathematically by the neutron transport equation (Boltzmann equation):

$$\begin{aligned}&\frac{1}{v}\frac{\partial\psi\left(\vec{r},\vec{\Omega},E,t\right)}{\partial t}+\vec{\Omega}\cdot\nabla\psi\left(\vec{r},\vec{\Omega},E,t\right)+\Sigma_t\left(\vec{r},E,t\right)\psi\left(\vec{r},\vec{\Omega},E,t\right)\\&=\frac{\chi(E)}{4\pi}\int_\infty dE'\int_{4\pi}d\vec{\Omega}'\left[\nu\left(E'\right)\Sigma_f\left(\vec{r},E',t\right)\psi\left(\vec{r},\vec{\Omega}',E',t\right)\right]\\&\quad+\int_\infty dE'\int_{4\pi}d\vec{\Omega}'\left[\Sigma_s\left(\vec{r},E'\to E,\vec{\Omega}'\to\vec{\Omega},t\right)\psi\left(\vec{r},\vec{\Omega}',E',t\right)\right]\end{aligned} \tag{2.6}$$

where

$\psi\left(\vec{r},\vec{\Omega},E,t\right)$: angular neutron flux $[cm^{-2}\cdot\sec^{-1}\cdot sr^{-1}\cdot MeV^{-1}]$

$\Sigma_t\left(\vec{r},E,t\right)=N\left(\vec{r},t\right)\sigma_t\left(E\right)$: macroscopic total cross section $[cm^{-1}]$

$\Sigma_f\left(\vec{r},E',t\right)=N\left(\vec{r},t\right)\sigma_f\left(E\right)$: macroscopic fission cross section $[cm^{-1}]$

$\Sigma_s\left(\vec{r},E'\to E,\vec{\Omega}'\to\vec{\Omega},t\right)=N\left(\vec{r},t\right)\sigma_s\left(E'\to E,\vec{\Omega}'\to\vec{\Omega}\right)$: macroscopic scattering cross section $[cm^{-1}]$

www.manaraa.com

$\sigma_x(E)$: microscopic reaction cross section (x can be t, f and s) [cm^2]

$N(\vec{r},t)$: nuclide number density at time t [$\#/cm^3$]

$\chi(E)$: fission spectrum

v : neutron velocity [$cm \cdot \sec^{-1}$]

$\nu(E)$: neutron yield per fission

$\vec{r}$: independent variable for space (3 dimension)

$\vec{\Omega}$: independent variable for neutron direction (2 dimension)

E : independent variable for energy [MeV] (1 dimension)

t : independent variable for time [sec] (1 dimension)

Note that the Eq. (2.6) can be considered as a problem to find a solution of angular neutron flux distribution $\psi(\vec{r},\vec{\Omega},E,t)$ with input coefficients determined by material properties, i.e. reaction cross sections, $\Sigma_t(\vec{r},E,t)$, $\Sigma_f(\vec{r},E',t)$, $\Sigma_s(\vec{r},E' \to E,\vec{\Omega}' \to \vec{\Omega},t)$, $\chi(E)$ and $\nu(E)$. The Eq. (2.6) can be solved analytically only in limited conditions with significant simplifications. One of the issues in Eq. (2.6) is the nuclide number density change. Because the nuclides are changed into other nuclides due to reactions, the material composition would be changed as the reactions occur. Note that the reaction is induced by neutrons, therefore there is a coupling between the flux and the nuclide concentration, i.e. the neutron transport equation requires the nuclide number density as material data while the nuclide density calculation (i.e. depletion calculation) requires the flux distribution. To

www.manaraa.com

resolve this issue, the quasi-static assumption is introduced. The reactor core is assumed to steady-state and the depletion calculation is separated from the flux calculation, i.e. when calculating the flux, the number density is assumed to static, and vice versa. In order to balance the production and the loss of neutrons, the k-eigenvlaue is introduced; thus Eq. (2.6) becomes the eigenvalue problem.

$$\begin{aligned}&\vec{\Omega}\cdot\nabla\psi\left(\vec{r},\vec{\Omega},E\right)+\Sigma_t\left(\vec{r},E\right)\psi\left(\vec{r},\vec{\Omega},E\right)\\&=\frac{1}{k}\frac{\chi(E)}{4\pi}\int dE'\int_{4\pi}d\vec{\Omega}'\left[\nu\left(E'\right)\Sigma_f\left(\vec{r},E'\right)\psi\left(\vec{r},\vec{\Omega}',E'\right)\right]\\&\quad+\int_{\infty}dE'\int_{4\pi}d\vec{\Omega}'\left[\Sigma_s\left(\vec{r},E'\to E,\vec{\Omega}'\to\vec{\Omega}\right)\psi\left(\vec{r},\vec{\Omega}',E'\right)\right]\end{aligned}\tag{2.7}$$

where k is k-eigenvalue (multiplication factor).

Another issue is the energy dependency of the reaction cross sections. As shown in **Figure 2-7**, the cross sections are varied in a complicated way, which means that the cross sections cannot be expressed with a simple functional form. To deal with cross section energy dependency, one can discretize the continuous energy range into discrete energy intervals or groups. By integrating Eq. (2.7) over the g th energy group characterized by energies $E_g<E<E_{g-1}$, the Multi-Group (MG) equation can be obtained:

$$\begin{aligned}&\vec{\Omega}\cdot\nabla\psi_g\left(\vec{r},\vec{\Omega}\right)+\Sigma_{tg}\left(\vec{r}\right)\psi_g\left(\vec{r},\vec{\Omega}\right)\\&=\frac{1}{k}\frac{\chi_g}{4\pi}\sum_{g'=1}^{G}\int_{4\pi}d\vec{\Omega}'\left[\nu_{g'}\Sigma_{fg'}\left(\vec{r}\right)\psi_g\left(\vec{r},\vec{\Omega}'\right)\right]\\&\quad+\sum_{g'=1}^{G}\int_{4\pi}d\vec{\Omega}'\left[\Sigma_{s,g'\to g}\left(\vec{r},\vec{\Omega}'\to\vec{\Omega}\right)\psi_g\left(\vec{r},\vec{\Omega}'\right)\right]\end{aligned}\tag{2.8}$$

with the group constants $\Sigma_{tg}\left(\vec{r}\right)$, χ_g, ν_g, $\Sigma_{fg}\left(\vec{r}\right)$ and $\Sigma_{sg'\to g}\left(\vec{r}\right)$. The total number of groups G can be determined by the required level of accuracy.

www.manaraa.com

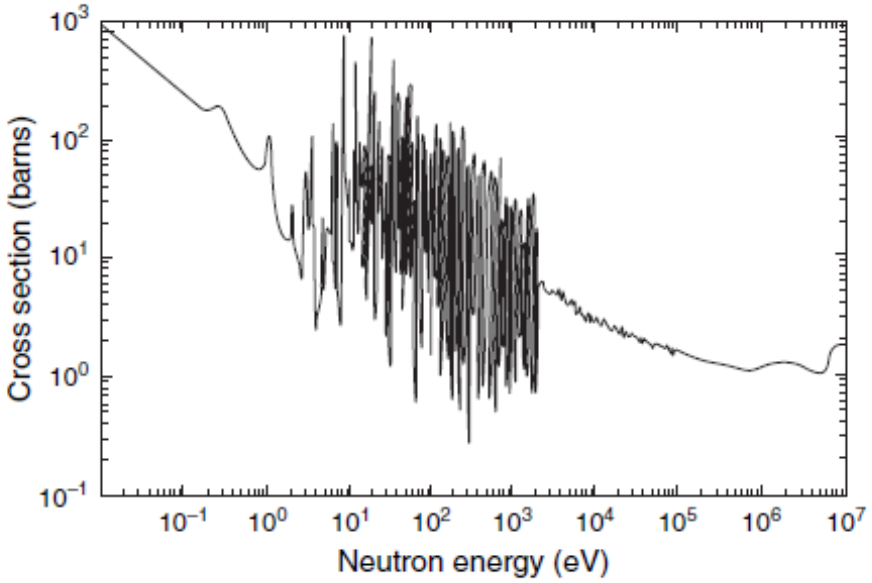

Figure 2-7. Microscopic Fission Cross Section σ_f of ^{235}U [Lewis (2008)]

The Eq. (2.8) can be solved by using spatial discretization method, e.g. method of characteristic (MOC) or nodal expansion methods [Lewis & Miller (1984)]. Note that if the space $\vec{r}$ is discretized into N nodes, the energy E into G groups and the angle $\vec{\Omega}$ into A, the total number of equations to be solved would be $N \times G \times A$.

2. 3 Conventional Reactor Core Calculations

Nuclear reactor cores are constructed in a highly heterogeneous configuration to facilitate thermal design (coolant channels, heat-transfer surfaces), mechanical design (structural

www.manaraa.com

integrity, fuel fabrication and handling), and reactivity control (control rods, burnable poisons, instrumentation). Such heterogeneities in the reactor fuel array or lattice must be taken into account in nuclear design since they will cause a local spatial variation in the neutron flux which may strongly influence core multiplication.

One example is the self-shielding effect [Duderstadt & Hamilton (1976), p.404]. Note that neutrons born in fission events in the fuel have to slow down in the moderator, i.e. thermalize, and then must diffuse back into the fuel to induce a further fission. However, the highly absorbing nuclei near the surface of the fuel pin tend to absorb the thermal neutron diffusing back in from the moderator and hence in effect shield the fuel nuclei in the interior of the pin. This leads to the depression of the thermal flux in the fuel. If the fuel pin is homogenized or calculated by coarse mesh without properly considering self-shielding effect, the multiplication factor would be incorrect.

Another example is the hot channel factor [Duderstadt & Hamilton (1976), p.503]:

$$F = \frac{\text{average heat flux of the hot channel}}{\text{average heat flux of the channels in core}} \tag{2.9}$$

where the hot channel is defined as the coolant channel in which the maximum heat flux occurs. Because the fuel has very low heat conductivity, the temperature is varied significantly inside of the fuel pin. In order to ensure the fuel integrity, the hot channel factor is used as a design and an operation limitation. If one can ensure that thermal conditions of this channel remain below the core limitations, the remaining channels in the entire core will presumably fall within design limitations. Note that the heat source is calculated by multiplying the fission reaction rate density by the recoverable energy released per fission

www.manaraa.com

event. Therefore, in order to calculate the hot channel factor correctly, the neutron distribution should be provided accurately.

Note that the number of equations to be solved is $N \times G \times A$ where N is the number of spatial nodes, G is the number of energy groups and A is the number of angular meshes. If only one dimension is considered, the N increases proportionally. However, for example, two dimension (i.e., x and y direction) is considered, the N increases exponentially, i.e. $N_1 \times N_2$ where N_1 and N_2 is the number of discretization along x and y direction, respectively. Though a powerful computer is used, the detailed treatment both of the spatial variation and the energy group dependency would be unmanageable.

In practice, full-core calculations are divided into three steps, i.e. pin-cell, assembly and core calculations and in each step, the each energy and spatial dependencies are considered in different levels. Also, in each step, the resonance self-shielding calculations are involved as a pre-processing of the group constants. For pin-cell calculations, a very finely structured many-group calculation is performed to calculate the intra-group fluxes while the spatial dependency is ignored or crudely approximated. These intra-group fluxes are then used to calculate the multi-group (MG) constants for a coarse group calculation including spatial dependence by [Duderstadt (1976), p.409]:

$$\Sigma_g^i = \frac{\int_{E_g}^{E_{g-1}} dE \int_{V^i} d\vec{r}^3 \Sigma(\vec{r}, E) \phi(\vec{r}, E)}{\int_{E_g}^{E_{g-1}} dE \int_{V^i} d\vec{r}^3 \phi(\vec{r}, E)} \tag{2.10}$$

www.manaraa.com

where V^i is the volume of the pin cell. Note that the MG constants defined by Eq. (2.10) can be considered as the flux weighted, energy group collapsed and volume homogenized very fine-group constants. After pin-cell calculation, the assembly calculation is conducted with MG constants and heterogeneity considerations, i.e. spatial dependency, to generate few-group (FG) constants in the same way with the pin-cell calculation. Then, as the final step, these assembly-averaged group constants are used to determine the flux and power distribution over the entire core. For the heterogeneous full-core calculations, each assembly is considered as a node, and power reconstruction methods or form factor methods can be used if the detailed distributions inside the nodes are required. In this way, one can characterize each unit by effective group constants accounting for the inhomogeneous flux distribution. This scheme is summarized in **Figure 2-8**.

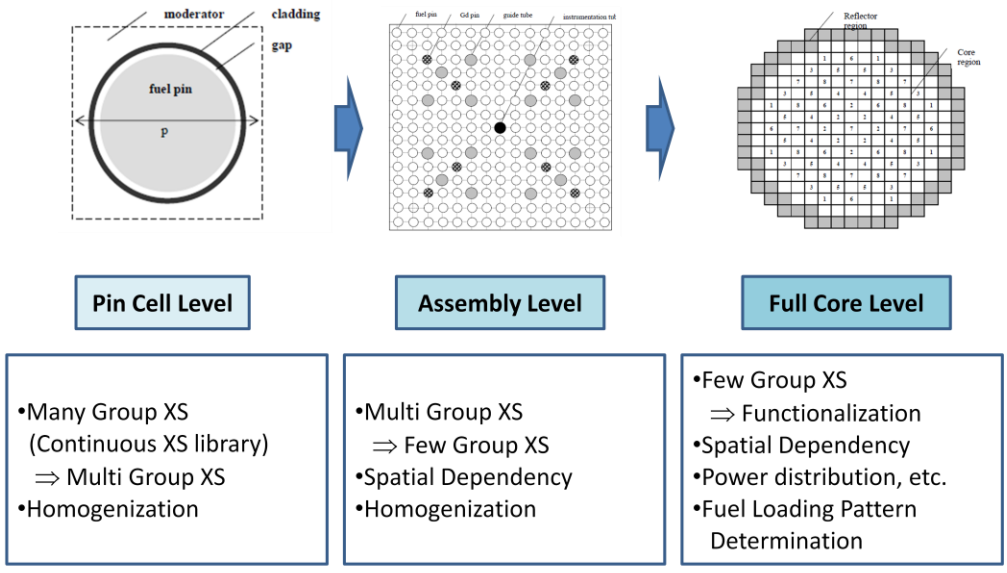

Figure 2-8. Heterogeneous Core Calculations

www.manaraa.com

As explained above, the reactor physics calculations are divided into several steps to alleviate the computational cost. Consider the lattice calculations, i.e. assembly calculation, for generation of the few-group homogenized cross sections. The core simulators are using them as input parameters to calculate the full-core neutron distribution and power distribution. Note that the core simulations are typically conducted by nodal methods, i.e. each assembly is considered as a node characterized as a single homogenized and group-condensed mixture. Because the homogenization and the group condensation are approximation techniques, the calculation results have discrepancy to the heterogeneous calculation (no approximation). In order to improve the accuracy and preserve the reaction rate and leakage rate, the discontinuity theory is introduced and assembly discontinuity factors (ADF) are used for full core nodal calculations. Also, to reconstruct the neutron distribution in the assembly, the power reconstruction techniques, e.g. form factor, have been suggested. The group constants, i.e. few-group cross sections, and other factors are called as ***homogenization parameters***.

It is important to note that the homogenization parameters are varied according to physical conditions, which is not known before the core design is fixed. For example, the resonance parameters are functions of the temperature, e.g. Doppler effects. However, the temperature of the assembly can be found after the location of the assembly is determined and the other factors, e.g. thermal-hydraulic heat transfer, are known. Note that the purpose of the core simulation is to determine the fuel loading pattern and design optimization; thus,

www.manaraa.com

the temperature is not known a priori. Therefore, another approximation technique is introduced to core simulators; ***few-group constant functionalization***.

For functionalization, the assembly lattice calculations are conducted with several different conditions as branch calculations and then, a set of FG constants are provided to the core simulator. The core simulator builds each FG constant as a function of the physical conditions, i.e. moderator density, fuel temperature, burnup, etc. Then, taking into account all possible physical condition changes, the reference FG constants are adjusted before put into nodal equations.

As an example, the FORMOSA-B updates the FG cross sections as [Moore et al. (1999)]:

$$\Sigma = \Sigma^{VH,IV} + \Delta\Sigma^{CRH} + \Delta\Sigma^{TF} + \Delta\Sigma^{FP} + \Delta\Sigma^{CRD} \tag{2.11}$$

where, given explicit arguments,

$\Sigma^{VH,IV} = \Sigma^{VH,IV}\left(\left[BU, \bar{\rho}, \bar{R}_f\right], \rho\right)$: moderator density history and instantaneous moderator density,

$\Sigma^{CRH} = \Sigma^{CRH}\left(\left[BU, \bar{\rho}, \bar{R}_f\right], \rho\right)$: control rod history,

$\Sigma^{TF} = \Sigma^{TF}\left(\left[BU, \bar{\rho}\right], \rho, T_f\right)$: fuel temperature,

$\Sigma^{FP} = \Sigma^{FP}\left(\sigma^{FP}\left(\left[BU, \bar{\rho}, \bar{R}_f\right], \rho\right), \phi_g\right)$: fission products,

$\Sigma^{CRD} = \Sigma^{CRD}\left(\left[BU, \bar{\rho}\right], \rho, R_f\right)$: control rod insertion.

Note that the nodal exposure, moderator density history (void history) and control rod history are given as:

www.manaraa.com

nodal exposure : $BU(i) = \int_0^{BU(i)} d\left[BU(i)\right]$

moderator density history (void history): $\bar{\rho}(i) = \frac{1}{BU(i)} \int_0^{BU(i)} \rho(i) d\left[BU(i)\right]$

control rod history: $\bar{R}_f(i) = \frac{1}{BU(i)} \int_0^{BU(i)} R_f d\left[BU(i)\right]$

where BU is a burnup (exposure), ρ is an instantaneous moderator density, R_f is a control rod insertion $0 \le R_f \le 1$ and T_f is a fuel temperature. One can notice that the FG constants are functionalized with the parameters, i.e. burnup, moderator density, control rod insertion and fuel temperature.

The lattice calculation is also divided into several calculations: resonance calculation, transport calculation, and depletion calculation. The schematic of the procedure is depicted in **Figure 2-9**. According to the physical configurations, e.g. geometry, material composition, temperature, the reaction cross sections are prepared to take into account the resonance and the temperature effects. Then, the transport calculation is conducted to calculate the neutron flux distributions. After that, the depletion calculation can be performed to calculate the nuclide number density at the next time step with an assumption that the flux is not changed, i.e. quasi-static assumption. The few-group constants can be calculated by using the flux and the resonance self-shielded macroscopic cross sections. Note that the most computational load is on the transport calculation.

www.manaraa.com

As mentioned above, in the level of FG constant generation, the physical conditions of the assembly are not fully provided, i.e. the fuel temperature and moderator temperature and density are not known yet. The core simulator, e.g. FORMOSA-B, requires the branch calculations to functionalize the FG constants. In every depletion steps, the branch cases with different conditions, e.g. fuel temperature or moderator density, are also evaluated and sets of FG constants are constructed.

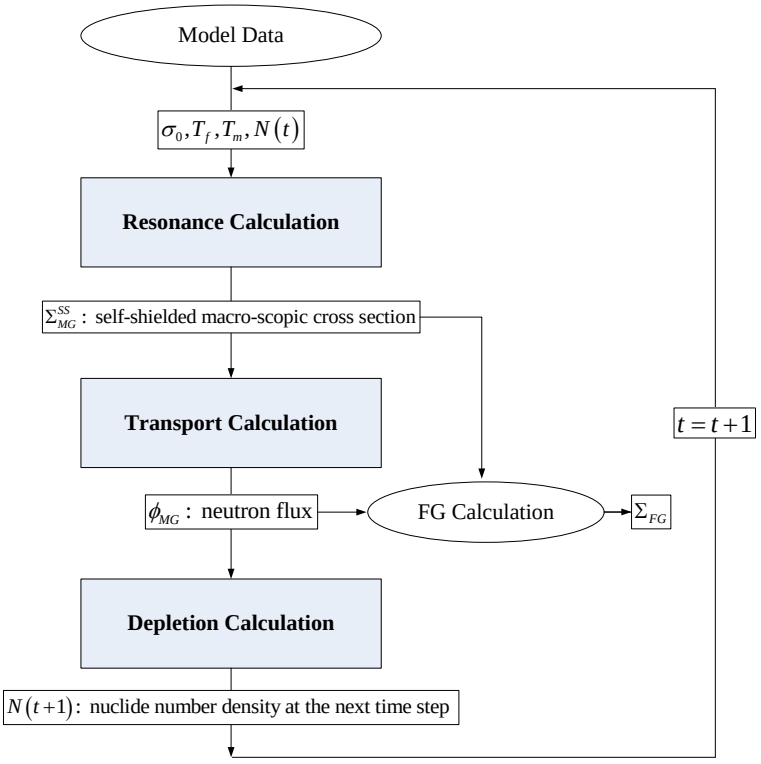

Figure 2-9. Schematic of Lattice Calculation

www.manaraa.com

The main focus of this dissertation is on the assembly averaged group constant generation (i.e. FG constant generation). In realistic core calculations, the required number of assembly calculations is very large. As an example, consider TMI-1 reactor core [Ivanov (1999)] which consists of 241 assemblies, 177 fuel assemblies and 64 reflector assemblies. Assuming one-eight symmetry of the core, the 30 different types of assemblies should be considered for radial geometry for each axial layer. Some assemblies may contain different types of control rods. For the power distribution change due to depletion, the burnup of the fuel material, the temperature change of the fuel and the moderator density variations should be considered. As an example, assume that 2 control rod insertion cases (in or out), 3 fuel temperature and 3 moderator density are required for all assembly types, i.e. 30 different types at 40 depletion time steps. Therefore, the total required number of assembly calculations for FG constant generation would be:

$$30 \times 40 \times 2 \times 3 \times 3 = 21,600 \tag{2.12}$$

Just for the flux distribution (power distribution) calculation, 21,600 sets of FG constants are required, which implies that the MG neutron equation should be solved 21,600 times. One can see that this number would increase easily if one put more data points, e.g. more depletion time steps or assembly types. Moreover, if considering safety criteria or feedback from thermal-hydraulics or material structures, the physical configuration would be changed and the whole process of reactor physics calculation should be repeated. In this case, the uncertainty quantification or data assimilation are out of question because they require

www.manaraa.com

inevitably repetitive code executions to capture the input parameter variations due to uncertainty.

www.manaraa.com

CHAPTER 3. LITERATURE REVIEWS

This dissertation employs the surrogate modeling techniques and the reduced order modeling techniques to reduce the computational cost in nuclear reactor calculations and to utilize the high fidelity codes efficiently. Though those methods have been already suggested by many researchers and used in variety fields which are dealing with expensive computer codes, those are yet not popular in nuclear engineering community. In this chapter, the brief literature survey about the related works is presented to figure out the current issues. First, the overview of the surrogate modeling techniques and recent trends are summarized. Second, the reduced order modeling techniques and related works are reviewed. The other works related to this dissertation are also addressed. The conclusion of literature review is followed to highlight the motivation and the objectives of this dissertation.

3.1 Surrogate Modeling Techniques

The surrogate model is also called as a ***meta-model*** or an ***approximated model*** according to research communities and authors. There are many different surrogate models and those have been widely used in many different areas: for some examples, Isukapalli et al. (1998) used stochastic response surface methods for uncertainty propagation and applied to a biological system (i.e. estimate the effective doses of toxic chemical in human body) and

www.manaraa.com

environmental problem (i.e. estimate pollutant concentrations in the atmosphere). Doebling et al. (2002) suggested a framework to employ the meta-model to enhance the model validation procedure. Anile et al. (2003) employed the stochastic response surface method to microelectronics to determine the effect of parameter variations on the output of a given system. Giunta et al. (2004) compared three types of sampling methods (i.e. Monte Carlo sampling, Latin hypercube sampling, and orthogonal array sampling) to generate data to build the response surface approximation along with two types of approximation methods (i.e. kriging interpolation and multivariate adaptive regression splines) for a Rosenbrock function. Chen et al. (2006) derived Tensor-product basis functions and analytical formulation for sensitivity analysis and uncertainty quantification and demonstrated on the design optimization of engine piston. Ghanmi et al. (2006) proposed a method to determine the optimal and robust design with respect to the uncertainties of design parameters of finite element models using stochastic response surface method and demonstrated the method on the coupled beam problem and the helicopter landing gear modeling. Liem (2007) introduced the multi-agent collective method to reduce the computational cost in aviation system model for environmental impact estimation. Laurenceau & Meaux (2008) investigated the response surface (kriging) based optimization framework and compared to traditional quasi-Newton gradient method with CFD problems. Kewlani & Iagnemma (2008) employed the stochastic response surface approach to take into account the terrain parameter uncertainty in mobile robot mobility. (for more application examples, see Goel (2007), Viana (2011) and website of SUMO Lab. http://www.sumo.intec.ugent.be).

www.manaraa.com

In nuclear engineering, there were attempts to use the surrogate modeling[2] for the plant control, the signal monitoring and diagnosis, the prediction of the system parameters and the artificial neural network (ANN) were dominant. Excellent reviews can be found in Pazsit & Kitamura (1996), Uhrig & Tsoukalas (1998), Schirru et al. (1999), Hines & Uhrig (2005), Guo et al. (2010) and Faghihi et al. (2011). For examples of the application to the plant control, Ku et al. (1992) used the diagonal recurrent neural networks with adaptive learning rate scheme to control nuclear reactor temperature. Boroushaki et al. (2003) and Boroushaki et al. (2004) used an updatable recurrent neural network to design an on-line intelligent core controller for load following operations and the axial offset control of PWR nuclear reactor core during load following operation, respectively. For the plant monitoring and diagnosis, Hwang (1993) studied an approach based on neural networks for detecting and diagnosing instrument failures in nuclear power plants. Kim & Bartlett (1996) developed artificial neural networks to monitor and control nuclear power plant systems and support plant personnel providing a faulty diagnosis. Na et al. (2003) used the fuzzy neural network to estimate an output signal for failure detection. Vinod et al (2003) developed an operator support system known as Symptom Based Diagnostic System (SBDS) to identify the initiating event and inform the operator with the proper corrective actions. Lee et al. (2005) also developed an accident diagnosis advisory system (ADAS) using modified dynamic neural network (MDNN) and dynamic neuro-fuzzy network (DNFN) to help operators with information gathering, planning and decision making during abnormal conditions. Santosh et al. (2007),

[2] In nuclear engineering literature, it is called as ***data-based model*** or ***information-driven model*** (cf, physical model) instead of surrogate model.

www.manaraa.com

Kupka & Meloun (2009) and Santosh et al. (2009) used the artificial neural networks for identification of accident scenarios and proper actions. The neural networks was also used to predict the thermal power distribution of nuclear power plant [Roh et al. (1991), Tanabe and Yamamoto (1993), Dubey et al. (1998), Na et al. (2004), Montes et al. (2009), Malik et al. (2010)]. Bakal et al. (1995) and Ortiz & Requena (2003) used neural networks to predict core parameter changes in transient. Choi et al. (2004), Ridluan et al. (2009), Wei et al. (2009) and Patra et al. (2010) used artificial neural networks to simulate the thermohydraulic behaviors of nuclear power plants. Mazrou & Hamadouche (2004), Perez-Cruz & Poznyak (2007) and Khalafi & Terman (2009) designed a research reactor by neural networks model. The prediction capability of neural networks introduced into fuel reloading optimization [Jang et al. (2001), Yamamoto (2003), Sadighi et al. (2002), Erdogan & Geckinli (2003), Ortiz & Requena (2004) and Hedayat et al. (2009)]. Ramu et al. (2010) employed the response surface modeling, Kriging and neural network to optimize the design of the roof slab of a nuclear reactor using finite element software ANSYS. Other than the neural networks, Roderick et al. (2010) applied the polynomial regression method to estimate the temperature on the centerline of the fuel pin and Lockwood & Anitescu (2010) suggested the gradient-enhanced kriging to improve the accuracy of the kriging model and demonstrated it with nuclear reactor simulation code. Also, kriging is used to analyze the LB-LOCA [Joucla et al. (2011)].

In reactor physics (neutronics problems), the ***first order Taylor expansion*** has been used to estimate the response changes due to input parameter variations. The ***adjoint based***

www.manaraa.com

approach has been recognized as the most efficient method to calculate the first order derivative information, which is further used in uncertainty propagation and data assimilation [Cacuci (2003)].

Note that the surrogate is basically constructed by executing the original model at different points in the parameter space as many times as can be afforded and a functional form for the surrogate is assumed with some undetermined coefficients, which are determined via a minimization procedure that reduces the discrepancies between the surrogate and the original model's predictions at all available points. For more rigorous surrogate modeling, the framework for constructing and utilizing a surrogate model is established by many authors [Booker et al. (1998), Queipo et al. (2005), Barton (2009), Forrester & Keane (2009)]. The main procedure can be summarized as in **Figure 3-1**. First step is to determine the variables to be considered. Because the number of unknown coefficients in a surrogate model increases super-linearly, the screening of dominant input parameters are recommended to reduce the computational cost. Next step is to generate the training sets to determine the unknown coefficients. These samples can be generated simply by random sampling, i.e. Monte Carlo sampling, however, to achieve the better design space representation, the structured sampling techniques, e.g. Latin Hypercube sampling [McKay (1989)], orthogonal array (OA) [Owen (1992)] and other optimal methods [Tang (1984), Johnson et al. (1990)] are recommended. The unknown coefficients in a surrogate model are determined by minimizing the discrepancy between the original model calculations and the surrogate model estimations.

www.manaraa.com

The prominent surrogate modeling techniques may be response surface modeling (RSM) [Myer et al. (2008)], kriging [Sacks et al. (1989a)], radial-basis function [Hardy (1971)], kernel-based function [Nadaraya (1964)], multivariate adaptive regression spline (MARS) [Friedman (1991)] and neural network [Smith (1993)]. Those are compared in **Table 3-1** based on the discussions of Goel (2007), Barton (2009) and Forrester et al. (2009). As the final step, the constructed surrogate has to be validated to ensure its accuracy. Split sample (SS), Cross-validation (CV) and Bootstrapping methods can be used to estimate the error of the surrogate model [Queipo et al. (2005)].

www.manaraa.com

Table 3-1. Functional Form of Surrogate Models

Surrogate Type	Functional Form	Applicability	Comp. Cost	Recommended Condition
RSM	$y_{est}(\vec{x}) = \sum_{i=1}^{N_\beta} \beta_i f_i(\vec{x}_j)$	Local	Low	$N_v < 20, N_s < 500$ Only for smooth functions
KRG	$y_{est}(\vec{x}) = \sum_{i=1}^{N_\beta} \beta_i f_i(\vec{x}) + \varepsilon(\vec{x})$	Global	High	$N_v < 20, N_s < 500$ smooth and fast varying functions
RBF	$y_{est}(\vec{x}) = \sum_{i=1}^{N_{RBF}} w_i h_i(\vec{x})$	Local	High	$N_v > 20, N_s > 500$ good for fast varying functions
KBR	$y_{est}(\vec{x}) = \sum_{i=1}^{N_s} \alpha_i G(\vec{x}, \vec{x}^{(i)}) + b$	Global	Low	$N_v > 20, N_s > 500$
BNN	$y_{est}(\vec{x}) = \int_{\Re} f_N(\vec{x}, \vec{w})\, p_{w\|D}(\vec{w})\, d\vec{w}$	Global	High	good for complex functions
SPD	$y_{est}(\vec{x}) = \frac{\sum_{i=1}^{N_b} w_i(\vec{x}) P_i(\vec{x})}{\sum_{i=1}^{N_b} w_i(\vec{x})}$	Global	High	Not Found

* RSM: response surface model, KRG: Kriging, RBF: radial basis function, KBR: kernel-based regression, BNN: Bayesian neural network, SPD: Shepard
* N_v: number of variables, N_s: number of samples (training data)

www.manaraa.com

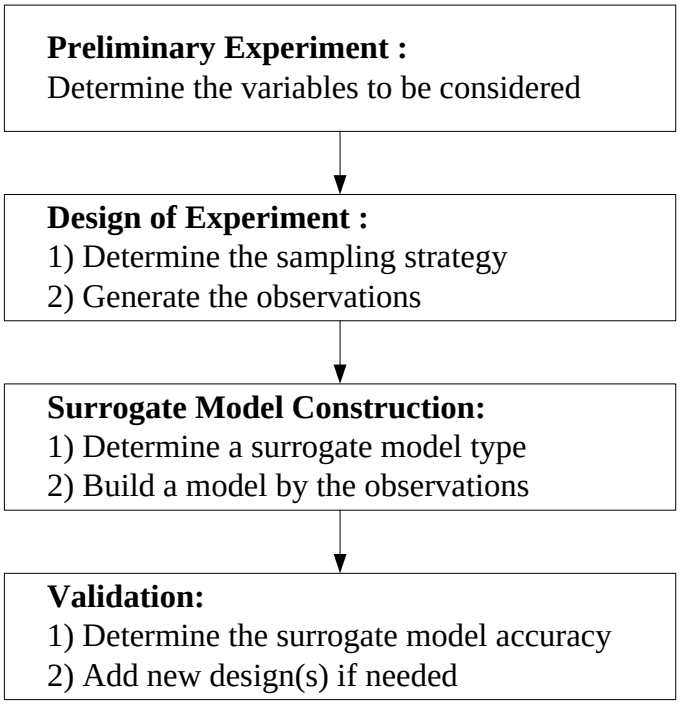

Figure 3-1. General Framework of Surrogate Model Construction

Comparative studies on different combinations of sampling strategies and surrogate modeling types have conducted by many researchers [Friedman and Stuetzel, 1981, Yakowitz & Szidarovsky, 1985, Laslett, 1994, Giunta & Watson, 1998, Jin et al., 2001, Simpson et al., 2001, Macdonald, 2009, Zhao & Xue, 2009]. The common conclusion is that, depending on the problem under consideration, a particular modeling scheme (i.e. sampling strategy + surrogate model type) may outperform the others, however, in general, ***it is not known a priori which one should be selected*** [Goel, 2007].

As an effort to improve the accuracy of the surrogate, hybrid surrogate modeling techniques are suggested. Varadarajan et al. (2000) suggested the combined RSM+ANN

www.manaraa.com

(response surface modeling + artificial neural network) approach to improve the prediction accuracy and complement each other's limitations. Qian et al. (2006) proposed 2-step approach (approximate simulation stage and detailed simulation stage) to reduce the number of computationally expensive simulations. Recently, multiple surrogate-based analysis and optimization approaches have been suggested. Zhou et al. (2007) suggested an approach to calculate many surrogate models simultaneously and choose best one for optimization. Zerpa et al. (2005), Goel et al. (2006b) and Glaz et al. (2009) proposed the multiple surrogate-based analysis approach utilizing the weighted average of the individual surrogates. Zhao & Xue (2009) combined the multi-surrogate methods by Bayes' theorem in view of conditional probability.

3.2 Reduced Order Modeling Techniques

Several reduced order modeling methods are available and those are well-summarized by Villemagne & Skelton (1987), Freund (1999, 2000), Bai (2002), Fodor (2002), Antoulas et al. (2006) and Penzl (2006). Reduced order modeling techniques have been used in various fields and extended by many authors. For example, Park & Jung (2000) developed a recursive algorithm employing Karhunen-Loève Galerkin procedure for multidimensional inverse heat conduction problems. Banks et al. (2002) utilized the proper orthogonal decomposition method to analyze the feedback control of thin film growth in a high-pressure chemical vapor decomposition reactor. Phillips (2003) explored the Krylov-subspace-based reduction methods for nonlinear time-varying circuit systems. Rewienski & White (2006)

www.manaraa.com

extended the reduced order modeling techniques for nonlinear dynamical systems based on trajectory piecewise-linear (TPWL) approximations and demonstrated on a micromachined switch, nonlinear electronic circuits and shock propagation modeled by Burgers' equation. Daescu & Navon (2007) developed a proper orthogonal decomposition-based reduced second-order adjoint model to facilitate a Hessian-free truncated Newton (HFTN) minimization algorithm for 4D-Var data assimilation.

The reduced order modeling methods appear in literatures are Balanced Trucation [Moore (1981)], optimal Hankel norm approximation [Glover (1981)], Krylov-based methods [Bai (2002)] and Proper Orthogonal Decomposition (POD). In circuit modelings (i.e. linear time-invariant (LTI) and linear time-varying (LTV) problems), the Krylov-based method [Feldmann & Freund (1995)] and the balanced truncation methods [Moore (1981)] are popular. For nonlinear fluid dynamics problems, the POD methods are dominant [Lumley (1967), Berkooz et al. (1993), Holmes et al. (1996)].

As pointed by Antoulas et al. (2006), most of the model reduction methods are based on ***projection***. Most works have been conducted to reduce the system of equations, i.e. ***reducing the state variables***. To illustrate this, consider an time-dependent nonlinear partial differential equation in a form [Chaturantabut & Sorensen (2009)]:

$$\frac{\partial y(x,t)}{\partial t} = L\left(y(x,t)\right) + F\left(y(x,t)\right) \tag{3.1}$$

where L denotes a linear spatial differential operator and F is a nonlinear function of a scalar variable. By spatially discretizing, a system of nonlinear ordinary differential equations can be given by:

www.manaraa.com

$$\frac{d}{dt}\vec{y}(t) = \mathbf{A}\vec{y}(t) + \mathbf{F}\left(\vec{y}(t)\right) \tag{3.2}$$

where $t \in [0,T]$ denotes time, $\vec{y}(t) = \begin{bmatrix} y_1(t) & \cdots & y_n(t) \end{bmatrix}^T \in \mathbb{R}^n$, $\mathbf{A} \in \mathbb{R}^{n \times n}$ is a discrete approximation matrix of the operator L, $\mathbf{F}$ is a nonlinear function evaluated at $\vec{y}(t)$, i.e., $\mathbf{F} = \begin{bmatrix} F\left(y_1(t)\right) & \cdots & F\left(y_n(t)\right) \end{bmatrix}^T$ with appropriate initial conditions. Let the $\mathbf{V} \in \mathbb{R}^{n \times r}$ be a matrix whose orthonormal columns are the vectors in the reduced basis. Then, the $\vec{y}(t)$ can be projected onto the basis by:

$$\mathbf{V}\mathbf{V}^T\vec{y}(t) = \mathbf{V}\vec{y}_r(t) \tag{3.3}$$

where $\vec{y}_r(t) \in \mathbb{R}^r$. Substitute Eq. (3.3) to Eq. (3.2), then the reduced-order system can be obtained by:

$$\frac{d}{dt}\vec{y}_r(t) = \mathbf{A}_r\vec{y}_r(t) + \mathbf{V}^T\mathbf{F}\left(\mathbf{V}\vec{y}_r(t)\right) \tag{3.4}$$

where $\mathbf{A}_r = \mathbf{V}^T\mathbf{A}\mathbf{V} \in \mathbb{R}^{r \times r}$ is an approximation of the matrix $\mathbf{A}$. Due to reduced dimensionality, the problem can be solved efficiently with lowered computational cost, e.g. floating point operations and memory requirements. Note that the choice of the reduced basis would determine the quality of the approximated solution.

The POD may be the most famous method because its derivation is numerically tractable for very large scale systems [Astrid (2004)]. According to Berkooz et al. (1993), POD rediscovered independently by several scientists, e.g. Kosambi (1943), Loève (1945), Karhunen (1946), Pougachev (1953) and Obukhov (1954). Depending on the field of

www.manaraa.com

research, the POD is also called as principal component analysis (e.g. statistics), Karhunen-Loève decomposition (signal analysis and pattern recognition) and the method of empirical orthogonal function (EOF) in geophysical fluid dynamics and meteorology [Homescu et al. (2007)]. Originally POD was used as a data representation technique (i.e. data analysis and compression), combined with the Galerkin projection procedure, POD can be used to generate lower dimensional models of dynamical systems [Rathinam & Petzold (2003)].

POD has been widely used in various fields (e.g. fluid mechanics, image processing, electrical circuit, pattern recognition, control, inverse problems) and extended by many authors. For example, Astrid et al. (2008) developed the method of missing point estimation (MPE) to enhance the efficiency in computing Galerkin projections over a restricted subset of the spatial domain. Varshney & Armaou (2008) suggested POD with updates in which the empirical eigenfunctions are continuously modified as additional data from the process becomes available. Chaturantabut & Sorensen (2009) combined the POD with discrete empirical interpolation method (DEIM) to further reduce the complexity of nonlinear models. Xu et al. (2010) introduced the recursive proper orthogonal decomposition (rPOD) method based on the operator perturbation theory to incorporate new data at each sampling time for cyber-physical systems.

Error due to reduced approximation has been extensively studied. For POD, the error bound can be estimated by [Lall et al. (2002), Astrid & Verhoeven (2006), Bui-Thanh et al. (2007), Chaturantabut & Sorensen (2000)]:

$$\left\| \vec{y} - \vec{y}_r \right\|_2^2 = \sum_{i=r+1}^{n} \sigma_i^2 \tag{3.5}$$

www.manaraa.com

or in a relative sense,

$$\gamma \le \frac{\sum_{i=1}^{r} \sigma_i^2}{\sum_{i=1}^{n} \sigma_i^2} \tag{3.6}$$

where σ_i for $i = 1,...,n$ are singular values of the snapshot matrix $\mathbf{Y} = \mathbf{U\Sigma V}^T \in \mathbb{R}^{n \times n}$ in which $\mathbf{\Sigma} = diag\left[\sigma_1 \quad \cdots \quad \sigma_n\right]$. Benner et al. (2003) summarized the error estimates of balanced truncation, singular perturbation approximation and Hankel-norm approximation for stable and unstable systems. Reis & Stykel (2005) derived the error bounds for coupled system. For approximation approaches of nonlinear dynamic problems, Rathinam & Petzold (2000) and Rewienski & White (2006) derived the error estimation for power series expansion method and piecewise-linear approximation, respectively.

When the parametrized system (i.e. the system of equations contains uncertain parameters) is considered, the error estimation of a reduced model becomes very complicated. Grepl & Patera (2005) proposed the error estimation for greedy adaptive reduced-basis approach for parametrized parabolic PDEs. Homescu et al. (2007) derived the error estimation based on the small sample statistical condition estimation method and adjoint method to define regions of validity of the reduced models. Haasdonk & Ohlberger (2008) suggested the error estimation of reduced basis techniques for finite volume approximation of parametrized evolution equations. Klindworth et al. (2011) employed the empirical interpolation method to approximate the parametrized functions and provided associated error bound. On the other hand, Galbally et al. (2009), Buithanh & Willcox (2008)

www.manaraa.com

and Liberman et al. (2010) simply used a set of test samples to evaluate the state variable representation accuracy of a reduced order model:

$$\varepsilon_{rel} = \underset{\vec{\mu}\in\Xi^{test}}{mean} \frac{\left\|\vec{y}(\vec{\mu}) - \vec{y}_r(\vec{\mu})\right\|}{\left\|\vec{y}(\vec{\mu})\right\|} \qquad \text{[Galbally et al. (2009)]} \qquad (3.7)$$

where Ξ^{test} is the test set.

$$\varepsilon = \frac{\sqrt{\int_0^{t_f} \left\|\vec{y}_e - \vec{y}_a\right\|_2^2 dt}}{\sqrt{\int_0^{t_f} \left\|\vec{y}_e - \vec{y}_0\right\|_2^2 dt}} \times 100\% \qquad \text{[Bui-Thanh \& Willcox (2008)]} \qquad (3.8)$$

where $\vec{y}_e$, $\vec{y}_a$ and $\vec{y}_0$ are the exact, approximate and nominal outputs, respectively.

$$E\left(\left\|\vec{y} - \vec{y}_r\right\|_2\right) \text{ and } \text{var}\left(\left\|\vec{y} - \vec{y}_r\right\|_2\right) \quad \text{[Liberman et al., (2010)]} \qquad (3.9)$$

where $E(\bullet)$ is a sample mean and $\text{var}(\bullet)$ is a sample variance.

3.3 Randomized Matrix Approximation

Though low rank matrix factorization is one of the most useful tools in scientific computing and data analysis, classical methods for low-rank factorization of an $m \times n$ matrix into two matrices of rank k require $O(mnk)$ floating-point operations and at least k passes from the data storage [Sapp, (2011)]. In modern applications with very large matrices, the classical methods may not be suitable due to computational cost. Randomized algorithms have been recently received a great attention as a powerful tool for accelerating the

www.manaraa.com

approximate matrix decomposition methods. Compared to traditional techniques, randomized low-rank approximation methods have several advantages: 1) smaller computational cost, e.g. $O\left(mn\log\left(k\right)+\left(m+n\right)k^2\right)$ flops for an approximate SVD, 2) inherent stability, 3) parallelism [Halko et al., (2011)].

Given an $m\times n$ matrix $\mathbf{A}$, the basic challenge in low-rank matrix approximation is to find a matrix with k orthonormal columns such that

$$\left\|\mathbf{A}-\mathbf{Q}\mathbf{Q}^T\mathbf{A}\right\|_2 \le \varepsilon \tag{3.10}$$

where ε is a positive error tolerance. Note that the range of $\mathbf{Q}$ is a k-dimensional subspace that captures most of the action of $\mathbf{A}$. Once the matrix $\mathbf{Q}$ is given, the low-rank factorization can be constructed by forming $\mathbf{A}=\mathbf{Q}\mathbf{B}$ where $\mathbf{B}=\mathbf{Q}^T\mathbf{A}$. One can compute a standard factorization (QR, SVD, etc) on the matrix $\mathbf{B}\in\mathbb{R}^{k\times n}$ with reduced cost and recover a standard factorization by pre-multiplying $\mathbf{Q}$ on it. With random sampling, the matrix $\mathbf{Q}$ can be constructed efficiently.

To illustrate the range finding algorithm with random samples, suppose the problem of finding basis for the range of a matrix $\mathbf{A}$ with exact rank k. Repeat a process of drawing random vector $\vec{x}$ of which entries are randomly generated and forming the product $\vec{y}=\mathbf{A}\vec{x}$:

$$\vec{y}^{(i)}=\mathbf{A}\vec{x}^{(i)}, \quad i=1,...,k \tag{3.11}$$

Owing to randomness, one can assume that the randomly generated vectors $\vec{x}^{(i)}$ for $i=1,...,k$ are linearly independent and resulting vectors $\vec{y}^{(i)}$ for $i=1,...,k$ are also linearly independent

www.manaraa.com

[Abdel-Khalik, (2004)]. By linear algebra, the vectors $\vec{y}^{(i)}$ for $i=1,...,k$ spans the range of the matrix $\mathbf{A}$; thus, the orthonormal basis of range of the matrix $\mathbf{A}$ can be constructed by orthonormalizing the vectors $\vec{y}^{(i)}$ for $i=1,...,k$. Basic algorithm can be summarized as follows [Halko et al., (2011)]:

Given an $m\times n$ matrix $\mathbf{A}$, a tolerance ε_{tol} and an integer s, an matrix $\mathbf{Q}$ whose columns are orthonormal and whose range approximates the range of $\mathbf{A}$ can be constructed with standard Gaussian random vectors[3]. The constructed basis $\mathbf{Q}$ satisfies the following statement with probability at least $1-10^{-s}$:

$$\left\|\left(\mathbf{I}-\mathbf{Q}\mathbf{Q}^T\right)\mathbf{A}\right\|_2 \le 10\sqrt{\frac{2}{\pi}}\max_{i=1,...,s}\left\|\left(\mathbf{I}-\mathbf{Q}\mathbf{Q}^T\right)\mathbf{A}\vec{z}^{(i)}\right\|_2$$

Step 1) Pick t standard Gaussian random vectors: $\vec{x}^{(1)},...,\vec{x}^{(t)}$

Step 2) Calculate: $\vec{y}^{(i)}=\mathbf{A}\vec{x}^{(i)},\ i=1,...,t$

Step 3) Find an orthonormal set such that: $span\left\{\vec{y}^{(1)},...,\vec{y}^{(t)}\right\}=span\left\{\vec{q}_1,...,\vec{q}_t\right\}$

Step 4) Let $\mathbf{Q}=\begin{bmatrix}\vec{q}_1 & \cdots & \vec{q}_t\end{bmatrix}\in\mathbb{R}^{n\times t}$

Step 5) Pick s standard Gaussian random vectors: $\vec{w}^{(1)},...,\vec{w}^{(s)}$

Step 6) Calculate: $\vec{z}^{(i)}=\mathbf{A}\vec{w}^{(i)},\ i=1,...,s$

Step 7) Calculate: $\left(\vec{z}^{(i)}\right)^{\perp}=\left(\mathbf{I}-\mathbf{Q}\mathbf{Q}^T\right)\vec{z}^{(i)},\ i=1,...,s$

Step 8) If $\max_{i=1,...,s}\left\|\left(\vec{z}^{(i)}\right)^{\perp}\right\|<\varepsilon_{tol}$, let $r=t$

[3] Standard Gaussian random vector is the one of which entries are independent Gaussian random variables with mean zero and variance one.

www.manaraa.com

Otherwise, increase t and go back to Step 1.

To achieve faster implementation, i.e. smaller flops, many researchers suggested improved algorithms with probabilistic error bound. One can fine excellent review in Halko et al (2011) and Mahoney (2011).

Independently, Abdel-Khalik (2004) proposed the efficient subspace methods (ESM) to approximate the action of very large, dense and numerically rank-deficient matrix operators only by matrix-vector operations. In ESM, the random perturbed input parameters are utilized to extract the influential subspace with respect to output response and to reconstruct the operator in a lower rank. Focusing on the numerical tests, ESM-based algorithms for sensitivity analysis, uncertainty quantification and data assimilation were suggested for linear or quasi-linear problems [Abdel-Khalik et al. (2008)].

3.4 Other Related Works

Spectral Expansion

The spectral expansion approach for the stochastic partial differential equations (SPDEs) is suggested by Ghanem & Spanos (1991) to deal with parametrized problems. In that, the random algebraic equations arising from spatial discretization of stochastic PDEs are solved using a polynomial chaos (PC) expansion approach. The basic idea is to represent the response process by a linear combination of multidimensional polynomials with

www.manaraa.com

undertermined coefficients, which can be uniquely computed by Galerkin scheme. Eldred (2009) summarized the set of polynomials which provide an optimal basis for different continuous probability distribution types. The stochastic expansion can also be formed as a sum of a set of multidimensional Lagrange interpolation polynomials, in which there is no need for tailoring of the expansion form as there is for polynomial chaos expansion [Webster (2007)]. In these methods, the solution is approximated by:

$$R = \sum_{i=0}^{N} \alpha_i \Psi_i(\xi) \tag{3.12}$$

where α_i is a coefficient and $\Psi_i(\xi)$ is a multivariate polynomial of random variable ξ. N is the number of terms in spectral expansion and given as $(n+r)/(n!r!)$ where n is the number of inputs and r is the order of expansion. Note that as the number of inputs or order increases, the number of terms increases super-linearly and so does the number of coefficients. Note that ***the solution is approximated in these spectral expansion methods while the model is approximated in surrogate modeling methods***.

The spectral expansion approach can be boiled down to determine the unknown coefficients α_i. Basically, those can be determined by intrusive methods [Ghanem & Spanos (1991)] or non-intrusive methods [Acharjee & Zabaras (2007)]. When it comes to intrusive methods, one can calculate the coefficients exactly by utilizing the orthogonality. However, it requires to solve a very large size of problem. On the other hands, in non-intrusive methods, numerical integration can be used to determine the unknown coefficients which requires a large number of samples. Tensor product quadrature or Smolyak sparse grid method are one

www.manaraa.com

way to calculate the coefficients efficiently [Eldred (2009)]. However, it is the fact that the spectral expansion approach suffers from the curse of dimensionality.

To alleviate the difficulties, Nair & Keane (2000a, 2000b), Nair (2001) and Nair & Keane (2003) have been suggested the reduced order modeling polynomial chaos expansion method (ROM-PCE) in which the reduced order modeling is incorporated to spectral expansion. This idea has been further studied and used by Acharjee & Zabaras (2006), Sachdeva et al. (2006a, 2006b), Maute et al. (2009) and Boraval et al. (2010). According to Maute et al. (2009), there are two approaches: ROM-PCE (i.e. model reduction and then polynomial expansion) and PCE-ROM (i.e. polynomial expansion and then model reduction).

3.5 Conclusion

As a summary of the surrogate modeling techniques,

- The surrogate modeling techniques have been used in various fields (e.g. fluid dynamics, structural mechanics, biochemistry, oceanic geophysics, aerodynamics and nuclear engineering).
- There are several surrogate modeling methods available (e.g. polynomial regression, Kriging, radial-basis functions, kernel-based regression, neural network, multivariate adaptive regression splines).

www.manaraa.com

- Except the original function form is known are a priori, ***the analytical error estimation is not available***. Therefore, the test set is used to validate the surrogate model and the surrogate modeling construction should be in adaptive way.
- Comparative studies pointed out that a surrogate modeling technique may be superior than others according to the problem conditions, i.e. ***there is no absolutely superior surrogate modeling technique***. Thus, the ***multi-surrogate modeling*** has been studied to complement other individual techniques.
- The curse of dimensionality is widely recognized. In the reviewed works, the surrogate modeling was applied to small dimensional problems (< 20) and the training set of which the size is more than 10 times larger than the number of inputs are used to construct (learn) the surrogate model to guarantee the accuracy.

For the reduced order modeling techniques,

- The reduced order modeling techniques have been used in various fields and most of methods are based on the projection and focused on the state variable reduction.
- Proper orthogonal decomposition (POD) method is prominent for nonlinear problems and Krylov subspace methods are popular for linear time-varying (LTV) and linear time-invariant problems (LTI).
- Because the basis construction is crucial for accuracy, many authors proposed formula for error estimation. This issue is also related to the reducibility (i.e. how much the system can be reduced).

www.manaraa.com

- For POD, one issue is to determine the number of sample sets to extract the subspace basis. For that, adaptive approaches are proposed (e.g. adaptive POD, POD with updates).
- Reduced order modeling techniques are combined with spectral expansion methods (e.g. polynomial chaos expansion, stochastic collocation) for stochastic (parametrized) equations to reduce the computational cost.

As a result of the survey, this dissertation can be located as an extension of the surrogate modeling approach with pre-processing of the input parameters to reduce the required cost. The surrogate modeling techniques could suffer from the curse of dimensionality and would be impractical for large parameter problems. Note that the reviewed surrogate application cases in this chapter have less than 20 input parameters. Most of efforts to alleviate it have been focused on the efficient sampling strategy (i.e. design of experiment). As shown above, the reduced order modeling techniques can be used to reduce the system dimensionality, i.e. the number of input parameters or state variables. However, there were (in our best knowledge) no explicit attempts to combine the reduced order modeling techniques to surrogate modeling approach.

This dissertation hybridizes the existing surrogate modeling and reduced order modeling methods to achieve the accurate and efficient estimation of the response change. Main effort is focused on the ***dimensionality reduction.*** The motivating works and methods used in this dissertation are listed below:

1. Efficient subspace methods & randomized range finder (reduced order model)

www.manaraa.com

2. Multiple-surrogate (multi-metamodeling) methods
3. Reduced order polynomial chaos expansion method (PCE-ROM & ROM-PCE)
4. Design of Experiment & surrogate modeling (sampling approach)
5. Adjoint sensitivity analysis (variational approach)

www.manaraa.com

CHAPTER 4. HYBRID REDUCED ORDER MODELING AND GOAL-ORIENTED SURROGATE MODELING

As found out in the previous chapter, the current surrogate modeling methods suffer from computational cost due to curse of dimensionality. Especially, nuclear reactor physics utilizes a very large number of input parameters which has been a severe problem to introduce surrogate modeling techniques. To circumvent it, we construct the goal-oriented surrogate model instead of reproducing the original model's entire features. In other words, only influential components of the model with respect to purpose of simulations are extracted and the surrogate model would be constructed with only those components. To identify those components, we utilize the reduced order modeling with subspace methodologies.

In reduced order modeling (ROM), a vector of interests is recast as a sum of sub-components:

$$\vec{x} = \sum_{i=1}^{n} \alpha_i \vec{q}_i \simeq \sum_{i=1}^{r} \alpha_i \vec{q}_i \tag{4.1}$$

where n is the number of elements in a vector $\vec{x}$ and r is the reduced dimension. Note that the entries of the vector $\vec{x}$ can be input parameters or state variables. If the vector $\vec{x}$ is defined as state variables, the vector $\vec{q}_i$ can be interpreted as a ***pattern*** in state variable changes due to variations of input parameters or initial/boundary conditions. On the other

www.manaraa.com

hand, if the vector $\vec{x}$ is input parameters whose reduction is the main focus of this dissertation, the component $\vec{q}_i$ is a ***sensitive component*** with respect to the output response changes. Then, the scalar value α_i can be considered as a significance of the component $\vec{q}_i$. ROM can be constructed by collecting only influential component, i.e. large α_i. Note that if the components $\vec{q}_i$ are known, the vector $\vec{x}$ can be represented with α_i and the number of α_i is determined by the number of $\vec{q}_i$. It has been observed that the number of basis vectors is smaller than the original dimension, i.e. $r \ll n$ which means that there are ***correlations*** between input parameters or state variables.

The vector $\vec{x}$ transformed by ROM cannot be the same with the original one because basis vectors with small importance are discarded, which implies that ROM transformation inevitably introduces an error for the price of reducing dimensionality. However, a certain level of error can be tolerated because there are already numerical errors in computerized calculations due to 1) modeling error: mathematical representation of physical phenomena; 2) discretizing error: converting mathematical function to algebraic equation for computerized machines; 3) convergence error: iterative solution for large scale problems. For illustration, assume that discretization error is in the order of 10^{-4} in relative sense. Then, the tighter convergence criteria of iteration solver than 10^{-4} would be meaningless because the values smaller than 10^{-4} are contaminated by discretization error. There is no reason to solve the equation very accurately and a little more accurate than the error of discretization scheme would be sufficient. In the same sense, one can achieve dimensionality reduction within

www.manaraa.com

numerical precision and by properly controlling the error introduced in ROM transformation, a significant impact of additional error can be avoided.

Mathematically, Eq. (4.1) can be considered as basis transformation. Once the basis is given, the original vector can be transformed by projection. Therefore, accurate basis construction is critical for ROM. Existing ROM techniques are distinguished by methods to construct the basis. in this dissertation, we hybridize the existing surrogate modeling and reduced order modeling techniques. Reduced order modeling can be constructed at two-levels: input-level and state-level. As noticed in Chapter 3, the most current reduced order modeling techniques are focused on the state variables. In this dissertation, the input-level reduction is more emphasized to directly address the difficulty from curse of dimensionality. However, the state-level reduction is also briefly explained. The main tool to identify the active subspace basis and to estimate the error due to ROM transformation is the subspace methodologies. In this chapter, the mathematical derivations and the algorithms for input parameter reduction are presented. First, the basic idea and the principles of subspace methodologies are presented. Next, the hybrid ROM construction methods are proposed for reductions at the state-level, the input-level and the interface between codes. As a collection of the methodologies, a general framework for constructing a surrogate model with ROM is discussed.

www.manaraa.com

4.1 Basis Construction

Basis (Coordinate) Transformation

In linear algebra, a basis is a linearly independent spanning set. Given a basis of a vector space, every element of a vector space can be expressed uniquely as a finite linear combination of basis vectors. For illustration, a three-dimensional example is shown in **Figure 4-1**. A vector $\vec{X}$ can be expressed as a linear combination of three basis vectors, i.e. $\vec{e}_1$, $\vec{e}_2$ and $\vec{e}_3$, with coefficients a_1, a_2 and a_3. It is important to note that the basis vectors can be chosen to other set of linearly independent vectors, i.e. orthonormal vectors. The right side of the **Figure 4-1** shows that the vector $\vec{X}$ can be expressed by another set of coefficients α_1, α_2 and α_3 and basis vectors $\vec{q}_1$, $\vec{q}_2$ and $\vec{q}_3$. This idea can be used to extract a basis of a subspace and further used in reduced order modeling.

To demonstrate the reduced order modeling, consider the following example:

$$\vec{X}^{(1)} = \begin{bmatrix} 4 \\ 3 \\ 2 \\ 5 \end{bmatrix} = 2\begin{bmatrix} 2 \\ 0 \\ 1 \\ 1 \end{bmatrix} + 3\begin{bmatrix} 0 \\ 1 \\ 0 \\ 1 \end{bmatrix} = \begin{bmatrix} 2 & 0 \\ 0 & 1 \\ 1 & 0 \\ 1 & 1 \end{bmatrix}\begin{bmatrix} 2 \\ 3 \end{bmatrix} = \mathbf{Q}\begin{bmatrix} 2 \\ 3 \end{bmatrix}$$

$$\vec{X}^{(2)} = \begin{bmatrix} 6 \\ 2 \\ 3 \\ 5 \end{bmatrix} = 3\begin{bmatrix} 2 \\ 0 \\ 1 \\ 1 \end{bmatrix} + 2\begin{bmatrix} 0 \\ 1 \\ 0 \\ 1 \end{bmatrix} = \begin{bmatrix} 2 & 0 \\ 0 & 1 \\ 1 & 0 \\ 1 & 1 \end{bmatrix}\begin{bmatrix} 3 \\ 2 \end{bmatrix} = \mathbf{Q}\begin{bmatrix} 3 \\ 2 \end{bmatrix} \tag{4.2}$$

$$\vec{X}^{(3)} = \begin{bmatrix} 6 \\ 3 \\ 3 \\ 6 \end{bmatrix} = 3\begin{bmatrix} 2 \\ 0 \\ 1 \\ 1 \end{bmatrix} + 3\begin{bmatrix} 0 \\ 1 \\ 0 \\ 1 \end{bmatrix} = \begin{bmatrix} 2 & 0 \\ 0 & 1 \\ 1 & 0 \\ 1 & 1 \end{bmatrix}\begin{bmatrix} 3 \\ 3 \end{bmatrix} = \mathbf{Q}\begin{bmatrix} 3 \\ 3 \end{bmatrix}$$

www.manaraa.com

As can be seen, the vectors $\vec{X}^{(1)}$, $\vec{X}^{(2)}$ and $\vec{X}^{(3)}$ can be expressed as linear combinations of the two vectors $\begin{bmatrix}2 & 0 & 1 & 1\end{bmatrix}^T$ and $\begin{bmatrix}0 & 1 & 0 & 1\end{bmatrix}^T$. If those vectors are considered as basis vectors, i.e. the columns of the matrix $\mathbf{Q}$, only two coefficients are required to represent the vectors $\vec{X}^{(1)}$, $\vec{X}^{(2)}$ and $\vec{X}^{(3)}$. In other words, once a basis is given, only the coefficients as many as the number of basis vectors would be required to represent the vector. Note that in this example, the original dimension $\mathbb{R}^4$ is reduced to $\mathbb{R}^2$.

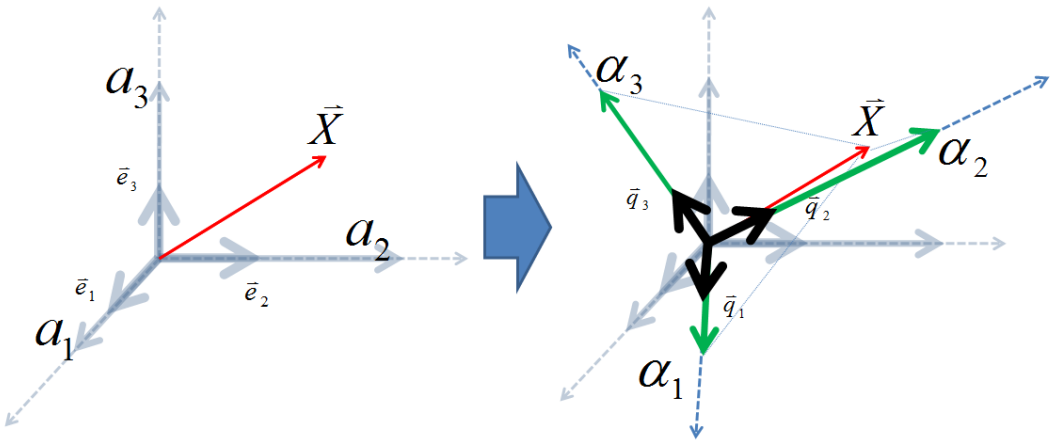

Figure 4-1. Basis (Coordinate) Transformation

Active Subspace

Consider a linear operation as following:

$$\vec{y} = \mathbf{A}\vec{x} \tag{4.3}$$

where $\vec{y} \in \mathbb{R}^m$, $\vec{x} \in \mathbb{R}^n$ and $\mathbf{A} \in \mathbb{R}^{m \times n}$. Suppose that $\vec{x}$ is the vector of input parameters and $\vec{y}$ is the vector of state variables, and active subspace can be defined for both.

www.manaraa.com

Note that $\vec{y}$ can be represented by a sum of columns of $\mathbf{A}$. In linear algebra, this is expressed that $\vec{y}$ spans the column space of $\mathbf{A}$, i.e. the range of $\mathbf{A}$. If the rank of $\mathbf{A}$ is exactly k (some of columns of $\mathbf{A}$ can be represented with other columns), $\vec{y}$ can be represented exactly with k basis vectors. Therefore, the ***active subspace*** of $\vec{y}$ can be the range of $\mathbf{A}$, i.e. $\mathrm{R}(\mathbf{A})$.

If denote the i^{th} element of $\vec{y}$ as y_i and the i^{th} row of the matrix $\mathbf{A}$ as $\vec{A}_i^T$, then Eq. (4.3) can be re-written as:

$$y_i = \vec{A}_i^T \vec{x} \tag{4.4}$$

Note that y_i can be considered as an inner product of $\vec{A}_i$ and $\vec{x}$. As explained in **Figure 4-2**, only the component of $\vec{x}$ parallel to $\vec{A}_i$ would contribute to y_i. This means that in terms of y_i, we only need to consider $\vec{x}^{\parallel}$ which is given by projecting the $\vec{x}$ onto the direction of $\vec{A}_i$, i.e. $\hat{A}_i = \vec{A}_i / \left\|\vec{A}_i\right\|$. Therefore, the active subspace of $\vec{x}$ is the row space of $\mathbf{A}$, i.e. $\mathrm{R}\left(\mathbf{A}^T\right)$.

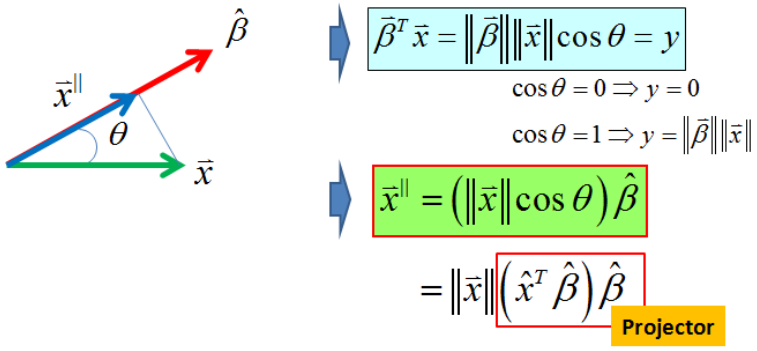

Figure 4-2. Inner Product and Influential Component

www.manaraa.com

In mathematical language, the vector $\vec{x}$ can be decomposed as:

$$\vec{x} = \vec{x}^{\parallel} \oplus \vec{x}^{\perp} \tag{4.5}$$

where $\vec{x}^{\parallel} \in \mathrm{R}\left(\mathbf{A}^T\right)$ and $\vec{x}^{\perp} \in \mathrm{N}\left(\mathbf{A}\right)$. Note that $\mathrm{R}\left(\bullet\right)$ denotes the range and $\mathrm{N}\left(\bullet\right)$ is the null space. By definition, $\mathbf{A}\vec{x}^{\perp} = 0$ which means that the component $\vec{x}^{\perp}$ has no contribution to $\vec{y}$. Thus, we only need to consider $\vec{x}^{\parallel}$ that is included in the $\mathrm{R}\left(\mathbf{A}^T\right)$, which can be called as active subspace. Note that the $\vec{x}^{\parallel}$ can be calculated by projecting $\vec{x}$ onto the active subspace:

$$\vec{x}^{\parallel} = \mathbf{Q}\mathbf{Q}^T\vec{x} = \mathbf{Q}\vec{\alpha} \tag{4.6}$$

where the columns of the matrix $\mathbf{Q}$ are basis vectors of the active subspace, i.e. $\mathrm{R}\left(\mathbf{A}^T\right)$.

This idea can be extended to the nonlinear surrogate modeling approach. Notice that the surrogate models shown in **Table 3-1** can be considered as a sum of linear combinations of functions. Assuming that an unknown original model is smooth enough to be well-represented by a surrogate model, the output response can be approximated by the ***Tensor-Free expansion*** [Abdel-Khalik & Hite (2011)]:

$$\begin{aligned} R\left(\vec{x}\right) = R\left(\vec{x}_0\right) + \sum_{i_1=1}^{n} \psi_{i_1}^{(1)}\left(\vec{\beta}_{i_1}^{(1)T}\Delta\vec{x}\right) + \sum_{i_1,i_2=1}^{n} \psi_{i_1}^{(2)}\left(\vec{\beta}_{i_1}^{(2)T}\Delta\vec{x}\right)\psi_{i_2}^{(2)}\left(\vec{\beta}_{i_2}^{(2)T}\Delta\vec{x}\right) \\ + \sum_{i_1,i_2,i_3=1}^{n} \psi_{i_1}^{(3)}\left(\vec{\beta}_{i_1}^{(3)T}\Delta\vec{x}\right)\psi_{i_2}^{(3)}\left(\vec{\beta}_{i_2}^{(3)T}\Delta\vec{x}\right)\psi_{i_3}^{(3)}\left(\vec{\beta}_{i_3}^{(3)T}\Delta\vec{x}\right) + ... \end{aligned} \tag{4.7}$$

where $\vec{x} \in \mathbb{R}^n$ is a vector of n input parameters which is given by $\vec{x} = \vec{x}_0 + \Delta\vec{x}$, $\vec{x}_0$ is a vector of input parameters at reference configuration, $\Delta\vec{x}$ is a vector of input parameter variations from $\vec{x}_0$, $\beta_{i_l}^{(k)} \in \mathbb{R}^n$ is a coefficient vector and $\psi_{i_l}^{k}$ is an arbitrary once-differentiable scalar

www.manaraa.com

function depending on an assumed surrogate model form. In a compact form, the above expansion becomes:

$$R(\vec{x}) - R(\vec{x}_0) = \Delta R(\vec{x}) = \sum_{k=1}^{\infty} \sum_{i_1,\ldots i_l,\ldots i_k=1}^{n} \psi_{i_1}^{(k)}\left(\vec{\beta}_{i_1}^{(k)T}\Delta\vec{x}\right)..\psi_{i_l}^{(k)}\left(\vec{\beta}_{i_l}^{(k)T}\Delta\vec{x}\right)..\psi_{i_k}^{(k)}\left(\vec{\beta}_{i_k}^{(k)T}\Delta\vec{x}\right) \quad (4.8)$$

The tensor-free expansion can be considered as a generalization of existing series expansions. According to choosing the spanning sets and functions, i.e. $\vec{\beta}_i^{(k)}$ and $\psi_i^{(k)}$, it reduces to well-known expansions. For example, in case of $\psi_i\left(\vec{\theta}\right) = \vec{\theta}$, Eq. (4.7) would be multi-variate Taylor series expansion and the mathematical proof is presented in Appendix A. The important advantage of the tensor-free expansion notation is that one can investigate and match the structure of the original model more explicitly, which ultimately enables to truncate the expansion according to user-defined error tolerance [Abdel-Khalik, 2011]. Note that the scalar functions $\psi_{i_l}^{k}$ are functions of inner product of a coefficient vector $\vec{\beta}_{i_l}^{(k)}$ and input parameter perturbation $\Delta\vec{x}$. In the same sense with the previous linear mapping case, only components of $\Delta\vec{x}$ parallel to $\vec{\beta}_{i_l}^{(k)}$ would contribute to the response change. The subspace formed by the directions $\left\{\vec{\beta}_{i_l}^{(k)}\right\}$ would be the active subspace [Bang et al., 2012].

Basis Construction with Random Samples

The basis construction of the active subspace is the key for the projection-based reduced order modeling. In this dissertation, the randomized algorithm is employed. It is based on the assumption that the probability to generate the same random vectors would be negligibly

www.manaraa.com

small [Abdel-Khalik, 2004]. Therefore, the randomly generate vectors $\vec{x}^{(1)}$, …, $\vec{x}^{(r)}$ would be independent and $\mathbf{G}\vec{x}^{(1)}$, $\mathbf{G}\vec{x}^{(2)}$, …, $\mathbf{G}\vec{x}^{(r)}$ are also independent, where $\mathbf{G}$ is the orthogonal projector onto a pre-defined subspace spanned by basis vectors numbering $r \le s$. This means that each randomly generated vector $\mathbf{G}\vec{x}^{(i)}$ for $i = 1,...,r$ contains information about the pre-defined subspace. Clearly, when $r = s$, the vectors $\mathbf{G}\vec{x}^{(1)}$, $\mathbf{G}\vec{x}^{(2)}$, …, $\mathbf{G}\vec{x}^{(r)}$ span the entire subspace $\vec{Y}$; therefore, the projection of more randomly generated vectors will not be linearly independent and will not have any more information about the pre-defined subspace.

The above idea can be used to construct the active subspace basis. First, consider the active subspace of $\vec{y}$ which is linear case. The $\vec{y}$ in the Eq. (4.3) can considered as a linear combination of the column vectors of the matrix $\mathbf{A}$, which span the active subspace. It is straightforward to extract the active subspace from $\vec{y}$ because $\vec{y}$ itself is in the active subspace and each randomly generated $\vec{y}$ has information about the active subspace. Therefore, the orthonormal basis of the active subspace can be constructed simply by orthonormalizing $\vec{y}$ vectors [Golub & Van Loan, 1996]. It is obvious that this procedure would be applicable to nonlinear cases because only thing needs to do is examine the random samples of $\vec{y}$ to identify the patterns in $\vec{y}$.

For an illustration, two-dimensional case is shown in **Figure 4-3**. Consider that the subspace which we want to find is spanned by two vectors, i.e. $\vec{A}_1$ and $\vec{A}_2$. Let the first sample point as $\vec{y}^{(1)}$ which is calculated with perturbed input parameters. Then, the first basis vector can be given as:

www.manaraa.com

$$\vec{q}_1 = \frac{\vec{y}^{(1)}}{\left\| \vec{y}^{(1)} \right\|_2} \tag{4.9}$$

Let the second sample point as $\vec{y}^{(2)}$. The component orthogonal to the first basis vector can be calculated by:

$$\vec{y}^{(2)\perp} = \left(\mathbf{I} - \vec{q}_1 \vec{q}_1^T \right) \vec{y}^{(2)} \tag{4.10}$$

where $\mathbf{I}$ is the identity matrix. Then, the second orthonormal basis vector can be constructed by normalizing the $\vec{y}^{(2)\perp}$. As can be seen in **Figure 4-3**, the two orthonormal basis vectors, i.e. $\left(\vec{A}_1, \vec{A}_2 \right)$ and $\left(\vec{q}_1, \vec{q}_2 \right)$, span the same subspace. This illustrates that we can identify the orthonormal basis by examining the samples. This idea can be easily extended to higher dimensional cases.

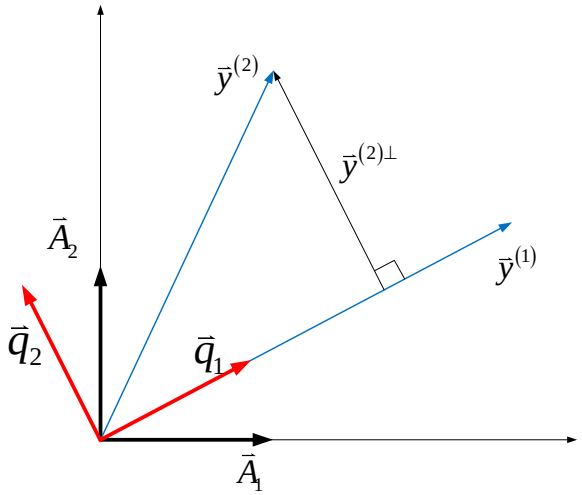

Figure 4-3. Illustration of Orthonormal Basis Construction

www.manaraa.com

Constructing the active subspace of input parameters is not straightforward like state variables' and the main contribution of this dissertation is devoted to this part. Consider the linear model first as in Eq. (4.3). Remind that the active subspace of input parameters $\vec{x}$ is the row space of $\mathbf{A}$, i.e. $\mathrm{R}\left(\mathbf{A}^T\right)$ which is not directly accessible. If the full matrix $\mathbf{A}$ is available, the orthonormal basis of $\mathrm{R}\left(\mathbf{A}^T\right)$ can be calculated by singular value decomposition. In this dissertation, we assume that the mapping with transpose of $\mathbf{A}$ be available due to popularity of adjoint sensitivity analysis in reactor physics codes [Cacuci (2003)]:

$$\vec{z} = \mathbf{A}^T \vec{w} \tag{4.11}$$

Then, the random samples of $\vec{z}$ spans the column space of $\mathbf{A}^T$ which is the same with row space of $\mathbf{A}$. Once the orthonormal basis of $\mathrm{R}\left(\mathbf{A}^T\right)$ is constructed to $\mathbf{Q}$, the input parameters can be recast by projecting onto that subspace as $\vec{\omega} = \mathbf{Q}\mathbf{Q}^T \vec{w}$ and this transformation should not change in $\vec{z}$.

For nonlinear case, the active subspace can be found via the first order derivative of the response [Bang et al., 2012]. As shown in the previous section, the orthonormal basis we seek spans the same subspace formed by the coefficients vectors. Note that the first order derivative of Eq. (4.7) is given as:

$$\vec{\nabla} R\left(\vec{x}\right) = \sum_{k=1}^{\infty} \sum_{i_1,\ldots i_l \ldots i_k=1}^{n} \psi_{i_1}^{(k)}\left(\vec{\beta}_{i_1}^{(k)T}\Delta\vec{x}\right)..\psi_{i_l}^{(k)'}\left(\vec{\beta}_{i_l}^{(k)T}\Delta\vec{x}\right)..\psi_{i_k}^{(k)}\left(\vec{\beta}_{i_k}^{(k)T}\Delta\vec{x}\right)\vec{\beta}_{i_l}^{(k)} \tag{4.12}$$

www.manaraa.com

Each term of this summation represents a vector in the parameters space pointed by the $\left\{\vec{\beta}_{i_l}^{(k)}\right\}$ vectors. Accordingly, the gradient of the response function $\vec{\nabla}R(\vec{x})$ may be viewed as a linear combination of all the $\left\{\vec{\beta}_{i_l}^{(k)}\right\}$ vectors, which means the first order derivatives at random points spans the range of active subspace [Abdel-Khalik, 2004]. In the same sense with before, orthonormal basis can be constructed by orthonormalizing the first order derivatives at the random points. The premise is that all parameter variations that are orthogonal to the active subspace produce negligible response change.

The above idea of the basis construction can be extended to the multi-responses cases by defining the following pseudo response [Bang & Abdel-Khalik, 2011a]:

$$R_{pseudo} = \sum_{i=1}^{m} R_i w_i \tag{4.13}$$

where R_i is a i^{th} response and w_i is an arbitrary number for $i = 1,...,m$. Note that the gradient of the pseudo response would still be random linear combinations of all responses' coefficients vectors.

The ideas for the basis construction are combined into one algorithm: ***Range Finding Algorithm*** (RFA).

Step 1) Pick the k random input vectors: $\vec{x}^{(i)}$ for $i = 1,...,k$

Step 2) Calculate the random samples:

- if state-level reduction,

www.manaraa.com

calculate the state variables with random inputs: $\vec{y}^{(i)} = f\left(\vec{x}^{(i)}\right)$ for $i = 1,...,k$

- if input-level reduction,

calculate the gradient of random pseudo-responses: $\left.\frac{\partial y_{pseudo}}{\partial \vec{x}}\right|_{\vec{x}^{(i)}}$ for $i = 1,...,k$

Step 3) Construct the orthonormal basis by orthonormalizing the samples:

- if state-level reduction, $span\left[\vec{q}_1 \quad \cdots \quad \vec{q}_k\right] = span\left[\vec{y}^{(1)} \quad \cdots \quad \vec{y}^{(k)}\right]$

- if input-level reduction, $span\left[\vec{q}_1 \quad \cdots \quad \vec{q}_k\right] = span\left[\left.\frac{\partial y_{pseudo}}{\partial \vec{x}}\right|_{\vec{x}^{(1)}} \quad \cdots \quad \left.\frac{\partial y_{pseudo}}{\partial \vec{x}}\right|_{\vec{x}^{(k)}}\right]$

Step 4) Check the basis

- if k is not sufficient, then increase k and repeat from Step 1)

- otherwise, the active subspace basis is $\mathbf{Q} = \left[\vec{q}_1 \quad \cdots \quad \vec{q}_k\right]$

It is noteworthy to mention that the idea for finding matrix structure only using random matrix-vector products was first proposed by Abdel-Khalik (2004). However, at the time, only numerical experiments were employed to decide on an acceptable rank for the matrix, which is often acceptable from an engineering/practical viewpoint. Recently, the above algorithm developed in the applied mathematics community employing the basic idea of using random matrix-vector products, has been shown to provide an upper-bound on the error resulting from the randomized range identification [Liberty et al., 2007, Halko et al., 2011].

www.manaraa.com

4.2 Projection based Reduced Order Modeling

Once the orthonormal basis is available, the reduced order model can be constructed by projecting the model onto the active subspace.

State Level Reduction

Consider an unsteady nonlinear partial differential equation for a state function $\phi(x,t)$ with n input parameters represented by a vector $\vec{p}$:

$$\frac{\partial \phi(x,t)}{\partial t} = L(\vec{p})\phi(x,t) + F\left(\vec{p}, \phi(x,t)\right) \tag{4.14}$$

where L denotes a linear spatial differential operator and F is a nonlinear function of a scalar variable. By discretization, a system of nonlinear ordinary differential equations can be given by:

$$\frac{d}{dt}\vec{\phi}(t) = \mathbf{A}\vec{\phi}(t) + \mathbf{F}\left(\vec{\phi}(t)\right) \tag{4.15}$$

where $t \in [0,T]$ denotes time, $\vec{\phi}(t) = \left[\phi_1(t) \quad \cdots \quad \phi_m(t)\right]^T \in \mathbb{R}^m$, $\mathbf{A} \in \mathbb{R}^{m \times n}$ is a discrete approximation matrix of the operator L, $\mathbf{F}$ is a nonlinear function evaluated at $\phi(t)$, i.e., $\mathbf{F} = \left[F(\phi_1(t)) \quad \cdots \quad F(\phi_m(t))\right]^T$ with appropriate initial conditions and boundary conditions. Let the $\mathbf{V} \in \mathbb{R}^{m \times r_V}$ be a matrix whose orthonormal columns are the vectors in the reduced basis. Then, the $\vec{\phi}(t)$ can be projected onto the basis by:

$$\mathbf{V}\mathbf{V}^T\vec{\phi}(t) = \mathbf{V}\vec{\phi}_r(t) \tag{4.16}$$

www.manaraa.com

where $\vec{\phi}_r \in \mathbb{R}^{r_V}$. Substitute Eq. (4.16) to Eq.(4.15), then the reduced-order system can be obtained by:

$$\frac{d}{dt}\vec{\phi}_r(t) = \mathbf{A}_r\vec{\phi}_r(t) + \mathbf{V}^T\mathbf{F}\left(\mathbf{V}\vec{\phi}_r(t)\right) \tag{4.17}$$

where $\mathbf{A}_r = \mathbf{V}^T\mathbf{A}\mathbf{V} \in \mathbb{R}^{r_V \times r_V}$ is an approximation of the matrix $\mathbf{A}$.

Input Level Reduction

Assume that a state function is mildly nonlinear with respect to the input parameter variations so it can be expanded using a tensor-free infinite series expansion as follows (to simplify the expressions, the spatial and the temporal notations are omitted):

$$\begin{aligned}\phi(\vec{p}) = &\sum_{i_1=1}^{n}\psi_{i_1}^{(1)}\left(\vec{\beta}_{i_1}^{(1)T}\vec{p}\right) + \sum_{i_1,i_2=1}^{n}\psi_{i_1}^{(2)}\left(\vec{\beta}_{i_1}^{(2)T}\vec{p}\right)\psi_{i_2}^{(2)}\left(\vec{\beta}_{i_2}^{(2)T}\vec{p}\right) \\ &+ \sum_{i_1,i_2,i_3=1}^{n}\psi_{i_1}^{(3)}\left(\vec{\beta}_{i_1}^{(3)T}\vec{p}\right)\psi_{i_2}^{(3)}\left(\vec{\beta}_{i_2}^{(3)T}\vec{p}\right)\psi_{i_3}^{(3)}\left(\vec{\beta}_{i_3}^{(3)T}\vec{p}\right) + \cdots\end{aligned} \tag{4.18}$$

where ψ_i can be any kind of scalar function. In a compact form, the above expansion becomes:

$$\phi(\vec{p}) = \sum_{k=1}^{\infty}\sum_{i_1,\ldots,i_l,\ldots,i_k=1}^{n}\psi_{i_1}^{(k)}\left(\vec{\beta}_{i_1}^{(k)T}\vec{p}\right)\cdots\psi_{i_l}^{(k)}\left(\vec{\beta}_{i_l}^{(k)T}\vec{p}\right)\cdots\psi_{i_k}^{(k)}\left(\vec{\beta}_{i_k}^{(k)T}\vec{p}\right) \tag{4.19}$$

If the basis $\mathbf{Z}$ is given such that

$$\vec{p} = \sum_{i=1}^{r_Z}\alpha_i\vec{z}_i = \mathbf{Z}\vec{\alpha} \tag{4.20}$$

www.manaraa.com

where $\mathbf{Z} = \left[\vec{z}_1 \quad \cdots \quad \vec{z}_{r_\mathbf{z}} \right] \in \mathbb{R}^{n \times r_\mathbf{z}}$ and $\vec{\alpha} = \left[\alpha_1 \quad \cdots \quad \alpha_{r_\mathbf{z}} \right]^T$, the system of equation can be re-defined as:

$$\begin{aligned} \phi(\vec{p}) \simeq \hat{\phi}(\vec{\alpha}) &= \sum_{k=1}^{\infty} \sum_{i_1,..,i_l,..,i_k=1}^{n} \psi_{i_1}^{(k)}\left(\vec{\beta}_{i_1}^{(k)T} \mathbf{Z}\mathbf{Z}^T \vec{p}\right) \cdots \psi_{i_l}^{(k)}\left(\vec{\beta}_{i_l}^{(k)T} \mathbf{Z}\mathbf{Z}^T \vec{p}\right) \cdots \psi_{i_k}^{(k)}\left(\vec{\beta}_{i_k}^{(k)T} \mathbf{Z}\mathbf{Z}^T \vec{p}\right) \\ &= \sum_{k=1}^{\infty} \sum_{i_1,..,i_l,..,i_k=1}^{n} \psi_{i_1}^{(k)}\left(\hat{\beta}_{i_1}^{(k)T} \vec{\alpha}\right) \cdots \psi_{i_l}^{(k)}\left(\hat{\beta}_{i_l}^{(k)T} \vec{\alpha}\right) \cdots \psi_{i_k}^{(k)}\left(\hat{\beta}_{i_k}^{(k)T} \vec{\alpha}\right) \end{aligned} \tag{4.21}$$

where $\hat{\beta}_i^{(k)} = \mathbf{Z}^T \vec{\beta}_i^{(k)} \in \mathbb{R}^{r_\mathbf{z}}$.

In view of surrogate modeling, one can consider the Eq. (4.21) as an approximate model to be constructed with the unknowns $\vec{\beta}_i^{(k)} \in \mathbb{R}^n$. Note that if Eq. (4.19) is reduced to Eq. (4.21), the unknown coefficients are also reduced to $\hat{\beta}_i^{(k)} \in \mathbb{R}^{r_\mathbf{z}}$. It implies that the smaller number of simulations would be required and, opposed to the curse of dimensionality, one can save significant amount of computational cost.

To identify the influential basis of the inputs, consider the first order derivative of Eq. (4.19) given as:

$$\vec{\nabla}\phi(\vec{p}) = \sum_{k=1}^{\infty} \sum_{i_1,..,i_l,..,i_k=1}^{n} \psi_{i_1}^{(k)}\left(\vec{\beta}_{i_1}^{(k)T} \vec{p}\right) \cdots \frac{\partial \psi_{i_l}^{(k)}}{\partial \vec{p}}\left(\vec{\beta}_{i_l}^{(k)T} \vec{p}\right) \cdots \psi_{i_k}^{(k)}\left(\vec{\beta}_{i_k}^{(k)T} \vec{p}\right) \vec{\beta}_{i_l}^{(k)} \tag{4.22}$$

Note that each term of this summation represents a vector in the input parameter space pointed by the $\left\{\vec{\beta}_{i_l}^{(k)}\right\}$ vectors. Accordingly, the gradient of the function $\vec{\nabla}\phi(\vec{p})$ may be viewed as a linear combination of all the $\left\{\vec{\beta}_{i_l}^{(k)}\right\}$ vectors. Given that any subspace could be described by an infinite number of the basis, one can find a basis by sampling gradient information in Eq. (4.22) at random points in the input parameter space, where each sample

www.manaraa.com

represents a new vector from the input parameter subspace. The above idea can be extended to the case of multiple state variables by defining the following pseudo variable:

$$\phi_{pseudo} = \sum_{i=1}^{m} \phi_i w_i \tag{4.23}$$

where ϕ_i is a i^{th} state variable (or response) and w_i is an arbitrary number for $i = 1, ..., m$. Note that each ϕ_i can be represented as in Eq. (4.19) and the gradient of the pseudo variable would still be a random linear combination of all state variables' (or responses') coefficient vectors.

It is important to note that the proposed input-level reduced order modeling approach utilizes only the first order derivatives which are recognized as local information to capture the higher order effects which are related to global behavior. Therefore, this implies that it could be applied not only to the uncertainty quantification, but also to the problems, e.g. design optimization in which the input parameter variations could be large.

The construction of the active subspace requires the first order derivative information of the response. This can be done via adjoint sensitivity analysis. In the nuclear engineering community, since Wigner (1945) introduced perturbation theory into reactor physics, the sensitivity analysis has been extended under the name of generalized perturbation theory to the analysis of reactivities and reaction-rates which are linear or bilinear functionals of the forward and/or adjoint fluxes [Stacey (1974), Williams (1986), Cacuci (2003)]. Using first order generalized perturbation theory, one can calculate the first order derivatives for a given

www.manaraa.com

response with respect to all parameters using only one forward and one adjoint mode executions.

4.3 Intersection Subspace Basis Construction

In multi-physics problems, the further reduction can be achieved by considering the active subspace of all multiple physical models [Bang & Abdel-Khalik (2012e)]. Assume that we have Model **A** and Model **B** whereby outputs of Model **A** are passed as inputs to Model **B** and consider the construction of the surrogate model for Model **B**:

Model **A**: $f_{\mathbf{A}}(\vec{x}) = \vec{y}$, where $\vec{x} \in \mathbb{R}^m$, $\vec{y} \in \mathbb{R}^n$

Model **B**: $f_{\mathbf{B}}(\vec{y}) = \vec{z}$, where $\vec{y} \in \mathbb{R}^n$, $\vec{z} \in \mathbb{R}^l$

Note that the outputs of Model **A** can be reduced by identifying a subspace determined solely by Model **A**, using the snapshots algorithms described earlier:

$$\vec{y} \simeq \mathbf{Q}_{\mathbf{A}}\mathbf{Q}_{\mathbf{A}}^T\vec{y} = \mathbf{Q}_{\mathbf{A}}\vec{\alpha}, \text{ where } \mathbf{Q}_{\mathbf{A}} \in \mathbb{R}^{n \times r_{\mathbf{A}}}, \ \vec{\alpha} \in \mathbb{R}^{r_{\mathbf{A}}} \tag{4.24}$$

This means that the reduced output of Model **A** will be confined to the active subspace spanned by the column vectors of the matrix $\mathbf{Q}_{\mathbf{A}}$, implying that Model B will not see any components that are orthogonal to the active subspace generated by Model A. Therefore, by a simple transformation, the inputs to model B are now effectively reduced to $r_{\mathbf{A}}$ components only. Note that, at this point, Model B has not been utilized yet.

Now, considering Model **B** and for now independently of the reduction rendered by Model **A**, the vector $\vec{y}$ represents the inputs to Model **B** and therefore can be reduced using

www.manaraa.com

an ROM algorithm by sampling the derivatives of the outputs of Model $\mathbf{B}$ with respect to its inputs, as mentioned earlier:

$$\vec{y} \simeq \mathbf{Q_B}\mathbf{Q_B}^T\vec{y} = \mathbf{Q_B}\vec{\beta}, \quad \text{where } \mathbf{Q_B} \in \mathbb{R}^{n\times r_B},\ \vec{\beta} \in \mathbb{R}^{r_B} \tag{4.25}$$

This means that the components of $\vec{y}$ belonging to the active subspace spanned by the column vectors of $\mathbf{Q_B}$ are the most influential to the outputs of Model $\mathbf{B}$. The implication is that one need not consider the impact of all $\vec{y}$ components that are orthogonal to the active subspace as determined solely by Model $\mathbf{B}$.

Now, in general, one would not expect the active subspace represented by $\mathbf{Q_A}$ to be the same as the $\mathbf{Q_B}$ subspace. In other words, the components of the active subspace belonging to the $\mathbf{Q_A}$ subspace which are also orthogonal to the $\mathbf{Q_B}$ subspace will not be influential to the overall output of the combined model, therefore these components should be discarded, leading to further reduction of the active subspace at the interface between the two models. If the two subspaces determined by Model $\mathbf{A}$ and $\mathbf{B}$ happen to be exactly the same, an unlikely situation, then one would not be able to render any further reduction.

Mathematically, this situation may be described as follows: among the r_A components of $\vec{y}$ determined from Model $\mathbf{A}$, only the components spanned by $\mathbf{Q_B}$ subspace can contribute to the output response of Model $\mathbf{B}$. Therefore, we can define the matrix $\mathbf{Q} \in \mathbb{R}^{n\times r}$ whose range spans the common components (i.e. the intersection between the two subspace) in the $\mathbf{Q_A}$ and $\mathbf{Q_B}$ subspaces. It is natural to expect that the size of the intersection subspace to be smaller than the minimum of the two model-specific subspaces, i.e.,

www.manaraa.com

$$r \le \min\left\{r_{\mathbf{A}}, r_{\mathbf{B}}\right\} \tag{4.26}$$

If r is smaller than either values, one could further reduce the input parameters for Model $\mathbf{B}$; thereby leading to a more efficient construction of the surrogate model.

The intersection algorithm is summarized below in two steps. Step 1 is a standard snapshots reduced order modeling algorithm applied to Model $\mathbf{A}$. In Step 2, the derivatives of Model $\mathbf{B}$'s outputs are employed to construct an active subspace for its input parameters. The two subspaces are combined using a projection technique which filters out all the components that lie outside the intersection subspace. Once determined, the ROMs for both Model $\mathbf{A}$ and Model $\mathbf{B}$ can be constructed. Note that the inputs of Model $\mathbf{B}$ which is also the outputs of Model $\mathbf{A}$ can be transformed by:

$$\vec{y} \approx \mathbf{Q}\mathbf{Q}^T\vec{y} = \mathbf{Q}\vec{y}, \quad \text{where } \mathbf{Q} \in \mathbb{R}^{n\times r} \tag{4.27}$$

Algorithm: Intersection Subspace Construction

Step 1) Construct the active subspace for Model $\mathbf{A}$

Generate the random inputs $\left[\vec{x}^{(1)} \quad \cdots \quad \vec{x}^{(k)}\right]$

Compute the outputs $\mathbf{Y} = \left[\vec{y}^{(1)} \quad \cdots \quad \vec{y}^{(k)}\right]$

Determine the rank $r_{\mathbf{A}}$ using a range finding algorithm

Calculate QR decomposition of $\mathbf{Y} = \mathbf{Q}_{\mathbf{A}}\mathbf{R}_{\mathbf{A}}$

Step 2) Construct the intersection subspace:

Generate random inputs $\left[\vec{y}^{(1)} \quad \cdots \quad \vec{y}^{(k)}\right]$

Calculate derivatives of pseudo responses of Model B

www.manaraa.com

$$\mathbf{D} = \left[\frac{\partial z_{pseudo}^{(1)}}{\partial \vec{y}^{(1)}} \quad \cdots \quad \frac{\partial z_{pseudo}^{(k)}}{\partial \vec{y}^{(k)}} \right]$$

where $z_{pseudo}^{(j)} = \sum_i \gamma_i^{(j)} z_i^{(j)}$

Project onto the basis of Model $\mathbf{A}$

$$\mathbf{U} = \mathbf{Q_A} \mathbf{Q_A}^T \mathbf{D}$$

Using a range finding algorithm, determine the rank r

Calculate QR decomposition of $\mathbf{U} = \mathbf{QR}$

4.4 General Framework for Surrogate Modeling with Reduced Order Transformation

The general framework for surrogate modeling with reduced order modeling methods is depicted in **Figure 4-4**. One can notice that, compared to the surrogate modeling framework in **Figure 3-1**, the Step 2 and the Step 3 are added due to incorporation of the reduced order approximation. Step 4 – 6 are the same as described in the Chapter 3.

Note that, for surrogate modeling with ROM, there are two possible error sources to be considered; ***reduced order modeling*** and ***surrogate modeling***. In the reduced order step, the error may be introduced by insufficient basis vectors, i.e. the variations of the input parameters are not fully captured. There are three ways to estimate the error due to ROM transformation and determine the size of the active subspace basis: singular value spectrum, portion of in-active subspace component and κ-metric.

www.manaraa.com

The singular value decomposition [Golub & Van Loan (1996)] of a matrix $\mathbf{A} \in \mathbb{R}^{n \times n}$ is given by:

$$\mathbf{A} = \mathbf{U}\mathbf{\Sigma}\mathbf{V} = \sum_{i=1}^{n} \sigma_i \vec{u}_i \vec{v}_i^T \approx \sum_{i=1}^{r} \sigma_i \vec{u}_i \vec{v}_i^T \tag{4.28}$$

where $\vec{u}_i$ and $\vec{v}_i$ are the orthonormal vectors. Thus, the σ_i can be considered as the importance of the subspace spanned by $\vec{u}_i$ and $\vec{v}_i$. As can be seen in Eq. (4.28), by considering only components with large importance, one can construct the low-rank approximation of the matrix $\mathbf{A}$. Same idea can be used to determine the number of basis by examining the singular value spectrum of the matrix of which columns are sample vectors:

for linear case, $\mathbf{Y} = \left[\vec{y}^{(1)} \quad \cdots \quad \vec{y}^{(r)} \right]$ where $\vec{y}^{(i)} = \mathbf{A}^T \vec{x}^{(i)}$,

for nonlinear case, $\mathbf{G} = \left[\left. \frac{\partial R_{pseudo}}{\partial \vec{x}} \right|_{\vec{x}^{(1)}} \quad \cdots \quad \left. \frac{\partial R_{pseudo}}{\partial \vec{x}} \right|_{\vec{x}^{(r)}} \right]$ where $R_{pseudo} = \sum_{i=1}^{m} R_i w_i$.

The components associated with small singular values have small impacts on the basis representation and may be contaminated by the numerical errors. Because of no additional code execution, this method may be the easiest and straightforward way to determine the number of basis vectors.

Second, we can explicitly compare the original vector and the transformed vector and examine the portion of discarded components, i.e. in-active component. This can be done by:

$$\vec{x}^{\perp} = \left(\mathbf{I} - \mathbf{Q}\mathbf{Q}^T \right) \vec{x} \tag{4.29}$$

www.manaraa.com

where $\vec{x}^{\perp}$ is the component discarded in ROM transformation process. Especially for state variable reduction, this approach can be easy to use because $\vec{x}^{\perp}$ can be interpreted directly as error. However, the error estimation by Eq. (4.29) requires additional samples.

Note that the above two methods can be used to determine the number of basis vectors in terms of the active subspace basis construction. Note that for input parameters, it may be difficult to connect $\vec{x}^{\perp}$ to error in output responses. Because the reduction is performed on the input parameters and an original model is assumed to unknown, there is no way to relate the transformed input parameters directly to the output responses which is what we actually need to calculate. Only way to estimate the error introduced to the responses may be a statistical method by utilizing the additional samples as test sets. For rigorous validation of the basis vectors in view of the output responses, κ-metric can be used to measure the error in responses (or states) introduced by transforming the input parameters [Kennedy et al., 2011]:

$$\kappa^{(i)} = \left| R^{(i)}\left(\vec{x}_0 + \Delta\vec{x}^{\perp}\right) - R\left(\vec{x}_0\right) \right| \quad \text{for } i = 1,\ldots,N \tag{4.30}$$

where $R\left(\vec{x}_0\right)$ is a response value at the reference configuration, $R^{(i)}\left(\vec{x}_0 + \Delta\vec{x}^{\perp}\right)$ is a response value with input parameters perturbed orthogonal to the subspace spanned by the basis vectors, i.e. $\Delta\vec{x}^{\perp} = \left(\mathbf{I} - \mathbf{Q}\mathbf{Q}^T\right)\Delta\vec{x}$, N is the number of test samples, $\mathbf{I}$ is the identity matrix and the columns of the matrix $\mathbf{Q}$ is the basis vectors. Note that if the basis vectors which spans the influential subspace are constructed properly, the κ-metric should be very small, i.e. the input parameter perturbations orthogonal to the influential subspace would not

www.manaraa.com

contribute to the response change. The κ-metric characterizes the effect of the components that are considered non-influential, i.e. the components that are not represented in reduced order transformation.

Once the basis vectors $\mathbf{Q}$ for the influential subspace are obtained, the input parameters can be transformed into low dimension by projection. Then, a surrogate model can be constructed by examining the relationship between the dimensionally reduced input parameters and the responses. The training sample sets are required in this step. Note that due to reduced order transformation, the required number of training sample sets would be reduced. In this surrogate modeling step, an additional error may be introduced. As noted in the literature review, the analytical estimation of the error due to surrogate approximation is not available because the original model is not known as a priori. Though the original model is known, a functional form of a surrogate model may be different from the original one so that the analytical relationship between the original model and the surrogate model cannot be derived and analytical error estimation would not be available. Therefore, statistical methods employing test sample sets, e.g. split samples, cross-validation and bootstrapping, may be the only way to estimate the error introduced by the surrogate approximation. Note that it is difficult to separate the error due to the reduced order modeling and the surrogate modeling because this procedure is sequential so that both error sources are combined in the ultimate response estimation. In practice, it is recommended that the test sample sets are generated in the Step 1 and reuse them for subsequent validations in Step 6. The main error estimation is conducted on the predictions of the surrogate model and considered as convergence criteria

www.manaraa.com

for determining the required number of basis vectors, i.e. the Steps 2 – 5 are repeated until the error estimated by the test sample sets is small enough to satisfy the user-defined tolerance of the response estimation. The κ-metric for the Step 3 can be considered as a supplementary tool.

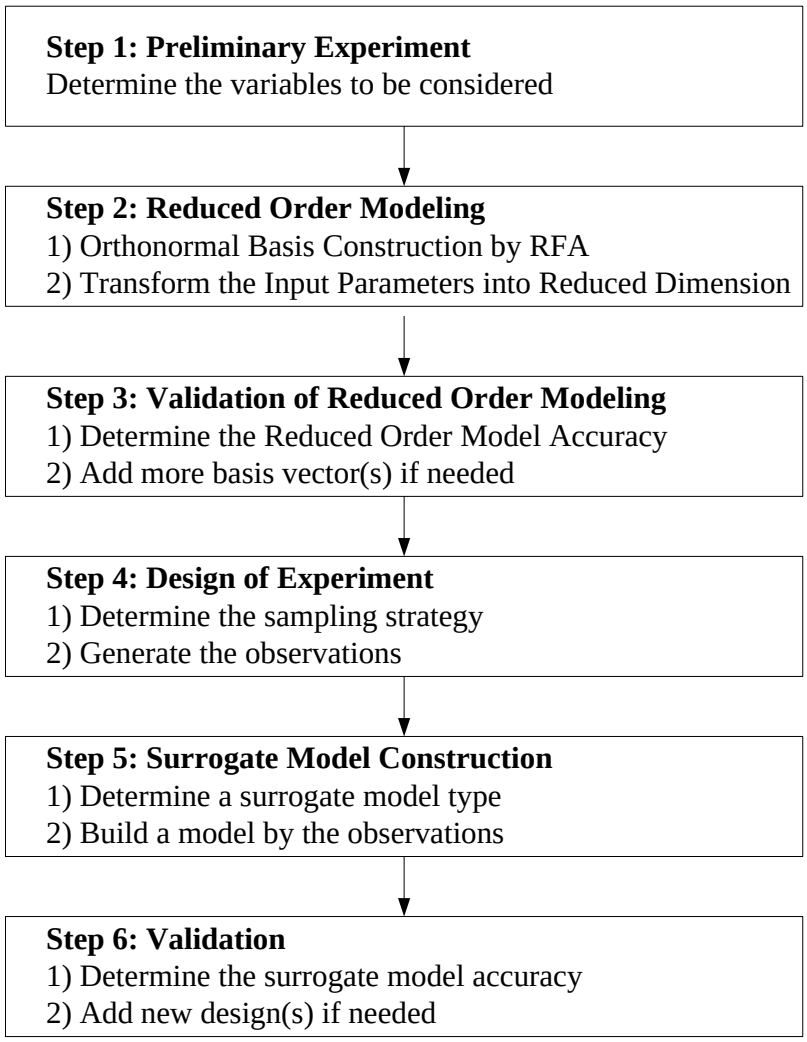

Figure 4-4. General Framework of Reduced Order Surrogate Model Construction

www.manaraa.com

CHAPTER 5. REDUCED ORDER INITIAL CONDITION PERTURBATION THEORY

In subsequent chapters (Chapter 5 ~ Chapter 9), the proposed methods are implemented for reactor physics calculations to examine the feasibility and the applicability. As a first example, the state-level reduced order modeling is incorporated into the traditional initial condition perturbation theory in this Chapter. Taking advantage of the state-level reduced order transformation, the adjoint system of equations to be solved would be reduced so one can connect the initial condition variations to state variable changes with reduced computational cost. This work has been published in Transport Theory and Statistical Physics [Bang et al. (2012b)].

5.1 Problem Description

Consider the spatially and temporally discretized form of a non-homogeneous partial differential equation representing a dynamical system:

$$\begin{aligned} \vec{\phi}(t+1) &= \mathbf{A}(t)\vec{\phi}(t), \quad t = 0,1,....,T-1 \\ \vec{R}(t) &= \mathbf{C}\vec{\phi}(t), \quad t = 0,1,....., T \end{aligned} \tag{5.1}$$

www.manaraa.com

with a given initial condition $\vec{\phi}(0)=\vec{\phi}_0$, where $\vec{\phi}(t)\in\mathbb{R}^n$ and $\vec{R}(t)\in\mathbb{R}^m$ denote state and responses at time step t, respectively. The $\mathbf{A}(t)\in\mathbb{R}^{n\times n}$ and $\mathbf{C}\in\mathbb{R}^{m\times n}$ are coefficient matrices. In reactor physics, Eq. (5.1) can be used to describe the time-dependent diffusion equation. By defining the system of equations:

$$\mathbf{A}_s=\begin{bmatrix} \mathbf{I} & 0 & 0 & & & 0 \\ -\mathbf{A}(1) & \mathbf{I} & 0 & & & \vdots \\ 0 & -\mathbf{A}(2) & \mathbf{I} & & & \\ & & \ddots & \ddots & \ddots & 0 \\ \vdots & & \ddots & \ddots & \mathbf{I} & 0 \\ 0 & \cdots & & 0 & -\mathbf{A}(T-1) & \mathbf{I} \end{bmatrix}, \mathbf{F}_s=\begin{bmatrix} \mathbf{I} \\ 0 \\ 0 \\ \vdots \\ \\ 0 \end{bmatrix} \text{ and } \vec{\boldsymbol{\phi}}_s=\begin{bmatrix} \vec{\phi}(0) \\ \vdots \\ \vec{\phi}(T) \end{bmatrix} \tag{5.2}$$

where $\mathbf{I}\in\mathbb{R}^{n\times n}$ identity matrix and $\mathbf{A}_s\in\mathbb{R}^{nT\times nT}$, $\mathbf{F}_s\in\mathbb{R}^{nT\times n}$, and $\vec{\boldsymbol{\phi}}_s\in\mathbb{R}^{nT\times 1}$, we can get:

$$\begin{aligned} \mathbf{A}_s\vec{\boldsymbol{\phi}}_s&=\mathbf{F}_s\vec{\phi}_0 \\ \vec{\boldsymbol{R}}_s&=\mathbf{C}_s\vec{\boldsymbol{\phi}}_s \end{aligned} \tag{5.3}$$

where $\mathbf{C}_s\in\mathbb{R}^{m\times nT}$ is a coefficient matrix for calculating responses and $\vec{\boldsymbol{R}}_s\in\mathbb{R}^{m\times 1}$ is a vector of responses. This is a compact representation for a dynamical system with *n* initial conditions given by the elements of the $\vec{\phi}_0$ vector.

One may need to calculate the change of the response $\vec{\boldsymbol{R}}_s$ due to the variations of the initial condition $\vec{\phi}_0$. The simplest way is to re-solve Eq. (5.3), i.e. calculate the state variables with perturbed initial condition and compute the responses again. However, if Eq. (5.3) requires a lot of computation time or storages, re-solving may be not a preferred choice. Instead, the initial condition perturbation theory can be used to predict the response change. If one can solve the adjoint equation defined by:

www.manaraa.com

$$\mathbf{A}_s^T \vec{\boldsymbol{\phi}}_s^* = \mathbf{C}_s^T \tag{5.4}$$

Then, the initial condition variation can be directly connected to the response change by taking advantages of the adjoint property:

$$\Delta \vec{\boldsymbol{R}}_s = \mathbf{C}_s \Delta \vec{\boldsymbol{\phi}}_s = \left(\mathbf{A}_s^T \vec{\boldsymbol{\phi}}_s^*\right)^T \Delta \vec{\boldsymbol{\phi}}_s = \left(\vec{\boldsymbol{\phi}}_s^*\right)^T \mathbf{A}_s \Delta \vec{\boldsymbol{\phi}}_s = \left(\vec{\boldsymbol{\phi}}_s^*\right)^T \mathbf{F}_s \Delta \vec{\phi}_0 \tag{5.5}$$

This means that once the adjoint system of equations given in Eq. (5.4) is solved at the reference configuration, the response changes can be accurately predicted without solving any more equations. Note that in this initial condition perturbation theory, the adjoint equation defined in Eq. (5.4) should be solved as many as the number of responses, i.e. *m* times. Therefore, if the number of response is large, its applicability would be limited.

Another approach has been proposed by Bashir et al. (2008). In their one-shot Hessian-based approach, the state $\vec{\phi}(t)$ is considered as a linear combination of basis vectors:

$$\vec{\phi}_r(t) = \mathbf{V}^T \vec{\phi}(t) \tag{5.6}$$

where $\mathbf{V} \in \mathbb{R}^{n \times r}$ contains *r* orthonormal basis vectors as columns. The ROM discrete dynamic system can be derived by projection of Eq. (5.1) onto the subspace spanned by the basis $\mathbf{V}$ as:

$$\begin{aligned} \vec{\phi}_r(t+1) &= \tilde{\mathbf{A}}(t)\vec{\phi}_r(t), \quad t = 0,1,....,T-1 \\ \vec{R}_r(t) &= \tilde{\mathbf{C}}\vec{\phi}_r(t), \quad t = 0,1,....., T \end{aligned} \tag{5.7}$$

where $\tilde{\mathbf{A}} = \mathbf{V}^T \mathbf{A} \mathbf{V} \in \mathbb{R}^{r \times r}$ and $\tilde{\mathbf{C}} = \mathbf{C}\mathbf{V} \in \mathbb{R}^{m \times r}$. By defining the system of equations:

www.manaraa.com

$$\mathbf{A}_r = \begin{bmatrix} \mathbf{V} & 0 & 0 & & & 0 \\ -\tilde{\mathbf{A}}(1) & \mathbf{V} & 0 & & & \vdots \\ 0 & -\tilde{\mathbf{A}}(2) & \mathbf{V} & & & \\ & & \ddots & \ddots & \ddots & 0 \\ \vdots & & \ddots & \ddots & \mathbf{V} & 0 \\ 0 & \cdots & & 0 & -\tilde{\mathbf{A}}(T-1) & \mathbf{V} \end{bmatrix}, \ \mathbf{F}_r = \begin{bmatrix} \mathbf{V}^T \\ 0 \\ 0 \\ \vdots \\ \\ 0 \end{bmatrix},$$

$$\mathbf{C}_r = \begin{bmatrix} \tilde{\mathbf{C}} & 0 & 0 & & & 0 \\ 0 & \tilde{\mathbf{C}} & 0 & & & \vdots \\ 0 & 0 & \tilde{\mathbf{C}} & & & \\ & & \ddots & \ddots & \ddots & 0 \\ \vdots & & \ddots & \ddots & \tilde{\mathbf{C}} & 0 \\ 0 & \cdots & & 0 & 0 & \tilde{\mathbf{C}} \end{bmatrix} \text{ and } \vec{\boldsymbol{\phi}}_r = \begin{bmatrix} \mathbf{V}^T \vec{\phi}(0) \\ \vdots \\ \mathbf{V}^T \vec{\phi}(T) \end{bmatrix} \tag{5.8}$$

one can get more compact form,:

$$\begin{aligned} \mathbf{A}_r \vec{\boldsymbol{\phi}}_r &= \mathbf{F}_r \vec{\phi}_0 \\ \vec{\boldsymbol{R}}_r &= \mathbf{C}_r \vec{\boldsymbol{\phi}}_r \end{aligned} \tag{5.9}$$

Now the problem can be simplified to find the appropriate basis $\mathbf{V} \in \mathbb{R}^{n \times r}$ where $r \ll n$ such that the error between the original model's responses $\vec{\boldsymbol{R}}_s$ and the reduced model responses $\vec{\boldsymbol{R}}_r$ is minimized for all initial conditions of interest. This is done by solving an associated optimization problem of the form:

$$\vec{\phi}_0^* = \arg\max_{\vec{\phi}_0 \in \chi_0} \left(\vec{\boldsymbol{R}}_s - \vec{\boldsymbol{R}}_r \right)^T \left(\vec{\boldsymbol{R}}_s - \vec{\boldsymbol{R}}_r \right) \tag{5.10}$$

where the initial condition $\vec{\phi}_0^*$ are chosen to maximize the error between the original and the reduced order model responses via a greedy sampling algorithm. Eq. (5.10) can be re-written as:

www.manaraa.com

$$\vec{\phi}_0^* = \arg\max_{\vec{\phi}_0 \in \chi_0} \vec{\phi}_0^T \mathbf{H}^e \vec{\phi}_0 \tag{5.11}$$

where $\mathbf{H}^e = \left(\mathbf{C}_s\mathbf{A}_s^{-1}\mathbf{F}_s - \mathbf{C}_r\mathbf{A}_r^{-1}\mathbf{F}_r\right)^T \left(\mathbf{C}_s\mathbf{A}_s^{-1}\mathbf{F}_s - \mathbf{C}_r\mathbf{A}_r^{-1}\mathbf{F}_r\right)$, and $\mathbf{A}_r$, $\mathbf{C}_r$ and $\mathbf{F}_r$ are coefficient matrices for the reduced model. Consider that a initial condition vector can be decomposed as:

$$\vec{\phi}_0 = \vec{\phi}_0^{\parallel} \oplus \vec{\phi}_0^{\perp} \tag{5.12}$$

where $\vec{\phi}_0^{\parallel}$ is the component of $\vec{\phi}_0$ in the subspace of current basis and $\vec{\phi}_0^{\perp}$ is the orthogonal complement of $\vec{\phi}_0^{\parallel}$. By assuming that:

$$\mathbf{C}_s\mathbf{A}_s^{-1}\mathbf{F}_s\vec{\phi}_0^{\parallel} = \mathbf{C}_r\mathbf{A}_r^{-1}\mathbf{F}_r\vec{\phi}_0^{\parallel} \tag{5.13}$$

Eq. (5.11) can be simplified to:

$$\vec{\phi}_0^* = \arg\max_{\vec{\phi}_0 \in \chi_0} \left(\vec{\phi}_0^{\perp}\right)^T \mathbf{H}\left(\vec{\phi}_0^{\perp}\right) \tag{5.14}$$

where $\mathbf{H} = \left(\mathbf{C}_s\mathbf{A}_s^{-1}\mathbf{F}_s\right)^T \left(\mathbf{C}_s\mathbf{A}_s^{-1}\mathbf{F}_s\right)$. By considering initial conditions of unit norm, the solution $\vec{\phi}_0^*$ is equivalent to maximizing the Rayleigh quotient of the form:

$$\vec{\phi}_0^* = \arg\max_{\vec{\phi}_0 \in \chi_0} \frac{\left(\vec{\phi}_0^{\perp}\right)^T \mathbf{H}\left(\vec{\phi}_0^{\perp}\right)}{\left(\vec{\phi}_0^{\perp}\right)^T \left(\vec{\phi}_0^{\perp}\right)} \tag{5.15}$$

The solution of this maximization problem is the eigenvector corresponding to the largest eigenvalue of $\mathbf{H}$, which also solves the optimization problem in Eq. (5.14). This process could be repeated to find the remaining dominant eigenvectors. This one-shot Hessian-based approach is basically constructing a reduced order model and solving the system of equations with different initial conditions with reduced cost. Note that because the reduced order model

www.manaraa.com

is constructed with respect to pre-defined responses (which can be called Goal-oriented reduced order modeling), in case that the other responses which is not considered in reduced order modeling are to be calculated, the whole process should be repeated.

5.2 Proposed Method

We would like to devise the method for a large number of responses and for general responses, i.e. not pre-defined in the reduced order modeling stage. For that, our reduced order model is constructed on the state level. Therefore, any response can be calculated with predicted state variables. In our state-based approach, $\vec{\phi}_s$ in Eq. (5.3) is considered as a linear combination of basis vectors:

$$\vec{\phi}_s \simeq \sum_{i=1}^{r} \bar{q}_i \alpha = \mathbf{Q}\mathbf{Q}^T \vec{\phi}_s \tag{5.16}$$

where $\mathbf{Q} \in \mathbb{R}^{nT \times r}$ contains r orthonormal basis vectors as columns. The range finding algorithm (RFA) explained in the previous chapter can be used to identify the active subspace of the state variables with respect to initial condition variations, in which the initial conditions are randomly perturbed within their permitted ranges, and the forward model is executed. The variations in $\vec{\phi}_s$ are recorded and the process is repeated until the reduced subspace is identified via RFA. Note that the number of basis vectors is determined by the initial condition variations not by the coefficient matrix $\mathbf{A}_s$ which has larger size of dimension. That means that even though the dimension of the entire state vector $\vec{\phi}_s$ is nT,

www.manaraa.com

the rank of the subspace cannot be larger than n which is the dimension of the initial condition vector. If there is a correlation in initial values, then the rank of the subspace must be less than n.

We denote the subspace spanned by the columns of the converged $\mathbf{Q}$ matrix as the active state subspace. The inactive subspace refers to the orthogonal complement subspace. In a similar manner, the columns of another matrix $\mathbf{Q}^{\perp}$ are assumed to form a basis for the inactive state subspace. Since the two subspaces are orthogonally complementary to each other then:

$$\mathrm{R}(\mathbf{Q}) \oplus \mathrm{R}\left(\mathbf{Q}^{\perp}\right) = \mathbb{R}^{nT \times nT} \text{ and } \mathbf{Q}\mathbf{Q}^{T} + \mathbf{Q}^{\perp}\mathbf{Q}^{\perp T} = \mathbf{I}_{nT \times nT} \tag{5.17}$$

The above identity could be used to express the change in the response due to a general initial condition change as follows:

$$\Delta\vec{R} = \mathbf{C}_s \Delta\vec{\boldsymbol{\phi}}_s = \mathbf{C}_s \left(\mathbf{Q}\mathbf{Q}^{T} + \mathbf{Q}^{\perp}\mathbf{Q}^{\perp T}\right)\Delta\vec{\boldsymbol{\phi}}_s \tag{5.18}$$

Since all possible variations $\Delta\vec{x}$ are assumed to belong to the active state subspace, the term $\mathbf{Q}^{\perp}\mathbf{Q}^{\perp T}\Delta\vec{\boldsymbol{\phi}}_s$ is equal to zero (within the precision of the calculations). The above equation could therefore be re-written as:

$$\Delta\vec{R} = \mathbf{C}_s \mathbf{Q}\mathbf{Q}^{T} \Delta\vec{\boldsymbol{\phi}}_s \tag{5.19}$$

Note again that the rank of the matrix $\mathbf{C}_s\mathbf{Q}\mathbf{Q}^{T}$ could not be greater than r. This implies that in case of multi-response, especially, the number of the responses are larger than the number of the initial condition values, the responses may be correlated, and their variations will belong to a subspace of dimension r, given by the range $\mathrm{R}\left(\mathbf{C}_s\mathbf{Q}\mathbf{Q}^{T}\right)$. This subspace is

www.manaraa.com

denoted as the active response subspace. Secondly, the above system of equations could be represented by r independent linear equations as follows:

$$\Delta\hat{R}^j = \mathbf{C}_s^j \vec{q}_i \vec{q}_i^T \Delta\vec{\phi}, \quad \text{for } i = 1,...,r \tag{5.20}$$

where $\Delta\hat{R}^j$ represents the j th component of the response variation vector $\Delta\vec{R}^j$ along the active response subspace and $\mathbf{C}_s^j$ is the j th row of $\mathbf{C}_s$.

To evaluate the change in the response without calculating the changes in the state vector, the adjoint approach is employed. Given that the active subspace has a dimension r, the adjoint model is executed r times as follows:

$$\mathbf{A}_s^T \vec{z}_i = \vec{q}_i, \quad \text{for } i = 1,...,r \tag{5.21}$$

The corresponding changes in responses (as projected on the active response subspace) could then be calculated from: $\Delta\vec{R}^j = \mathbf{C}_s^j \vec{q}_j \vec{z}_j^T \Delta\vec{\phi}_0$. The active components could then be mapped back to the original response space. Note that in this development, the right hand side for the adjoint equations depends only on the flux variations rather than on the response. This represents a major difference to existing adjoint methods, where the solution of the adjoint model is dependent on the given response of interest. If one is interested in calculating another response, the same solution of the r adjoint functions could be used to calculate the corresponding change in the new responses, whereas in existing adjoint methods, the adjoint models must be re-solved. We therefore distinguish this approach from existing adjoint methods by denoting this method by the state-based adjoint, where the adjoints are only dependent on the state variations rather than on the responses.

www.manaraa.com

State-Based Adjoint Initial Condition Perturbation Theory :

1. Randomly generate $\vec{\phi}_0$ by r_0 times, denote by: $\left\{\vec{\phi}_0^{\,i}\right\}_{i=1}^{r_0}$
2. Calculate $\left\{\vec{\boldsymbol{\phi}}_s^{\,i}\right\}_{i=1}^{r_0}$ and build $\mathbf{W} = [\vec{\boldsymbol{\phi}}_s^{\,1} - \vec{\boldsymbol{\phi}}_s^{\,0} \quad \cdots \quad \vec{\boldsymbol{\phi}}_s^{\,r_0} - \vec{\boldsymbol{\phi}}_s^{\,0}]$
3. Decompose $\mathbf{W} = \mathbf{Q}\boldsymbol{\Sigma}\mathbf{V}^T$ using SVD decomposition, where $\mathbf{Q} \in \mathbb{R}^{nT \times r_0}$, $\mathbf{V} \in \mathbb{R}^{r_0 \times r_0}$, and $\boldsymbol{\Sigma} \in \mathbb{R}^{r_0 \times r_0}$
4. Determine the rank r, and re-iterate Step 1-3 if necessary.
5. Solve $\mathbf{A}_s^T \vec{z}_i = \vec{q}_i$ for $i = 1, ..., r$
6. Calculate $\Delta\vec{R} = \mathbf{C}_s\mathbf{Q}\left[\vec{z}_1^{\,T} \quad ... \quad \vec{z}_r^{\,T}\right]^T \Delta\vec{\phi}_0$

5.3 Numerical Test

The three linear time-invariant (LTI) cases which are based on one-dimensional diffusion models are presented here. The basic data for model configurations are adopted from Mckinley (2000, 2002) and modified for the purpose of this study. The objective of these studies is to compare the sb-ROM (state-based adjoint ROM approach) and the go-ROM (goal-oriented Hessian-based one-shot ROM approach) with regard to their associated computational cost and accuracy of their reduced order model predictions. The first case employs a time-independent $\mathbf{A}$ matrix with an external neutron source term and emulates a single assembly model; and the second and third cases employ a time-dependent $\mathbf{A}(t)$ matrix to emulate a multi-assembly model. In the go-ROM implementation, the Hessian matrix $\mathbf{H}$ is explicitly formed using *n* forward model executions.

www.manaraa.com

For the sake of comparison, a discrepancy metric is calculated for each ROM model. The metric measures in a root-mean-square sense the discrepancy between the actual responses (evaluated with direct perturbations of the forward model) and ROM model estimate defined as:

$$discrepancy = \frac{1}{m \times T} \left\| \frac{\vec{R}^{actual} - \vec{R}^{estimate}}{\Delta \vec{R}^{actual}} \right\|_2 \tag{5.22}$$

where m denotes the number of responses at each time step and T is the number of time steps. This metric is calculated for both sb-ROM and go-ROM approaches. Two cases are considered; the first case involves only one response representing the flux at the center location and the second case represents the responses at locations near the center.

5.3.1. Case Study No. 1

The first case employs a heterogeneous model that emulates some of the basic details of a fuel assembly, and employs an external source term:

$$\frac{1}{v}\frac{\partial \phi(x,t)}{\partial t} = \frac{\partial}{\partial x} D(x) \frac{\partial \phi(x,t)}{\partial x} + \left(\nu \Sigma_f(x) - \Sigma_a(x)\right)\phi(x,t) + S_{ext}(x) \tag{5.23}$$

The material layout is shown in **Figure 5-1** and material data (reaction cross sections) is listed in the **Table 5-1**. Through discretization, the system of equations can be constructed as in Eq. (5.3) with $\mathbf{A}_s \in \mathbb{R}^{1000\times1000}$, $\vec{\boldsymbol{\phi}}_s \in \mathbb{R}^{1000\times1}$, $\mathbf{F}_s \in \mathbb{R}^{1000\times20}$, and $\vec{\phi}_0 \in \mathbb{R}^{20\times1}$. As initial conditions, use: $\vec{\phi}_0 = 1$. **Table 5-2** summarizes the computational overheads for both the go-ROM and sb-ROM approaches, where m is the number of model's responses, n is the

www.manaraa.com

number of state dimensions, s is the extra samples to determine the size of the active subspace via the range finding algorithm (in this study, $s=10$) and r is the size of the active subspace for the sb-ROM approach or the truncated rank for the go-ROM approach. The results of this study are shown in **Table 5-3**.

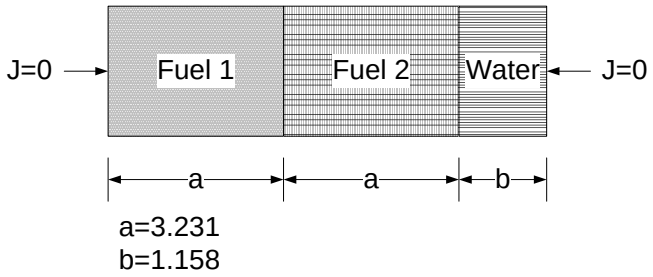

Figure 5-1. Layout for Case Study No. 1

Table 5-1. Specifications for Case Study No. 1

Material	D $[cm]$	Σ_a $[cm^{-1}]$	$\nu\Sigma_f$ $[cm^{-1}]$	v [m/s]	Source [#/sec]
Fuel 1	1.2069	0.0284	0.0416	2200	1.0×10^{25}
Fuel 2	1.2069	0.0252		2200	1.0×10^{25}
Water	9.6618	0	0.034 0	2200	0

Table 5-2. Comparison Between the go-ROM and sb-ROM approaches

	go-ROM	**sb-ROM**
Step 1	Construction of Hessian Matrix	Construction of Active Subspace
	n forward or m adjoints	$r+s$ forward
Step 2	Construction of ROM model	Construction of ROM model
	r adjoints	r adjoints

www.manaraa.com

Table 5-3. Results for Case Study No. 1

Response (m)	Approach	System Size	No. Basis (r)	Discrepancy	Major Computation	
					Step 1	Step 2
1	sb-ROM	1000x1000	20	7.9248e-017	30	20
	go-ROM	250x250	5	1.7157e-004	1	5
		500x500	10	4.5114e-008	1	10
		750x750	15	1.5967e-008	1	15
		1000x1000	20	1.1861e-016	1	20
3	sb-ROM	1000x1000	20	7.2051e-017	30	20
	go-ROM	250x250	5	0.0045	3	5
		500x500	10	0.0017	3	10
		750x750	15	0.0099	3	15
		1000x1000	20	2.1561e-016	3	20

The information in **Table 5-3** may be described as follows: the first column refers to the number of responses employed to construct the go-ROM model. The third column describes the size of the various problems analyzed, each corresponding to a different refinement of the mesh. The fourth column determines the size of the active subspace. The size of the active subspace for the sb-ROM approach is based on machine precision tolerance, while for the go-ROM approach, different ranks for the Hessian matrix are assumed which sets the size of the reduced model. The fifth column calculates the discrepancies according to Eq. (5.22). The final columns shows the computational effort (the number of simulations in forward or adjoint mode) for each of the two steps required for the construction of both the sb-ROM and go-ROM approaches as described in **Table 5-2**. With r=20, both go-ROM and sb-ROM approaches have similar accuracy. The sb-ROM expends 10 extra oversamples to verify the accuracy of the active subspace.

www.manaraa.com

For the case of m=3, the go-ROM model is constructed based on three responses at the center of the model at the last time step. Notice that as the rank of the Hessian is reduced below 20, the accuracy is degraded more than the single response case (m=1). The sb-ROM approach however always determines a subspace of r=20, implying that one cannot find a subspace of smaller dimension to accurately capture all response variations. This behavior is expected because the sb-ROM optimizes the selection of the active subspace over all responses, and hence the size of its active subspace must always be bigger than the go-ROM approach.

5.3.2. Case Study No. 2

This case study emulates a multi-assembly model, and also simulates depletion of fuel materials. This is done by changing the cross-sections exponentially through time. Consider the time-dependent one-group diffusion equation with time-varying coefficients:

$$\frac{\partial \phi(x,t)}{\partial t} = \frac{\partial}{\partial x} D(x) e^{\lambda t} \frac{\partial \phi(x,t)}{\partial x} + \left(\nu \Sigma_f(x) - \Sigma_a(x)\right) e^{-\lambda t} \phi(x,t) \qquad (5.24)$$

The model layout and specifications are shown in **Figure 5-2** and **Table 5-4**. Through discretization, the system of equations is constructed such that: $\mathbf{A}_s \in \mathbb{R}^{2800\times 2800}$, $\vec{\phi}_s \in \mathbb{R}^{2800\times 1}$, $\mathbf{F}_s \in \mathbb{R}^{2800\times 140}$, and $\vec{\phi}_0 \in \mathbb{R}^{140\times 1}$. As initial conditions, use $\vec{\phi}_0 = 1$. The maximum system size of 2800 was used as a reference for the accuracy for both the sb-ROM and go-ROM approaches.

www.manaraa.com

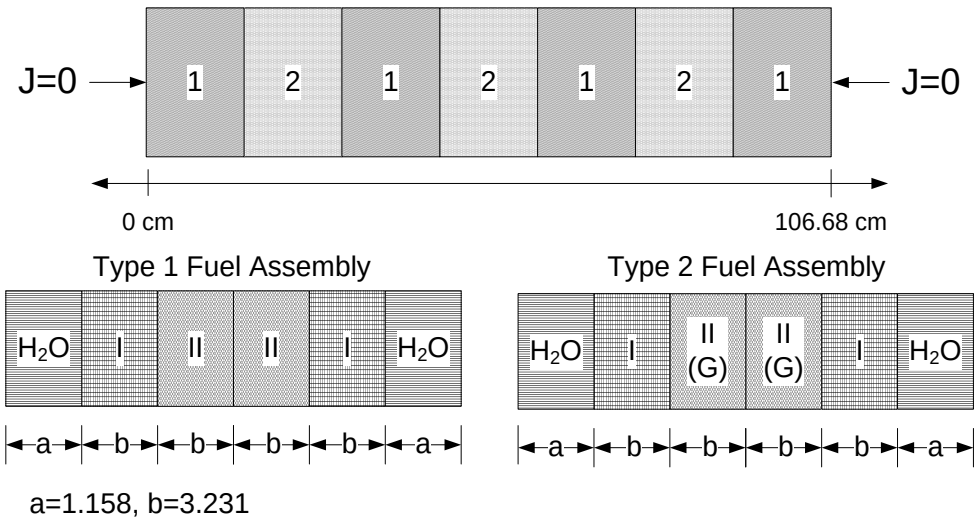

Figure 5-2. Layout for Case Study No. 2

Table 5-4. Specifications for Case Study No. 2

	Type 1 Fuel Assembly			**Type 2 Fuel Assembly**		
	Water	**Region I**	**Region II**	**Water**	**Region I**	**Region II**
$D[cm]$	1.41	1.21	1.22	1.47	1.26	1.30
$\Sigma_a\left[cm^{-1}\right]$	0.00230	0.0252	0.0284	0.00188	0.0224	0.075
$\nu\Sigma_f\left[cm^{-1}\right]$	0.0	0.0340	0.0416	0.0	0.0289	0.00844

The results of this case study are shown in **Table 5-5**. First consider the sb-ROM case for a system size of 2800 corresponding to n=140 and T=20. With r=140, the discrepancy as before is very small and within numerical tolerance of the calculations. Now with the rank of the active subspace reduced to r=130, the accuracy is degraded for all responses as would be expected. Depending on the user-defined accuracy, one can select the desired rank r. Next, for the go-ROM case, consider the case of system size 200 with n=10 and T=20. For this case, after constructing the go-ROM model based a single response (m=1), it is employed to

www.manaraa.com

estimate the variations for other sets of responses (m=11, m=21 and m=41). Notice that the accuracy is degraded for the responses not included in the construction of the go-ROM model. This is again would be expected since the go-ROM is designed for a particular response only. This process is repeated for system sizes of 600, and 1000. Notice also that the level of accuracy degradation is different for different system sizes; notice for example the case of system size equal to 1000 with n=50 and T=20, and r=50. This phenomenon is expected as it is difficult to make any quantitative statements about the size of the discrepancy error for any responses that are not included in the construction of the go-ROM model.

In conclusion, we note that the go-ROM approach is very effective is generating the most computationally efficient ROM when few responses are desired. On the other hands, the sb-ROM approach has an advantage of flexibility in allowing the user to generate an reduced order model that is independent of the choice of the responses.

www.manaraa.com

Table 5-5. Results for Case Study No. 2

Approach	System Size	No. Basis (r)	No. Response (m)	Discrepancy
sb-ROM	2800x2800	140	1	2.9299E-15
			11	1.4109E-16
			21	3.6632E-16
			41	1.8916E-16
	2800x2800	130	1	2.9000E-03
			11	7.4583E-04
			21	9.8884E-04
			41	4.6280E-04
go-ROM	200x200	10	**1**	**2.4704E-08**
			11	4.0000E-03
			21	1.9800E-02
			41	2.6400E-02
	600x600	30	**1**	**3.2221E-14**
			11	4.2903E-06
			21	6.6096E-04
			41	1.9300E-02
	1000x1000	50	**1**	**3.6895E-16**
			11	4.6729E-08
			21	2.8850E-05
			41	1.4900E-02
	2800x2800	140	**1**	**1.6043E-16**
			11	1.1307E-16
			21	9.3616E-17
			41	6.9009E-17

www.manaraa.com

5.3.3. Case Study No. 3

In this case study, we consider the case that initial values are correlated with an ill-conditioned covariance matrix; thus, the initial values are perturbed in r directions, i.e. r degree of freedom of the initial value variations, where r is the numerical rank of the covariance matrix. Different with the previous two cases in that the initial values are perturbed randomly and independently and n forward runs and n adjoint runs are required for the sb-ROM approach, the forward run and the adjoint run would be required only r times ($\ll n$), respectively.

The same model in the case study No.2 is used here again and, for clear demonstrations, two covariance matrices are manufactured to ill-conditioned ($r = 30$ and $r = 50$). The singular values of the covariance matrices are shown in **Figure 5-3**. Ignoring the components associated with small singular values, which have very small effects, the initial value variations are only in 30 directions and 50 directions, respectively. The test results are compared in **Table 5-6**. The first column in **Table 5-6** represents the number of basis vectors, which is denoted as r, used to construct a sb-ROM. Note that the computational cost in fourth and fifth columns would be determined by the number of basis vectors to be considered. The discrepancies in second and third columns are defined in Eq. (5.22) as a metric for error. It can be seen that if the number of basis is not enough to capture the state variable variations, the discrepancy would be large, i.e. sb-ROM would not be accurate. However, once the sufficient number of basis vectors is extracted, i.e. 30 basis vectors for the rank 30 covariance matrix and 50 basis vectors for the rank 50 covariance matrix, we can

www.manaraa.com

build an accurate ROM with smaller computational cost (number of code runs in forward and adjoint mode) than the size of the system, i.e. $r < n$. It is important to distinguish that the computational cost of the go-ROM approach is determined by the number of responses, on the other hand, the computational cost of the sb-ROM approach is determined by the active subspace.

Table 5-6. Results for Case Study No. 3

# of basis	Discrepancy		Computational Cost	
	Cov. rank=30	Cov. rank=50	Forward	Adjoint
10	1.7010E-01	2.0790E-01	10	10
20	7.6733E-02	1.9927E-01	20	20
30	**1.7827E-15**	1.0793E-01	30	30
40	4.3946E-16	6.1200E-02	40	40
50	5.9064E-16	**6.1510E-15**	50	50
60	4.4981E-16	7.5985E-16	60	60
70	5.9817E-16	1.7439E-15	70	70
100	3.7814E-16	7.0416E-16	100	100
140	**6.7294E-16**	**5.1618E-16**	**140**	**140**

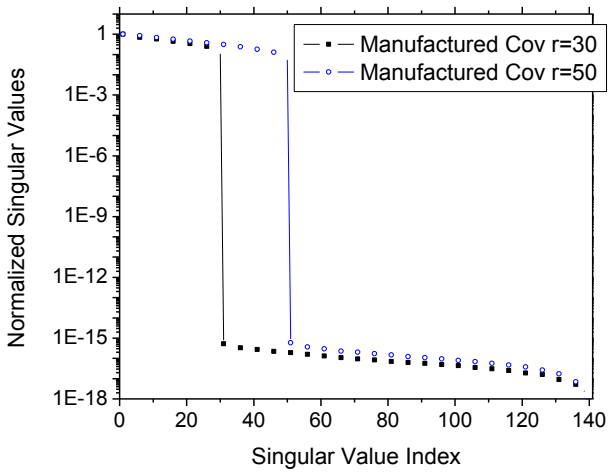

Figure 5-3. Singular Values of Manufactured Covariance Matrices

www.manaraa.com

CHAPTER 6. REDUCED ORDER HESSIAN CONSTRUCTION

The Hessian matrix which is the second order derivatives of the response with respect to the input parameters is constructed by utilizing reduced order modeling (i.e. low rank approximation). In nuclear community, Taylor expansion-based perturbation theory has been used to estimate response changes due to input parameter variations. In practice, the first order adjoint based approach has been recognized as the most powerful tool for sensitivity analysis, uncertainty propagation and data assimilation [Cacuci (2003)] because it requires only one forward mode and one adjoint mode code execution to calculate the first order derivatives with respect to all input parameters. However, for more rigorous sensitivity analysis, the interrelations between parameters should be considered. In addition, the sandwich rule with the linear assumption would not guarantee the accurate response uncertainty propagation for large input parameter uncertainty (i.e. variations) due to nonlinear effects. Though the higher order sensitivity analysis methods have been well-established [Gandini (1978a, 1978b), Greenspan et al. (1978), Greenspan & Gilai (1978)], the computational cost to calculate the higher order derivatives limits the applicability in practice because the number of simulations would increase according to the number of input parameters. By combining the reduced order modeling techniques and the first order adjoint-based sensitivity analysis, the reduced order Hessian matrix can be constructed and the

www.manaraa.com

second order Taylor series approximation can be built with reduced computational cost. This work has been published in Annals of Nuclear Energy [Bang and Abdel-Khalik (2012c)].

6.1 Mathematical Derivation

Consider that the second order Taylor expansion for a response $R(\vec{x})$ is given by:

$$R(\vec{x}) = R(\vec{x}_0) + \left(\left. \frac{\partial R}{\partial \vec{x}} \right|_{\vec{x}_0} \right)^T (\Delta \vec{x}) + \frac{1}{2} (\Delta \vec{x})^T \left(\left. \frac{\partial^2 R}{\partial \vec{x} \partial \vec{x}} \right|_{\vec{x}_0} \right) (\Delta \vec{x})$$
$$\text{or } R = R_0 + \vec{S}_0^{\,T} (\Delta \vec{x}) + \frac{1}{2} (\Delta \vec{x})^T \mathbf{H}_0 (\Delta \vec{x}) \tag{6.1}$$

where $R(\vec{x}_0)$ is the zeroth order term, i.e. reference response, $\left. \frac{\partial R}{\partial \vec{x}} \right|_{\vec{x}_0}$ is the first order derivative vector $\vec{S}_0 \in \mathbb{R}^n$ at the reference configuration, $\left. \frac{\partial^2 R}{\partial \vec{x} \partial \vec{x}} \right|_{\vec{x}_0}$ is the second order derivative matrix, i.e. Hessian matrix $\mathbf{H}_0 \in \mathbb{R}^{n \times n}$, $\Delta \vec{x} \in \mathbb{R}^n$ is the perturbed input parameters given by $\vec{x} - \vec{x}_0$, i.e. difference between perturbed and reference configurations and n is the number of input parameters. The main focus is given on constructing the Hessian matrix.

Differentiating the Eq. (6.1) gives:

$$\vec{S} = \vec{S}_0 + \mathbf{H}_0 (\Delta \vec{x}) \tag{6.2}$$

where $\vec{S} = \left. \frac{\partial R}{\partial \vec{x}} \right|_{\vec{x}}$, i.e. the first order derivatives at the perturbed configuration. Rewriting Eq. (6.2) as:

www.manaraa.com

$$\vec{U} = \mathbf{H}_0 \vec{V} \tag{6.3}$$

where $\vec{U} = \vec{S} - \vec{S}_0$ and $\vec{V} = \Delta\vec{x} = \vec{x} - \vec{x}_0$, then one can see that the Eq. (6.3) has the same form with Eq. (4.3), i.e. the linear mapping. Because the Hessian matrix is symmetric, the active subspace basis construction and the reduced order Hessian matrix construction can be conducted simultaneously.

Note that the vector $\vec{U}$ spans the active subspace which is in $\mathrm{R}\left(\mathbf{H}_0^T\right) = \mathrm{R}\left(\mathbf{H}_0\right)$. By using the range finding algorithm with perturbed input parameters, i.e. $\vec{V}^{(i)}$ for $i = 1,...,r$, the basis vectors in the matrix form $\mathbf{Q}$ can be constructed. Then, Eq. (6.3) can be transformed into reduced order form as:

$$\mathbf{Q}^T\vec{U} = \mathbf{Q}^T\mathbf{H}_0\mathbf{Q}\mathbf{Q}^T\vec{V} \quad \Rightarrow \quad \vec{U}_r = \mathbf{H}_{0,r}\vec{V}_r \tag{6.4}$$

where $\vec{U}_r = \mathbf{Q}^T\vec{U}$, $\vec{V}_r = \mathbf{Q}^T\vec{V}$ and $\mathbf{H}_{0,r} = \mathbf{Q}^T\mathbf{H}_0\mathbf{Q}$. Note that the Hessian matrix $\mathbf{H}_0 \in \mathbb{R}^{n\times n}$ in the original Eq. (6.3) is transformed into lower dimension $\mathbf{H}_{0,r} \in \mathbb{R}^{r\times r}$. The error due to the transformation can be estimated by three ways as explained in the previous chapter: singular value spectrum, in-active component and κ-metric.

Defining the matrix $\mathbf{U}_r$ and $\mathbf{V}_r$ by $\mathbf{U}_r = \left[\vec{U}_r^{(1)} \quad \cdots \quad \vec{U}_r^{(r)}\right]$ and $\mathbf{V}_r = \left[\vec{V}_r^{(1)} \quad \cdots \quad \vec{V}_r^{(r)}\right]$, the reduced order Hessian matrix can be calculated by solving:

$$\mathbf{H}_{0,r} = \mathbf{U}_r\mathbf{V}_r^{-1} \tag{6.5}$$

In order to eliminate the effect of numerical error, e.g. rounding, the regularization parameter can be introduced into Eq. (6.5) as [Bang & Abdel-Khalik (2011b)]:

www.manaraa.com

$$\mathbf{H}_{0,r} = \left(\mathbf{R}_{\mathbf{V}_r}^T \mathbf{R}_{\mathbf{V}_r} + \alpha \mathbf{I}\right)^{-1} \mathbf{R}_{\mathbf{V}_r}^T \mathbf{Q}_{\mathbf{V}_r}^T \mathbf{U}_r^T \tag{6.6}$$

where $\mathbf{V}_r^T = \mathbf{Q}_{\mathbf{V}_r} \mathbf{R}_{\mathbf{V}_r}$, i.e. QR decomposition, α is a regularization factor and $\mathbf{I}$ is an identity matrix. Note that $\mathbf{U} = \left[\vec{U}^{(1)} \quad \cdots \quad \vec{U}^{(r)}\right]$ and $\mathbf{V} = \left[\vec{V}^{(1)} \quad \cdots \quad \vec{V}^{(r)}\right]$ are used both for the basis construction and the Hessian construction, i.e. the total number of simulation sequences (i.e. forward mode and adjoint mode) is only $r+1$, i.e. 1 at the reference configuration and r at the perturbed configuration.

Once the basis vectors and the reduced order Hessian matrix are obtained, the response change can be estimated by the second order approximation:

$$R = R_0 + \vec{S}_0^{\,T} \left(\Delta \vec{x}\right) + \frac{1}{2}\left(\mathbf{Q}^T \Delta \vec{x}\right)^T \mathbf{H}_{0,r} \left(\mathbf{Q}^T \Delta \vec{x}\right) \tag{6.7}$$

The original Hessian matrix can be recovered by:

$$\mathbf{H}_0 = \mathbf{Q}\mathbf{H}_{0,r}\mathbf{Q}^T \tag{6.8}$$

The RO Hessian construction algorithm is summarized as follows:

Algorithm: Reduced Order Hessian Construction Method

Consider that the 2nd order Taylor expansion of a single-valued response $R(\vec{x})$ around $\vec{x}_0$:

$$R(\vec{x}) \simeq R(\vec{x}_0) + (\vec{x} - \vec{x}_0)^T \vec{S}_0 + \frac{1}{2}(\vec{x} - \vec{x}_0)^T \mathbf{H}_0 (\vec{x} - \vec{x}_0)$$

where $\vec{x} = \left(x_1 \quad \ldots \quad x_n\right)^T$ represents a vector of n input data, $\vec{x}_0$ denote the reference values for the input parameters, $\vec{S}_0$ is the gradient vector containing the response's first order derivatives evaluated at the input parameters reference values, and $\mathbf{H}_0$ is the

www.manaraa.com

unknown Hessian matrix containing all second order derivatives. This algorithm requires running the forward model and the adjoint model $r+s$ times, where r is the user's estimate of the rank, and s are oversamples needed to check whether the user-defined tolerance is met. For all practical purposes, s is a small integer, e.g., $s=10$. The reduced order 2nd order Taylor expansion model can be constructed employing a user-defined tolerance ε as follows:

Step 1) Draw random vectors $\vec{V}^{(i)}$, $i=1,...,r+s$.

Step 2) Perturb input parameters as follows: $\vec{x}^{(i)}=\vec{x}_0+\vec{V}^{(i)}$, $i=1,...,r+s$

Step 3) DO $i=1,2,...,r+s$,

compute $\vec{U}^{(i)}=\vec{S}^{(i)}-\vec{S}_0$,

where $\vec{S}^{(i)}$ are the sensitivities calculated with perturbed input parameters $\vec{x}^{(i)}$.

END DO

Step 4) Set $j=0$ and $\mathbf{Q}_0=[\ ]$, the $n\times 0$ empty matrix

Step 5) $j=j+1$

Step 6) $\vec{U}^{(j)}\leftarrow\left(\mathbf{I}-\mathbf{Q}_{j-1}\mathbf{Q}_{j-1}^T\right)\vec{U}^{(j)}$

Step 7) $\vec{q}_j=\vec{U}^{(j)}/\left\|\vec{U}^{(j)}\right\|$

Step 8) $\mathbf{Q}_j=\left[\mathbf{Q}_{j-1}\quad \vec{q}_j\right]$

Step 9) Compute $\vec{z}^{(i)}=\left(\mathbf{I}-\mathbf{Q}_j\mathbf{Q}_j^T\right)\vec{U}^{(r+i)}$, $i=1,...,s$

Step 10) If $\max\left\{\left\|\vec{z}^{(1)}\right\|,\left\|\vec{z}^{(2)}\right\|,...,\left\|\vec{z}^{(s)}\right\|\right\}<\varepsilon$, go to Step 11,

else increases r and go back to Step 1,

Step 11) $\mathbf{Q}=\mathbf{Q}_j$, $\mathbf{U}=\left[\vec{U}^{(1)}\quad\cdots\quad\vec{U}^{(j)}\right]$, $\mathbf{V}=\left[\vec{V}^{(1)}\quad\cdots\quad\vec{V}^{(j)}\right]$, and rank $r=j$

Step 12) Compute the projected matrices: $\mathbf{V}_r=\mathbf{Q}^T\mathbf{V}$ and $\mathbf{U}_r=\mathbf{Q}^T\mathbf{U}$

Step 13) Compute the reduced order Hessian matrix:

www.manaraa.com

$$\mathbf{H}_{0,r} = \left(\mathbf{R}_{\mathbf{V}_r}^T \mathbf{R}_{\mathbf{V}_r} + \alpha \mathbf{I}\right)^{-1} \mathbf{R}_{\mathbf{V}_r}^T \mathbf{Q}_{\mathbf{V}_r}^T \mathbf{U}_r^T$$

where regularization parameter α

Step 14) Construct the reduced order 2nd order Taylor expansion model:

$$R = R_0 + \vec{S}_0^{\,T}\left(\Delta\vec{x}\right) + \frac{1}{2}\left(\mathbf{Q}^T\Delta\vec{x}\right)^T\left(\mathbf{Q}^T\mathbf{H}_0\mathbf{Q}\right)\left(\mathbf{Q}^T\Delta\vec{x}\right)$$

6.2 Numerical Test

Problem Description

The Hessian construction approach is tested for k_{eff} value estimation. Note that the neutron transport equation is given by:

$$\begin{aligned}&\vec{\Omega}\cdot\nabla\psi\left(\vec{r},\vec{\Omega},E\right)+\Sigma_t\left(\vec{r},E\right)\psi\left(\vec{r},\vec{\Omega},E\right)\\&=\frac{1}{k_{eff}}\frac{\chi(E)}{4\pi}\int_{\infty}dE'\int_{4\pi}d\vec{\Omega}'\left[\nu\left(E'\right)\Sigma_f\left(\vec{r},E'\right)\psi\left(\vec{r},\vec{\Omega}',E'\right)\right]\\&\quad+\int_{\infty}dE'\int_{4\pi}d\vec{\Omega}'\left[\Sigma_s\left(\vec{r},E'\to E,\vec{\Omega}'\to\vec{\Omega}\right)\psi\left(\vec{r},\vec{\Omega}',E'\right)\right]\end{aligned} \tag{6.9}$$

By applying a numerical method, Eq. (6.9) can be represented in a operator form:

$$\mathbf{L}\left(\vec{\Sigma}\right)\vec{\psi} = \frac{1}{k_{eff}}\mathbf{F}\left(\vec{\Sigma}\right)\vec{\psi} \tag{6.10}$$

where $\mathbf{L}\left(\vec{\Sigma}\right)\vec{\psi}$ can be interpreted as a loss of neutrons and $\mathbf{F}\left(\vec{\Sigma}\right)\vec{\psi}$ can be production and k_{eff} is an eigenvalue to balance the loss and the production of neutrons. Note that the operators $\mathbf{L}$ and $\mathbf{F}$ are functions of reaction cross sections $\vec{\Sigma}$. The problem considered here

www.manaraa.com

is to estimate the k_{eff} change due to reaction cross section variations from the reference configuration:

$$\mathbf{L}\left(\vec{\Sigma}_0+\Delta\vec{\Sigma}\right)\left(\vec{\psi}_0+\Delta\vec{\psi}\right)=\frac{1}{k_{eff,0}+\Delta k_{eff}}\mathbf{F}\left(\vec{\Sigma}_0+\Delta\vec{\Sigma}\right)\left(\vec{\psi}_0+\Delta\vec{\psi}\right) \tag{6.11}$$

where $\vec{\Sigma}_0$, $\vec{\psi}_0$ and $k_{eff,0}$ are reference configurations.

The perturbation theory based on the Taylor expansion can be used to estimate the response change due to input parameter variation:

$$\begin{aligned} k\left(\vec{\Sigma}\right) &\approx k\left(\vec{\Sigma}_0\right)+\left(\left.\frac{\partial k}{\partial\vec{\Sigma}}\right|_{\vec{\Sigma}_0}\right)^T\left(\Delta\vec{\Sigma}\right)+\frac{1}{2}\left(\Delta\vec{\Sigma}\right)^T\left(\left.\frac{\partial^2 k}{\partial\vec{\Sigma}\partial\vec{\Sigma}}\right|_{\vec{\Sigma}_0}\right)\left(\Delta\vec{\Sigma}\right)+\text{Higher Order Terms} \\ \text{or } k &\approx k_0+\vec{S}_0{}^T\left(\Delta\vec{\Sigma}\right)+\frac{1}{2}\left(\Delta\vec{\Sigma}\right)^T\mathbf{H}_0\left(\Delta\vec{\Sigma}\right)+\text{Higher Order Terms} \end{aligned} \tag{6.12}$$

where $k\left(\vec{\Sigma}_0\right)$ is the zeroth order term, i.e. reference response, $\left.\frac{\partial k}{\partial\vec{\Sigma}}\right|_{\vec{\Sigma}_0}$ is the first order derivative vector $\vec{S}_0$ at the reference configuration, $\left.\frac{\partial^2 k}{\partial\vec{\Sigma}\partial\vec{\Sigma}}\right|_{\vec{\Sigma}_0}$ is the second order derivative matrix, i.e. Hessian matrix $\mathbf{H}_0$ and $\Delta\vec{\Sigma}$ is perturbation of input parameters given by $\vec{\Sigma}-\vec{\Sigma}_0$, i.e. difference between perturbed and reference configurations. In this study, the second order Taylor expansion is considered as a surrogate model and reduced order modeling technique is used to reduce the computational cost to calculate the Hessian matrix $\mathbf{H}_0$.

www.manaraa.com

Implementation

For calculating the first order derivatives, TSUNAMI-2D control module of SCALE6.1 [RSICC (2011)] is used. TSUNAMI-2D control module generates the input files for resonance calculation module (e.g. NITAWL, BONAMI or CENTRM), transport solver (i.e. NEWT for forward and adjoint mode) and sensitivity calculation module (i.e. SAMS). The SAMS calculates the sensitivity coefficients (i.e. relative first order derivative) of user-defined responses, i.e. k_{eff} in this test, with respect to the self-shielded macroscopic cross sections. For testing the reduced order Hessian construction algorithm, the working library for self-shielded macroscopic cross sections is perturbed and NEWT (forward) – NEWT (adjoint) – SAMS sequences are performed to calculate the perturbed sensitivity coefficients. **Figure 6-1** depicts the model analyzed; it is a stand-alone benchmark model designed by OECD/NEA to assess the assumptions in current LWR standard lattice physics scheme for generation of few-group cross-sections [Ivanov et al. (2007)]. The 44 energy group library (v5-xn44) of SCALE6.1 is used and the reference k_{eff} is 1.08383475. With the perturbed self-shielded macroscopic cross sections $\vec{\Sigma}$ and the resulting sensitivity coefficients $\vec{S}$, the reduced order Hessian matrix construction and all subsequent calculations are conducted by using MATLAB 2011a.

www.manaraa.com

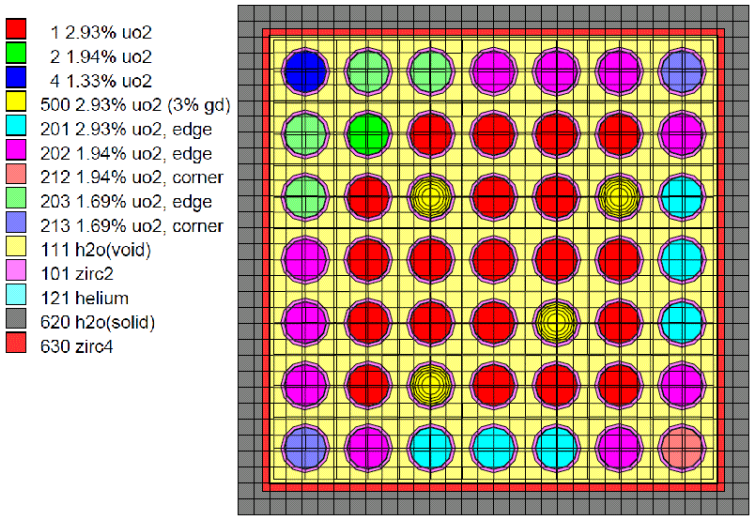

Figure 6-1. A 7x7 BWR Benchmark Assembly Model

Two cases are considered. First, the fission cross sections of four nuclides (i.e. U-234, U-235, U-236 and U-238) in 44 energy group in 9 fuel mixtures are perturbed by $\pm 50\%$ from uniform distribution, i.e. the dimension of input parameters is $\mathbb{R}^{1584}$. Second, the scattering cross sections, fission cross sections, capture cross sections and neutron yields per fission (nubar) of four nuclides (i.e. U-234, U-235, U-236 and U-238) in 44 energy group in 9 fuel mixtures are perturbed by $\pm 10\%$ from uniform distribution. In this case, the dimension of the input parameters is $\mathbb{R}^{6336}$. To estimate the accuracy of the second order approximation, the test sets are generated and the responses calculated by the original model, i.e. NEWT and the first order estimations are compared to the second order estimation with reduced order Hessian matrix. The accuracy of the surrogate model is measured by R^2 value:

www.manaraa.com

$$R^2 = 1 - \frac{\sum_i^N \left(y_{actual}^{(i)} - y_{estimate}^{(i)} \right)^2}{\sum_i^N \left(y_{actual}^{(i)} - \bar{y} \right)^2} \tag{6.13}$$

where $y_{actual}^{(i)}$ is the response calculated by the original model with the i^{th} test sample input parameters, $y_{estimate}^{(i)}$ is the response calculated by the reduced order surrogate model with the i^{th} test sample input parameters, $\bar{y}$ is the average value of N responses calculated by the original model and N is the number of test samples. As the R^2 value is closer to 1, the estimation is more accurate.

Results

As the first test case, the fission cross section perturbation case is considered, i.e. $\vec{\Sigma} \in \mathbb{R}^{1584}$. As noted in the previous chapter, the active subspace extraction and low rank approximation of the Hessian matrix can be conducted simultaneously. Differentiate Eq. (6.12) and stacking each sample side-by-side to define the matrix:

$$\mathbf{U} = \mathbf{H}_0 \mathbf{V} \tag{6.14}$$

where $\mathbf{U} = \left[\vec{U}^{(1)} \quad \cdots \quad \vec{U}^{(r)} \right] \in \mathbb{R}^{n \times r}$ and $\mathbf{V} = \left[\vec{V}^{(1)} \quad \cdots \quad \vec{V}^{(r)} \right] \in \mathbb{R}^{n \times r}$ with $\vec{U}^{(i)} = \vec{S}^{(i)} - \vec{S}_0$ and $\vec{V}^{(i)} = \Delta\vec{\Sigma}^{(i)} = \vec{\Sigma}^{(i)} - \vec{\Sigma}_0$. Note that by linear algebra:

$$\mathrm{R}\left(\mathbf{U}\right) = \mathrm{R}\left(\mathbf{H}_0\right) \tag{6.15}$$

where $\mathrm{R}(\bullet)$ is the range, i.e. column space. This implies that the columns of $\mathbf{U}$ and $\mathbf{H}_0$ span the same subspace, i.e. the subspace spanned by the columns of $\mathbf{U}$ and $\mathbf{H}_0$ can be

www.manaraa.com

represented by the same basis vectors. As can be seen in **Figure 6-2**, the spectrum of the singular values is decaying rapidly. Note that after 400^{th} singular value, the magnitudes of them are below 10^{-5} which is very small. Moreover, considering the precision of cross section values, i.e. single precision, the components associated to those small singular values are contaminated by numerical error and should be neglected.

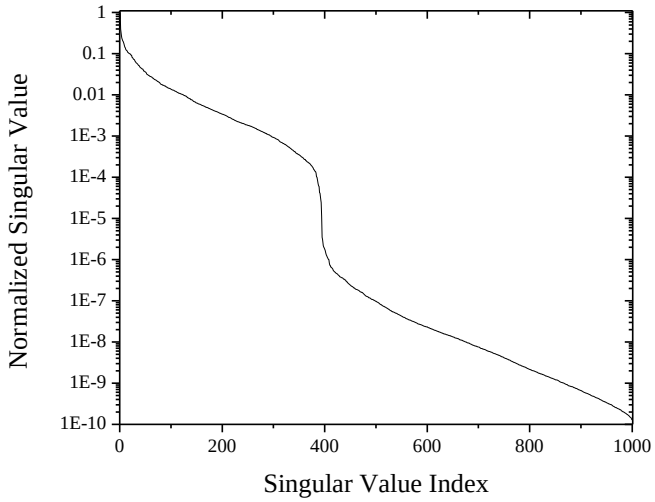

Figure 6-2. Normalized Singular Value Spectrum of the matrix $\mathbf{U}$
(Hessian construction, $\bar{\Sigma} \in \mathbb{R}^{1584}$)

In **Table 6-1**, the active subspace basis is examined by κ-metric. Note that if the basis is identified properly, the response change due to the parameter variation orthogonal to the subspace spanned by the basis should be zero. For test, 20 test cases, i.e. $\Delta\bar{\Sigma}^{(i)}$ for $i = 1,...,20$ are randomly generated and orthogonal perturbation is also generated by

www.manaraa.com

$\Delta\vec{\Sigma}^{(i)\perp} = \left(\mathbf{I} - \mathbf{Q}\mathbf{Q}^T\right)\Delta\vec{\Sigma}^{(i)}$ for $i = 1,...,20$. The 20 test cases are compared by using the root mean square change defined by:

$$\text{RMS [pcm]} = \sqrt{\frac{\sum_{i=1}^{N}\left(k^{(i)} - k_0\right)^2}{N}} \times 10^5 \tag{6.16}$$

where $k^{(i)}$ is the k_{eff} value in i^{th} test case, k_0 is k_{eff} value at the reference configuration and N is the number of test cases, i.e. 20. Also, the 2-norms of the inactive components are compared. As can be seen in **Table 6-1**, the k_{eff} change decreases as the more basis vectors are considered, which means that the subspace is captured more properly.

Table 6-1. Summary of Active Subspace Test (Hessian construction, $\vec{\Sigma} \in \mathbb{R}^{1584}$)

Rank	2-Norm of Inactive Components	RMS change [pcm]	
		$\Delta k\left(\Delta\vec{\Sigma}\right)$	$\Delta k\left(\Delta\vec{\Sigma}^{\perp}\right)$
100	2.898520e-002	1623.870501	80.185015
200	1.045743e-002	1925.696526	26.903832
300	4.004075e-003	1764.048116	9.347621
400	1.112478e-003	2113.337578	1.608435

The estimation accuracy is examined by using 100 test samples. The first order approximation and the second order approximation with reduced order Hessian construction are calculated by:

$$k_{1st} = k_0 + \vec{S}_0{}^T\left(\Delta\vec{\Sigma}\right) \tag{6.17}$$

$$k_{2nd} = k_0 + \vec{S}_0{}^T\left(\Delta\vec{\Sigma}\right) + \frac{1}{2}\left(\mathbf{Q}^T\Delta\vec{\Sigma}\right)^T\left(\mathbf{Q}^T\mathbf{H}_0\mathbf{Q}\right)\left(\mathbf{Q}^T\Delta\vec{\Sigma}\right) \tag{6.18}$$

www.manaraa.com

where the columns of the matrix $\mathbf{Q} \in \mathbb{R}^{n \times r}$ is the basis of the active subspace. The regularization parameter α is assumed to 0.5. The R^2 number defined in the Eq. (6.13) is used and the average absolute perturbation, the average absolute discrepancy and the average relative discrepancy is defined as:

$$\text{Avg.Abs.Perturbation [pcm]} = \frac{1}{N}\sum_{i=1}^{N}\left|k_{actual}^{(i)} - k_0\right| \times 10^5 \tag{6.19}$$

$$\text{Avg.Abs.Dis [pcm]} = \frac{1}{N}\sum_{i=1}^{N}\left|k_{actual}^{(i)} - k_{estimate}^{(i)}\right| \times 10^5 \tag{6.20}$$

$$\text{Avg.Rel.Dis [\%]} = \frac{\text{Avg.Abs.Dis}}{\text{Avg.Abs.Perturbation}} \times 100 \tag{6.21}$$

where $k_{actual}^{(i)}$ is the k_{eff} value calculated by the original model with the i^{th} test sample input parameters, $k_{estimate}^{(i)}$ is the k_{eff} value calculated by the reduced order surrogate model with the i^{th} test sample input parameters and N is the number of test samples, i.e. 100. As can be seen in **Table 6-2** and **Figure 6-3**, the second order approximation by reduced order Hessian construction approach can estimate the k_{eff} change more accurately than the first order approximation by an order level. Note that the reduction factor is defined as:

$$\text{Reduction Factor} = \frac{\text{reduced dimension}}{\text{original dimension}} = \frac{r}{n} \tag{6.22}$$

www.manaraa.com

Table 6-2. Summary of Estimation Results (Hessian construction, $\vec{\Sigma} \in \mathbb{R}^{1584}$)

			Avg. Abs. Perturbation [pcm]		
Original Model Δk_{actual}		-	1569.4220		-
	r	**Reduction Factor**	**Avg. Abs. Dis [pcm]**	**Avg. Rel. Dis [%]**	**R^2**
First Order Estimation Δk_{1st}		-	517.0471	32.9451	0.9220
Second Order Estimation Δk_{2nd}	100	0.0631	56.5675	3.6043	0.9989
	200	0.1263	32.4746	2.0692	0.9993
	300	0.1894	33.6016	2.1410	0.9992
	400	0.2525	30.7211	1.9575	0.9993
	500	0.3157	29.2548	1.8640	0.9994
	600	0.3788	26.8028	1.7078	0.9996
	700	0.4419	23.7559	1.5137	0.9996
	800	0.5051	25.1294	1.6012	0.9996
	900	0.5682	26.4121	1.6829	0.9996
	1000	0.6313	26.8600	1.7115	0.9996

www.manaraa.com

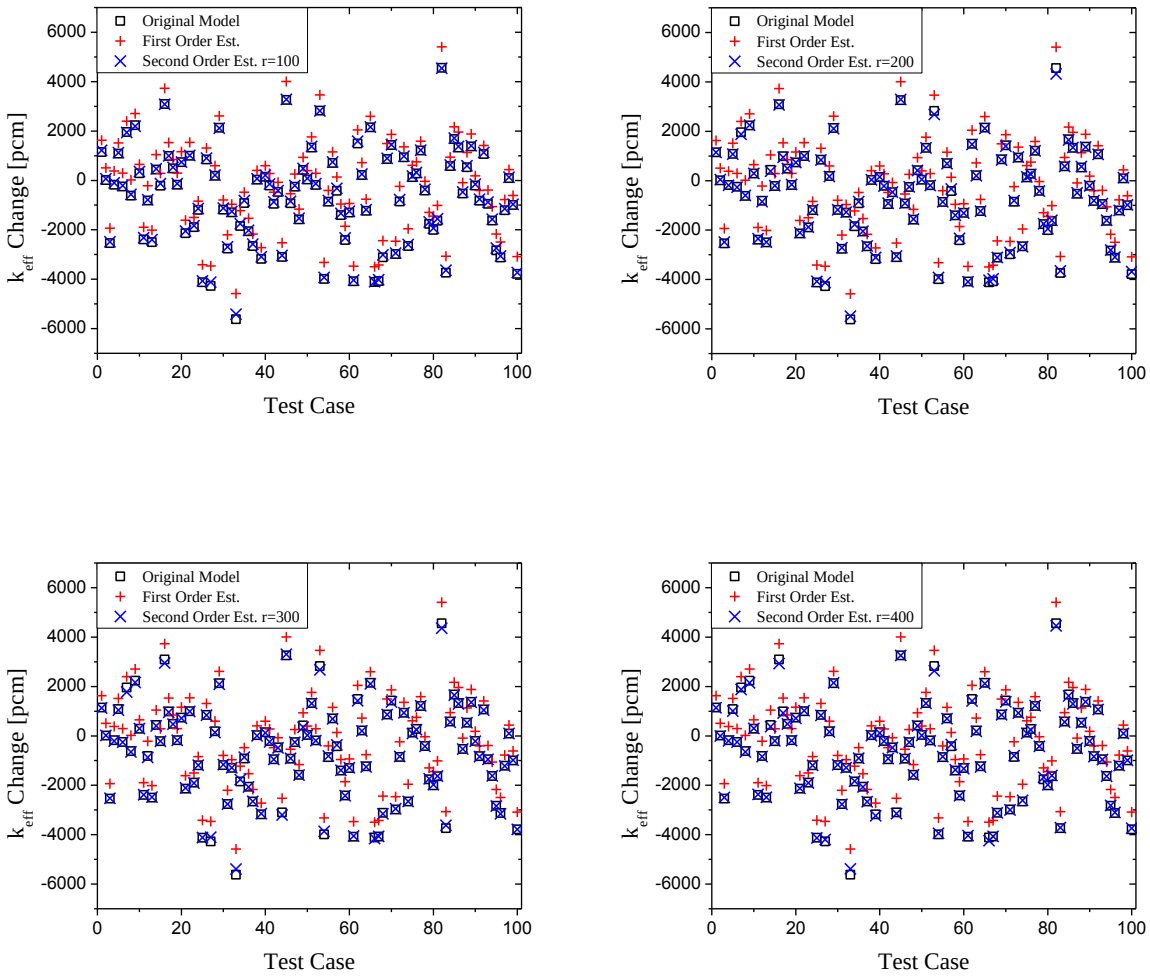

Figure 6-3. Comparison of Estimation Accuracy
(Hessian construction, $\vec{\Sigma} \in \mathbb{R}^{1584}$, random direction)

www.manaraa.com

To examine the estimation accuracy according to the perturbation magnitude, 30 test samples are generated by:

$$\Delta\vec{\Sigma}^{(i)} = \left(\Delta\vec{\Sigma}_{base}\right) \times i \qquad \text{for } i = 1,...,30 \tag{6.23}$$

where $\Delta\vec{\Sigma}_{base}$ is randomly generated by $\pm 1.5\%$ perturbation. As can be seen in **Figure 6-4**, the first order estimation loses the accuracy as the perturbation increases, while the second order approximation captures the nonlinear behavior of k_{eff} changes.

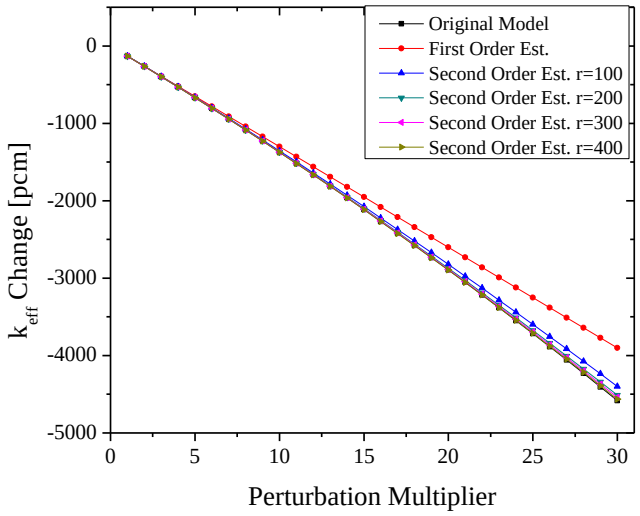

Figure 6-4. Comparison of Estimation Accuracy
(Hessian construction, $\vec{\Sigma} \in \mathbb{R}^{1584}$, one direction)

As the second test case, the problem with larger dimension but smaller perturbation is considered, i.e. $\vec{\Sigma} \in \mathbb{R}^{6336}$. The same tests are conducted. The singular value spectrum is shown in **Figure 6-5** and active subspace test is summarized in **Table 6-3**. The second order approximations are presented in **Figure 6-6**, **Figure 6-7** and **Table 6-4**. The results show that

www.manaraa.com

the reduced order Hessian construction approach improves the estimation accuracy and the computational cost to construct the Hessian matrix can be reduced successfully.

Table 6-3. Summary of Active Subspace Test (Hessian construction, $\vec{\Sigma} \in \mathbb{R}^{6336}$)

Rank	**Error Estimation Upper Bound**	**RMS change [pcm]**	
		$\Delta k\left(\Delta\vec{\Sigma}\right)$	$\Delta k\left(\Delta\vec{\Sigma}^{\perp}\right)$
100	3.186372e-002	908.924389	68.617675
200	1.816507e-002	1002.33654	56.248345
300	1.263442e-002	751.441779	44.177302
400	9.364596e-003	848.192897	35.475633

Table 6-4. Summary of Estimation Results (Hessian construction, $\vec{\Sigma} \in \mathbb{R}^{6336}$)

			Avg. Abs. Perturbation [pcm]		
Original Model Δk_{actual}		-	557.2634		-
	r	**Reduction Factor**	**Avg. Abs. Dis [pcm]**	**Avg. Rel. Dis [%]**	**R^2**
First Order Estimate Δk_{1st}		-	32.2087	5.7798	0.9965
Second Order Estimate Δk_{2nd}	100	0.0158	18.7735	3.3689	0.9989
	200	0.0316	12.7891	2.2950	0.9993
	300	0.0473	10.2140	1.8329	0.9992
	400	0.0631	9.7751	1.7541	0.9993
	500	0.0789	8.2644	1.4830	0.9994
	600	0.0947	7.7767	1.3955	0.9996
	700	0.1105	7.0500	1.2651	0.9996
	800	0.1263	6.8384	1.2271	0.9996
	900	0.1420	6.7094	1.2040	0.9996
	1000	0.1578	6.7239	1.2066	0.9996

www.manaraa.com

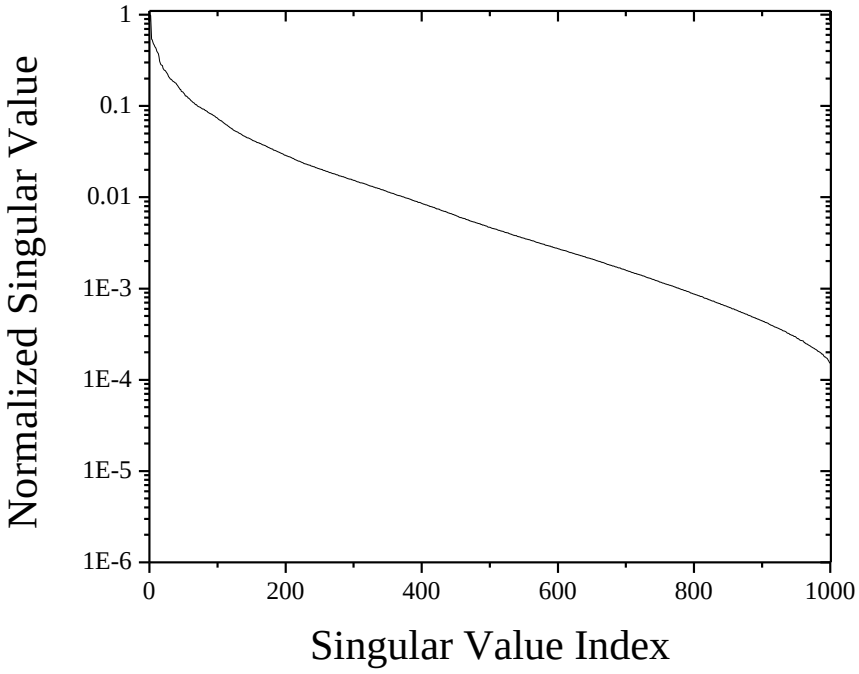

Figure 6-5. Singular Value Spectrum of the matrix **U**
(Hessian construction, $\vec{\Sigma} \in \mathbb{R}^{6336}$)

www.manaraa.com

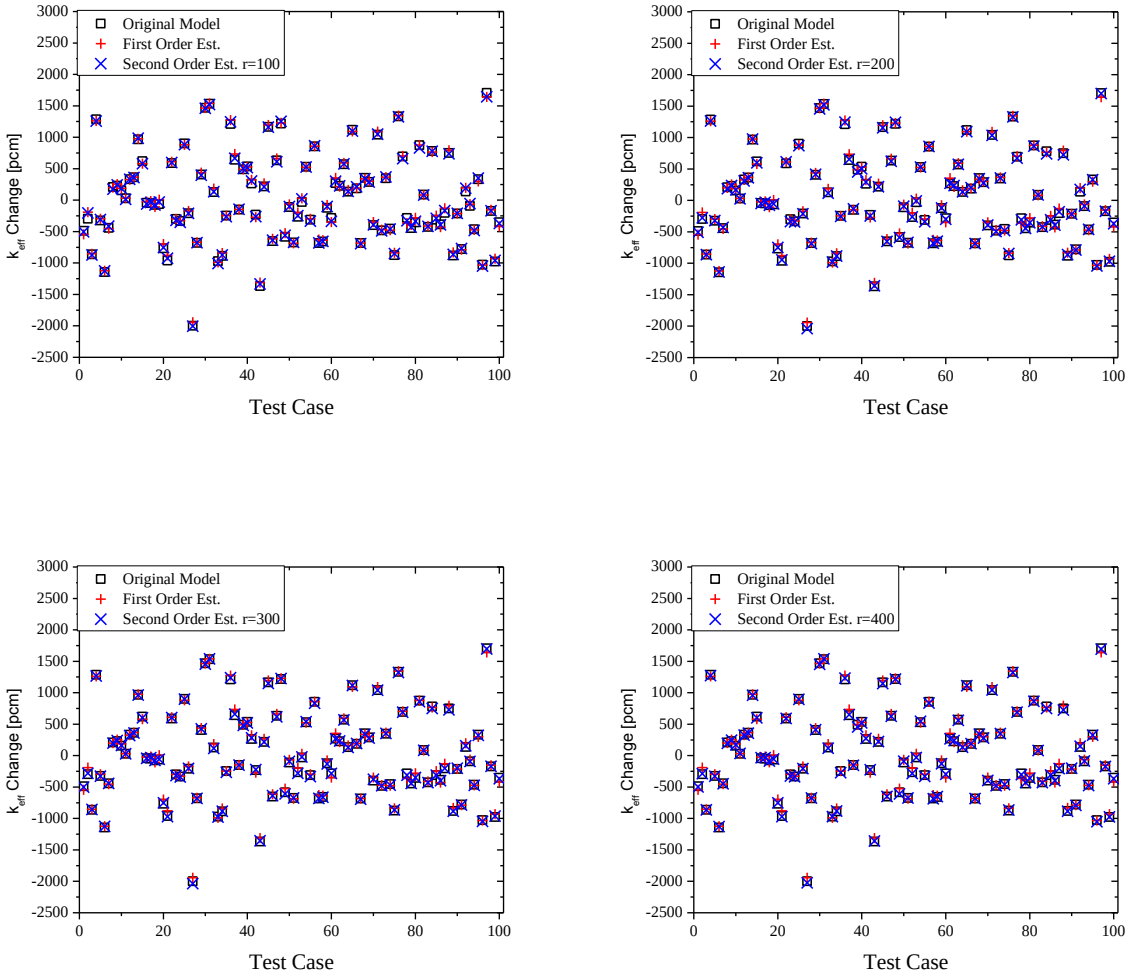

Figure 6-6. Comparison of Estimation Accuracy
(Hessian Construction, $\vec{\Sigma} \in \mathbb{R}^{6336}$, random direction)

www.manaraa.com

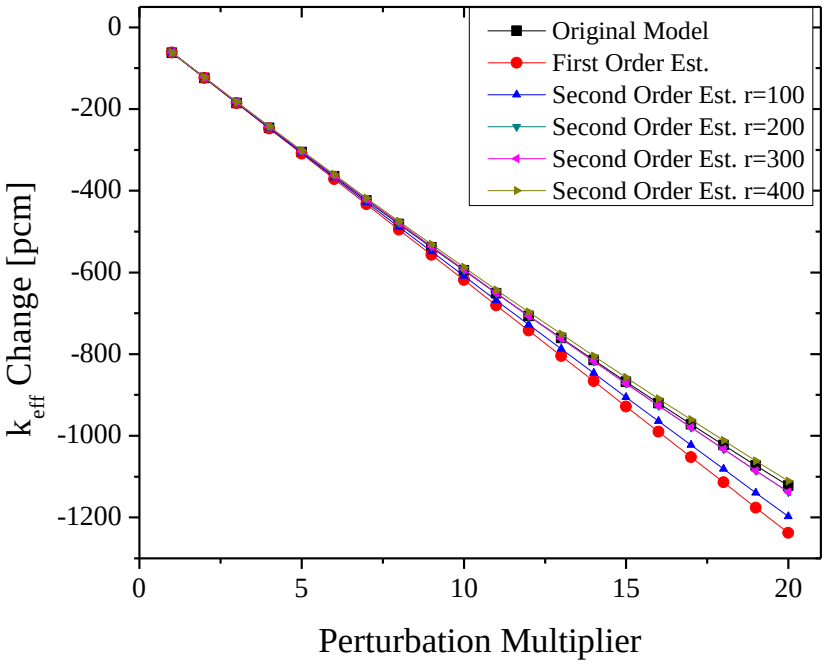

Figure 6-7. Comparison of Estimation Accuracy
(Hessian Construction, $\vec{\Sigma} \in \mathbb{R}^{6336}$, one direction)

Note that the nonlinear effects can appear in two different ways. First (left graph in **Figure 6-8**), the response change can be a sum of absolute linear effect and absolute nonlinear effect, i.e. $|\Delta R_{actual}| = |\Delta R_{linear}| + |\Delta R_{nonlinear}|$. In this case, the linear effect is greater than the nonlinear effect for the response change. Consider the linear portion and nonlinear portion defined as follows:

$$\text{Linear Portion } [\%] = \frac{|\Delta R_{linear}|}{|\Delta R_{actual}|} \times 100 \tag{6.24}$$

$$\text{Nonlinear Portion } [\%] = \frac{|\Delta R_{actual} - \Delta R_{linear}|}{|\Delta R_{actual}|} \times 100 \tag{6.25}$$

www.manaraa.com

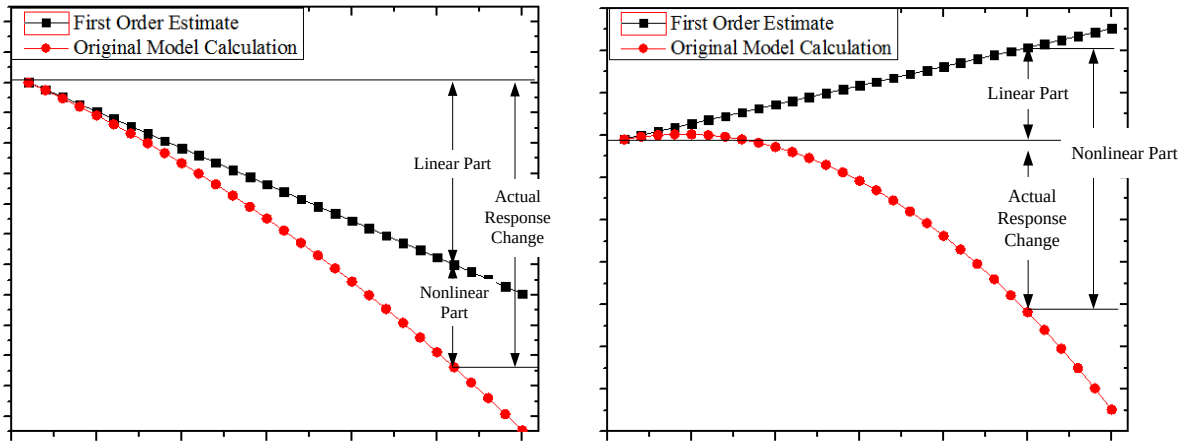

Figure 6-8. Response Change Shape and Linear/Nonlinear Effects Portion

Figure 6-9 shows that as the perturbation increases not only the magnitude of the nonlinear effect but also its portion in the response change would increase. On the other hand, in more highly nonlinear problems, the signs of the actual response change and the first order estimation may be different. In this case, the nonlinear effect would be larger than the linear effect, i.e. $|\Delta R_{linear}| < |\Delta R_{nonlinear}|$. This implies that the higher order effect would more important than the first order effect.

It is important to note that for the first test case, $r = 400$ is enough to capture all influential variations in the active subspace, i.e. the error due to input parameter transformation is negligible. On the other hand, for the second test case, $r = 400$ is not enough because the error due to input parameter transformation cannot be negligible in view of orthogonal test, i.e. **Table 6-3**. However, in both cases, the average absolute discrepancy,

www.manaraa.com

the average relative discrepancy and R^2 value show the same order of accuracy with $r = 400$. This implies that for the second case, much higher reduction is achieved within the same error tolerance. To explain this, the nonlinear/linear ratio is defined as:

$$\text{NL ratio} = \frac{\left|\Delta R_{actual} - \Delta R_{linear}\right|}{\left|\Delta R_{linear}\right|} \tag{6.26}$$

Figure 6-10 compares the distributions of the NL ratio for the first test case, i.e. $\pm 50\%$ perturbation and the second case, i.e. $\pm 10\%$, for 100 test sample sets. Because the first test case is more nonlinear than the second test case, the NL ratio is larger, which implies that the nonlinear effect has higher portion in the response change. The fact that NL ratio is larger than 1 means the nonlinear effect is more important than the linear effect in response changes. On the other hand, in the second test case, the NL ratio is small and most of them are distributed within 0.1 range. This means that the nonlinear effect is less important and as explained in the previous chapter, the error in the input parameter transformation and in the Hessian matrix construction would be damped, i.e. more reduction can be achieved. This observation leads to the important fact that ***the user-defined tolerance for reduced order modeling should be determined by considering the degree of the nonlinearity***.

www.manaraa.com

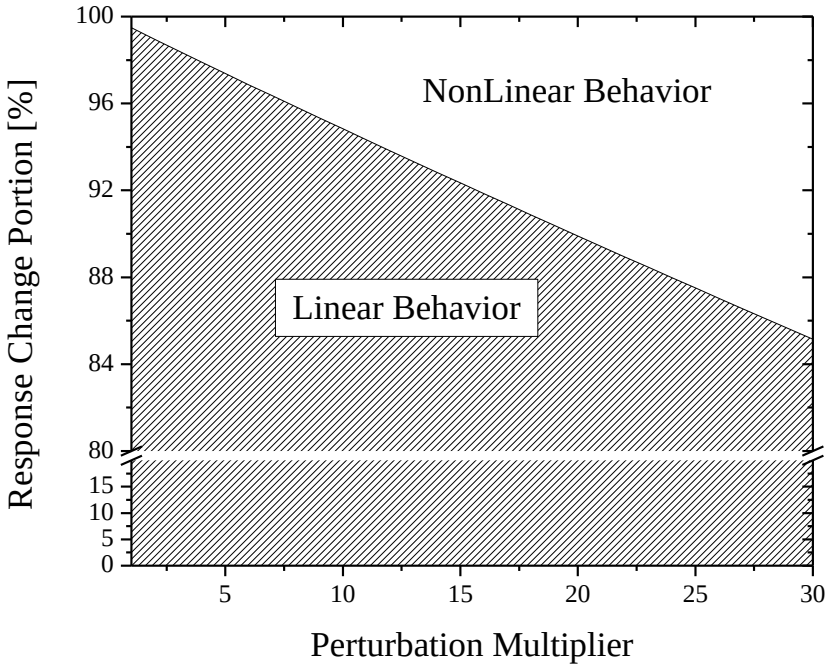

Figure 6-9. Comparison of Nonlinear/Linear Portion

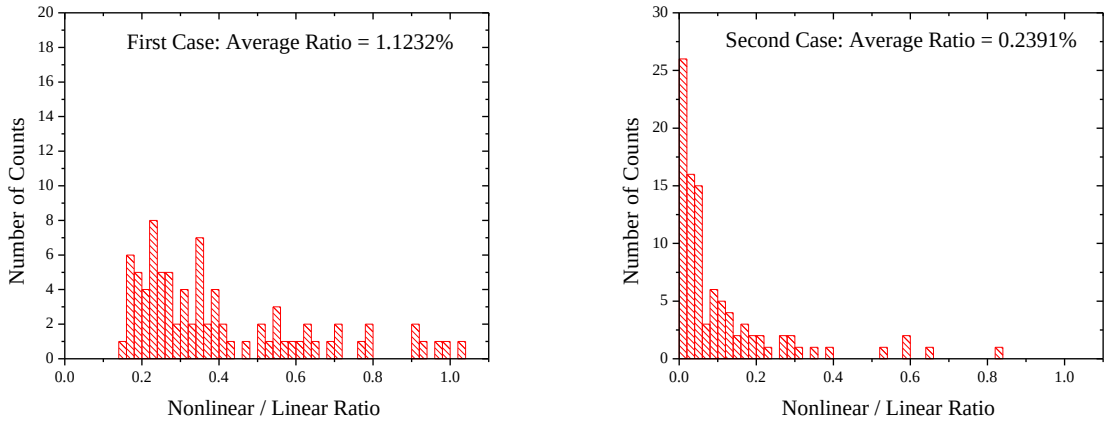

Figure 6-10. Comparison of Nonlinear/Linear Ratio

www.manaraa.com

CHAPTER 7. REDUCED ORDER REGRESSION ANALYSIS

Surrogate model can be constructed basically by assuming a certain functional form with some unknown features, e.g., expansion coefficients, and executing the original model at a set of points in the parameter space often referred to as a training set. The unknown surrogate features can then be identified via a minimization procedure that minimizes the discrepancies between the surrogate and original model's predictions for the training set. Despite their ease of implementation, all forward methods suffer from one major limitation; that is the so-called ***curse of dimensionality***. This 'curse' denotes that the computational cost increases exponentially with the number of input parameters. Adopting the reduced order modeling techniques, the input parameters are transformed into low dimension and then, the number of coefficients to be determined is reduced, which leads to the smaller number of training sets. Therefore, the surrogate modeling can be conducted with reduced computational overhead.

7.1 Proposed Method

Consider that the general Tensor-Free Expansion for the m^{th} response $R_m(\vec{x})$ around the reference configuration $\vec{x}_0$ is given by:

$$\Delta R_m(\vec{x}) = \sum_{k=1}^{\infty} \sum_{i_1,\ldots i_l,\ldots i_k=1}^{n} \psi_{i_1,m}^{(k)}\left(\vec{\beta}_{i_1,m}^{(k)T}\Delta\vec{x}\right)..\psi_{i_l,m}^{(k)}\left(\vec{\beta}_{i_l,m}^{(k)T}\Delta\vec{x}\right)..\psi_{i_k,m}^{(k)}\left(\vec{\beta}_{i_k,m}^{(k)T}\Delta\vec{x}\right) \qquad (7.1)$$

www.manaraa.com

The reduced order regression analysis can be two steps. First, the active subspace is extracted by examining the derivatives and then, a surrogate model is constructed with reduced input parameters. This procedure can be summarized as **Figure 7-1**. For multi-response problems, the procedure can be repeated for every response. On the other hands, by introducing a pseudo response [Bang & Abdel-Khalik, 2011a], the number of simulations to construct the basis vectors can be further reduced, i.e. the basis vectors for all responses are extracted simultaneously.

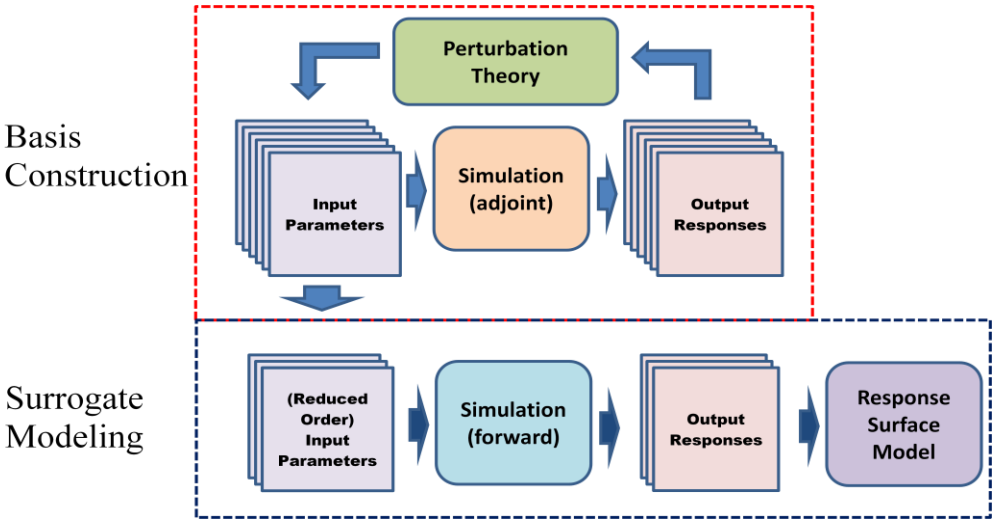

Figure 7-1. Schematic of Reduced Order Surrogate Modeling

For cases with very large number of input parameters, the reduced order input parameters may be still too large to construct a surrogate model by the existing methods. Note that for the second order regression analysis, the number of coefficients to be determined would be

www.manaraa.com

$\frac{(n+1)(n+2)}{2}$ and the required number of training sample sets are 2-3 times larger than the number of unknowns by rule of thumb. For example, consider that the number of the reduced order input parameters is 100. Then, the number of training sample sets would be more than 10,000, which may be impractical for expensive high-fidelity computer codes.

Instead of build a complete surrogate model by regression analysis, the multi-surrogate approach can be used [Bang and Abdel-Khalik (2012d)]. The basic idea is depicted in **Figure 7-2**. A response change can be considered as a sum of the linear component and the nonlinear component. Linear part can be captured by the first order Taylor expansion based on adjoint sensitivity analysis. Then, only the discrepancy between the original model and the first order estimation is fitted by the reduced order regression analysis, i.e. nonlinear reduced order surrogate model. One can consider that the nonlinear model is a correction model of the linear surrogate model.

Note that the major parameter variations can be captured by the first a few basis vectors. Considering more basis vectors produces more accurate representation of the input parameter variations, the accuracy improvement rate would be saturated. The main idea of the multi-surrogate approach is based on the observations that the effect of the nonlinear behavior, i.e. higher order terms, is relatively small compared to the linear portion. Therefore, the error due to insufficient basis vectors for higher order surrogate would be damped by the portion of the nonlinearity. This can be illustrated by an example. Consider that a response change is the sum of 90% linear part and 10% nonlinear part, i.e. higher order terms. If there is 10% error in the nonlinear part, the error in the response estimation would be only 1%. This implies that

www.manaraa.com

the higher order terms can be reduced further depending on the nonlinearity. The tolerance for reduced order modeling ε_{tol} should be determined by considering this point.

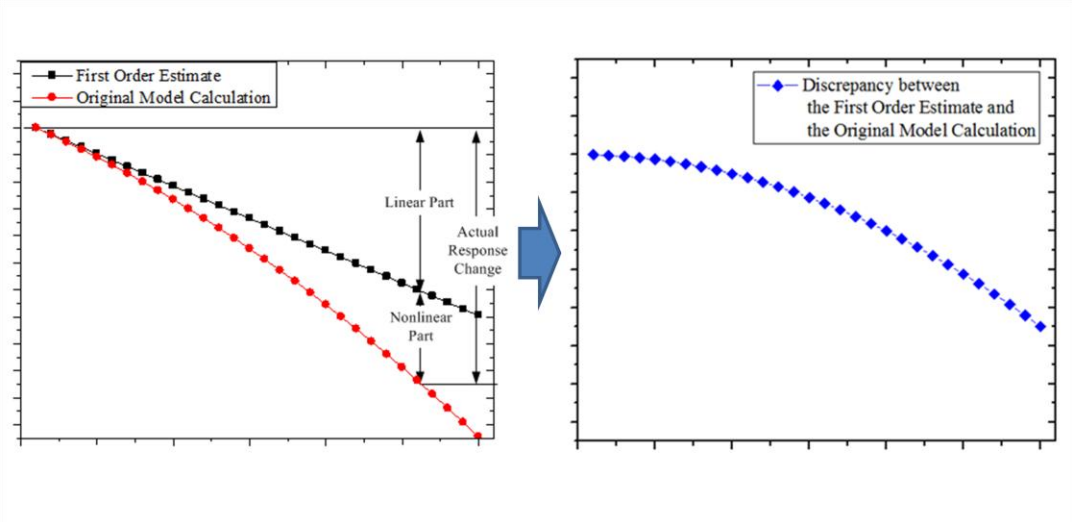

Figure 7-2. Schematic of the Multi-Surrogate Method

The RO regression analysis method is summarized as follows:

Algorithm: Reduced Order Regression Analysis Method

Consider that the Tensor-Free expansion of multi-valued response, i.e.

$\vec{R}(\vec{x}) = \left(R_1(\vec{x}) \quad ... \quad R_M(\vec{x})\right)^T$ around $\vec{x}_0$:

$$R_m\left(\vec{x}+\Delta\vec{x}\right) - R_m\left(\vec{x}_0\right) = \sum_{k=1}^{\infty} \sum_{i_1,...i_l,...i_k=1}^{n} \psi_{i_1,m}^{(k)}\left(\vec{\beta}_{i_1,m}^{(k)T}\Delta\vec{x}\right)..\psi_{i_l,m}^{(k)}\left(\vec{\beta}_{i_l,m}^{(k)T}\Delta\vec{x}\right)..\psi_{i_k,m}^{(k)}\left(\vec{\beta}_{i_k,m}^{(k)T}\Delta\vec{x}\right) \quad \text{for}$$

$$m = 1,...,M$$

where $\vec{x} = \left(x^1 \quad ... \quad x^n\right)^T$ is a vector of n input parameters which is given by $\vec{x} = \vec{x}_0 + \Delta\vec{x}$, $\vec{x}_0$ denote the reference values for the input parameters, $\Delta\vec{x}$ is a vector of input parameter variation from the $\vec{x}_0$, $\beta_{i_l,m}^{(k)} \in \mathbb{R}^n$ is a coefficient vector and $\psi_{i_l,m}^{k}$ is a

www.manaraa.com

scalar function depending on an assumed surrogate model form. This algorithm requires running the forward model and the adjoint model $r+s$ times to construct the basis of the active subspace, where r is the user's estimate of the rank, and s are oversamples needed to check whether the user-defined tolerance is met. For all practical purposes, s is a small integer, e.g., $s=10$. Once the input parameters are transformed into low dimension, a surrogate model can be constructed with reduced cost by utilizing the training sample sets generated by the original forward model.

Step 1) Build a pseudo response $R_{pseudo}^{(i)}=\sum_{m=1}^{M}R_m w_m^{(i)}$ for $i=1,...,r+s$

where R_m is the m^{th} response, $w_m^{(i)}$ is a randomly generated coefficient.

Step 2) Perturb input parameters as follows: $\vec{x}^{(i)}=\vec{x}_0+\Delta\vec{x}^{(i)}$ for $i=1,...,r+s$

Step 3) DO $i=1,2,...,r+s$,

compute $\nabla R_{pseudo}^{(i)}$ (first order derivatives at perturbed inputs $\vec{x}^{(i)}$)

END DO

Step 4) Set $j=0$ and $\mathbf{Q}_0=[\ ]$, the $n\times 0$ empty matrix

Step 5) $j=j+1$

Step 6) $\vec{U}^{(j)}\leftarrow\left(\mathbf{I}-\mathbf{Q}_{j-1}\mathbf{Q}_{j-1}^T\right)\vec{U}^{(j)}$

Step 7) $\vec{q}_j=\vec{U}^{(j)}/\left\|\vec{U}^{(j)}\right\|$

Step 8) $\mathbf{Q}_j=\left[\mathbf{Q}_{j-1}\quad\vec{q}_j\right]$

Step 9) Compute $\vec{z}^{(i)}=\left(\mathbf{I}-\mathbf{Q}_j\mathbf{Q}_j^T\right)\vec{U}^{(r+i)}$, $i=1,...,s$

Step 10) If $\max\left\{\left\|\vec{z}^{(1)}\right\|,\left\|\vec{z}^{(2)}\right\|,...,\left\|\vec{z}^{(s)}\right\|\right\}<\varepsilon$, go to Step 11,

else increases r and go back to Step 1

Step 11) $\mathbf{Q}=\mathbf{Q}_j$ and rank $r=j$

www.manaraa.com

Step 12) Generate the training sample set paired by

$$\left(\vec{x}^{(i)}, R_m^{(i)}\right) \text{ for } i = 1,\ldots,\frac{(r+1)(r+2)}{2}\times 2 \text{ or } 3 \quad \text{and } m = 1,\ldots,M$$

Step 13) Determine the reduced order coefficients and construct the surrogate model

$$R\left(\vec{x}_0 + \Delta\vec{x}\right) - R\left(\vec{x}_0\right)$$
$$= \sum_{k=1}^{\infty} \sum_{i_1,\ldots i_l,\ldots i_k=1}^{n} \psi_{i_1}^{(k)}\left(\vec{\beta}_{i_1}^{(k)T}\mathbf{Q}\mathbf{Q}^T\Delta\vec{x}\right)..\psi_{i_l}^{(k)}\left(\vec{\beta}_{i_l}^{(k)T}\mathbf{Q}\mathbf{Q}^T\Delta\vec{x}\right)..\psi_{i_k}^{(k)}\left(\vec{\beta}_{i_k}^{(k)T}\mathbf{Q}\mathbf{Q}^T\Delta\vec{x}\right)$$

Step 14) Generate the test sample set paired by $\left(\vec{x}^{(i)}, R_{m,actual}^{(i)}\right)$ for $i = 1,\ldots,N$ and $m = 1,\ldots,M$

Step 15) Compute the surrogate estimation by the test sample set

$$\left(\vec{x}^{(i)}, R_{m,estimate}^{(i)}\right) \text{ for } i = 1,\ldots,N \quad \text{and } m = 1,\ldots,M$$

Step 16) Compare the surrogate estimation $R_{m,estimate}^{(i)}$ to the original model calculation $R_{m,actual}^{(i)}$

7.2 Numerical Test

Problem Description

The reduced order regression approach is implemented to estimate the state variable (i.e. fluxes) change due to input parameter variation (i.e. reaction cross sections). The mixture flux estimated in this study is defined as:

$$\vec{\phi}_m^g = \sum_{i\in m}^{M} \vec{\phi}_i^g V_i \tag{7.2}$$

www.manaraa.com

where $\vec{\phi}_i^g$ is the flux in cell i and energy group g, V_i is the volume of the cell i, and M is the total number of cells. Therefore, the mixture flux is use for calculating any quantity related to the mixture. Note that the cell flux $\vec{\phi}_i^g$ is calculated by integrating the angular flux in Eq. (6.10) by angle and volume.

Implementation

The reduced order regression algorithm explained in the previous chapter is implemented. For calculating the first order derivatives, TSUNAMI-2D control module of SCALE6.1 can be used. TSUNAMI-2D control module generates the input files for resonance calculation module (e.g. NITAWL or CENTRM), transport solver (i.e. NEWT for forward and adjoint mode) and sensitivity calculation module (i.e. SAMS). The SAMS calculates the sensitivity coefficients (i.e. relative first order derivative) of self-shielded macroscopic cross with respect to user-defined responses. Note that the released TSUNAMI-2D supports only ratio type (e.g. reaction rate ratio) as a response. For this study, NEWT and SAMS are modified to support a linear type response (i.e. reaction rate) and verified in a systematic way [Bang & Abdel-Khalik, 2011c]. For testing the reduced order regression algorithm, the working library for self-shielded macroscopic cross sections is perturbed and NEWT (fundamental forward) – NEWT (fundamental adjoint) – NEWT (GPT adjoint) – SAMS sequences are performed to calculate the perturbed sensitivity coefficients. **Figure 7-3** depicts the model analyzed; it is a stand-alone benchmark model designed by OECD/NEA to assess the assumptions in current LWR standard lattice physics scheme for generation of few-group

www.manaraa.com

cross-sections [Ivanov et al. (2007)]. The 44 energy group library (v5-xn44) of SCALE6.1 is used and the reference k_{eff} is 1.08383475. With the perturbed self-shielded macroscopic cross sections $\vec{\Sigma}$ and the resulting sensitivity coefficients $\vec{S}$, the regression analysis and all subsequent calculations are conducted by using MATLAB 2011a.

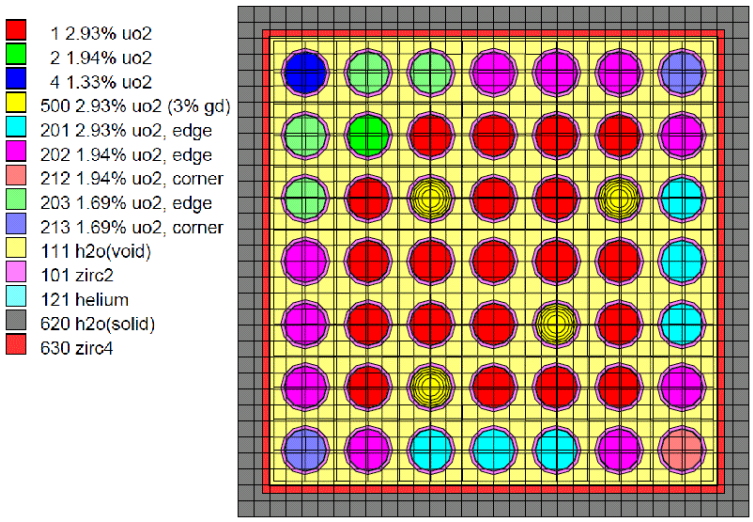

Figure 7-3. A 7x7 BWR Benchmark Assembly Model

The fission cross sections of four nuclides (i.e. U-234, U-235, U-236 and U-238) in 44 energy group in 9 fuel mixtures are perturbed by $\pm 30\%$ from uniform distribution, i.e. the dimension of input parameters is $\mathbb{R}^{1584}$. The responses are chosen to the mixture fluxes in the fuel mixture 1, i.e. the dimension of input parameters is $\mathbb{R}^{44}$. Note that the SAMS calculates the relative sensitivity coefficient, i.e. $\frac{\vec{\Sigma}}{R_i}\frac{\partial R_i}{\vec{\Sigma}}$. Therefore, if a pseudo response is built with randomly generated $\vec{w}$, the basis vectors are scaled by the magnitude of the response:

www.manaraa.com

$$\frac{\partial R_{pseudo}}{\partial \vec{\Sigma}} = \left(w_1 \frac{\partial R_1}{\partial \vec{\Sigma}} + \cdots + w_M \frac{\partial R_M}{\partial \vec{\Sigma}} \right)$$
$$\Rightarrow \frac{\vec{\Sigma}}{R_{pseudo}} \frac{\partial R_{pseudo}}{\partial \vec{\Sigma}} = \frac{\vec{\Sigma}}{R_{pseudo}} \left(w_1 \frac{\partial R_1}{\partial \vec{\Sigma}} + \cdots + w_M \frac{\partial R_M}{\partial \vec{\Sigma}} \right) \tag{7.3}$$
$$= w_1 \frac{R_1}{R_{pseudo}} \left(\frac{\vec{\Sigma}}{R_1} \frac{\partial R_1}{\partial \vec{\Sigma}} \right) + \cdots + w_M \frac{R_M}{R_{pseudo}} \left(\frac{\vec{\Sigma}}{R_M} \frac{\partial R_M}{\partial \vec{\Sigma}} \right)$$

In order to capture all active subspace of responses properly, the random coefficient are weighted by the magnitude of the response value, i.e.:

$$w_m = \frac{\hat{w}_m}{R_m} \tag{7.4}$$

where $\hat{w}_m$ is randomly generated from 0 to 1. To estimate the accuracy of the second order approximation, the test sets are generated and the responses calculated by the original model, i.e. NEWT, and first order estimation are compared.

Results

The singular value spectrum of the pseudo response sensitivity coefficients are shown in **Figure 7-4**. Considering the precision of the data used in this study, i.e. single precision, the components associated to singular values smaller than 10^{-5} are easy to be contaminated by numerical error, e.g. rounding error, and the impact on the response changes are negligible; therefore, in view of transforming the input parameter to low dimension, the number of basis vectors should be large enough up to the singular value index corresponding to singular value 10^{-5}. However, those numbers, i.e. more than 400, are too large to be practical to generate the training sample sets for regression analysis.

www.manaraa.com

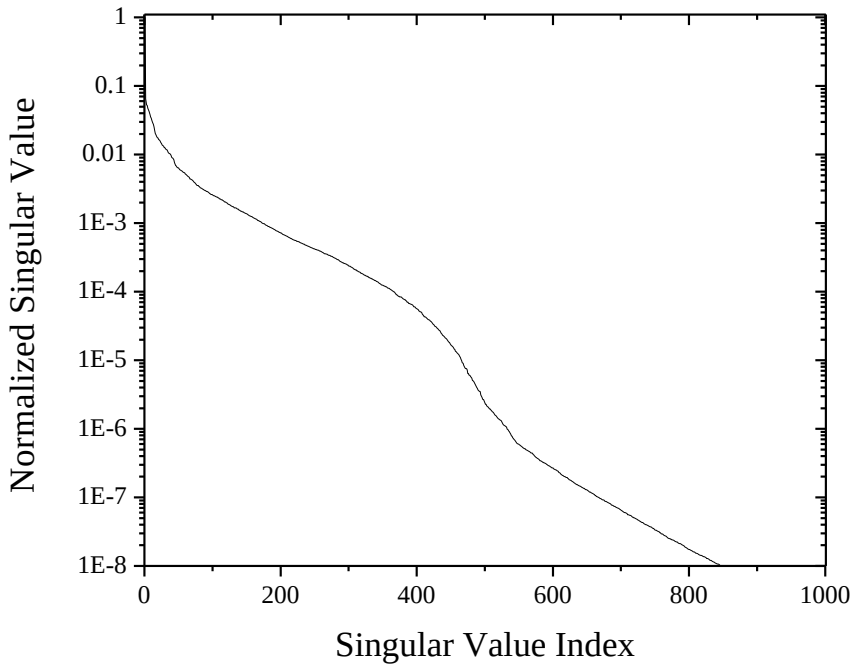

Figure 7-4. Singular Value Spectrum of Pseudo Response Sensitivity Vectors (Regression Analysis, $\vec{\Sigma} \in \mathbb{R}^{1584}$)

To estimate the nonlinearity of the problem, the NL ratios (see Eq. (6.26)) of each response for 100 test sample sets are compared in **Figure 7-5** and **Figure 7-6**. Note that because the second case described in the **Figure 7-2** increases the NL ratio severely, investigating that averaging values of the NL ratio may mislead the nonlinearity; thus, the distribution, i.e. histogram, is also checked. Note that in the histograms in **Figure 7-6**, very large NL ratios (outliers) are not included. As shown in the graphs, the linear components of

www.manaraa.com

the response changes are much greater than the nonlinear components, i.e. for all responses, the NL ratios are smaller than 0.3 in more than 50% of the test cases.

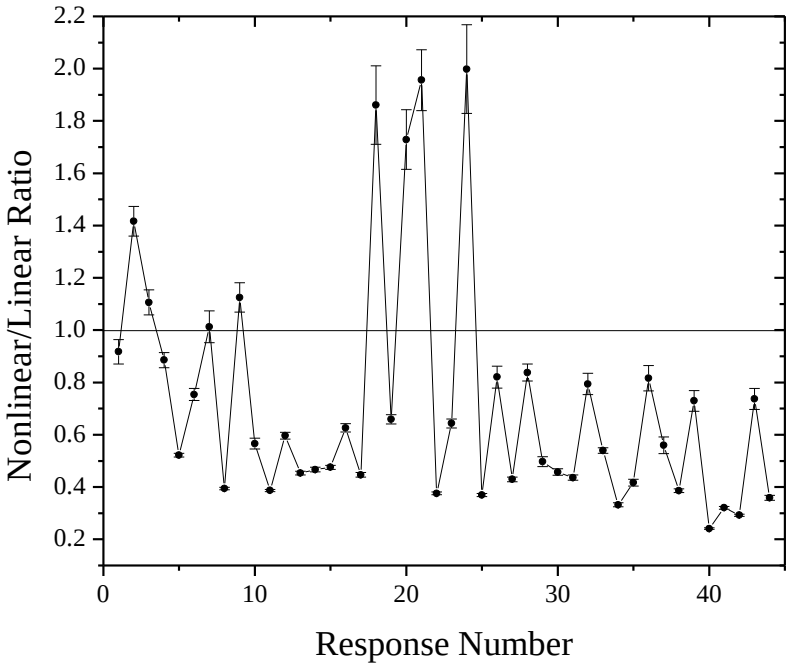

Figure 7-5. Comparison of the Nonlinear/Linear Ratio
(Regression Analysis, $\vec{\Sigma} \in \mathbb{R}^{1584}$)

www.manaraa.com

Figure 7-6. Comparison of Nonlinear/Linear Ratio

(Regression Analysis, $\vec{\Sigma} \in \mathbb{R}^{1584}$)

www.manaraa.com

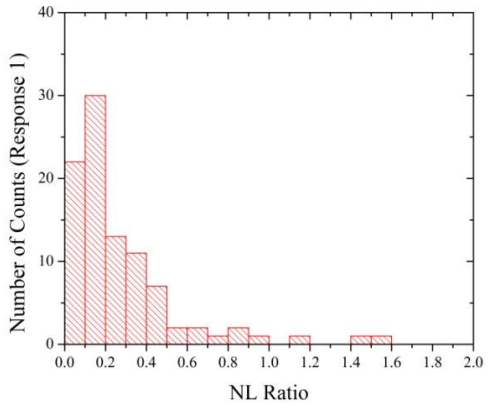

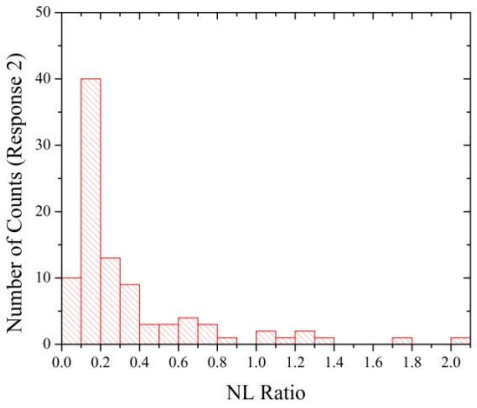

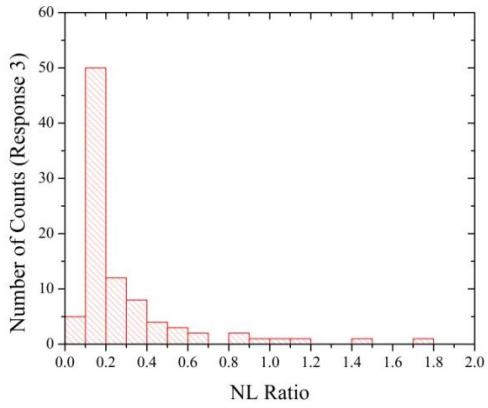

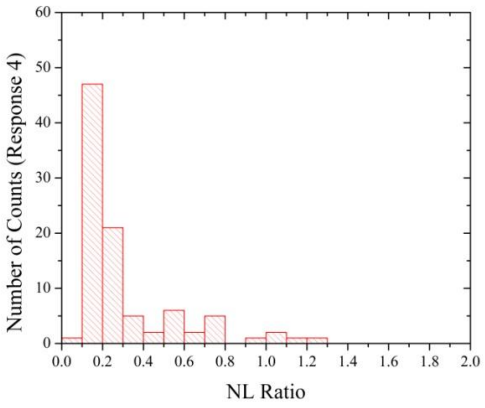

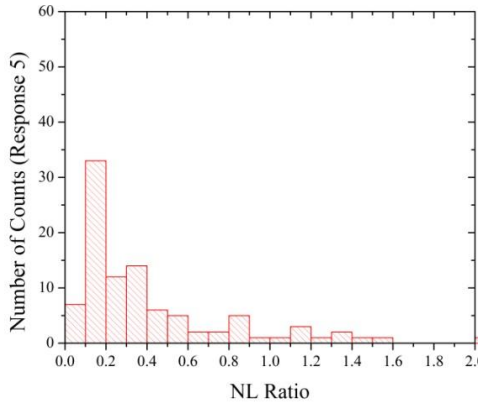

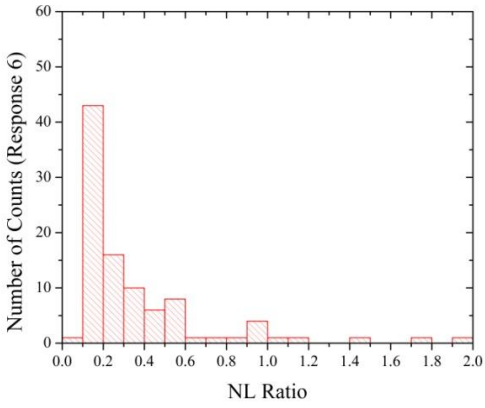

www.manaraa.com

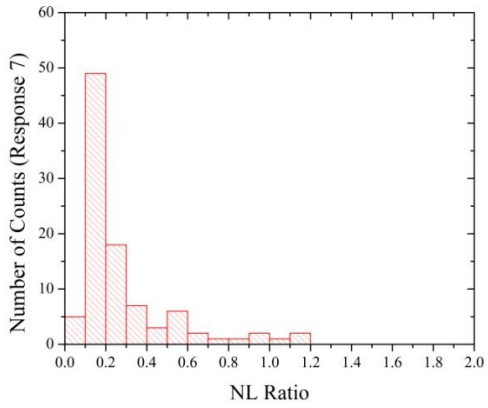

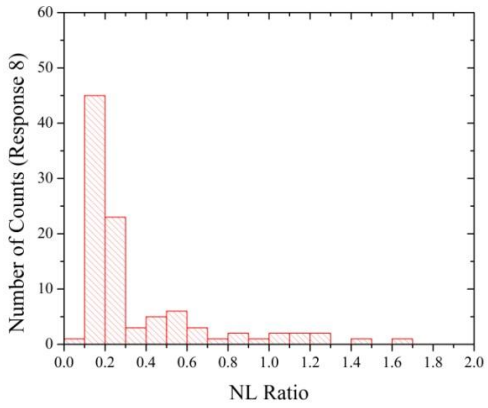

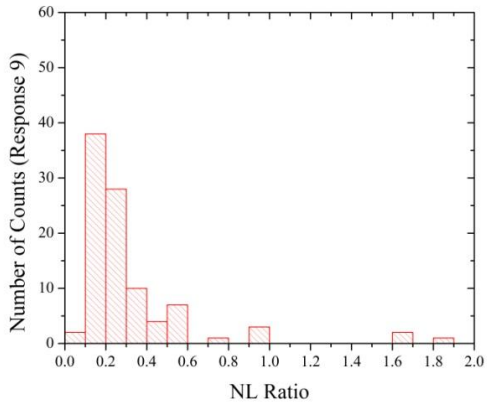

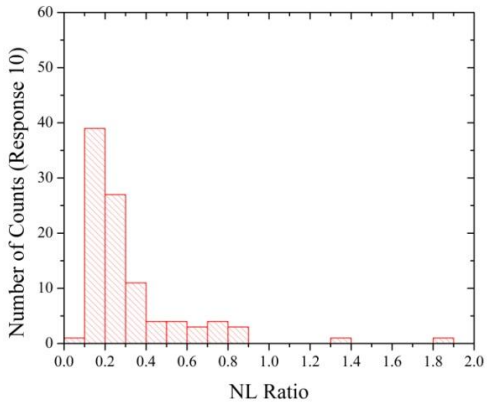

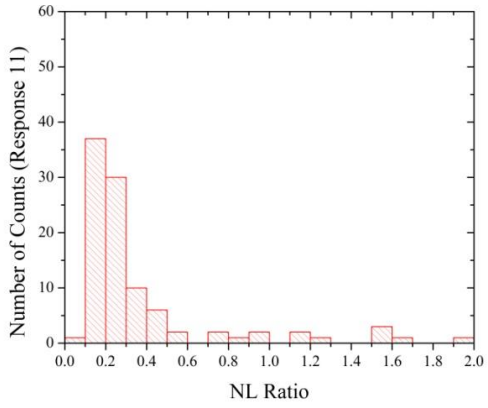

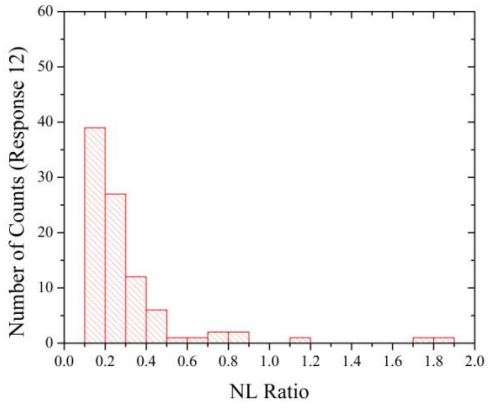

www.manaraa.com

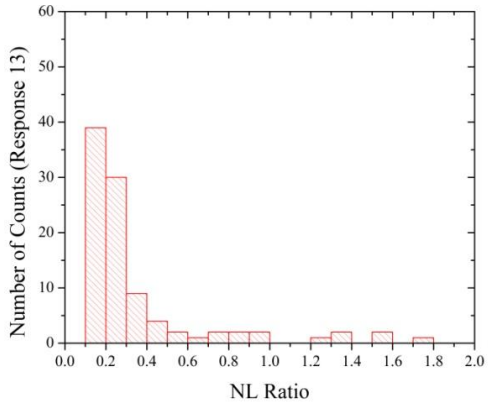

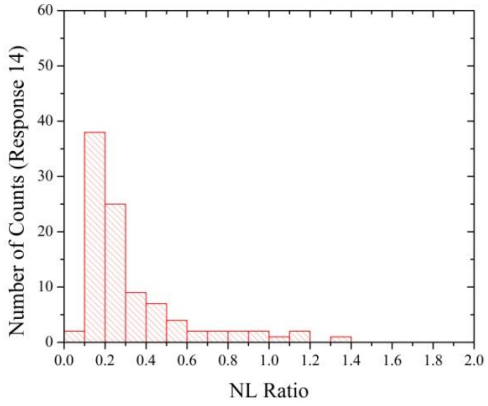

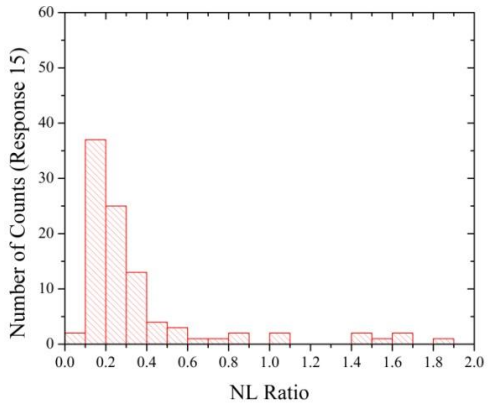

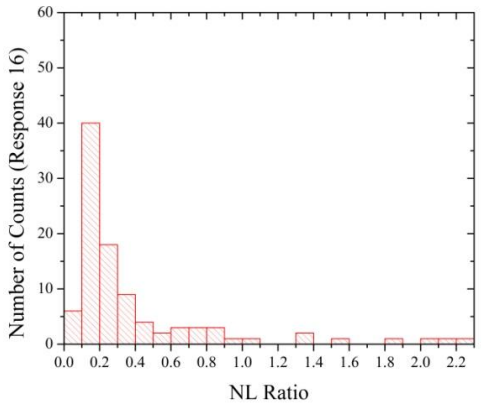

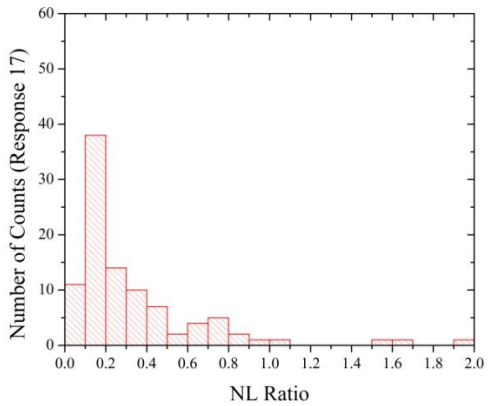

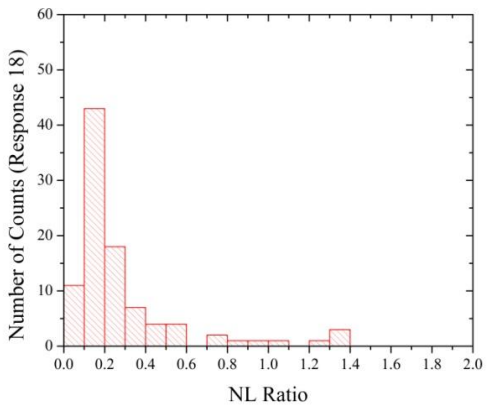

www.manaraa.com

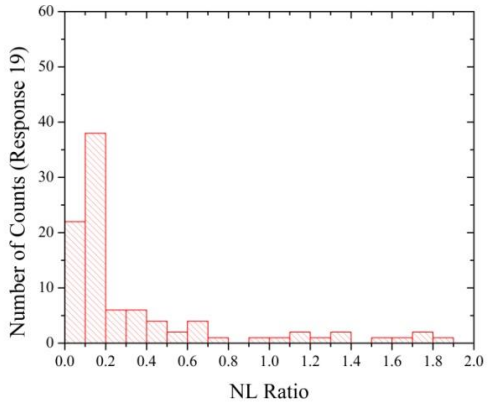

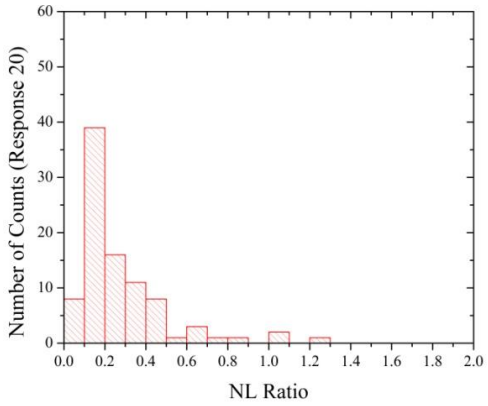

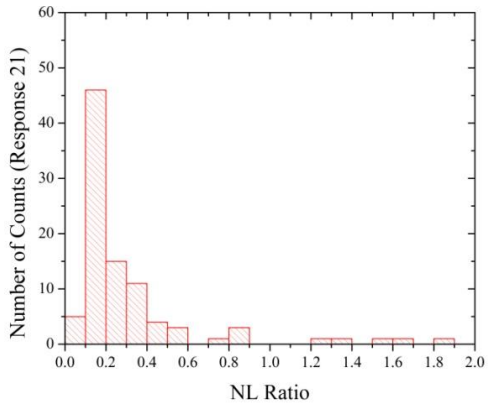

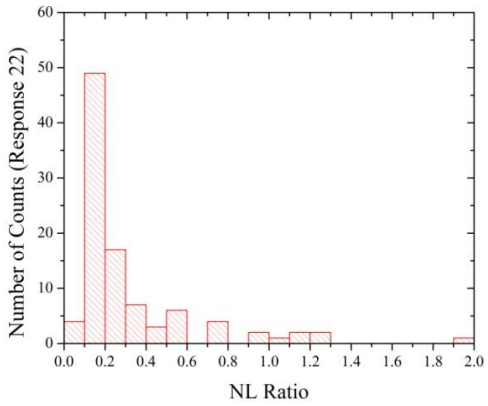

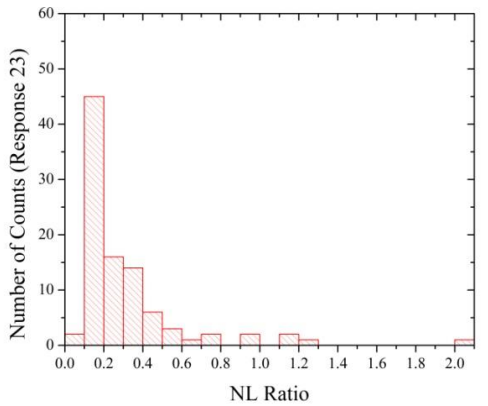

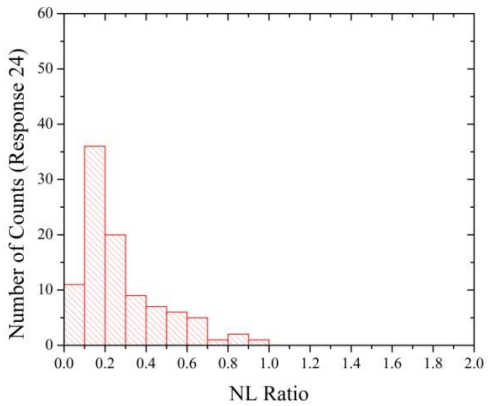

www.manaraa.com

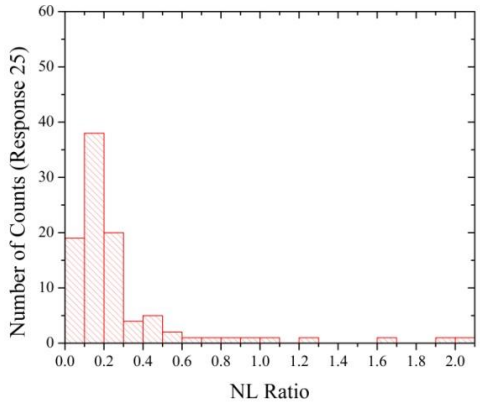

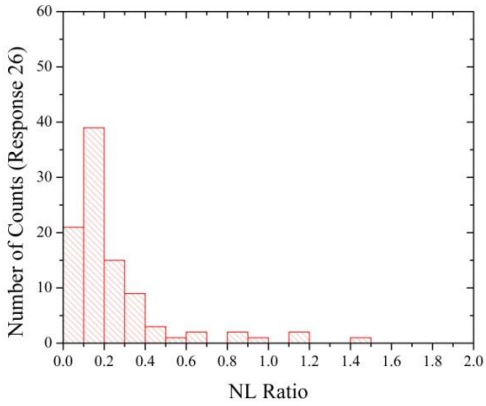

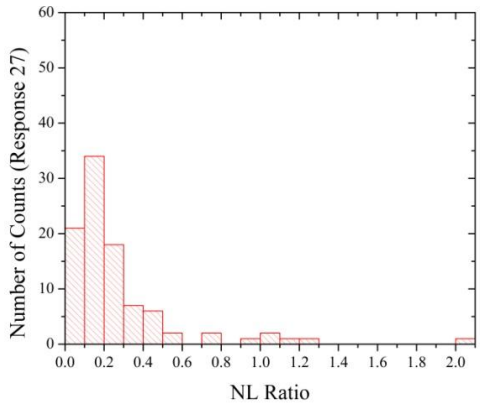

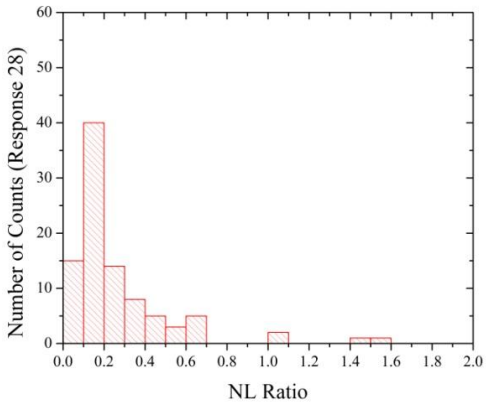

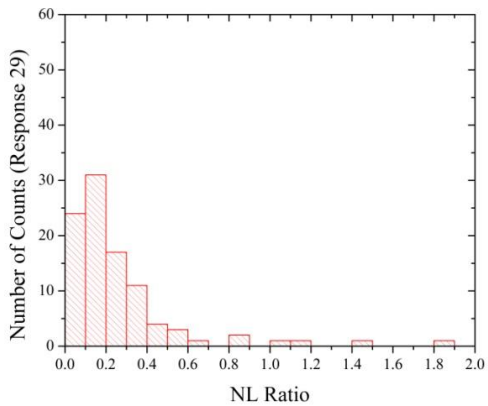

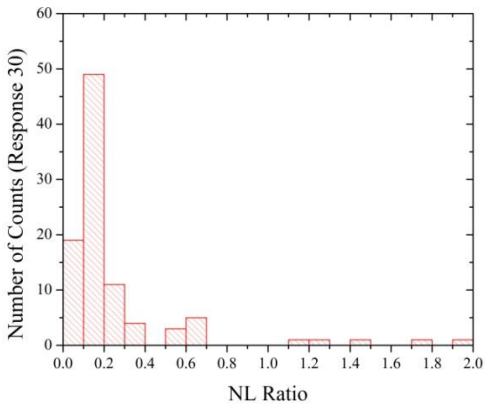

www.manaraa.com

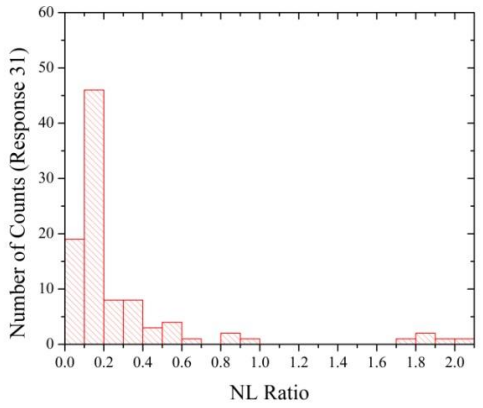

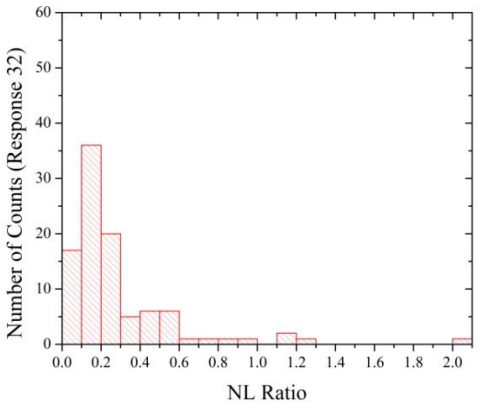

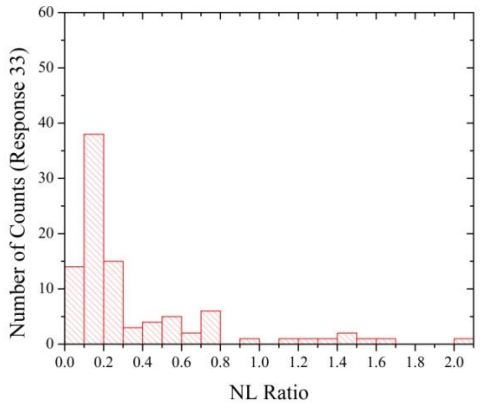

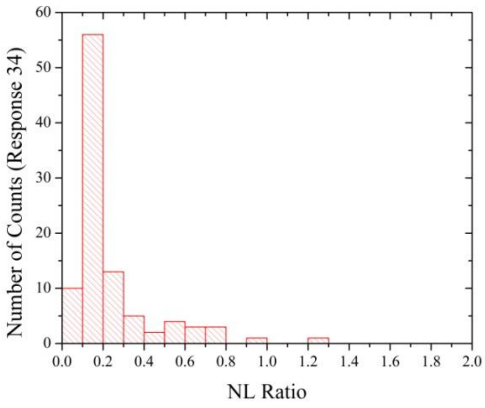

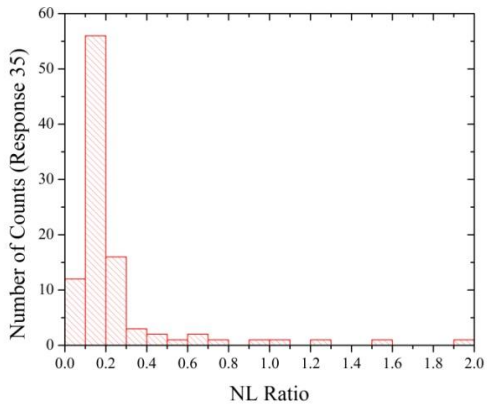

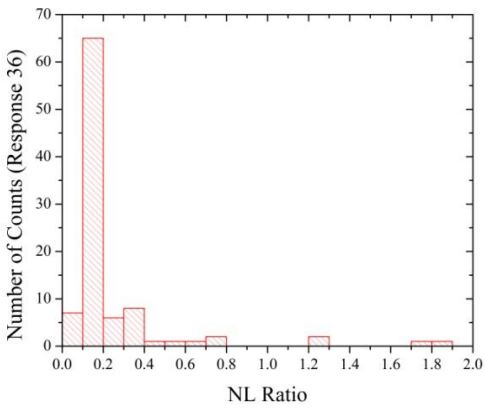

www.manaraa.com

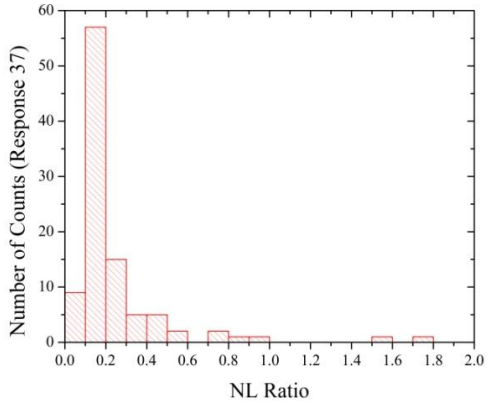

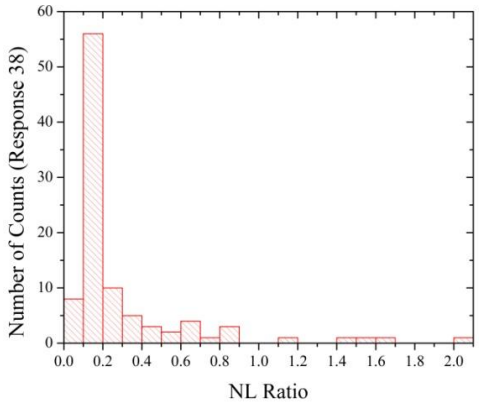

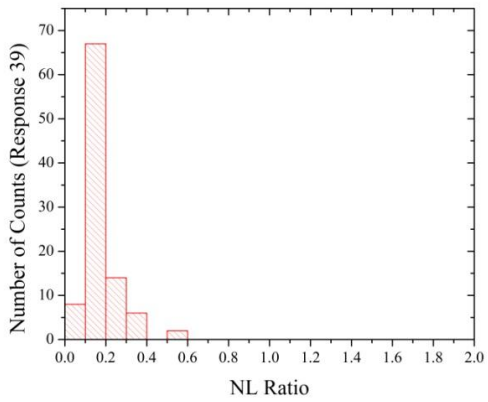

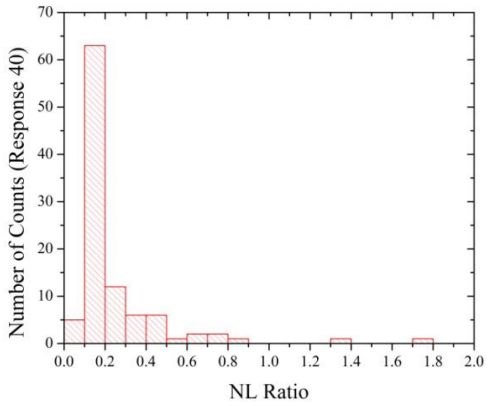

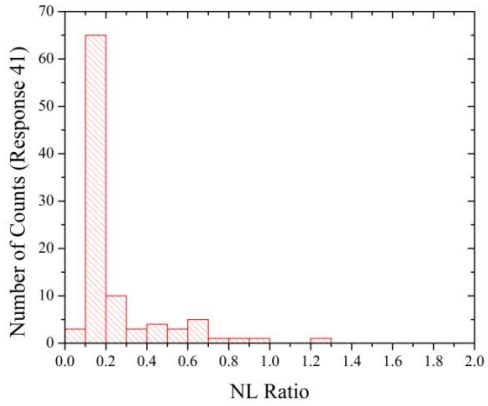

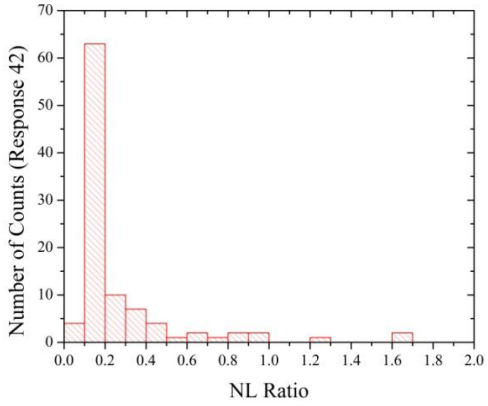

www.manaraa.com

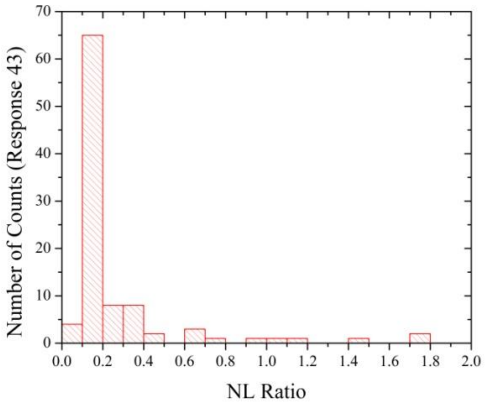

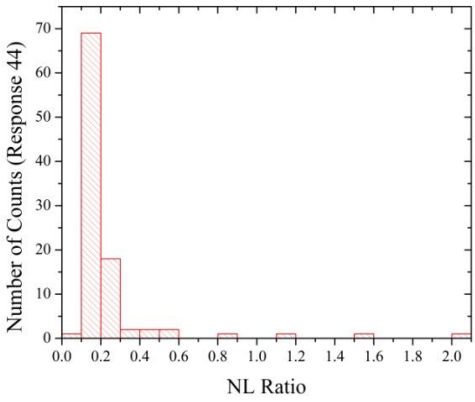

www.manaraa.com

As described in the previous chapter, the linear component is estimated by the adjoint sensitivity analysis. For reduced order regression analysis, the discrepancies between the actual response changes and the adjoint based first order estimation are corrected by the second order polynomial regression analysis with reduced order modeling, i.e.:

$$\begin{aligned} R_m\left(\vec{\Sigma}\right) &= R_m\left(\vec{\Sigma}_0\right) + R_{m,linear}\left(\vec{\Sigma}\right) + R_{m,nonlinear}\left(\vec{\Sigma}\right) \\ R_{m,linear}\left(\vec{\Sigma}\right) &= \left(\left. \frac{\partial R_m}{\partial \vec{\Sigma}} \right|_{\vec{\Sigma}_0} \right)^T \left(\vec{\Sigma} - \vec{\Sigma}_0\right) \\ R_{m,nonlinear}\left(\vec{\Sigma}\right) &= \vec{\beta}_{m,1}^T \mathbf{Q}^T \left(\vec{\Sigma} - \vec{\Sigma}_0\right) + \left\{ \vec{\beta}_{m,2}^T \mathbf{Q}^T \left(\vec{\Sigma} - \vec{\Sigma}_0\right) \right\}^2 \end{aligned} \tag{7.5}$$

where $\vec{\beta}_{m,1}, \vec{\beta}_{m,2} \in \mathbb{R}^r$ and $\mathbf{Q} \in \mathbb{R}^{n \times r}$. Two different number of basis vectors are tested; $r = 30$ and $r = 50$. As training sets, the 1000 and 3000 sample sets generated by Latin-Hypercube sampling (LHS) are used for $r = 30$ and $r = 50$, respectively. The coefficients are determined by least square method and the regularization factor is 10^{-5}. To measure the accuracy of the RO multi-surrogate method, i.e. second order approximation, 100 test sample sets are generated randomly and R^2 values are compared in **Table 7-1**. As can be seen, the second order approximations improve the estimation accuracy. Note that as the number of basis vectors increases, the accuracy is improved. To check the estimation accuracy according to the magnitude of the input parameter perturbation, the base perturbation is generated by ± 1% from uniform distribution and increases by multiplying integer values up to 30. The results are shown in **Figure 7-7**. The first order approximation loses the accuracy as the perturbation increases, while the second order approximation captures the nonlinear behavior. Note that the more basis vectors are included, the more accurate estimation can be expected.

www.manaraa.com

Table 7-1. R^2 Value Comparison of Reduced Order Regression Approach

Response No.	First Order Approx.	Second Order Approx.		Response No.	First Order Approx.	Second Order Approx.	
		r=30	*r*=50			*r*=30	*r*=50
1	0.97266	0.99281	0.99712	23	0.97325	0.99864	0.99953
2	0.97705	0.99644	0.99860	24	0.97797	0.99897	0.99960
3	0.97387	0.99769	0.99911	25	0.98308	0.99890	0.99968
4	0.97108	0.99777	0.99904	26	0.98439	0.99916	0.99968
5	0.97300	0.99777	0.99912	27	0.98369	0.99907	0.99969
6	0.97123	0.99670	0.99901	28	0.98226	0.99885	0.99962
7	0.97410	0.99809	0.99920	29	0.98479	0.99899	0.99957
8	0.97217	0.99790	0.99914	30	0.98548	0.99893	0.99968
9	0.96957	0.99781	0.99912	31	0.98396	0.99874	0.99958
10	0.96889	0.99807	0.99927	32	0.98113	0.99879	0.99963
11	0.96833	0.99820	0.99935	33	0.98244	0.99885	0.99963
12	0.96915	0.99833	0.99942	34	0.98256	0.99879	0.99957
13	0.96948	0.99836	0.99944	35	0.98443	0.99880	0.99971
14	0.96991	0.99841	0.99945	36	0.98407	0.99882	0.99972
15	0.97039	0.99845	0.99945	37	0.98317	0.99844	0.99959
16	0.97341	0.99864	0.99953	38	0.98316	0.99835	0.99945
17	0.97700	0.99872	0.99955	39	0.98336	0.99845	0.99947
18	0.97918	0.99897	0.99961	40	0.98198	0.99824	0.99934
19	0.98472	0.99918	0.99968	41	0.98177	0.99650	0.99941
20	0.97263	0.99865	0.99953	42	0.98046	0.99728	0.99937
21	0.97371	0.99869	0.99954	43	0.97959	0.99645	0.99938
22	0.97461	0.99872	0.99955	44	0.97460	0.99557	0.99938

www.manaraa.com

Figure 7-7. Comparison of Estimation Accuracy

(Regression Analysis, $\vec{\Sigma} \in \mathbb{R}^{1584}$)

www.manaraa.com

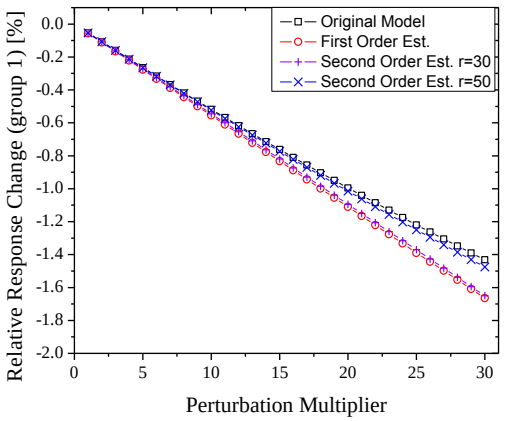

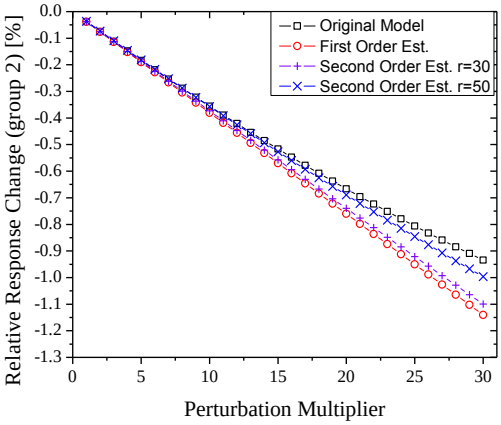

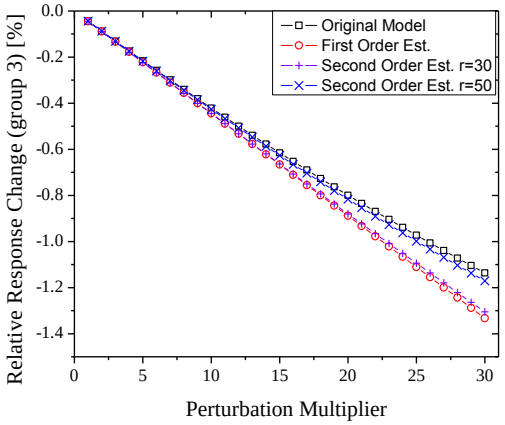

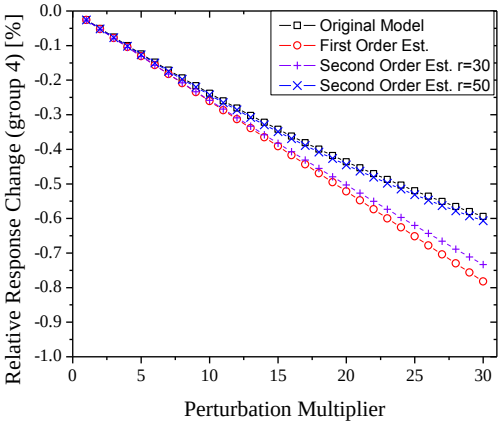

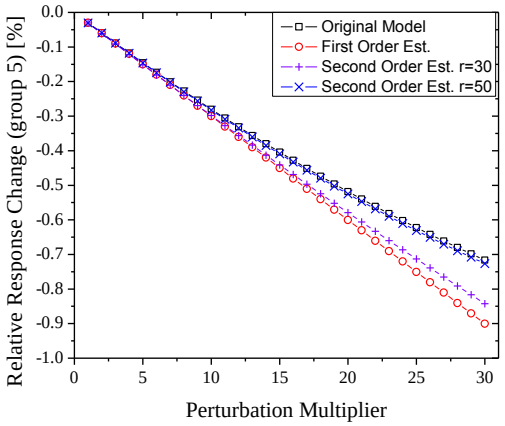

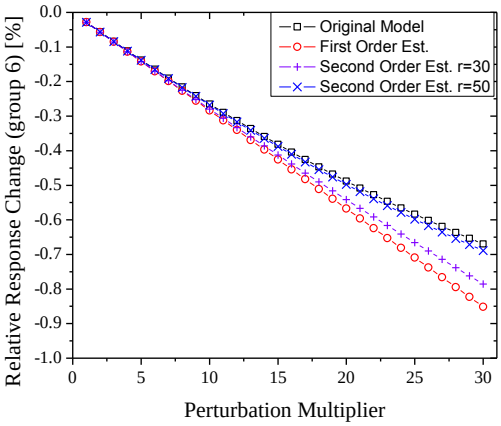

www.manaraa.com

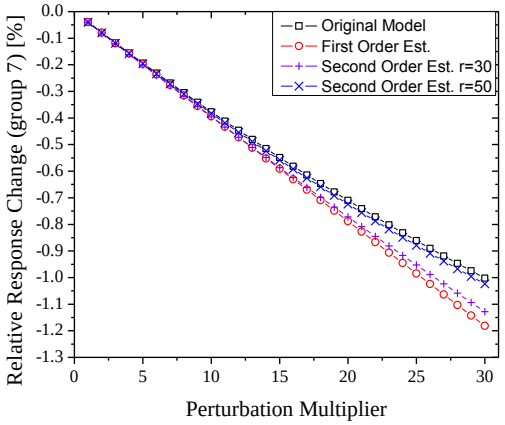

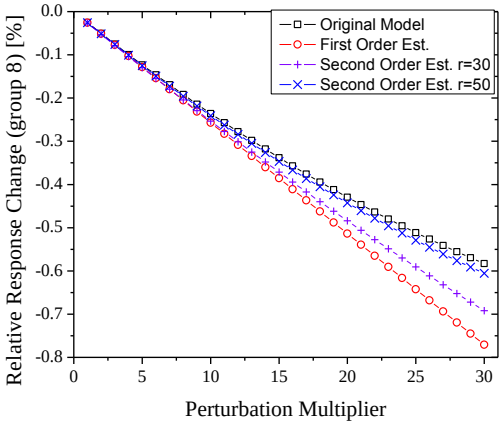

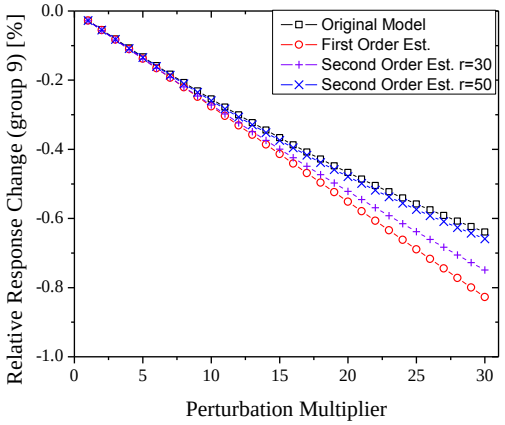

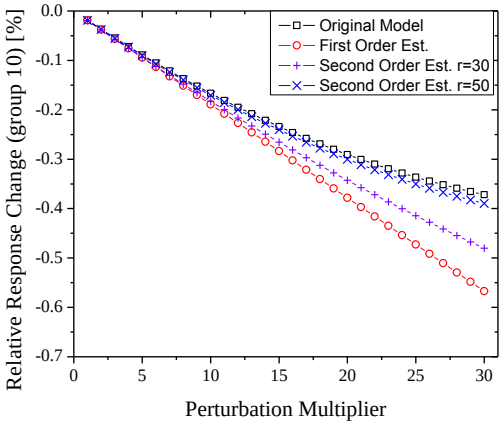

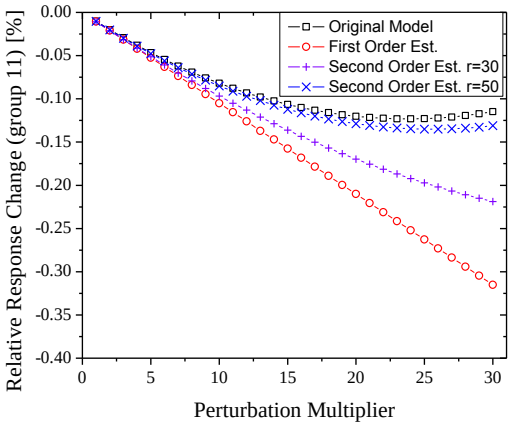

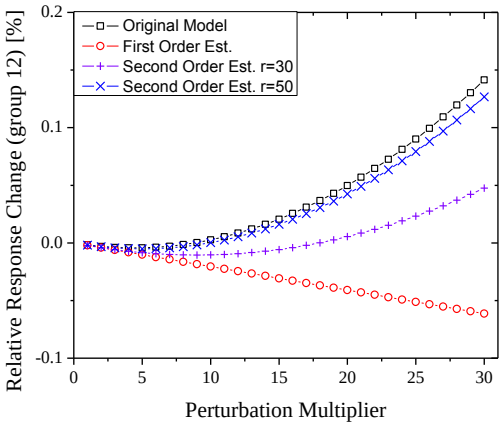

www.manaraa.com

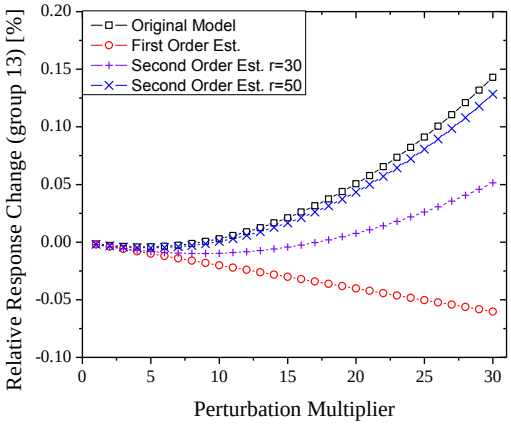

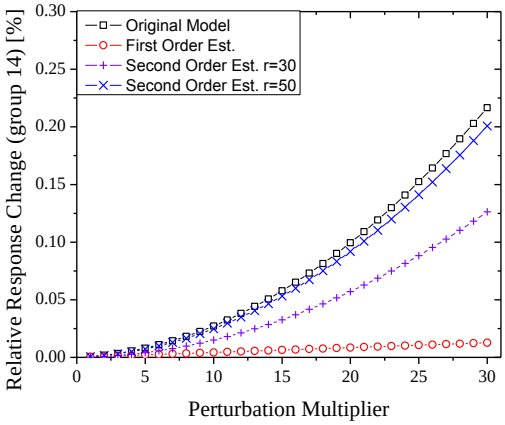

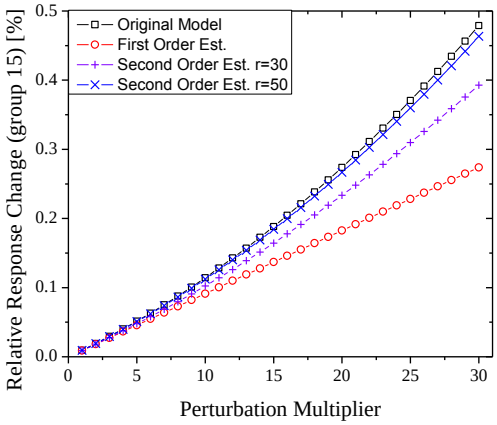

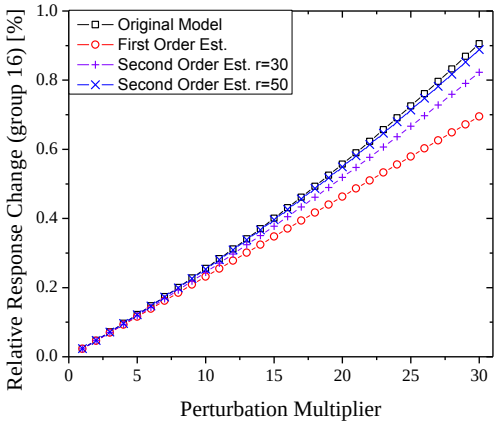

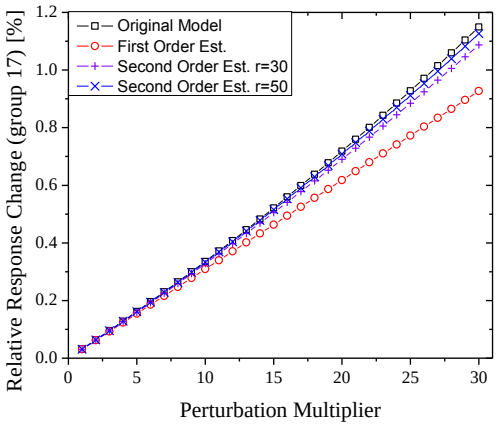

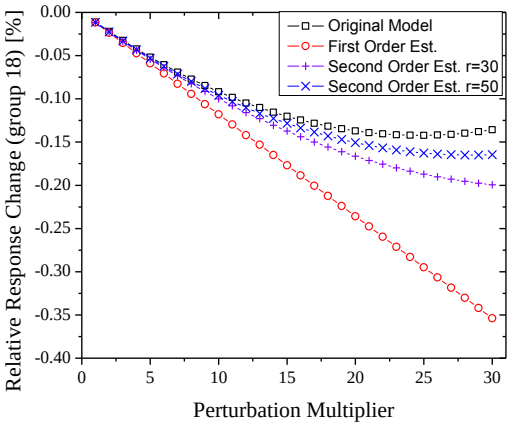

www.manaraa.com

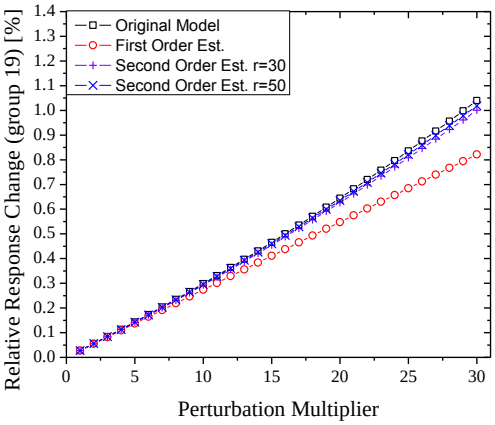

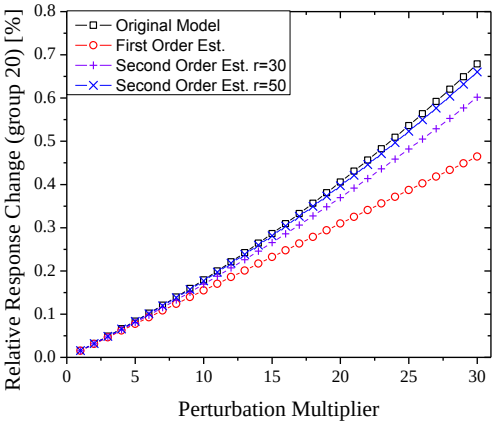

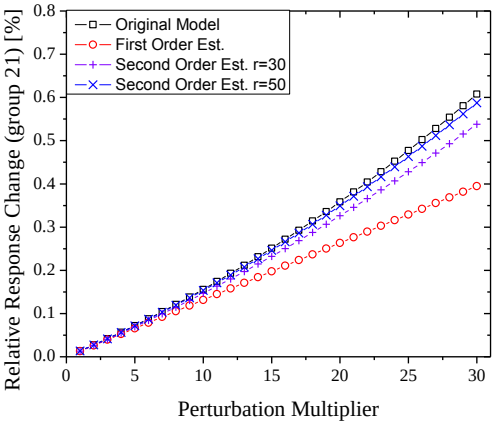

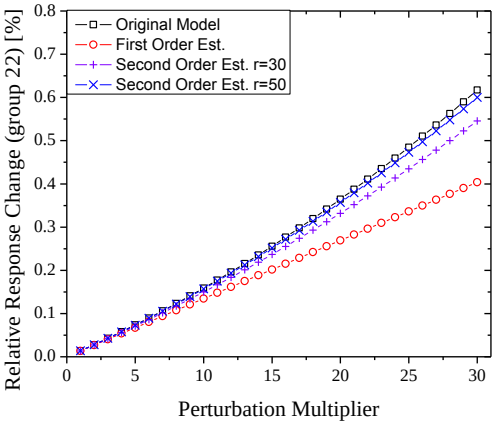

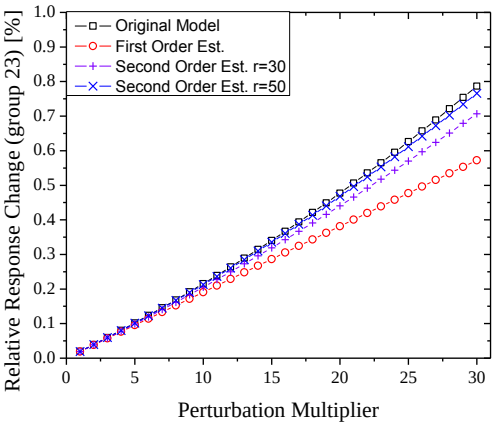

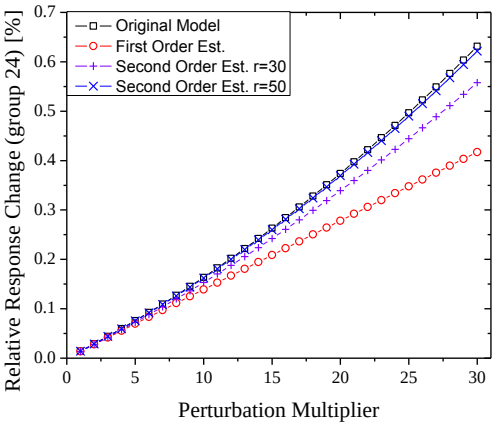

www.manaraa.com

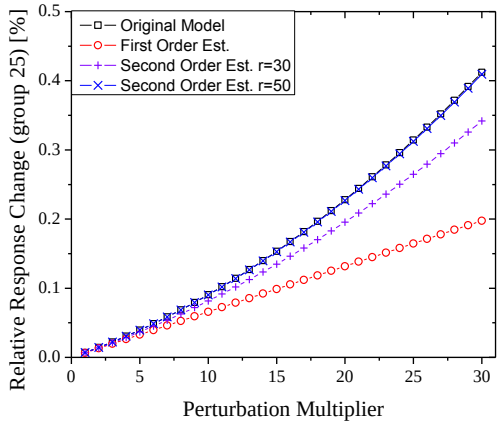

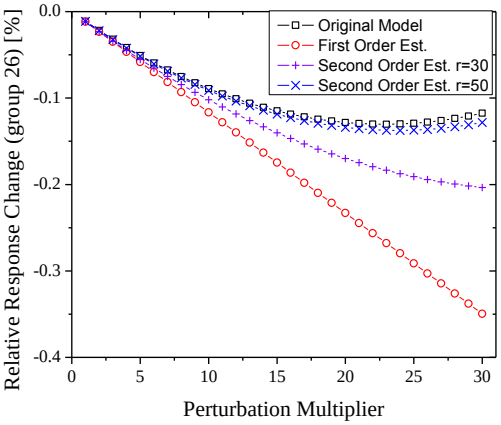

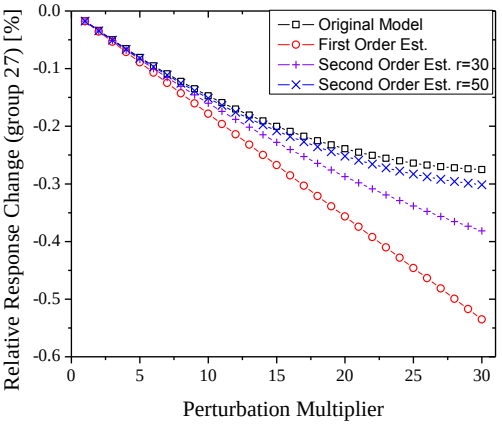

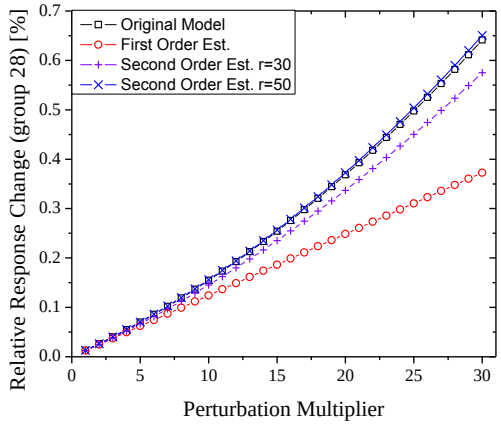

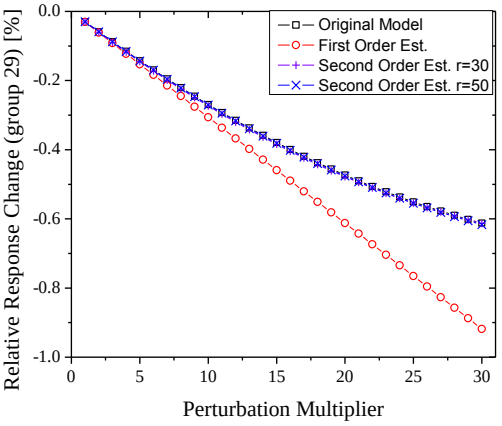

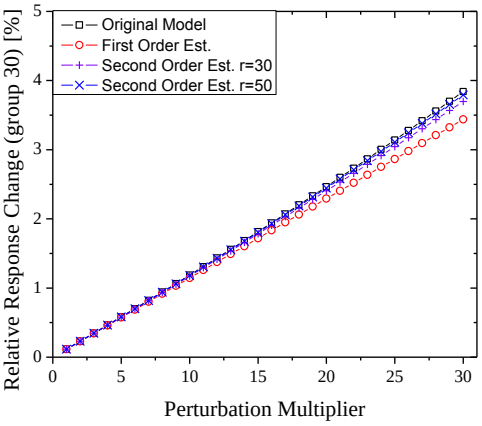

www.manaraa.com

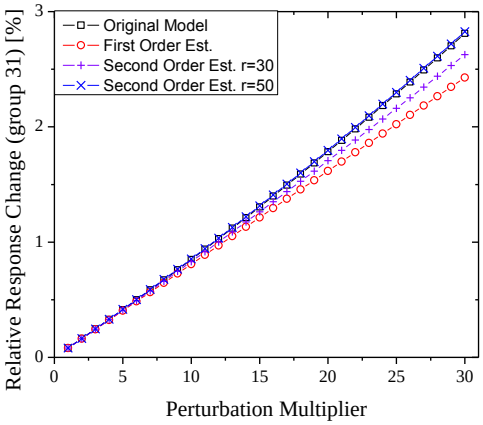

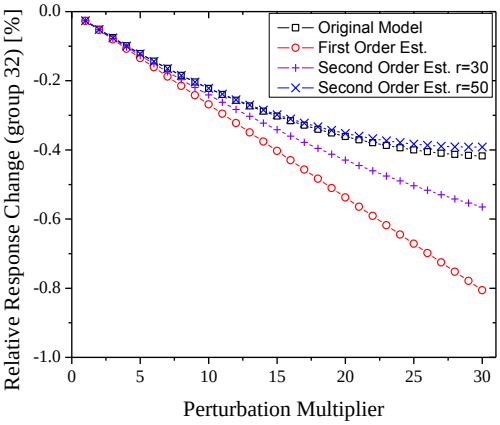

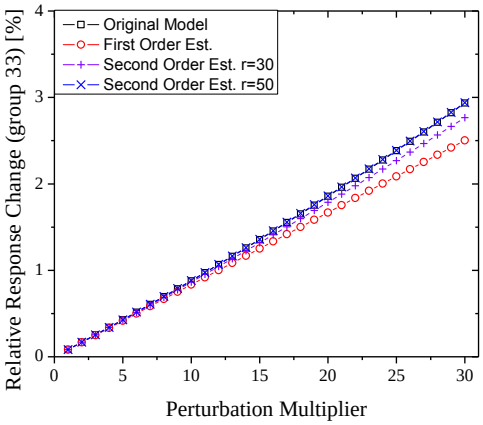

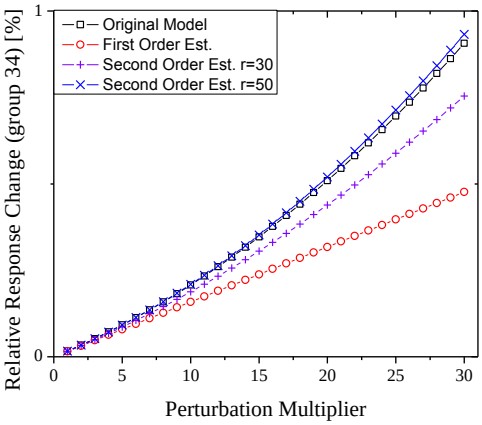

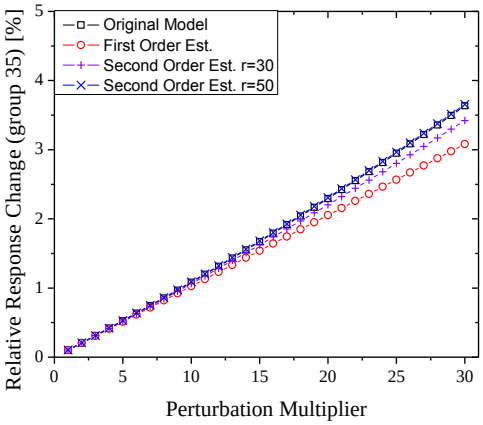

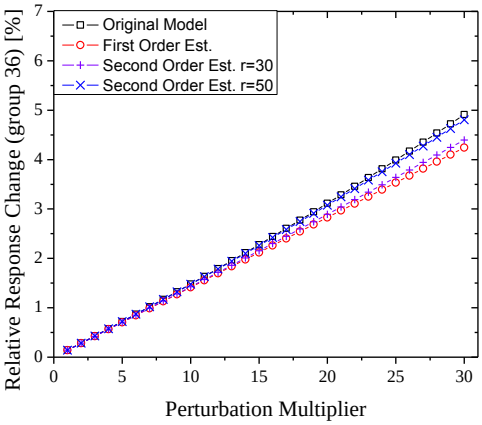

www.manaraa.com

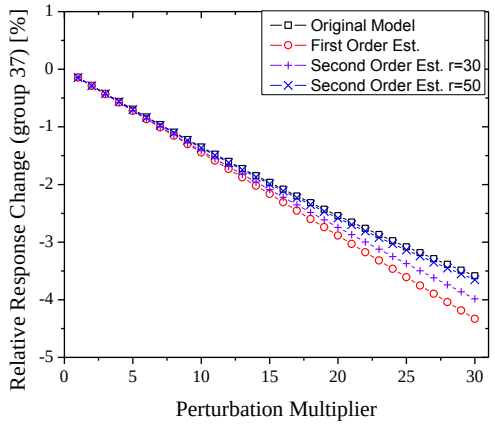

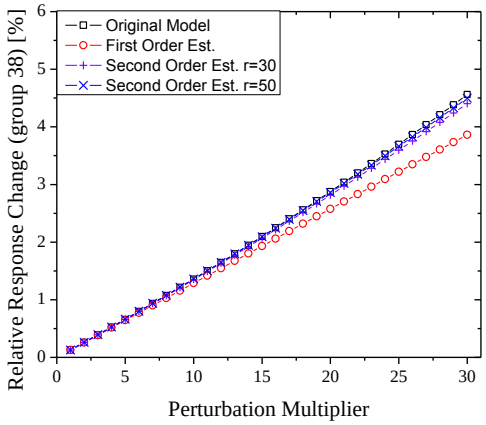

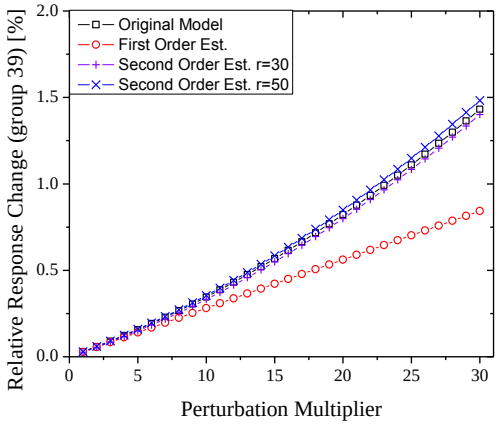

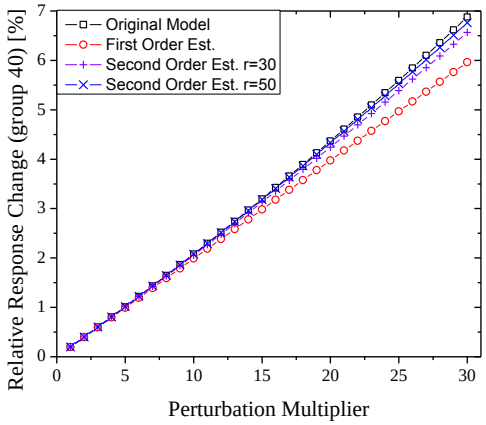

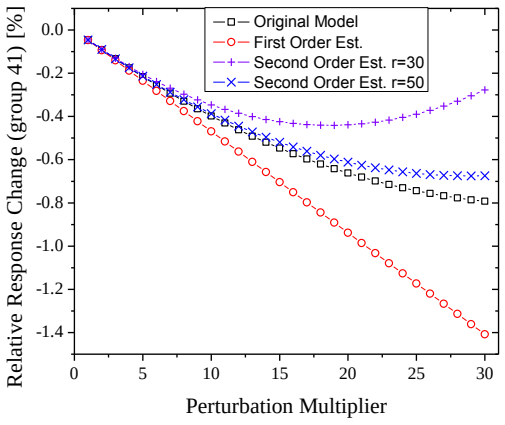

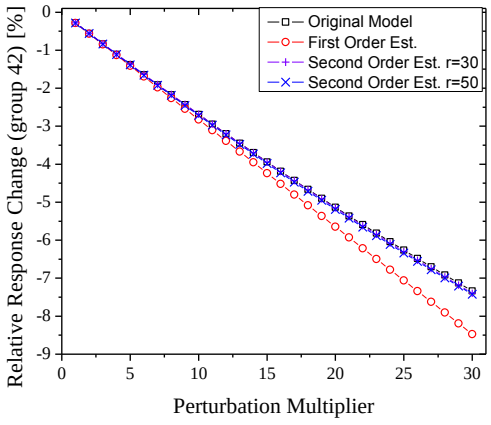

www.manaraa.com

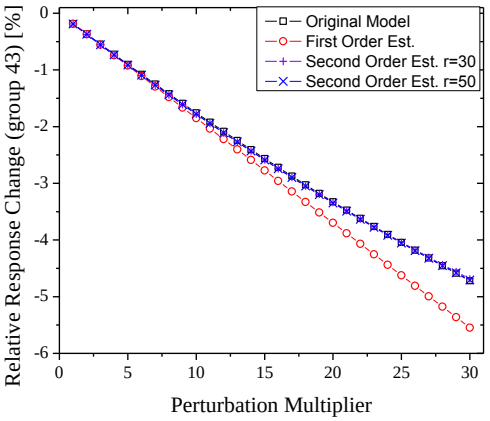

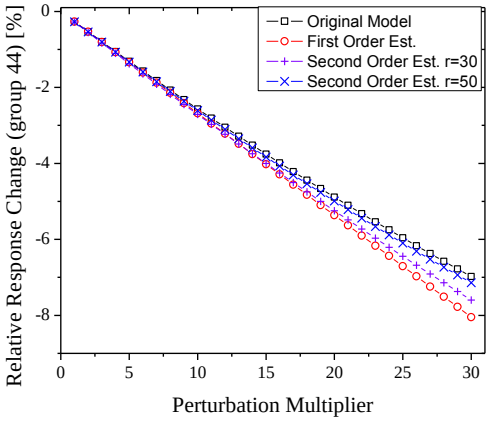

www.manaraa.com

CHAPTER 8. REDUCED ORDER UNCERTAINTY PROPAGATION

Uncertainty quantification requires repeated model executions to capture the impact of parameter uncertainty on the responses of interest. The Monte Carlo (MC) sampling approach has been widely recognized as the most versatile approach to complete uncertainty quantification. This is because it can be implemented in a non-intrusive manner and no assumptions have to be made about the model form, e.g. linear vs. nonlinear, single physics vs. multi-physics, etc. The idea is to execute the model many times, wherein each execution the parameters are sampled from their prior probability distribution functions and the resulting response variations are then used to approximate the response probability distribution function or calculate moments thereof.

The MC approach can be classified as a member of forward methods for uncertainty quantification; 'forward' implies that only the forward model is used to propagate uncertainties as opposed to the use of the adjoint model to be described later. Forward methods can be divided into two general approaches, first of which is the MC sampling approach. The second approach relies on surrogate modeling which approximates the behavior of the original model and can be executed inexpensively. Once constructed and its accuracy verified, the surrogate is used to propagate uncertainties. There are many different

www.manaraa.com

types of surrogate construction techniques: polynomial regression [Myers & Montgomer (1995)], Kriging [Sacks et al. (1989)], Multivariate Adaptive Regression Splines [Friedman (1991)], radial basis function approximations [Hardy (1971)], artificial neural networks [Smith (1993)], polynomial chaos [Ghanem & Spanos (1991)], etc. Although a great deal of differences exist between the various surrogate techniques, they are based on a common basic approach: that is to assume a certain functional form for the surrogate with some unknown features, e.g., expansion coefficients, and execute the original model at a set of points in the parameters space often referred to as a training set. The unknown surrogate features can then be identified via a minimization procedure that minimizes the discrepancies between the surrogate and original model's predictions for the training set.

Despite their ease of implementation, all forward methods suffer from one major limitation; that is the so-called curse of dimensionality. This 'curse' denotes that the computational cost increases exponentially with the number of input parameters. A great deal of research has therefore focused on identifying efficient sampling strategies known as Design of Experiment, which aim to reduce the number of samples while retaining an appropriate coverage of the parameter space. Unfortunately, with the increased demand for high fidelity predictions, the models continue to be more complex, more expensive to execute, and their associated parameters are too many to render a practical application.

To overcome the curse of dimensionality, the nuclear engineering community has leveraged the adjoint methods to constructing linear surrogate models via a sensitivity analysis (SA), whereby the coefficients are the first order derivatives of the response of

www.manaraa.com

interest with respect to parameters. Adjoint SA requires one to set up another model which represents the mathematical dual of the forward model. The advantage over forward methods is that the adjoint model needs to be executed only once per a given response. The adjoint solution could then be used in conjunction with the reference forward solution to estimate all first order derivatives of the given response with respect to all input parameters. This property has brought adjoint methods center stage in many scientific fields, especially dealing with a large number of parameters and few responses. In regard to the nuclear community, the adjoint SA has been employed to complete uncertainty quantification and data assimilation.

Although very powerful, adjoint methods start to lose their competitive advantage when higher order derivatives are sought. This is because the computational burden for higher order methods becomes dependent on other factors such as the number of parameters. For example, if second order derivatives are sought, one needs to execute the adjoint code n extra times, where n is the number of parameters. With first-order adjoint SA, the associated estimate for response variation with respect to parameter perturbation is only locally accurate, i.e. within a small range of perturbation around reference values for the parameters. This limits the utility of adjoint methods to exploratory studies only as opposed to routine design calculations where wide ranges of conditions must be analyzed in support of design, safety, and operation.

Moreover, adjoint methods are appropriate with the problems with large number of parameters and small number of responses. Note that for a general responses, one

www.manaraa.com

fundamental mode adjoint run and one general response mode adjoint run would be required in addition to the one fundamental mode forward run. Therefore, if the number of responses increases by Δm, the required additional code run would increase by $2\Delta m$. Generally, the adjoint run for general response would converge much slowly compared to forward run. Considering all these, constructing full sensitivity matrix would not be favorable for cases with large number of parameters. In practice, it is generally recommended that before conducting uncertainty study, insensitive parameters are screened out to reduce the number of parameters to be considered. However, those screening step requires a lot of computations and if not properly performed, it may result in inaccurate uncertainty propagation results.

Recognize that the fundamental issue comes from the large dimensionality. To circumvent it, we adopt reduced order modeling (ROM) techniques to reduce the required number of code runs. The reduction can be achieved by identifying only the subspace of parameter components with ***large uncertainties*** and ***high sensitivities***. The intersection approach with range finding algorithm can be utilized to identify the subspace, referring to as SU-Subspace. Once the basis for SU-Subspace is constructed, it can be incorporated to goal-oriented surrogate modeling, i.e. uncertainty propagation by 1) Conventional sandwich rule with linear assumption; and 2) MC sampling approach with nonlinear surrogate modeling. Both approaches are mathematically derived and demonstrated with numerical tests. Employing the reduced order modeling technique, the curse of dimensionality in constructing the surrogate model for uncertainty propagation would be relieved.

www.manaraa.com

8.1 Reduced Order Uncertainty Propagation with Linear Assumption

8.1.1 Mathematical Derivation

The law of the uncertainty propagation, so called sandwich rule, is given as:

$$\mathbf{C}_y = \mathbf{S}\mathbf{C}_x\mathbf{S}^T \tag{8.1}$$

where $\mathbf{S} = \left.\frac{\partial \vec{y}}{\partial \vec{x}}\right|_{\vec{x}_0} \in \mathbb{R}^{m\times n}$ is the first order derivatives of the responses with respect to the parameters, i.e. sensitivity matrix, $\mathbf{C}_x \in \mathbb{R}^{n\times n}$ and $\mathbf{C}_y \in \mathbb{R}^{m\times m}$ are the parameter and the response covariance matrix, respectively, and m and n are the number of output responses and input parameters, respectively. Note that the parameters are measured by experiments, thus the parameters may have an impact from a same uncertainty source, e.g. bias of the detector used to measure the multiple parameters and room temperature of the room where the experiments were conducted. Therefore, the uncertainty of parameters is usually expressed as a covariance matrix $\mathbf{C}_x$ which contains the correlations between parameters.

Two classes of methods have been proposed to evaluate Eq. (8.1); sensitivity-based and uncertainty-based methods. Uncertainty-based methods however recognize that the parameter covariance matrix could be decomposed using singular value decomposition [Golub & Van Loan (1996)], i.e., $\mathbf{C}_x = \mathbf{U}_x\mathbf{\Sigma}_x^2\mathbf{U}_x^T$, yielding:

www.manaraa.com

$$\mathbf{C}_y = \mathbf{S}\mathbf{U}_x\boldsymbol{\Sigma}_x^2\mathbf{U}_x\mathbf{S}^T = \left(\mathbf{S}\mathbf{U}_x\boldsymbol{\Sigma}_x\right)\left(\mathbf{S}\mathbf{U}_x\boldsymbol{\Sigma}_x\right)^T = \sum_{i=1}^{n}\left(\mathbf{S}\sigma_{x,i}\vec{u}_{x,i}\right)\left(\mathbf{S}\sigma_{x,i}\vec{u}_{x,i}\right)^T \tag{8.2}$$

where $\mathbf{U}_x = \left[\vec{u}_{x,1} \quad ... \quad \vec{u}_{x,n}\right] \in \mathbb{R}^{n\times n}$ is an orthonormal matrix and $\boldsymbol{\Sigma}_x = \left\{\sigma_{x,1},....,\sigma_{x,n}\right\} \in \mathbb{R}^{n\times n}$ a diagonal matrix. Notice that each term requires the product of the sensitivity matrix with a vector, i.e., $\sigma_{x,i}\vec{u}_{x,i}$. The $\vec{u}_{x,i}$ is the i th column of the matrix $\mathbf{U}_x$ and $\sigma_{x,i}$ is the r th singular value of the matrix $\boldsymbol{\Sigma}_x$. This matrix-vector product could be evaluated directly using finite differencing without explicit access to the elements of the sensitivity matrix as follows:

$$\mathbf{S}\sigma_{x,i}\vec{u}_{x,i} = \vec{y}\left(\vec{x}_0 + \sigma_{x,i}\vec{u}_{x,i}\right) - \vec{y}\left(\vec{x}_0\right) \tag{8.3}$$

This approach is often mentioned in the literature as Karhunen-Loève expansion acknowledging their first proposal for the spectral decomposition of uncertainty information in its continuous form [Karhunen (1946), Loève (1945)]. In linear algebra, this is equivalent to the singular value decomposition. This approach is effective as it does not require access to the sensitivity matrix which could be expensive to evaluate. However, it requires the execution of the model as many times as the number of non-zero singular values for the parameter covariance matrix. If the parameter covariance matrix is full rank with all singular values relatively large, the computational cost will be similar to the sensitivity-based approach using forward sensitivity analysis. If, however, many of the singular values can be considered small, i.e. effectively zero, the number of model executions can be reduced drastically. A small singular values imply a direction in the parameter space which has very small uncertainties. Discarding these directions means that the analyst believes its associated uncertainties will not impact the response's uncertainty, and hence a reduction in the number

www.manaraa.com

of uncertain input parameters is possible. This is the reason we denote this approach as uncertainty-based since it employs only uncertainty information to decide how to render reduction in the parameter space.

In sensitivity-based methods, one determines the matrix **S** using either a forward or an adjoint sensitivity analysis approach. After that, the response covariance matrix can be calculated directly using the sandwich rule in Eq. (8.1). Note that the derivative is the rate of change of the response with respect to the parameter calculated locally around some reference parameter value. Employing this definition, one can consider the parameter with a large derivative to be more sensitive, i.e., more influential, than one with a smaller derivative. This follows as a small variation in a parameter with large derivative implies a large variation in the response; whereas small variation in a parameter with small derivatives results in a small variation in the response. Therefore, derivatives could be used to determine the most influential parameters on the responses of interest which proves useful in a number of engineering applications such as design optimization to reach certain objectives. In the same sense, derivatives could be used to render reduction in the parameter space. The influential parameters are assumed to be the key contributors to the propagated uncertainties, as variations in the parameters with small sensitivities are not expected to lead to noticeable variations in the response. To explain how sensitivity information is used to render reduction in the parameter space, consider a singular value decomposition of the sensitivity matrix **S** as follows:

$$\mathbf{S} = \mathbf{U}_s \mathbf{\Sigma}_s \mathbf{V}_s^T = \sum_{i=1}^{\min(m,n)} u_{s,i} \sigma_{s,i} \vec{v}_{s,i}^T \tag{8.4}$$

www.manaraa.com

where $\mathbf{U}_s = \left[\vec{u}_{s,1} \quad ... \quad \vec{u}_{s,m} \right] \in \mathbb{R}^{m \times m}$ is an orthonormal matrix whose columns are referred to as the left singular vectors, $\mathbf{\Sigma}_s = \left\{ \sigma_{s,1}, ..., \sigma_{s,\min(m,n)} \right\} \in \mathbb{R}^{\min(m,n) \times \min(m,n)}$ a diagonal matrix, and $\mathbf{V}_s = \left[\vec{v}_{s,1} \quad ... \quad \vec{v}_{s,n} \right] \in \mathbb{R}^{n \times n}$ contains the right singular vectors. This decomposition provides great insight into the action of a matrix operator. One could describe the action of a matrix on a vector Δx as follows:

$$\Delta \vec{y} = \mathbf{S} \Delta \vec{x} = \sum_{i=1}^{\min(m,n)} \left(\vec{v}_{s,i}^T \Delta \vec{x} \right) \sigma_{s,i} \vec{u}_{s,i} = \sum_{i=1}^{\min(m,n)} \alpha_i \sigma_{s,i} \vec{u}_{s,i} \tag{8.5}$$

where $\alpha_i = \vec{v}_{s,i}^T \Delta \vec{x}$ is the component of $\Delta \vec{x}$ along the ith right singular vector $\vec{v}_{s,i}$. First, the vector $\Delta \vec{x}$ is decomposed along the right singular vectors. Second, its components are scaled by the singular values. The scaled components represent the components of the resultant vector $\Delta \vec{y}$ along the left singular vectors. Therefore, one can think of the singular vectors as simply rotating the vector $\Delta \vec{x}$ in the parameter space onto the vector $\Delta \vec{y}$ in the response space, with the core action of the operator contained in the singular values. During the scaling, some components are magnified, and some are damped. Depending on the variation in the singular values sometimes spreading over many orders of magnitude, some of the components vanish in comparison to others.

These observations could be used to render reduction in the parameter and response spaces when one has a model with many parameters and many responses which allows for more efficient implementations of the forward and adjoint approaches. For example, in the forward approach, one employs finite differencing to approximate the action of a matrix-

www.manaraa.com

vector product of the form: $\Delta\vec{y} = \mathbf{S}\Delta\vec{x}$. This process has to be repeated n times to cover all possible directions in the parameter space. Given however that some of these directions are associated with very small singular values, one can discard these directions as they are expected to cause very small response changes. Assuming that only the first r singular values are considered influential, the forward sensitivity analysis can be recast as follows:

$$\Delta\vec{y} = \mathbf{S}\Delta\vec{x} = \mathbf{S}\sum_{i=1}^{r} \alpha_i \vec{v}_{s,i} \tag{8.6}$$

where the summation runs to r only. This equation implies that $\Delta\vec{x}$ is constrained to the subspace spanned by the first r right singular vectors. Therefore, one only needs r forward model executions to cover this subspace. The assumption is that the remaining $n-r$ directions do not impact the responses and therefore can be discarded.

In the adjoint approach, one employs the adjoint model to calculate the action of a matrix-transpose on a vector of the form: $\Delta x = \mathbf{S}^T \Delta y$. This process has to be repeated m times to cover all possible directions in the response space. Given however that some of these directions vary very little due to parameter variations, one can exclude them from the adjoint SA. Assuming one considers only the first r singular values as done before, the adjoint sensitivity analysis can be recast as follows:

$$\Delta\vec{x} = \mathbf{S}^T \Delta\vec{y} = \mathbf{S}^T \sum_{i=1}^{r} \beta_i \vec{u}_{s,i} \tag{8.7}$$

This equation implies that $\Delta\vec{y}$ is constrained to the subspace spanned by the first r left singular vectors. Therefore, one only needs r adjoint model executions to cover this

www.manaraa.com

subspace. The assumption is that the remaining $m-r$ directions do not vary due to parameter variations.

If the singular value decomposition is known, the resulting error from the reduction may be estimated exactly as follows:

$$\left\| \mathbf{S} - \sum_{i=1}^{r} \vec{u}_{s,i} \sigma_{s,i} \vec{v}_{s,i}^{T} \right\| = \sigma_{s,r+1} \tag{8.8}$$

where $\sigma_{s,r+1}$ is the $r+1$ singular value of the matrix $\mathbf{S}$. In reality however, neither the matrix nor its singular value decomposition are known explicitly.

The proposed method hybridizes the sensitivity and uncertainty-based methods described above for completing uncertainty quantification. This approach may be thought of as finding an intersection between the two types of reduction: a sensitivity-based reduction which identifies directions in the parameter space that are considered the most sensitive, and an uncertainty-based reduction identifying the most uncertain directions. Each reduction is described by a subspace, whereby parameters perturbations orthogonal to this subspace are considered non-influential from sensitivity or uncertainty viewpoint. We denote the subspaces generated by sensitivity and uncertainty-based methods as ***S-active*** and ***U-active subspaces***, respectively. The complementary orthogonal subspaces are referred to as the S-inactive and U-inactive subspaces. The implicit assumption in these two classes of methods is that perturbations that belong to the inactive subspaces do not affect the response uncertainties. Since the response uncertainties are the product of two factors, the sensitivities and prior uncertainties, it becomes impossible to quantify the resulting error in the response

www.manaraa.com

uncertainties a priori, i.e. before the uncertainties are propagated. This follows as no information on the other factor is used to advise the reduction. In practice, the uncertainties are propagated and then compared to those calculated by a Monte Carlo sampling-based approach to provide confidence in the reduction employed.

What is proposed here is a hybrid approach that combines these two approaches and identifies an active subspace that represents both influential sensitivity and uncertainty information, denoted hereinafter as ***SU-active subspace***. In addition to reducing the computational cost, this approach allows one to establish an upper-bound on the error resulting from the reduction which provides an advantage over existing methods. The main idea is finding the basis of the SU-active subspace. This is illustrated in **Figure 8-1**. The S-active subspace and the U-active subspace are expressed as $\hat{\alpha}$ and $\hat{\beta}$ vectors. Note that the SU-active subspace is the intersection between those two subspaces expressed by $\hat{q}$ vectors.

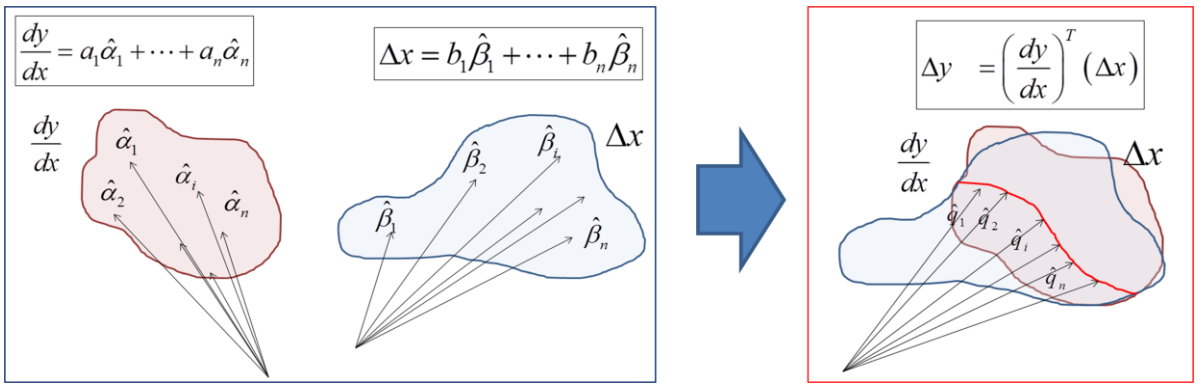

Figure 8-1. Illustration of SU-Active Subspace

www.manaraa.com

Consider re-writing Eq. (8.2) as follows:

$$\begin{aligned}\mathbf{C}_y &= \left(\mathbf{S}\mathbf{U}_x\boldsymbol{\Sigma}_x\left(\mathbf{Q}\mathbf{Q}^T+\mathbf{Q}^{\perp}\mathbf{Q}^{\perp T}\right)\right)\left(\mathbf{S}\mathbf{U}_x\boldsymbol{\Sigma}_x\left(\mathbf{Q}\mathbf{Q}^T+\mathbf{Q}^{\perp}\mathbf{Q}^{\perp T}\right)\right)^T \\ &= \mathbf{S}\mathbf{C}_x^{1/2}\left(\mathbf{Q}\mathbf{Q}^T+\mathbf{Q}^{\perp}\mathbf{Q}^{\perp T}\right)\mathbf{C}_x^{1/2T}\mathbf{S}^T \\ &= \left(\mathbf{S}\mathbf{C}_x^{1/2}\mathbf{Q}\mathbf{Q}^T\right)\left(\mathbf{S}\mathbf{C}_x^{1/2}\mathbf{Q}\mathbf{Q}^T\right)^T+\left(\mathbf{S}\mathbf{C}_x^{1/2}\mathbf{Q}^{\perp}\mathbf{Q}^{\perp T}\right)\left(\mathbf{S}\mathbf{C}_x^{1/2}\mathbf{Q}^{\perp}\mathbf{Q}^{\perp T}\right)^T\end{aligned} \tag{8.9}$$

Note that: $\mathbf{Q}\mathbf{Q}^T+\mathbf{Q}^{\perp}\mathbf{Q}^{\perp T}=\mathbf{I}\in\mathbb{R}^{n\times n}$, where the range of the matrix $\mathbf{Q}\in\mathbb{R}^{n\times r}$ is intended to describe the SU-active subspace (combining both sensitivity and uncertainty information). Assuming that $\mathbf{Q}$ is known, composed of r columns $\mathbf{Q}=\left[\vec{q}_1 \quad ... \quad \vec{q}_r\right]\in\mathbb{R}^{n\times r}$, one can employ finite differencing to evaluate response uncertainties as follows:

$$\mathbf{S}\mathbf{C}_x^{1/2}\vec{q}_i = y\left(\vec{x}_0+\vec{z}_i\right)-y\left(\vec{x}_0\right);\ i=1,...,r \tag{8.10}$$

where $\vec{z}_i=\mathbf{C}_x^{1/2}\vec{q}_i$ is a vector. The error resulting from this reduction may be described as follows:

$$\left\|\mathbf{C}_y-\mathbf{S}\mathbf{C}_x^{1/2}\mathbf{Q}\mathbf{Q}^T\mathbf{C}_x^{1/2T}\mathbf{S}^T\right\|=\left\|\mathbf{S}\mathbf{C}_x^{1/2}\mathbf{Q}^{\perp}\mathbf{Q}^{\perp T}\right\|^2=\left\|\mathbf{S}\mathbf{C}_x^{1/2}\left(\mathbf{I}-\mathbf{Q}\mathbf{Q}^T\right)\right\|^2 \tag{8.11}$$

We use a range finding algorithm to provide an error bound on the term $\left\|\mathbf{S}\mathbf{C}_x^{1/2}\left(\mathbf{I}-\mathbf{Q}\mathbf{Q}^T\right)\right\|$ which in turn limits the error on the response uncertainties.

Now, we discuss how the matrix $\mathbf{Q}$ is constructed. Let $\mathbf{A}=\mathbf{S}\mathbf{C}_x^{1/2}$ and employing the RFA algorithm, one needs to evaluate $\mathbf{A}^T\vec{w}=\left(\mathbf{S}\mathbf{C}_x^{1/2}\right)^T\vec{w}=\mathbf{C}_x^{1/2T}\mathbf{S}^T\vec{w}$. As discussed earlier, the adjoint approach can be used to evaluate a matrix-transpose-vector product of the form: $\mathbf{S}^T\vec{w}$. In earlier work [Bang & Abdel-Khalik, 2011a], we show that this is equivalent to setting up an adjoint model with a pseudo response of the form:

www.manaraa.com

$$y_{pseudo} = \vec{w}^T \vec{y} = \sum_{i=1}^{m} w_i y_i \tag{8.12}$$

where $\{w_i\}_{i=1}^{m}$ are random scalars. Therefore, one can employ pseudo responses with random weights then multiply the resultant vector with the matrix $\mathbf{C}_x^{1/2}$ to emulate the matrix-transpose-vector product $\mathbf{A}^T \vec{w}$. According to the RFA algorithm, this is repeated $r+s$ times to find a subspace spanned by r directions representing the columns of the matrix $\mathbf{Q}$.

The algorithm for the proposed method is summarized below:

Algorithm: Reduced Order Uncertainty Propagation with Linear Assumption

Given a user-defined tolerance ε and a user-defined small number s;

Step 1) Set $k=1$

Step 2) Generate the k^{th} random vector $\vec{w}^{(k)} \in \mathbb{R}^{m\times 1}$ where m is the number of responses.

Step 3) Construct a pseudo response: $y_{pseudo}^{(k)} = \vec{w}^{(k)T} \vec{y}$.

Step 4) Employing adjoint SA, calculate: $\dfrac{dy_{pseudo}^{(k)}}{d\vec{x}}$.

Step 5) Update: $\mathbf{G} = \mathbf{C}_x^{1/2T} \left[\dfrac{dy_{pseudo}^{(1)}}{d\vec{x}} \quad ... \quad \dfrac{dy_{pseudo}^{(k)}}{d\vec{x}} \right] \in \mathbb{R}^{n\times k}$.

Step 6) Determine the rank r of the sensitivity matrix G.

Step 7) Employ RFA algorithm until the tolerance ε is satisfied

Step 7) If the rank has not been reached yet, increase k and go back to step 2.

Step 8) Write $\mathbf{G} = \mathbf{QR}$, where $\mathbf{Q} \in \mathbb{R}^{n\times r}$.

www.manaraa.com

Step 9) Execute the simulation to calculate: $\Delta\vec{y}_i = \vec{y}\left(\vec{x}_0 + \mathbf{C}_x^{1/2}\vec{q}_i\right) - \vec{y}\left(\vec{x}_0\right)$ for $i = 1,...,r$.

Step 10) Determine $\mathbf{Y} = \left[\Delta\vec{y}_1 \quad \cdots \quad \Delta\vec{y}_r\right]$.

Step 11) Compute the propagated uncertainty: $\mathbf{C}_y = \mathbf{Y}\mathbf{Y}^T$.

Note that in this algorithm access to the matrix $\mathbf{C}_x^{1/2}$ is required. This is possible via an SVD decomposition as shown before, $\mathbf{C}_x^{1/2} = \mathbf{U}_x\boldsymbol{\Sigma}_x^{1/2} = \left[\sqrt{\sigma_{x,1}}\vec{u}_{x,1} \quad \cdots \quad \sqrt{\sigma_{x,n}}\vec{u}_{x,n}\right]$.

8.1.2 Numerical Test

Problem Description & Implementation

The reduced order uncertainty propagation method with linear assumption is used to calculate the response covariance matrix. For calculating the first order derivatives, TSUNAMI-2D control module of SCALE6.1 can be used. TSUNAMI-2D control module generates the input files for resonance calculation module (e.g. NITAWL or CENTRM), transport solver (i.e. NEWT for forward and adjoint mode) and sensitivity calculation module (i.e. SAMS). The SAMS calculates the sensitivity coefficients (i.e. relative first order derivative) of self-shielded macroscopic cross with respect to user-defined responses. Note that the released TSUNAMI-2D supports only ratio type (e.g. reaction rate ratio) as a response. For this study, NEWT and SAMS are modified to support a linear type response (i.e. reaction rate) and verified in a systematic way [Bang & Abdel-Khalik (2011c)]. For testing the reduced order regression algorithm, the working library for self-shielded macroscopic cross sections is perturbed and NEWT (fundamental forward) – NEWT

www.manaraa.com

(fundamental adjoint) – NEWT (GPT adjoint) – SAMS sequences are performed to calculate the perturbed sensitivity coefficients. **Figure 8-2** depicts the model analyzed; it is a stand-alone benchmark model designed by OECD/NEA to assess the assumptions in current LWR standard lattice physics scheme for generation of few-group cross-sections [Ivanov et al. (2007)]. The 44 energy group library (v5-xn44) of SCALE6.1 is used and the reference k_{eff} is 1.08383475. With the perturbed self-shielded macroscopic cross sections $\vec{\Sigma}$ and the resulting sensitivity coefficients $\vec{S}$, the regression analysis and all subsequent calculations are conducted by using MATLAB 2011a.

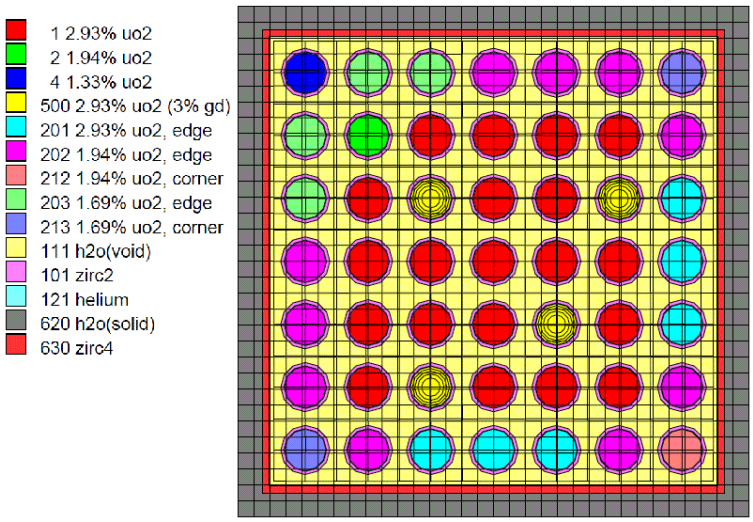

Figure 8-2. A 7x7 BWR Benchmark Assembly Model

As input parameters, the fission cross sections of four nuclides (i.e. U-234, U-235, U-236 and U-238) in 44 energy group in 9 fuel mixtures, i.e. the dimension of input parameters is $\mathbb{R}^{1584}$ are considered. The SCALE6.1 covariance data, i.e. 44groupcov, is used as the input

www.manaraa.com

parameter covariance matrix. The responses are chosen to the mixture flux defined in Eq. (7.2).

Results

First, the singular values are compared to get an insight about the required number of basis vectors. **Figure 8-3** compares the singular value spectrums of sensitivity matrix of the pseudo response and the pseudo response sensitivity pre-multiplied by $\mathbf{C}^{1/2T}$, i.e. S-active subspace and SU-active subspace. As can be seen, the singular value spectrum of the SU-active subspace is decaying more quickly than the one of the S-active subspace. This implies that the smaller number of basis vectors are required to achieve a certain level of accuracy and a less number of simulation with the proposed reduced order uncertainty propagation method than the one with sensitivity-based or uncertainty-based methods.

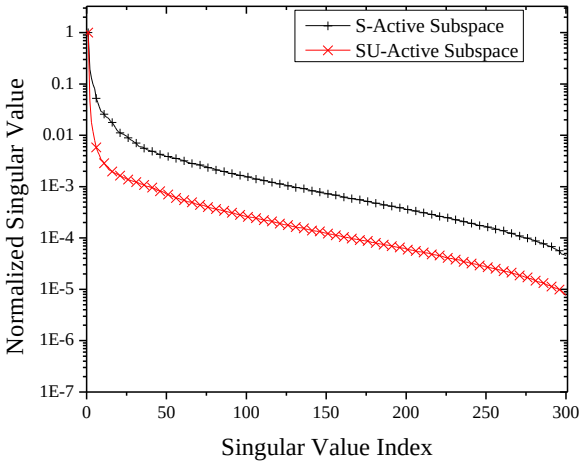

Figure 8-3. Singular Value Spectrum Comparison
(Linear Uncertainty Propagation, $\vec{\Sigma} \in \mathbb{R}^{1584}$)

www.manaraa.com

The response uncertainty is calculated with r =10, 20, 30, and 40 and compared in **Figure 8-4**. In **Figure 8-5**, the error norms explained in Eq. (8.11) are plotted according to the number of basis vectors. As the number of basis vectors increases, the error norm decreases. A user can determine the required number of basis vectors, i.e. order of reduction, for the purpose of the analysis, e.g. prioritization of the uncertainty factors. For comparison, the absolute sense uncertainty calculation results are presented in **Figure 8-6 ~ 9**. One can see more clearly that as the subspace size increases, the estimated uncertainty is getting closer to the one of the conventional sandwich approach.

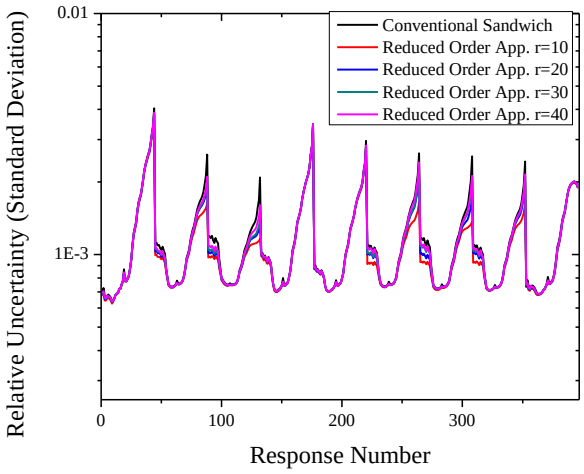

Figure 8-4. Comparison of Response (Relative) Uncertainty Calculation
(Linear Uncertainty Propagation, $\vec{\Sigma} \in \mathbb{R}^{1584}$)

www.manaraa.com

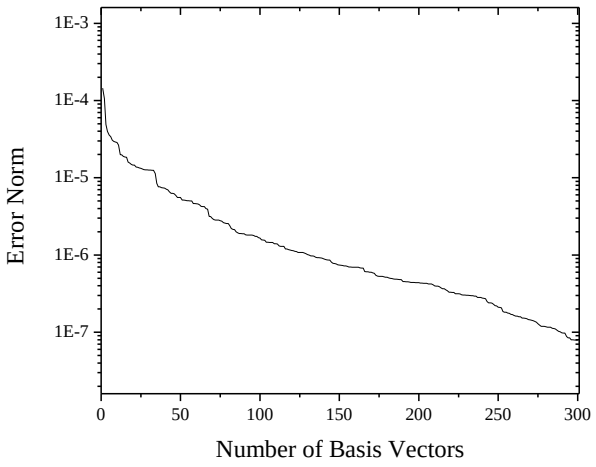

Figure 8-5. Error Norm for Reduced Order Uncertainty Propagation Method (Linear Uncertainty Propagation, $\vec{\Sigma} \in \mathbb{R}^{1584}$)

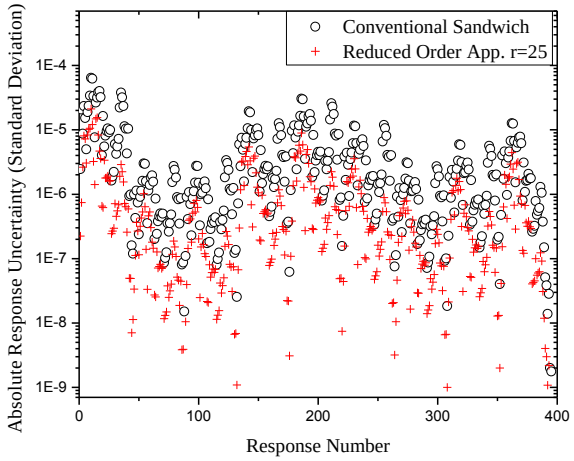

Figure 8-6. Comparison of Response (Absolute) Uncertainty Calculation (r=25) (Linear Uncertainty Propagation, $\vec{\Sigma} \in \mathbb{R}^{1584}$)

www.manaraa.com

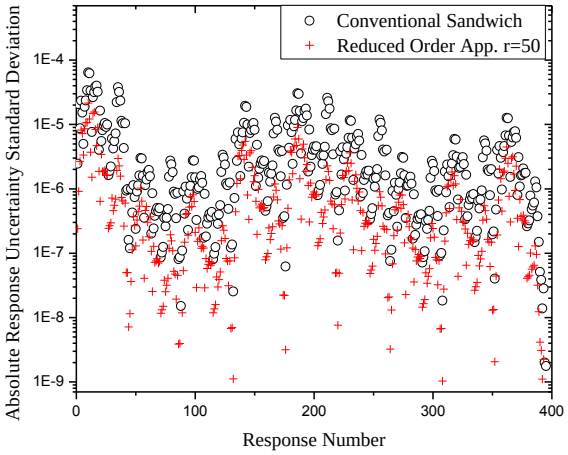

Figure 8-7. Comparison of Response (Absolute) Uncertainty Calculation (r=50) (Linear Uncertainty Propagation, $\vec{\Sigma} \in \mathbb{R}^{1584}$)

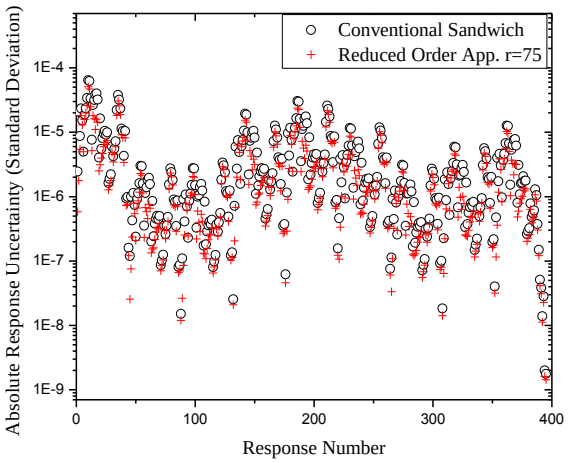

Figure 8-8. Comparison of Response (Absolute) Uncertainty Calculation (r=75) (Linear Uncertainty Propagation, $\vec{\Sigma} \in \mathbb{R}^{1584}$)

www.manaraa.com

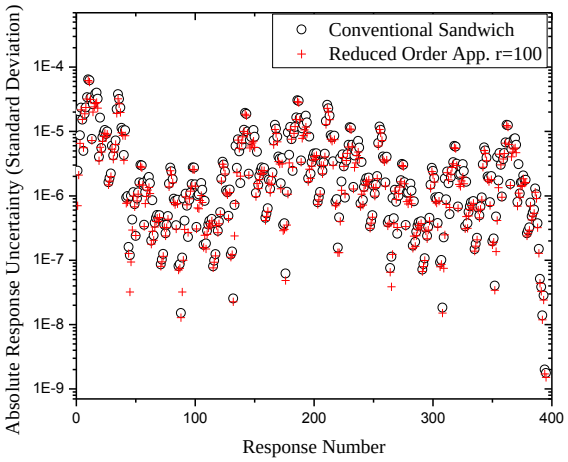

Figure 8-9. Comparison of Response (Absolute) Uncertainty Calculation (r=100) (Linear Uncertainty Propagation, $\vec{\Sigma} \in \mathbb{R}^{1584}$)

8.2 Reduced Order Uncertainty Propagation with Nonlinear Surrogate Modeling

8.2.1 Mathematical Derivation

The reduced order surrogate modeling can be extended to nonlinear uncertainty propagation. More specifically, one can construct the surrogate model only for uncertainty quantification, i.e. goal-oriented surrogate modeling. Consider that a parameter variation due to uncertainty can be expressed as:

$$\Delta\vec{x} = \mathbf{C}_x^{1/2}\vec{\xi} \tag{8.13}$$

www.manaraa.com

where $\vec{\xi} \in \mathbb{R}^n$ is a vector of which elements are randomly sampled from normal distribution with mean $\mu = 0$ and standard deviation $\sigma = 1$ and $\mathbf{C}_x^{1/2}$ is given by $\mathbf{C}_x = \mathbf{C}_x^{1/2}\mathbf{C}_x^{1/2T}$. Consider the singular value decomposition of $\mathbf{C}_x^{1/2} = \mathbf{U}_c\mathbf{\Sigma}_c\mathbf{V}_c^T$, then Eq. (8.13) can be rewritten as:

$$\Delta x = \mathbf{U}_c\mathbf{\Sigma}_c\mathbf{V}_c^T\vec{\xi} = \sum_{i=1}^{n}\sigma_{c,i}\vec{u}_{c,i}\vec{v}_{c,i}^T\vec{\xi} \tag{8.14}$$

Note that if the magnitude $\sigma_{c,i}\vec{v}_{c,i}^T\vec{\xi}$ (which is a scalar value) is small, the contribution of the direction $\vec{u}_{c,i}$ would be also small. This implies that the parameter variation $\Delta\vec{x}$ can be approximated by $\{\vec{u}_{c,i}\}$ vectors only corresponding to the large $\{\sigma_{c,i}\vec{v}_{c,i}^T\vec{\xi}\}$ and the only components of $\vec{\xi}$ which is parallel to the $\vec{v}_{c,i}$ would be contribute the $\Delta\vec{x}$. Therefore, we define U-active subspace as a subspace spanned by $\{\vec{v}_{c,i}\}$ vectors.

As explained before, the model has its own active subspace which is spanned by all coefficient vectors and this subspace is referred to as S-active subspace. Therefore, among the parameter variations, only components along the S-active subspace would contribute to the response changes. This implies that only the component of the random perturbation included in both U-active subspace and S-active subspace, i.e. SU-active subspace, would contribute to the response change. Define that the columns of the matrix $\mathbf{Q} \in \mathbb{R}^{n\times r}$ span the intersection of U-active subspace and S-active subspace. It is important to note that one can expect $r \le \min(r_U, r_S)$, where r_U and r_S are the numbers of the basis vectors of U-active subspace and S-active subspace, respectively.

www.manaraa.com

For illustration, assume that an unknown surrogate model has a form as:

$$\Delta R = f\left(\Delta\vec{x}\right) = \left(\vec{\beta}_1^T \Delta\vec{x}\right) + \left(\vec{\beta}_2^T \Delta\vec{x}\right)^2 = \left(\vec{\beta}_1^T \mathbf{C}^{1/2}\vec{\xi}\right) + \left(\vec{\beta}_2^T \mathbf{C}^{1/2}\vec{\xi}\right)^2 \tag{8.15}$$

where $\vec{\beta}_1, \vec{\beta}_2, \Delta\vec{x}, \vec{\xi} \in \mathbb{R}^n$ and $\mathbf{C}^{1/2} \in \mathbb{R}^{n\times n}$. Note that the random variations can be decomposed into:

$$\vec{\xi} = \vec{\xi}^{\parallel} \oplus \vec{\xi}^{\perp} \tag{8.16}$$

where $\vec{\xi}^{\parallel}$ is the component in SU-active subspace spanned by the columns of the matrix $\mathbf{Q}$ and $\vec{\xi}^{\perp}$ is the complementary component orthogonal to SU-active subspace. Note that $\vec{\xi}^{\parallel}$ can be calculated by projecting onto the SU-active subspace, i.e. $\mathbf{Q}\mathbf{Q}^T\vec{\xi} = \mathbf{Q}\vec{\alpha}$, which is a linear combination of the columns of the matrix $\mathbf{Q}$. This implies that once the matrix $\mathbf{Q}$ is given, the parameter variations can be represented by $\vec{\alpha} \in \mathbb{R}^r$ and, in the same sense described in the previous Chapter 4.2, the reduced order model of the surrogate model can be constructed as:

$$\begin{aligned}\Delta R = f\left(\Delta\vec{x}\right) &= \left(\vec{\beta}_1^T \mathbf{C}_x^{1/2}\vec{\xi}\right) + \left(\vec{\beta}_2^T \mathbf{C}_x^{1/2}\vec{\xi}\right)^2 \\ &\simeq \left(\vec{\beta}_1^T \mathbf{C}_x^{1/2}\mathbf{Q}\mathbf{Q}^T\vec{\xi}\right) + \left(\vec{\beta}_2^T \mathbf{C}_x^{1/2}\mathbf{Q}\mathbf{Q}^T\vec{\xi}\right)^2 \\ &= \left(\vec{\beta}_{1,r}^T\vec{\alpha}\right) + \left(\vec{\beta}_{2,r}^T\vec{\alpha}\right)^2\end{aligned} \tag{8.17}$$

where $\vec{\beta}_{1,r} = \mathbf{Q}^T\mathbf{C}_x^{1/2T}\vec{\beta}_1$, $\vec{\beta}_{2,r} = \mathbf{Q}^T\mathbf{C}_x^{1/2T}\vec{\beta}_2$ and $\vec{\alpha} = \mathbf{Q}^T\vec{\xi}$ and the dimension of all those vectors are $\mathbb{R}^r$. The surrogate model can be constructed by examining the pairs of $\left(\vec{\alpha}^{(i)}, \Delta R^{(i)}\right)$ where $\vec{\alpha}^{(i)}$ is $\mathbf{Q}^T\vec{\xi}^{(i)}$ and $\Delta R^{(i)}$ is calculated by running the simulation code with perturbed parameter given by $\Delta\vec{x}^{(i)} = \mathbf{C}_x^{1/2}\vec{\xi}^{(i)}$. Once the accurate surrogate model is

www.manaraa.com

constructed, the original model can be replaced by the surrogate mode and any existing sampling based uncertainty propagation methods, i.e. Monte-Carlo method, can be used to estimate the response uncertainty.

The basis of the SU-active subspace, i.e. the matrix $\mathbf{Q}$, can be constructed by the following way. First, define a pseudo response as random linear combination of all responses. As described in the above section, the first order derivative of pseudo responses at random points would span the S-active subspace. By pre-multiplying the $\mathbf{C}_x^{1/2T}$ to the derivatives, one can filter out the component only in the U-active subspace. Note that the resulting vectors would span the SU-active subspace. According to the RFA algorithm, this is repeated $r+s$ times to find a subspace spanned by r directions.

The algorithm for the proposed method is summarized below:

Algorithm: Reduced Order Uncertainty Propagation via Nonlinear Surrogate Modeling

Given a user-defined tolerance ε and a user-defined small number s;

Step 1) Set $k=1$

Step 2) Generate the k^{th} random vector $\vec{w}^{(k)} \in \mathbb{R}^m$ where m is the number of responses.

Step 3) Construct a pseudo response: $R_{pseudo}^{(k)} = \vec{w}^{(k)T}\vec{R} = \sum_{i=1}^{m} w_i^{(k)} R_i$.

Step 4) Employing adjoint SA, calculate: $\dfrac{dR_{pseudo}^{(k)}}{d\vec{x}}$.

Step 5) Update: $\mathbf{G} = \mathbf{C}_x^{1/2T}\left[\dfrac{dR_{pseudo}^{(1)}}{d\vec{x}} \quad \ldots \quad \dfrac{dR_{pseudo}^{(k)}}{d\vec{x}}\right] \in \mathbb{R}^{n\times k}$.

www.manaraa.com

Step 6) Determine the rank r of the sensitivity matrix $\mathbf{G}$.

Step 7) Employ RFA algorithm until the tolerance ε is satisfied

Step 8) If the rank has not been reached yet, increase k and go back to step 2.

Step 9) Write $\mathbf{G} = \mathbf{QR}$, where $\mathbf{Q} \in \mathbb{R}^{n \times r}$.

Step 10) Sample the training sets for reduced order surrogate model construction.

Step 11) Construct a reduced order surrogate model for each response.

Step 12) Generate the sample sets for uncertainty propagation.

Step 13) Calculate the responses by using the reduced order surrogate model.

Step 14) Compute the propagated uncertainty: $\sigma_j = \sqrt{\frac{1}{N}\sum_{i=1}^{N}\left(\Delta R_j^{(i)}\right)^2}$.

8.2.2 Numerical Test

Problem Description

The reduced order uncertainty propagation algorithm via reduced order surrogate modeling is implemented. The reduced order uncertainty propagation method is used to calculate the response covariance matrix and the distribution of the responses.

Implementation

For calculating the first order derivatives, TSUNAMI-2D control module of SCALE6.1 is used. TSUNAMI-2D control module generates the input files for resonance calculation module (e.g. NITAWL or CENTRM), transport solver (i.e. NEWT for forward and adjoint mode) and sensitivity calculation module (i.e. SAMS). The SAMS calculates the sensitivity coefficients (i.e. relative first order derivative) of self-shielded macroscopic cross with

www.manaraa.com

respect to user-defined responses. Note that the released TSUNAMI-2D supports only ratio type (i.e. reaction rate ratio) as a response. For this study, NEWT and SAMS are modified to support a linear type response (i.e. reaction rate) and verified in systematic way [Bang & Abdel-Khalik (2011)]. For testing the reduced order regression algorithm, the working library for self-shielded macroscopic cross sections is perturbed and NEWT (fundamental forward) – NEWT (fundamental adjoint) – NEWT (GPT adjoint) – SAMS sequences are performed to calculate the perturbed sensitivity coefficients. As input parameters, the fission cross sections of four nuclides (i.e. U-234, U-235, U-236 and U-238) in 44 energy group in 9 fuel mixtures, i.e. the dimension of input parameters is $\mathbb{R}^{1584}$ are considered. Note that with the covariance matrix provided with SCALE6.1, i.e. 44groupcov, the input parameter perturbation would be too small to see the nonlinear response change. Thus, to emulate the nonlinear problem, the manufactured covariance matrix is used for this test, i.e. the element of the covariance matrix for each nuclide is assumed 0.1. The responses are chosen to the mixture flux defined in Eq. (7.2). The pseudo response is built as explained in Eq. **Error! Reference source not found.**. With the perturbed self-shielded macroscopic cross sections $\vec{\Sigma}$ and the resulting sensitivity coefficients $\vec{S}$, all subsequent calculations are conducted by using MATLAB 2011a.

Results

First, the singular values are compared to get an insight about the required number of basis vectors. **Figure 8-10** compares the singular value spectrums of sensitivity matrix of the

www.manaraa.com

pseudo response and the pseudo response sensitivity pre-multiplied by $\mathbf{C}^{1/2T}$, i.e. S-active subspace and SU-active subspace. As can be seen, the singular value spectrum of the SU-active subspace is decaying more quickly than the one of the S-active subspace. This implies that the smaller number of basis vectors are required to achieve a certain level of accuracy and less number of simulation with the proposed reduced order uncertainty propagation method than the one with sensitivity-based or uncertainty-based methods.

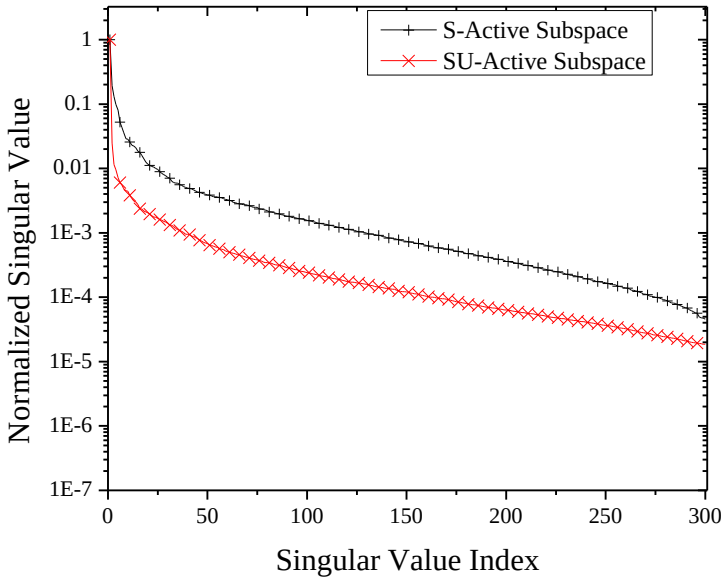

Figure 8-10. Singular Value Spectrum
(Nonlinear Uncertainty Propagation, $\vec{\Sigma} \in \mathbb{R}^{1584}$)

In **Table 8-1**, the average values of the 100 NL ratios defined in Eq. **(6.26)** are compared to see the nonlinearity of the responses. As can be seen, the average NL ratios are small, which means the linear behavior is much larger than the nonlinear behavior. Therefore, the

www.manaraa.com

impact of the error due to the reduction in the higher order terms would be damped, i.e. significant reduction of the dimension can be achieved.

Table 8-1. Average NL Ratio Comparison of the 100 Test Samples (Nonlinear Uncertainty Propagation, $\vec{\Sigma} \in \mathbb{R}^{1584}$)

Response No.	NL Ratio	Response No.	NL Ratio
1	5.8218E-02	23	3.1338E-02
2	4.3656E-02	24	1.7700E-02
3	2.2873E-02	25	1.2658E-02
4	3.4311E-02	26	1.2821E-02
5	1.7446E-02	27	1.7681E-02
6	4.7323E-02	28	7.3931E-02
7	2.9120E-02	29	3.1193E-02
8	3.9443E-02	30	2.1806E-02
9	9.8798E-02	31	2.6172E-02
10	2.6266E-02	32	2.0107E-02
11	3.9656E-02	33	1.4801E-02
12	2.8238E-02	34	1.4578E-02
13	9.1046E-02	35	1.1198E-01
14	3.7959E-02	36	6.1870E-02
15	4.2748E-02	37	2.7874E-02
16	3.3972E-02	38	2.5464E-02
17	1.8617E-02	39	2.5597E-02
18	3.1805E-02	40	2.7606E-02
19	7.1772E-01	41	2.9057E-02
20	1.7533E-02	42	2.2408E-02
21	1.4763E-02	43	2.0636E-02
22	2.2353E-02	44	1.9696E-02

In **Table 8-2**, the R^2 values for the first order approximation and the second order approximation with multi-surrogate modeling are listed. As can be seen, the second order approximation estimates the response changes very accurately; thus, it can replace the original model.

www.manaraa.com

Table 8-2. R^2 Value Comparison of Reduced Order Regression Approach ($r = 50$)

Response No.	First Order Approx.	Second Order Approx.	Response No.	First Order Approx.	Second Order Approx.
1	9.99238E-01	9.99889E-01	23	9.99861E-01	1.00000E+00
2	9.99632E-01	9.99965E-01	24	9.99873E-01	1.00000E+00
3	9.99771E-01	9.99992E-01	25	9.99880E-01	9.99999E-01
4	9.99835E-01	9.99998E-01	26	9.99883E-01	1.00000E+00
5	9.99892E-01	9.99998E-01	27	9.99877E-01	1.00000E+00
6	9.99860E-01	9.99997E-01	28	9.99873E-01	1.00000E+00
7	9.99877E-01	9.99998E-01	29	9.99870E-01	1.00000E+00
8	9.99849E-01	9.99998E-01	30	9.99864E-01	1.00000E+00
9	9.99848E-01	9.99998E-01	31	9.99858E-01	9.99999E-01
10	9.99839E-01	9.99999E-01	32	9.99852E-01	9.99999E-01
11	9.99830E-01	9.99999E-01	33	9.99848E-01	1.00000E+00
12	9.99825E-01	9.99999E-01	34	9.99841E-01	1.00000E+00
13	9.99825E-01	9.99999E-01	35	9.99834E-01	1.00000E+00
14	9.99825E-01	9.99999E-01	36	9.99828E-01	1.00000E+00
15	9.99836E-01	9.99999E-01	37	9.99822E-01	1.00000E+00
16	9.99836E-01	9.99999E-01	38	9.99816E-01	1.00000E+00
17	9.99836E-01	9.99999E-01	39	9.99810E-01	1.00000E+00
18	9.99851E-01	9.99999E-01	40	9.99805E-01	1.00000E+00
19	9.99868E-01	9.99999E-01	41	9.99798E-01	1.00000E+00
20	9.99852E-01	9.99999E-01	42	9.99779E-01	1.00000E+00
21	9.99850E-01	9.99999E-01	43	9.99749E-01	1.00000E+00
22	9.99856E-01	1.00000E+00	44	9.99637E-01	1.00000E+00

In **Figure 8-11**, the distribution of the response changes due to the input parameter variations are shown. The blue line is the normal distribution curve. Because the model is the thermal reactor model, the thermal region, i.e. energy group number > 25, is more sensitive than the fast region, i.e. energy group number < 25. Therefore, one can see larger uncertainty for responses in thermal region and larger deviation from the normal distribution. In **Table 8-**

www.manaraa.com

3 and **Figure 8-12**, the response uncertainties estimated by the nonlinear surrogate approach and the conventional sandwich rule are compared. One can see that the conventional sandwich underestimates the response uncertainty due to the linear assumption.

Table 8-3. Comparison of the Response Uncertainty Estimations (Nonlinear Uncertainty Propagation, $\vec{\Sigma} \in \mathbb{R}^{1584}$)

Response No.	Response Uncertainty Estimate		Response No.	Response Uncertainty Estimate	
	Nonlinear Surrogate	Conventional Sandwich		Nonlinear Surrogate	Conventional Sandwich
1	6.06042E-03	5.82048E-03	23	8.10094E-03	7.97372E-03
2	6.21874E-03	6.01350E-03	24	8.75438E-03	8.62924E-03
3	6.31496E-03	6.13785E-03	25	9.64688E-03	9.51095E-03
4	6.40806E-03	6.26321E-03	26	1.10161E-02	1.08555E-02
5	6.40889E-03	6.26446E-03	27	1.24038E-02	1.22079E-02
6	6.41212E-03	6.27744E-03	28	1.30603E-02	1.28499E-02
7	6.42623E-03	6.29069E-03	29	1.38409E-02	1.36209E-02
8	6.40477E-03	6.26900E-03	30	1.52814E-02	1.50600E-02
9	6.38215E-03	6.24486E-03	31	1.66131E-02	1.63870E-02
10	6.41187E-03	6.27566E-03	32	1.73436E-02	1.71056E-02
11	6.53713E-03	6.40194E-03	33	1.80558E-02	1.78083E-02
12	6.73082E-03	6.59879E-03	34	1.92486E-02	1.89864E-02
13	6.80460E-03	6.67260E-03	35	2.10391E-02	2.07538E-02
14	6.86512E-03	6.73472E-03	36	2.27006E-02	2.23907E-02
15	7.11772E-03	6.99188E-03	37	2.41212E-02	2.37920E-02
16	7.15222E-03	7.02825E-03	38	2.52877E-02	2.49449E-02
17	7.45622E-03	7.32506E-03	39	2.63234E-02	2.59713E-02
18	7.72519E-03	7.59841E-03	40	2.72784E-02	2.69175E-02
19	8.62395E-03	8.50377E-03	41	2.90935E-02	2.86996E-02
20	7.76254E-03	7.64102E-03	42	3.20503E-02	3.15785E-02
21	7.74099E-03	7.61439E-03	43	3.44596E-02	3.39301E-02
22	7.94718E-03	7.81521E-03	44	4.10244E-02	4.03679E-02

www.manaraa.com

Figure 8-11. Response Change Distribution due to Input Parameter Uncertainty

(Nonlinear Uncertainty Propagation, $\vec{\Sigma} \in \mathbb{R}^{1584}$)

www.manaraa.com

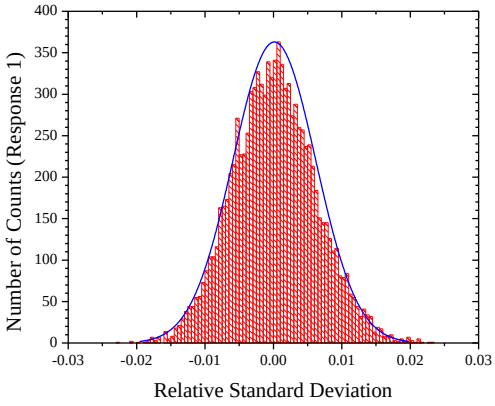

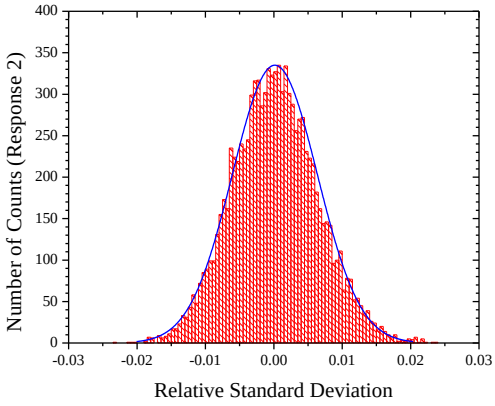

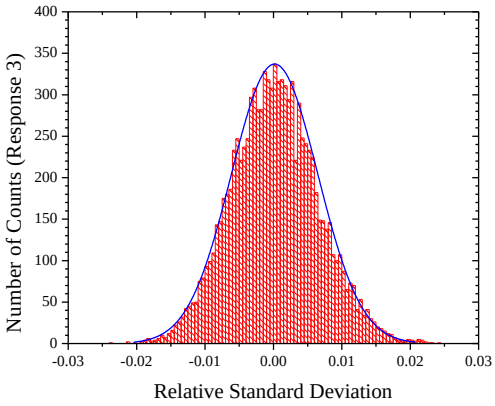

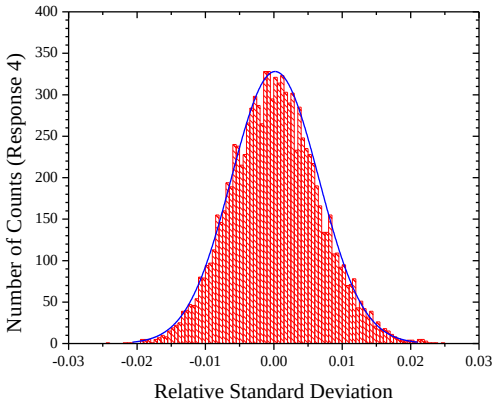

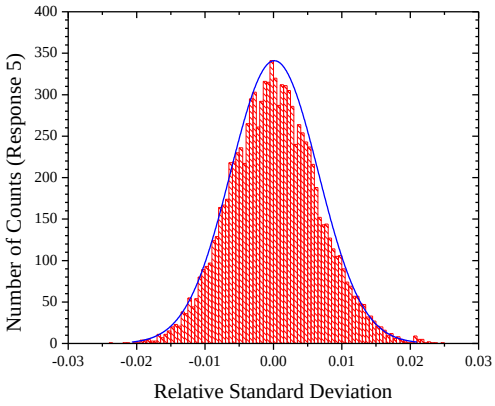

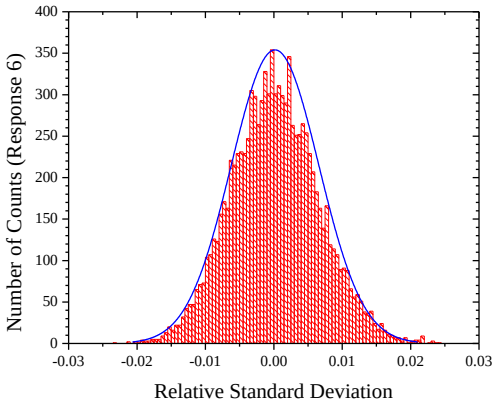

www.manaraa.com

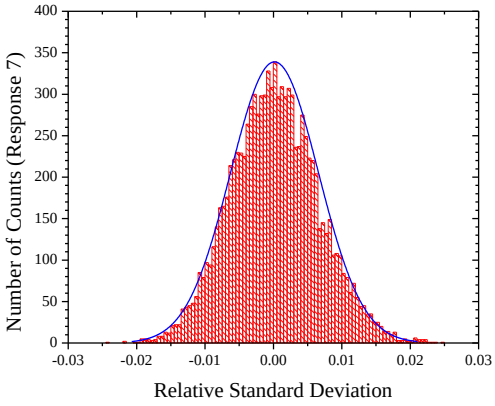

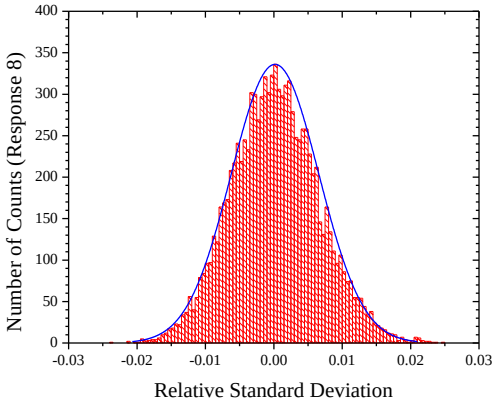

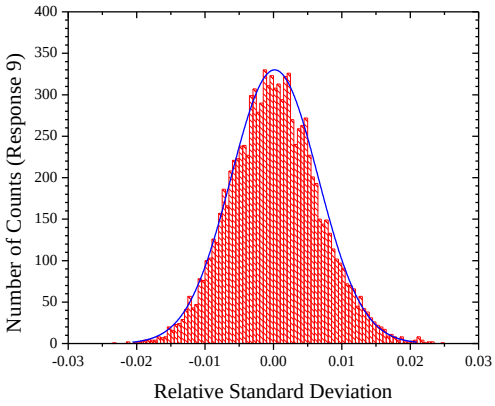

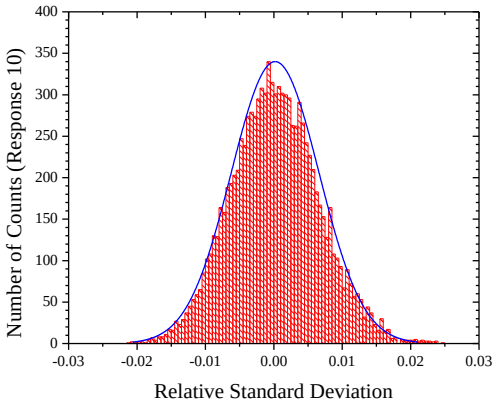

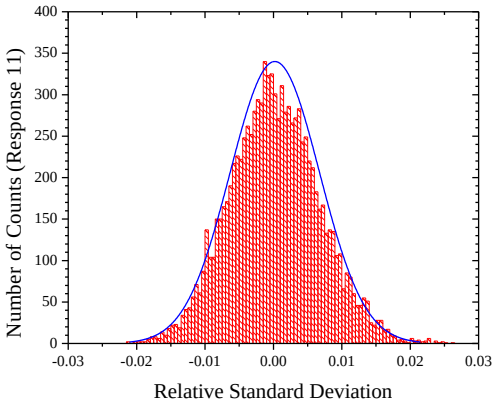

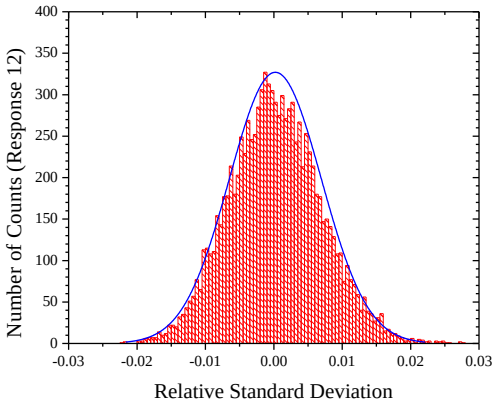

www.manaraa.com

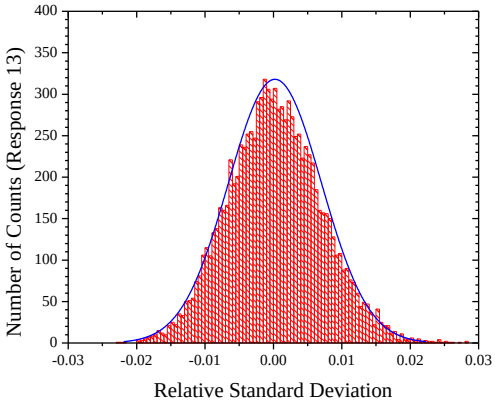

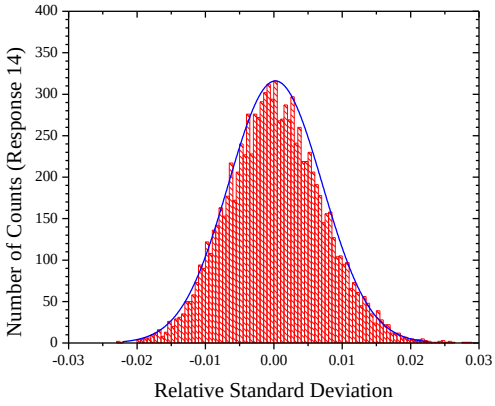

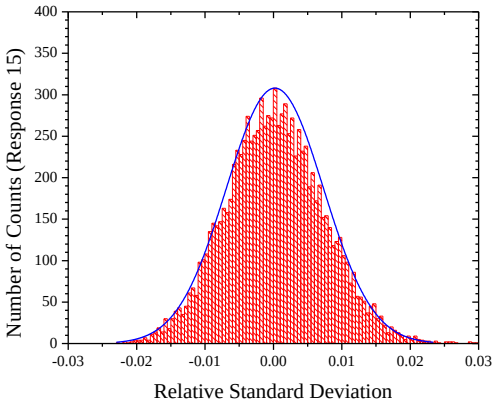

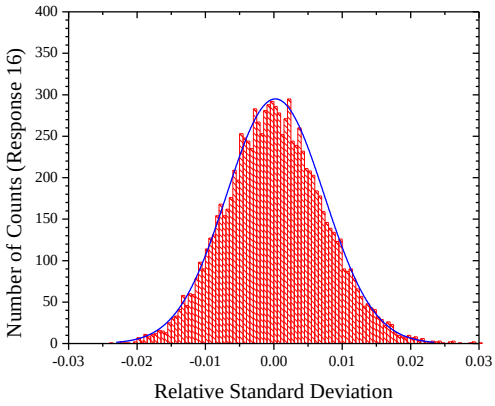

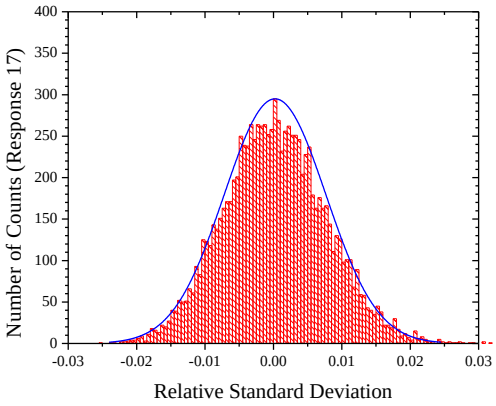

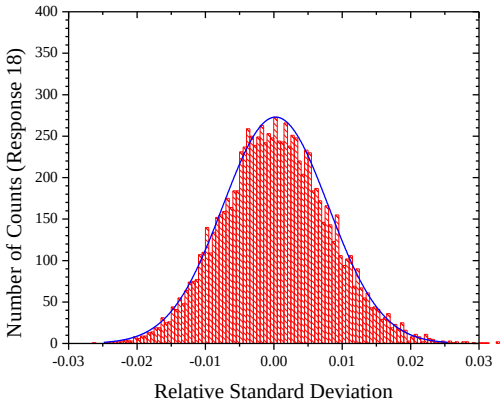

www.manaraa.com

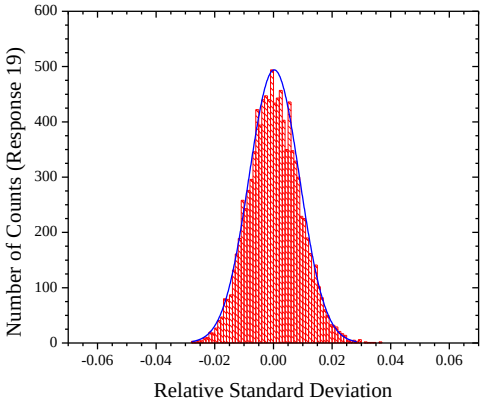

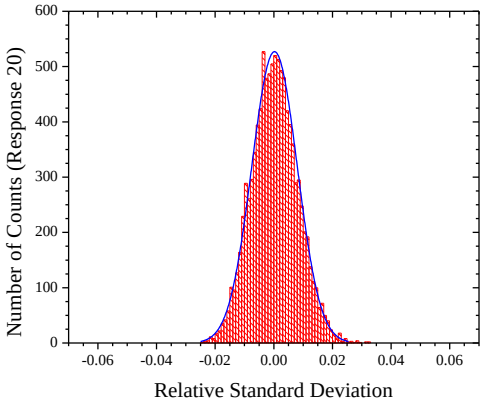

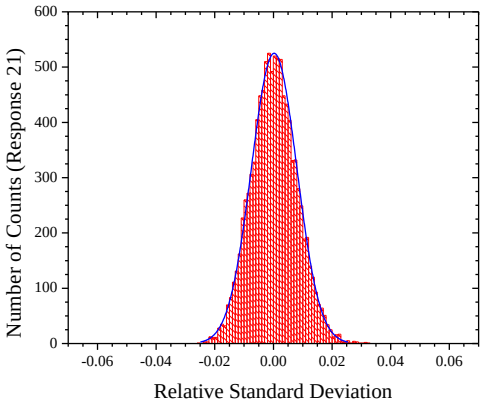

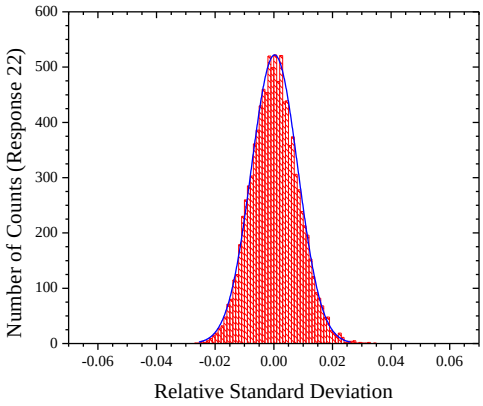

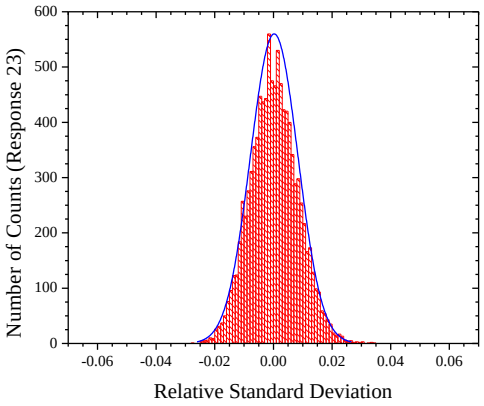

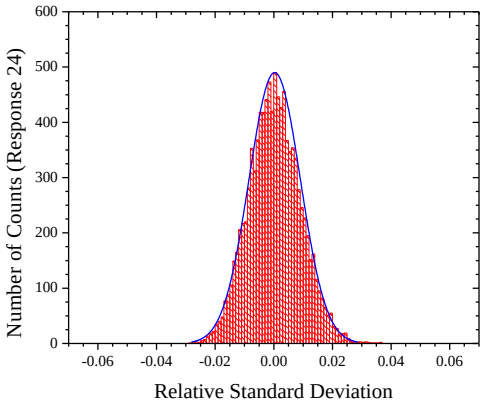

www.manaraa.com

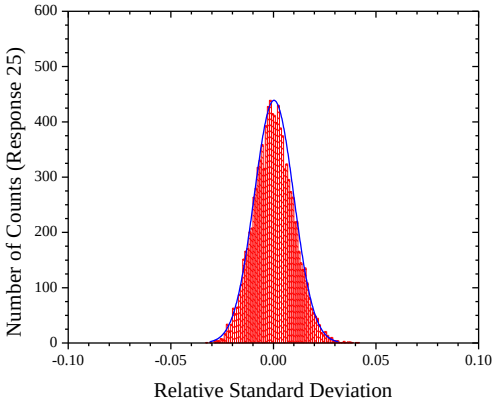

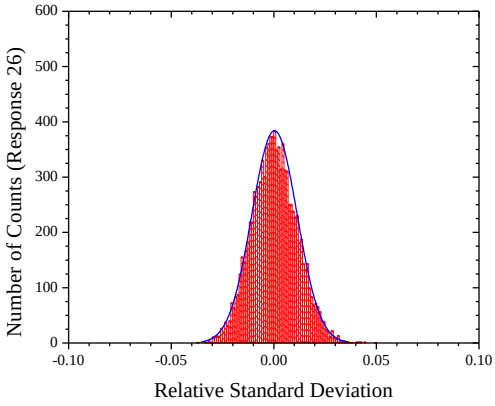

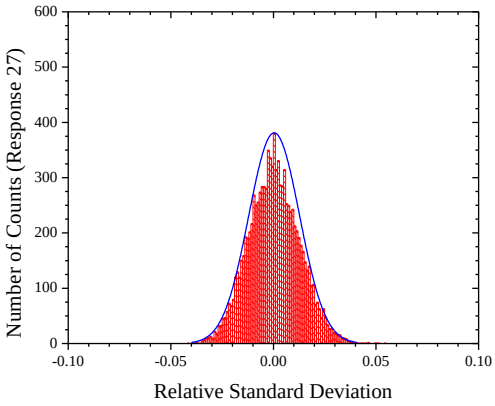

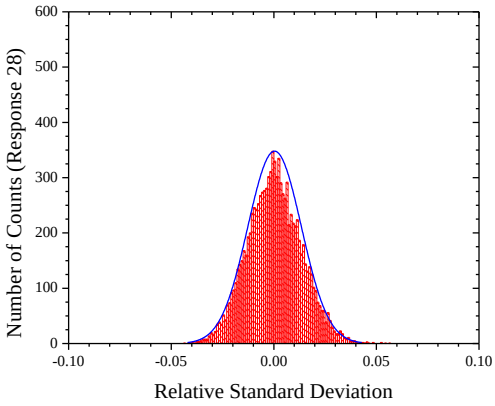

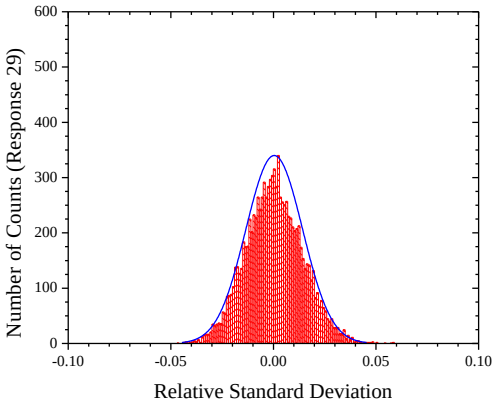

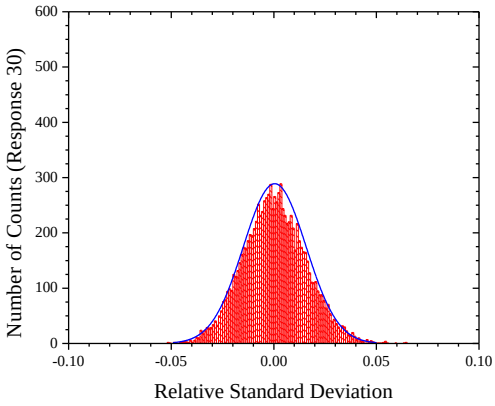

www.manaraa.com

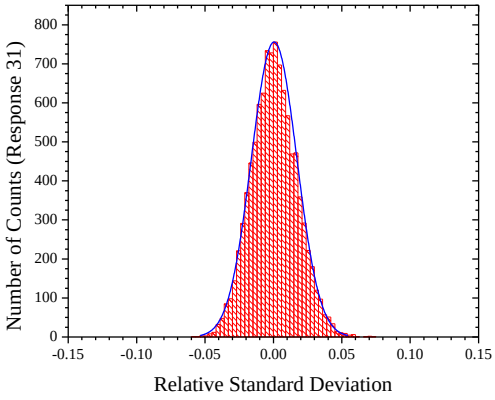

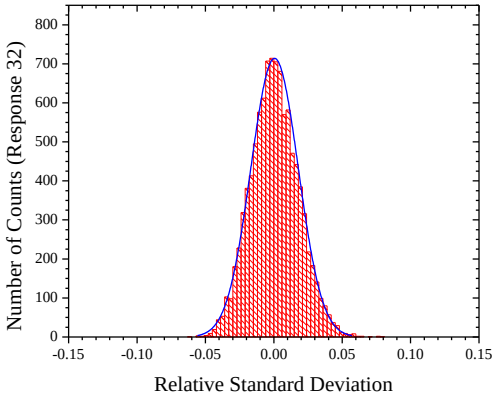

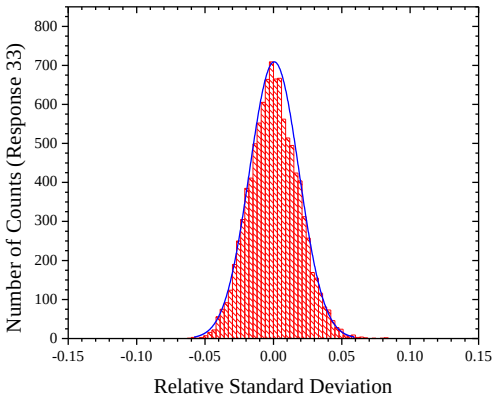

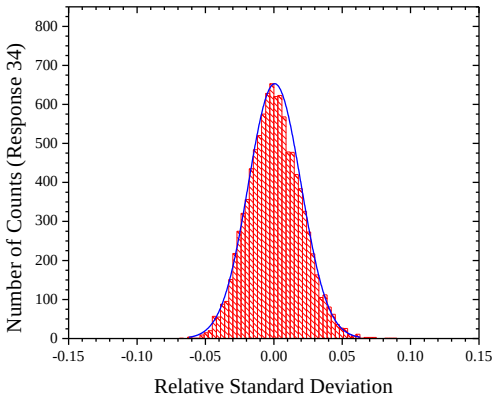

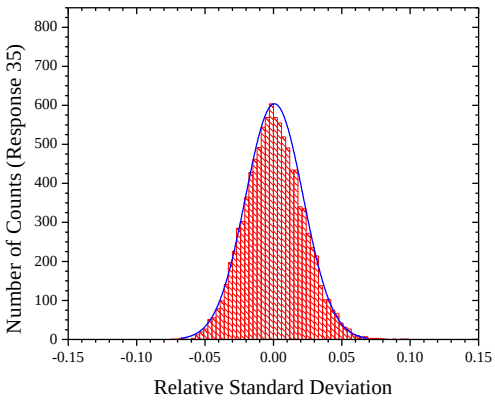

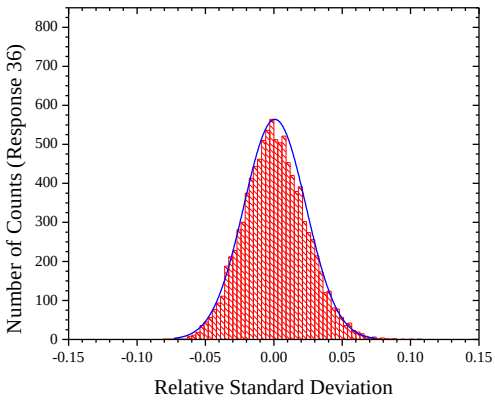

www.manaraa.com

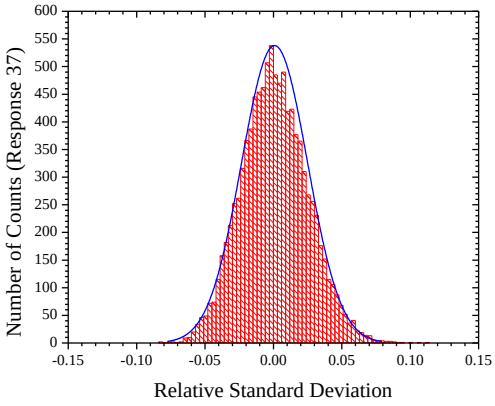

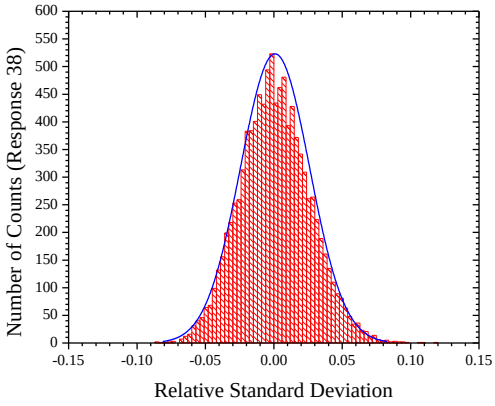

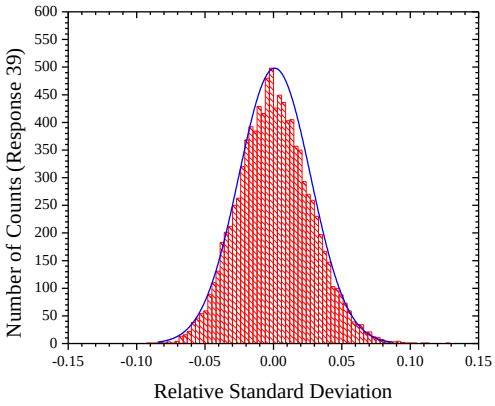

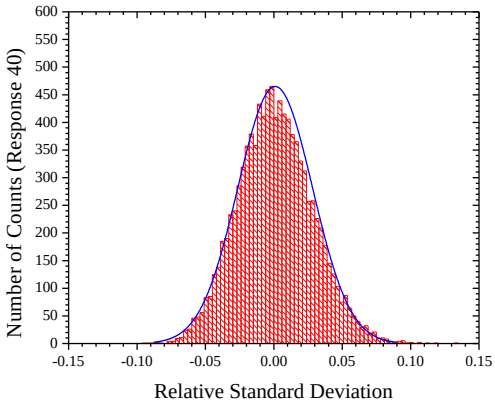

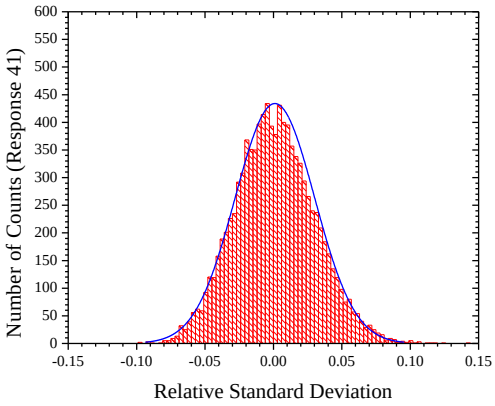

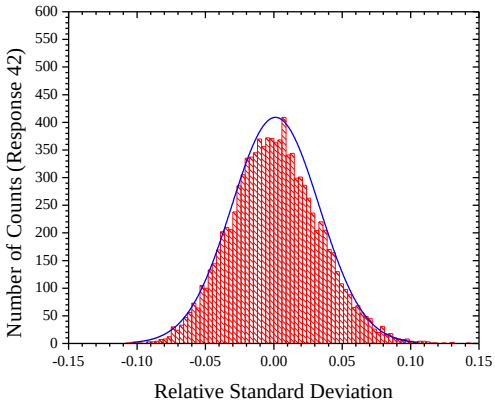

www.manaraa.com

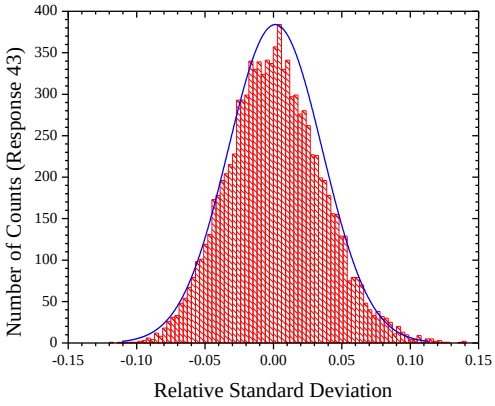

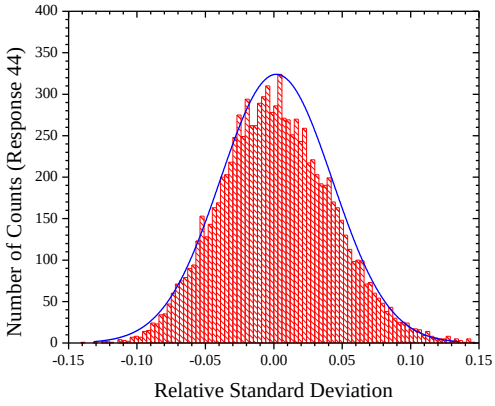

www.manaraa.com

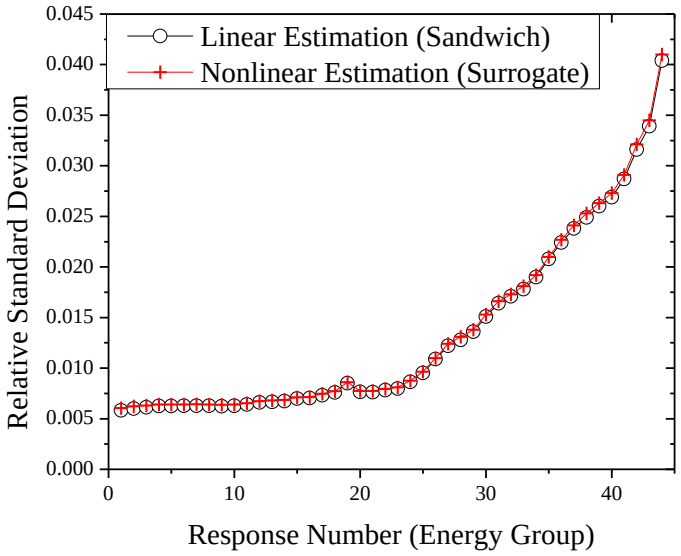

Figure 8-12. Comparison of the Response Uncertainty Estimations (Nonlinear Uncertainty Propagation, $\bar{\Sigma} \in \mathbb{R}^{1584}$)

www.manaraa.com

CHAPTER 9. REDUCED ORDER MODELING FOR DEPLETION CALCULATIONS

The intersection subspace approach is exercised on depletion calculations of semi-realistic assembly models. Not like uncertainty propagation in which only small input parameter variations need to be considered, the depletion process changes the material number density much more than the one in uncertainty quantification; thus, the nonlinear behavior (higher order effects) become more effective. Moreover, because the depletion produces many different nuclides due to fission and decay, much more nuclides should be taken into account which means the original dimension would be very large and complex correlations would appear.

The reduced order modeling with the range finding algorithm is applied to two assembly models; Peach Bottom Unit 2 Boiling Water Reactor (PB-2 BWR) and Watts Bar Unit 2 Pressurized Water Reactor (WB-2 PWR). BWR model contains Gadolinium (i.e. Gd-155 and Gd-157) materials as burnable poison which is burn-out fast in early stage of fuel cycle. Due to Gd-155 and Gd-157 burnt-out, it is expected that the flux distributions and the sensitivity profiles are changed significantly. The purpose of BWR model test is to examine the performance of the proposed reduced order modeling with the intersection approach in the highly nonlinear realistic assembly model depletion calculations. With the PWR model, more

www.manaraa.com

realistic depletion calculation is conducted. To capture the burn-up variations, each pin-cell is assigned to unique material identification number, which makes the original input parameter (macroscopic cross section) dimension very large. Moreover, to emulate the control rod insertion, burnable poison rods (BPR) are included in depletion calculations. Thus, the purpose of PWR model test is to examine the performance of the proposed reduced order modeling with the intersection approach with the full set of assembly calculations for few-group cross section generation.

Note that assembly calculation consists of two steps; problem-dependent cross section library preparation (resonance self-shielding calculation) and neutron distribution calculation by solving transport equation as can be seen in **Figure 9-1**. For SCALE calculation, BONAMI and NEWT are used for resonance calculation and transport calculation, respectively. Therefore, one can consider that the lattice physics calculation consists of two ***serially coupled models***. Note that BONAMI gets the material data and produces the resonance self-shielded macroscopic cross sections which are used by NEWT as input parameters to calculate k-eff and scalar fluxes. The purpose of this study is to exercise the reduced order modeling on macroscopic cross sections for entire depletion range. Note that as the materials are depleted, the number densities of them are changed, which are the inputs of BONAMI. First, the active subspace of macroscopic cross section variations determined by BONAMI due to number density and temperature variations is examined. This subspace will be called as a Variation Subspace ***(V-Subspace)***. Second, the active subspace of macroscopic cross section with respect to NEWT is investigated. This subspace will be called

www.manaraa.com

as a Sensitivity Subspace ***(S-Subspace)***. After that, the intersection subspace in terms of BONAMI and NEWT is compared. This subspace will be referred to as a Intersection Subspace ***(I-Subspace)***. The subspace approach can be expressed physically as shown in **Table 9-1**. Basically, the intersection subspace is intended to capture the component of **Component 1,** i.e. the component of large change and high sensitivity.

This study focus only on the reduced order modeling, i.e. basis construction for reducing input parameters (macroscopic cross sections). Those constructed basis vectors are verified by using three methods; singular value spectrum, portion of orthogonal component to active subspace and κ-metric.

Table 9-1. Subspaces Considered in Intersection Subspace Identification

		Macroscopic Cross Section Change (Active Subspace due to Resonance Model)	
		Large $\Delta\vec{\Sigma}$	(very) Small $\Delta\vec{\Sigma}$
Cross Section Change Sensitivity (Active subspace of transport model)	High Sensitivity	**Component 1**	**Component 2**
	(very) Low Sensitivity	**Component 3**	**Component 4**

www.manaraa.com

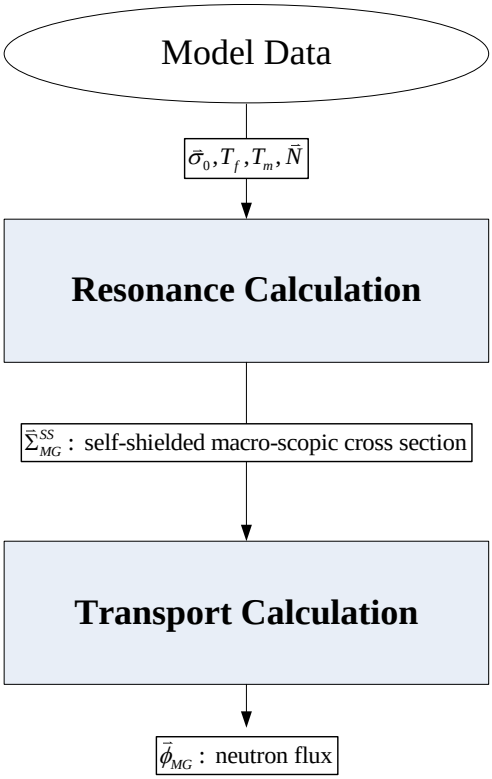

Figure 9-1. Schematics of Lattice Calculation

www.manaraa.com

9.1 BWR Assembly Model

9.1.1 Overview of Model

Peach Bottom Atomic Power Station Unit 2 (PB-2) is the 1112MWe Boiling Water Reactor (BWR) constructed by General Electric. For the need of uncertainty evaluations for Light Water Reactor (LWR) best-estimate calculations, the modeling aspects of uncertainty analysis and sensitivity analysis are recognized to be further developed and validated on scientific grounds. In consequence, OECD/NEA defined the reference LWR systems and scenarios for Uncertainty Analysis in Modeling (UAM) for design, operation and safety analysis of LWRs. PB-2 BWR is the first chosen LWR system because it is well documented [Ivanov et al. (2007)]. In this study, PB-2 SCALE model is used to study the depletion calculation and poison materials (e.g. Gd-155 and Gd-157) effects. **Figure 9-2** depicts the model analyzed; it is a stand-alone benchmark model designed by OECD/NEA to assess the assumptions in current LWR standard lattice physics scheme for generation of few-group cross-sections [Ivanov et al., 2007]. The 49 energy group library built by collapsing 238 energy group library (v7-238) is used and the reference k_{eff} is 1.11198246. The PB-2 Type 2 assembly model with initial fuel is depleted by SCALE6.1 TRITON module. Detailed model specifications are listed in **Table 9-2** and **Table 9-3**.

www.manaraa.com

Table 9-2. PB-2 Fuel Assembly Data

Assembly Type	2
No. of assemblies, initial core	263
No. of assemblies, Cycle 2	261
Geometry	7×7
Assembly pitch, mm	152.4
Fuel rod pitch, mm	18.75
Fuel rods per assembly	49
Water rods per assembly	0
Burnable poison positions	4
No. of spacer grids	7
Inconel per grid, kg	0.225
Zr-4 per grid, kg	1.183
Spacer width, cm	4.128
Assembly average fuel composition: **Gd2O3, g** **UO2, kg**	 441 212.21
Total fuel, kg	212.65

Table 9-3. PB-2 Assembly Design –Type 2 Initial Fuel

Rod Type	235U (wt.%)	Gd2O3 (wt.%)	No. of rods
1	2.93	0	26
2	1.94	0	12
3	1.69	0	6
4	1.33	0	1
5A	2.93	3.0	3
6B	2.93	3.0	1

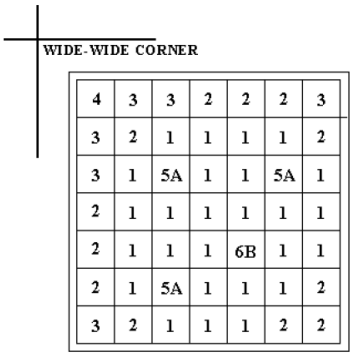

www.manaraa.com

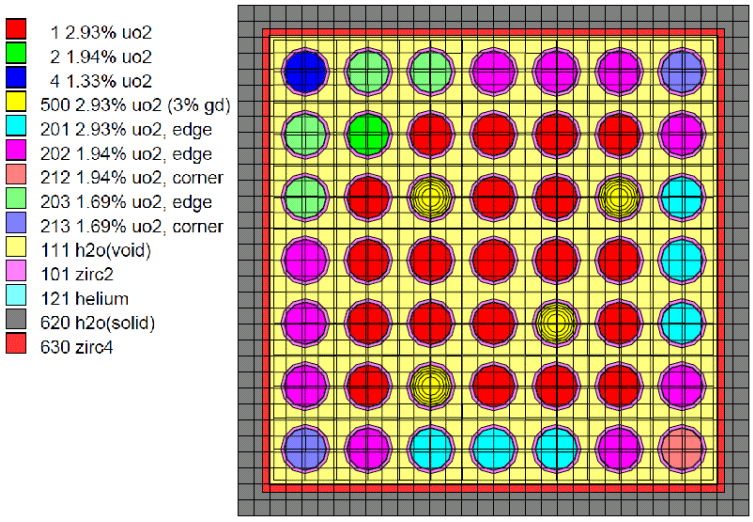

Figure 9-2. A 7x7 BWR Benchmark Assembly Model

Reference Depletion Calculation

For single depletion step calculation, the sequence of BONAMI (resonance self-shielding calculation) – NEWT (transport calculation for neutron flux distribution) – ORIGEN (nuclide depletion calculation) is conducted. Each depletion step is chosen to 40 days with 40 MW power. The k-eff variation due to depletion is shown in **Figure 9-3**. Interesting behavior is the k-eff value increases after about 12 steps (480 days) and after a few steps, starts to decrease again. That is because of Gd-155 and Gd-157 which is a strong absorber induces high nonlinearity because of its very strong spatial shielding effects [Lee et al. (2009)]. Those are depleted in early stage as can be seen in **Figure 9-4**; thus, in view of neutron economy, neutron loss is diminished after their burn-out. Therefore, the multiplication factor starts to increase during a few steps but due to U-235 depletion, it decreases again.

www.manaraa.com

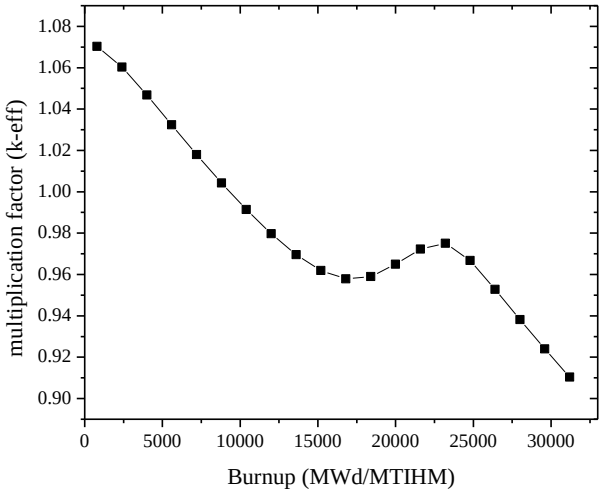

Figure 9-3. k-eff Change in Reference Depletion Calculation

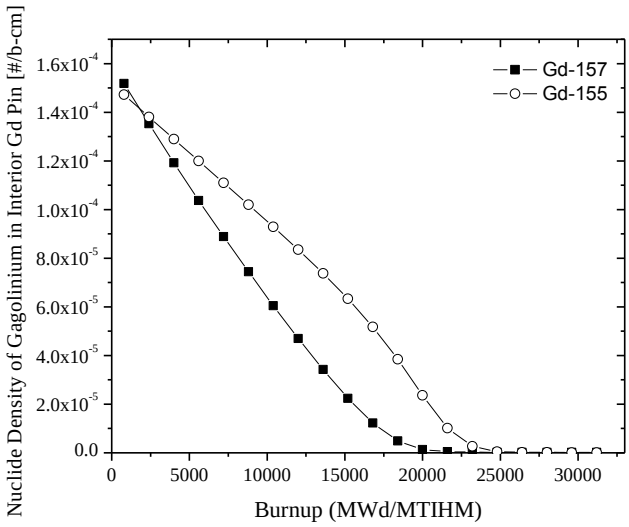

Figure 9-4. Gadolinium Nuclide Density Change due to Depletion

www.manaraa.com

9.1.2. V-Subspace Construction

In this stage, the resonance self-shielded macroscopic cross sections are considered as the output responses of the resonance calculation (BONAMI). Note that as the material depleted, the fuel materials are decreased while the fission fragments are increased. There can be two correlations in the resonance self-shielded macroscopic cross section changes; number density and depletion. First, note that the macroscopic cross section is defined as:

$$\vec{\Sigma}_i = N_i \vec{\sigma}_i \tag{9.1}$$

where $\vec{\Sigma}_i = \left[\Sigma_{1,i} \quad \cdots \quad \Sigma_{G,i} \right]^T$ is a vector of i th nuclide's macroscopic cross sections, $\vec{\sigma}_i = \left[\sigma_{1,i} \quad \cdots \quad \sigma_{G,i} \right]^T$ is a vector of i th nuclide's microscopic cross sections, N_i is the number density of i th nuclide and G is the number of energy groups. Therefore, if a number density of a nuclide is varied, the whole macroscopic cross sections of the nuclide are changed relatively same amount, i.e. changes together in the same direction. Due to resonance self-shielding effects, the changes of macroscopic cross sections are not exactly same amount but still one can see significant correlation between them. Second, the productions of some nuclides are come from other nuclides' depletion, e.g. fission or decay. For example, the uranium materials are only depleted not produced while other fission fragments, e.g. Xenon, Samarium, Ruthenium, Technetium, are increased. Therefore, one can also see significant correlations between number density changes. With those correlations, we expect that the size of the active subspace of the resonance self-shielded macroscopic cross section, i.e. V-subspace would be much smaller than its dimension.

www.manaraa.com

Sampling Scheme

Note that the nuclide density change for each isotope due to depletion is calculated by reference calculation. Thus, the ranges of nuclide number density changes are already known. One can generate the random sample sets simply by random-sampling from the each isotope's number density range. In this study, however, in order to consider the correlations due to depletion properly, the special sampling scheme is devised. First, sample the depletion step randomly and sample each nuclide's density from the density range at that depletion step. Note that we introduce ±20% variations in nuclide densities with respect to the reference case to consider more general cases (shaded area in **Figure 9-5**). The fuel and moderator temperatures are randomly perturbed by ±10%.

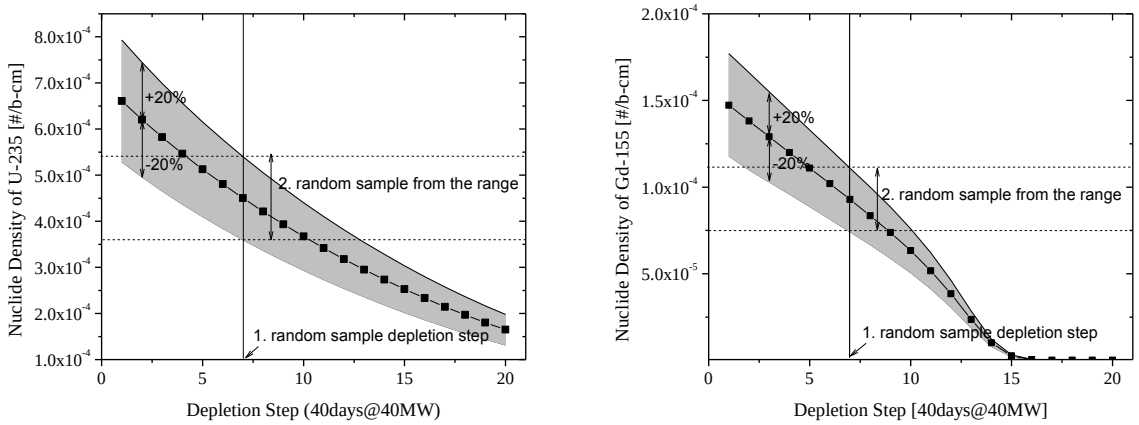

Figure 9-5. Sampling Scheme

www.manaraa.com

Active Subspace Identification

The active subspace of the resonance self-shielded macroscopic cross section changes due to number density and temperature variations (V-Subspace) is identified by the range finding algorithms. For sampling, the special sampling scheme described above is used. Identifying the active subspace can be considered as finding patterns in macroscopic cross section changes. Once those patterns are extracted, a macroscopic cross section change can be represented by a sum of those patterns:

$$\Delta\vec{\Sigma} = \sum_{i=1}^{r} \alpha_i \vec{q}_i \tag{9.2}$$

where $\vec{q}_i$ for $i = 1,...,r$ are the orthonormal basis of the active subspace, i.e. pattern, α_i for $i = 1,...,r$ are the coefficients and r is the size of the active subspace. Note that r is expected to be smaller than n which is the original dimension of the macroscopic cross sections.

In the PB-2 BWR SCALE model, all nuclides in all mixtures are considered, i.e. 914 nuclides with 49 energy groups. Thus, **the original dimension of the macroscopic cross section is 44,786**. To implement the range finding algorithm, the nominal configuration is specified and then, the random variations from the nominal configuration are examined. The nominal configuration N_0 is determined simply by taking median valued of the maximum and minimum nuclide densities for each nuclide as can be seen in **Figure 9-6**.

www.manaraa.com

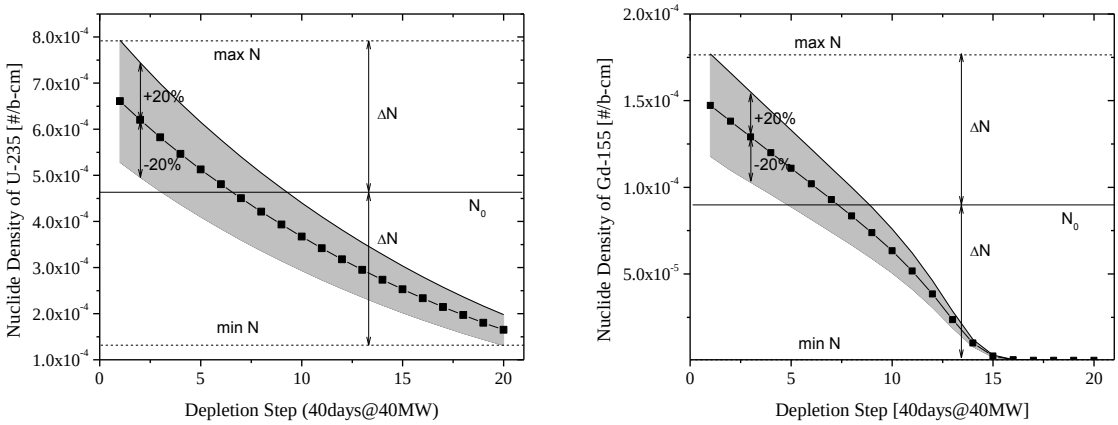

Figure 9-6. Determination of Nominal Configuration

The 1000 sets of macroscopic cross sections are calculated by executing BONAMI with sampled number densities and temperatures. For each calculated macroscopic cross section, the relative variation is calculated:

$$\frac{\Delta\Sigma_{i,g}^{(k)}}{\Sigma_{i,g}^{(0)}} = \frac{\Sigma_{i,g}^{(k)} - \Sigma_{i,g}^{(0)}}{\Sigma_{i,g}^{(0)}} \tag{9.3}$$

where $\Sigma_{i,g}^{(0)}$ is the i th nuclide and g th energy group macroscopic cross section calculated with nominal number density and temperatures and $\Sigma_{i,g}^{(k)}$ is the i th nuclide and g th energy group macroscopic cross section calculated with perturbed number densities and temperatures.

The size of the active subspace is investigated by three methods; singular value spectrum, portion of orthogonal component to active subspace and κ-metric.

www.manaraa.com

- **Singular Value Spectrum**

The singular value decomposition [Golub & Van Loan (1996)] of a matrix $\mathbf{A} \in \mathbb{R}^{n \times n}$ is given by:

$$\mathbf{A} = \mathbf{U}\boldsymbol{\Sigma}\mathbf{V} = \sum_{i=1}^{n} \sigma_i \vec{u}_i \vec{v}_i^T \approx \sum_{i=1}^{r} \sigma_i \vec{u}_i \vec{v}_i^T \tag{9.4}$$

where $\vec{u}_i$ and $\vec{v}_i$ are the orthonormal vectors. Thus, the σ_i can be considered as the importance of the subspace spanned by $\vec{u}_i$ or $\vec{v}_i$. As can be seen in Eq. (4.28), by considering only components with large importance, one can construct the low-rank approximation of the matrix $\mathbf{A}$. We examine the singular value spectrum of the matrix $\mathbf{X}$ which is defined by:

$$\mathbf{X} = \left[\frac{\Delta\vec{\Sigma}^{(1)}}{\vec{\Sigma}^{(0)}} \quad \cdots \quad \frac{\Delta\vec{\Sigma}^{(k)}}{\vec{\Sigma}^{(0)}} \right] \tag{9.5}$$

where $\vec{\Sigma}^{(0)} \in \mathbb{R}^{44,786}$ is the vector of all macroscopic cross sections at the nominal configuration and $\vec{\Sigma}^{(k)} \in \mathbb{R}^{44,786}$ is the vector of all macroscopic cross sections at the k th perturbed case. Therefore, the element of the matrix $\mathbf{X}$ is the relative change of the macroscopic cross section.

In **Figure 9-7**, the singular value spectrum of the matrix $\mathbf{X}$ is presented. One can see that the singular value spectrum decays gradually and has rapid drop around 900. Note that the number of nuclides considered is 914. As explained before, the macroscopic cross sections have correlations due to nuclide density. Therefore, with about 900 basis vectors, the major variations in the macroscopic cross sections can be represented accurately.

www.manaraa.com

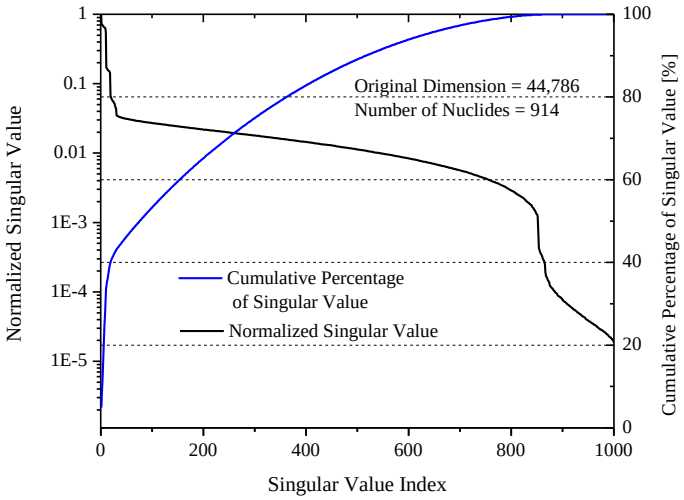

Figure 9-7. Singular Value Spectrum of V-Subspace

- **Portion of Orthogonal Component**

Given the basis $\mathbf{Q}$, the macroscopic cross section variations can be represented by:

$$\frac{\Delta\vec{\Sigma}}{\vec{\Sigma}^{(0)}} = \left(\frac{\Delta\vec{\Sigma}}{\vec{\Sigma}^{(0)}}\right)^{\|} + \left(\frac{\Delta\vec{\Sigma}}{\vec{\Sigma}^{(0)}}\right)^{\perp} = \mathbf{Q}\mathbf{Q}^{T}\frac{\Delta\vec{\Sigma}}{\vec{\Sigma}^{(0)}} + \left(\mathbf{I}-\mathbf{Q}\mathbf{Q}^{T}\right)\frac{\Delta\vec{\Sigma}}{\vec{\Sigma}^{(0)}} \tag{9.6}$$

where $\Delta\vec{\Sigma}^{\|}$ is the component in the active subspace and $\Delta\vec{\Sigma}^{\perp}$ is the component in the in-active subspace which is orthogonal to the active subspace. The main idea of the reduced order modeling is taking only the active subspace component and discarding the in-active subspace component. Thus, the discarded in-active subspace component can be considered as error due to reduced order transformation. In order to measure that discarded portion, the root mean square (RMS) error for random sample is calculated:

www.manaraa.com

$$r.m.s = \sqrt{\frac{1}{n}\left[\left(\frac{\Delta\vec{\Sigma}}{\vec{\Sigma}^{(0)}}\right)^{\perp}\right]^{T}\left[\left(\frac{\Delta\vec{\Sigma}}{\vec{\Sigma}^{(0)}}\right)^{\perp}\right]} = \sqrt{\frac{1}{n}\sum_{i=1}^{n}\left\{\left(\frac{\Delta\Sigma_i}{\Sigma_i^{(0)}}\right)^{\perp}\right\}^2} \tag{9.7}$$

Test is conducted by following way:

Step 1. Choose the size of the active subspace ($r = 50,100,150,...,1000$)
Step 2. Calculate the basis via Range Finding Algorithm with random samples
Step 3. For additional 10 random samples, calculate the RMS error metric
Step 4. Take the maximum among the 10 RMS error metrics

The results are shown in **Figure 9-8**. As the size increases, the RMS error decreases. Note that after the size of 900, the RMS error is less than 1%.

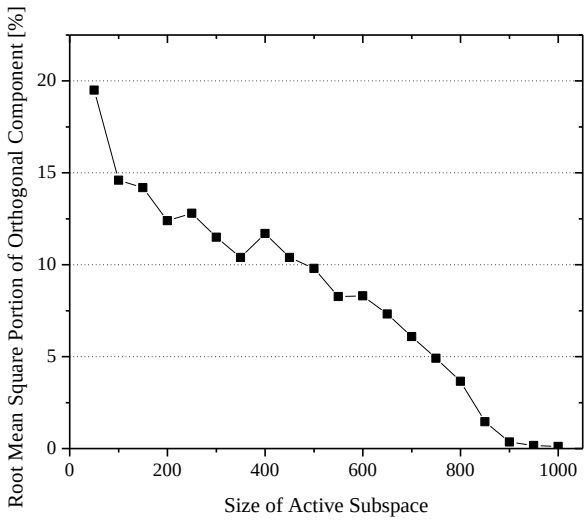

Figure 9-8. RMS Portion of Orthogonal Component of V-Subspace

www.manaraa.com

- **κ-metric**

The previous two approaches are based on completely mathematical sense. However, we need to consider the physical meaning of the subspace extracted. Only considering the mathematical sense, the subspace construction algorithm tends to discard the directions with small variations but physically those directions may have large importance. For example, the macroscopic cross section change of moderator material may be small but the output responses are very sensitive to them. To ensure the constructed basis capture the physics properly, the extra simulation can be used. The κ-metric method is examining the effect of the component not included in the active subspace. Simply, one can execute the code with input parameters perturbed along the direction orthogonal to the active subspace:

$$y = f\left(\Delta\vec{\Sigma}^{\perp}\right) = f\left(\left(\mathbf{I} - \mathbf{Q}\mathbf{Q}^{T}\right)\Delta\vec{\Sigma}\right) \tag{9.8}$$

where f can be considered as a model, e.g. NEWT, and y can be any response, e.g. k-eigenvalue or fluxes. The expected output response changes would be small if the basis is constructed correctly.

The test is conducted by following way:

Step1. The active subspace basis of the resonance self-shielded macroscopic cross section is constructed by the range finding algorithm with BONAMI executions: **Q**

Step 2. The resonance self-shielded macroscopic cross sections at every depletion steps

www.manaraa.com

are collected: $\vec{\Sigma}^{(i)}$ for $i = 1,...,n_{depletion}$

Step 3, The variations of those macroscopic cross sections from the nominal configuration are calculated: $\frac{\Delta\vec{\Sigma}^{(i)}}{\vec{\Sigma}^{(0)}}$ for $i = 1,...,n_{depletion}$

Step 4, The orthogonal components to the active subspace are calculated by projection: $\left(\mathbf{I}-\mathbf{Q}\mathbf{Q}^T\right)\frac{\Delta\vec{\Sigma}^{(i)}}{\vec{\Sigma}^{(0)}}$ for $i = 1,...,n_{depletion}$

Step 5, The transport solver (NEWT) is executed with those orthogonally perturbed macroscopic cross sections: $y^{(0)} + \Delta y^{(i)} = f\left(\vec{\Sigma}^{(0)} + \left(\mathbf{I}-\mathbf{Q}\mathbf{Q}^T\right)\Delta\vec{\Sigma}^{(i)}\right)$ for $i = 1,...,n_{depletion}$

Step 6, Check the changes in response, e.g. k-eff, fluxes and homogenized few group cross sections: $\Delta y^{(i)}$ for $i = 1,...,n_{depletion}$

First, the k-eff changes due to macroscopic cross section perturbation orthogonal to the active subspace are examined in **Figure 9-9**. Note that the original k-eff value changes are shown in **Figure 9-3** in which the k-eff values are varied from -1776 to 14215 [pcm]. As increasing the basis, the more components of the macroscopic cross section variations are captured; thus, the k-eff changes due to the components which are not included in the active subspace are decreased. With 1000 basis vectors, the k-eff changes are a few pcm, which are very small considering the computation precision (single precision) and convergence criteria (10^{-5}).

www.manaraa.com

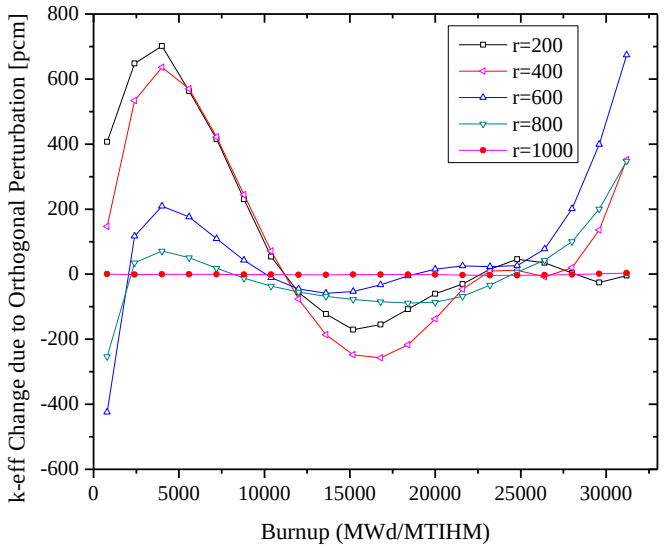

Figure 9-9. k-eff Change due to Macroscopic Cross Section Orthogonal Perturbation

Next, the flux changes due to the orthogonal perturbation are examined in **Figure 9-10** and **Figure 9-11**. In both cases, the flux changes due to in-active subspace components are decreased as the size of basis is increased. With 1000 basis, the flux changes are mostly less than 0.01%. It is important to note that there are very large flux changes in thermal region with Gadolinium (**Figure 9-11**). Especially, after Gd-155 and Gd-157 are burnt-out (after 400days), one can see more than 100% thermal flux changes due to large macroscopic cross section variations. However, the constructed basis can capture those variations properly.

www.manaraa.com

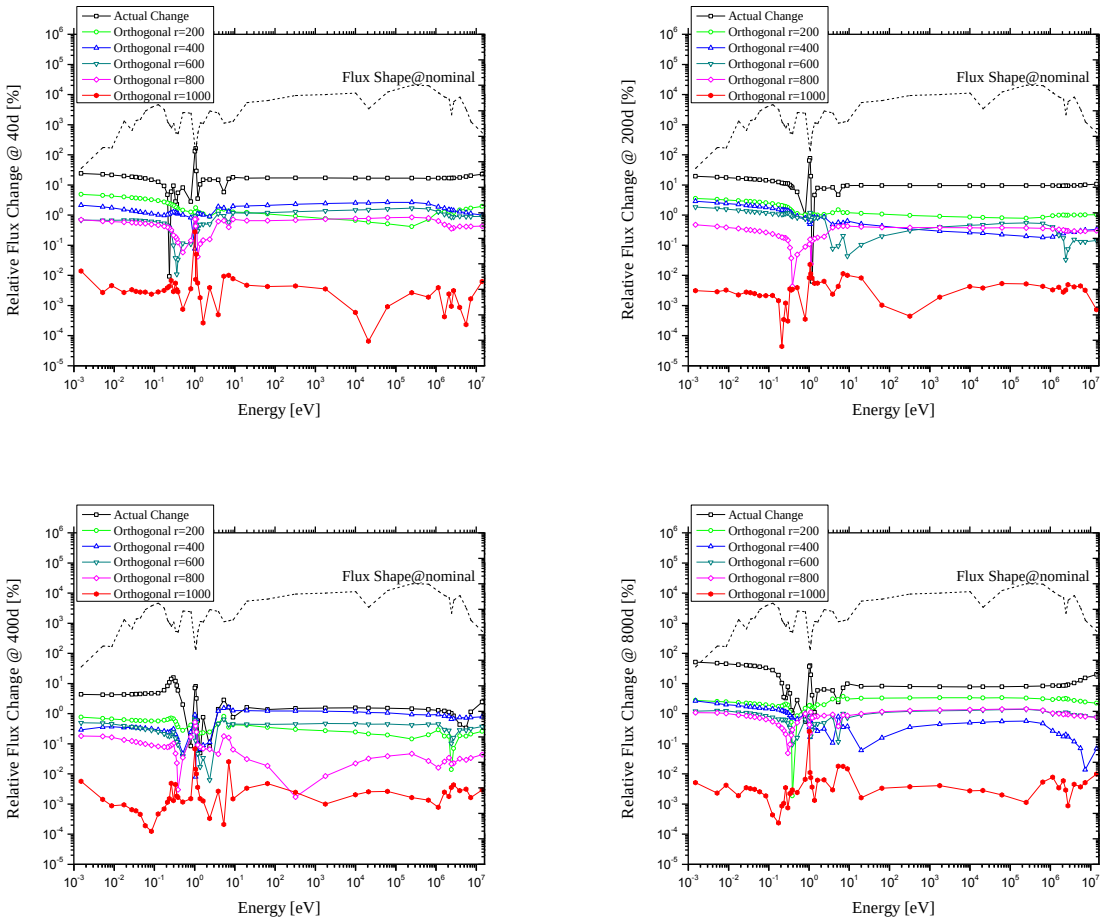

Figure 9-10. Flux Change due to Macroscopic Cross Section Orthogonal Perturbation (fuel pin)

www.manaraa.com

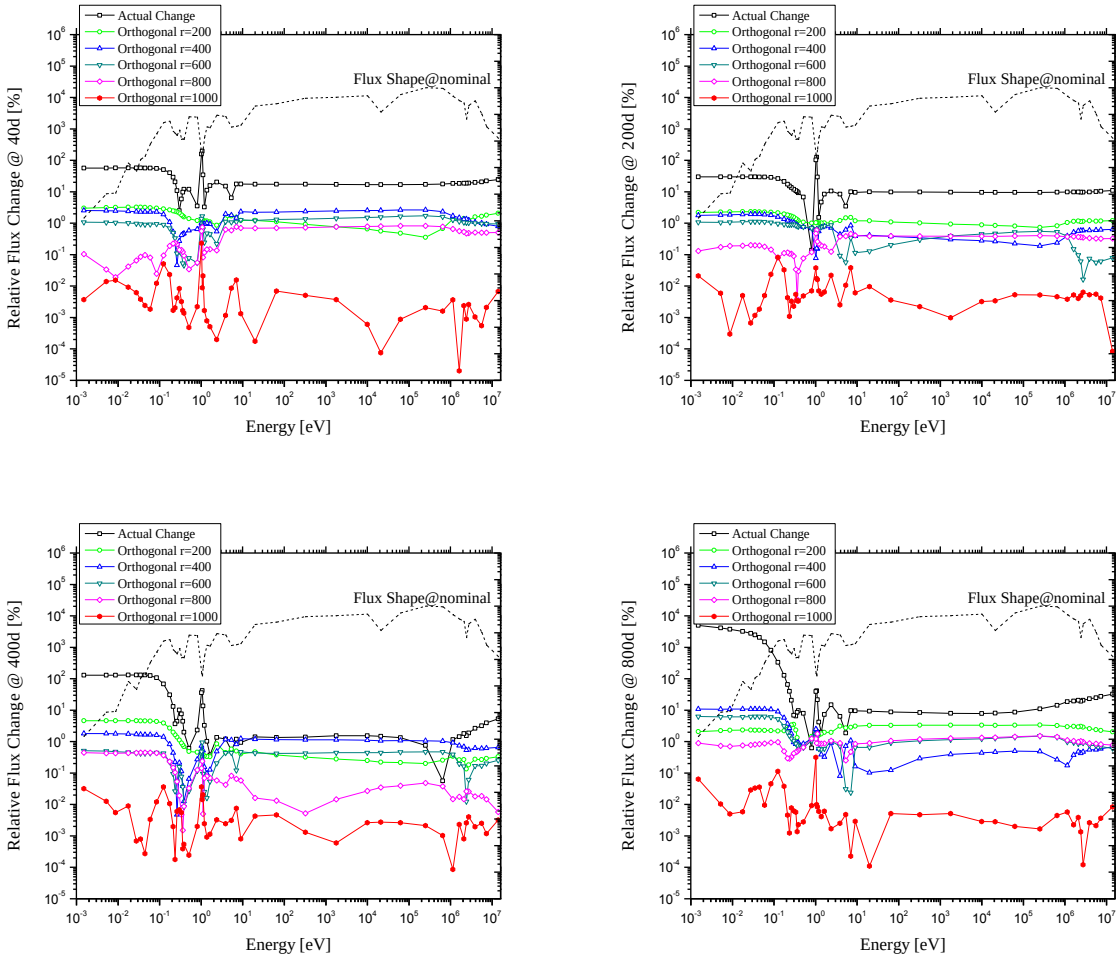

Figure 9-11. Flux Change due to Macroscopic Cross Section Orthogonal Perturbation (fuel + Gadolinium pin)

www.manaraa.com

Lastly, the assembly homogenized two group collapsed macroscopic cross sections are examined. In **Figure 9-12**, the total cross section Σ_t, the absorption cross section Σ_a, the nu*fission cross section $\nu\Sigma_f$, the elastic scattering cross section Σ_s, the capture cross section Σ_c and the diffusion coefficient D are presented. One can see the same behavior of the cross section changes according to the size of the active subspace.

www.manaraa.com

Figure 9-12. Few-Group Cross Section Change

due to Macroscopic Cross Section Orthogonal Perturbation

www.manaraa.com

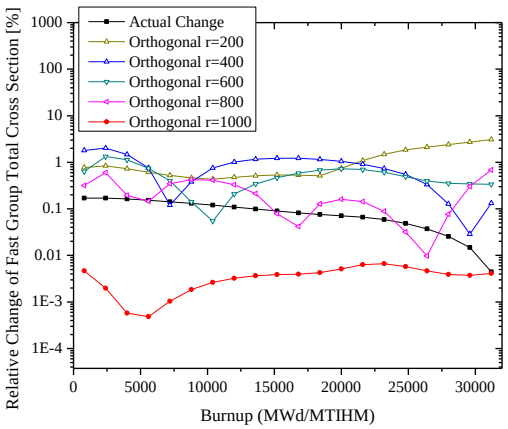

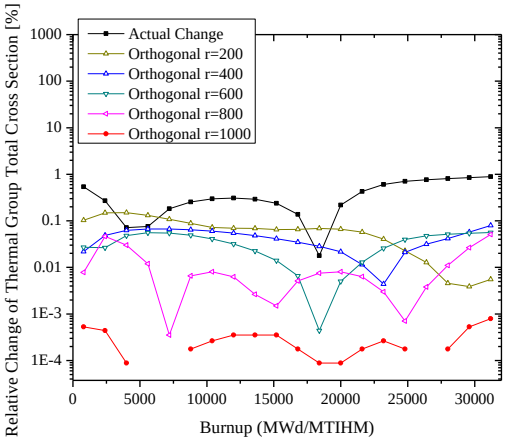

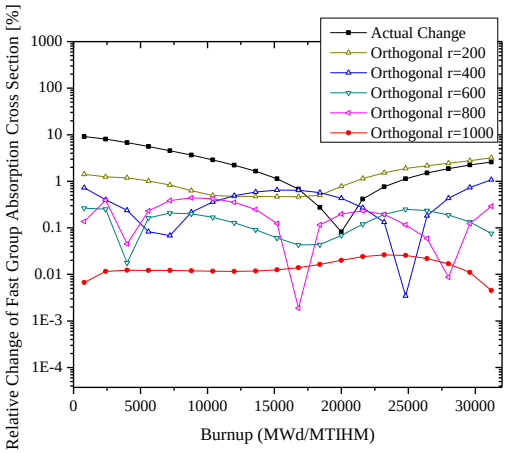

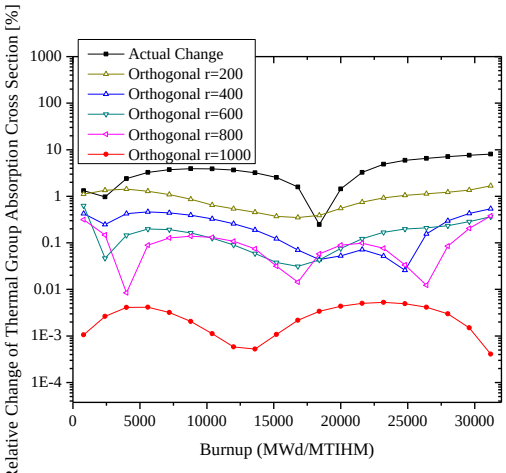

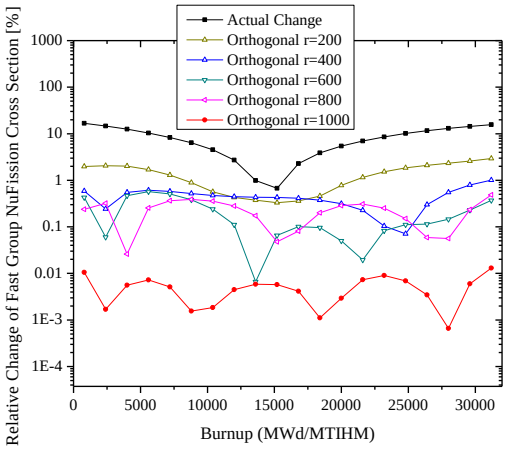

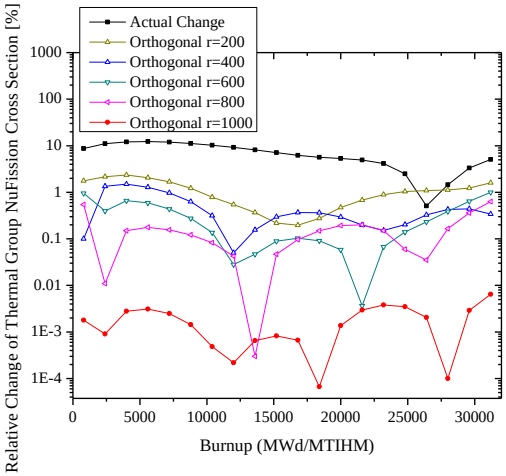

www.manaraa.com

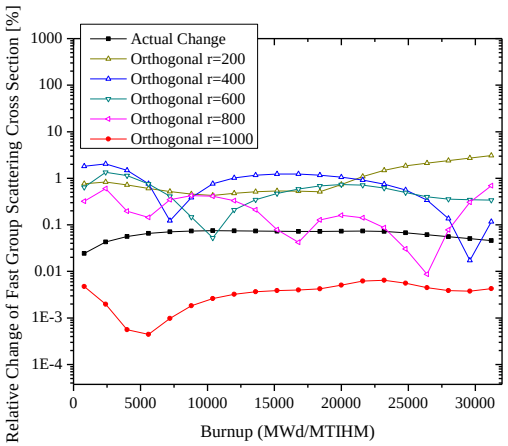

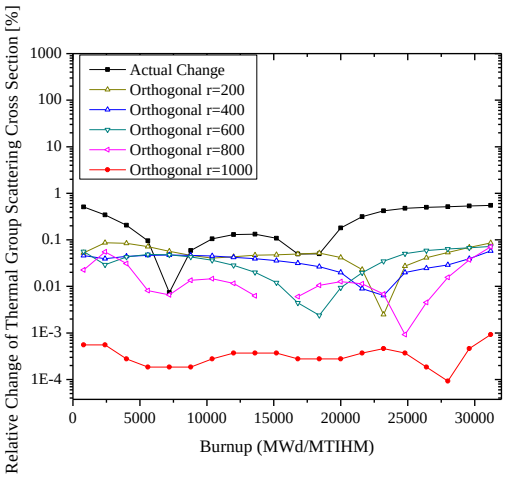

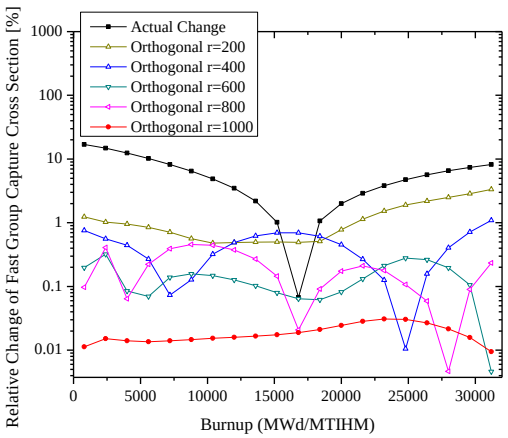

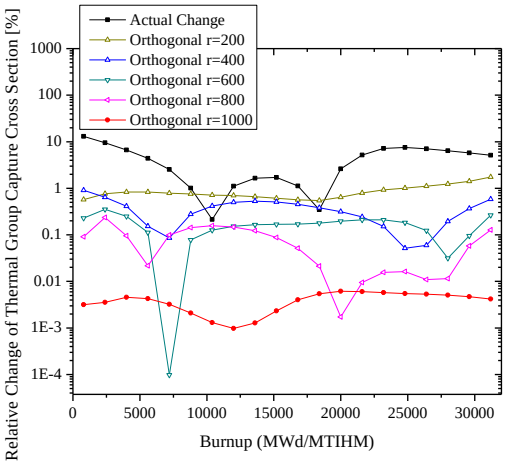

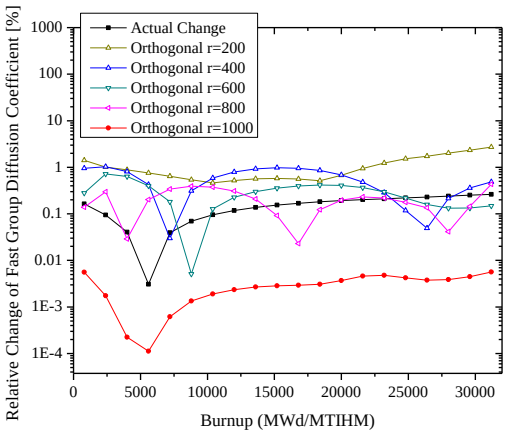

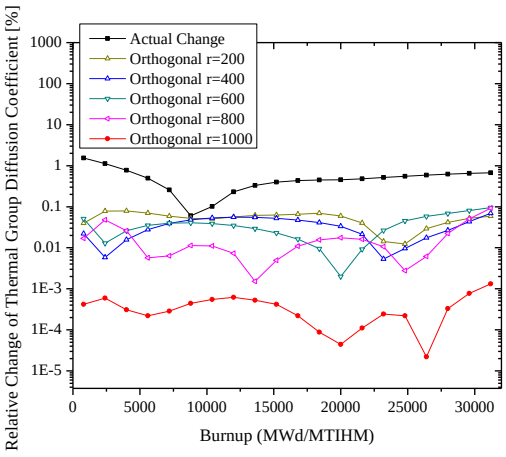

www.manaraa.com

9.1.3. S-Subspace Construction

The macroscopic cross section can be considered as input parameters to transport solver, i.e. NEWT and the active subspace of macroscopic cross section can be defined as sensitive components with respect to NEWT. It can be identified by examining sensitivity coefficient profiles (first order derivatives at the random configuration) with the range finding algorithm. Due to higher order (nonlinear) effects because of large macroscopic cross section variations, the size of the active subspace is expected to be very large; thus, the singular value spectrum decays gradually and slowly. Note that the first order derivative calculation via adjoint perturbation theory requires three calculations; one fundamental mode forward run, one fundamental mode adjoint run and one general perturbation theory mode adjoint run. Therefore, sampling a large number of derivatives is not a preferred option in computational and practical view points.

To estimate the size of the active subspace, the singular value spectrum is examined. For the random samples, the maximum macroscopic cross sections and the minimum macroscopic cross sections for each isotope over the entire depletion steps are collected and random configurations are sampled between those maximum and minimum values to ensure the complete coverage of the parameter domain. The matrix $\mathbf{S}$ is constructed by:

$$\mathbf{S} = \left[\frac{\vec{\Sigma}}{k_{eff}} \frac{\partial k_{eff}}{\partial \vec{\Sigma}} \bigg|^{(1)} \quad \cdots \quad \frac{\vec{\Sigma}}{k_{eff}} \frac{\partial k_{eff}}{\partial \vec{\Sigma}} \bigg|^{(k)} \right]$$
$$\text{or} \quad \mathbf{S} = \left[\frac{\vec{\Sigma}}{R^{pseudo}} \frac{\partial R^{pseudo}}{\partial \vec{\Sigma}} \bigg|^{(1)} \quad \cdots \quad \frac{\vec{\Sigma}}{R^{pseudo}} \frac{\partial R^{pseudo}}{\partial \vec{\Sigma}} \bigg|^{(k)} \right] \tag{9.9}$$

www.manaraa.com

where $\frac{\vec{\Sigma}}{k_{eff}}\frac{\partial k_{eff}}{\partial \vec{\Sigma}}$ is a relative k-eff sensitivity coefficient vector and $\frac{\vec{\Sigma}}{R^{pseudo}}\frac{\partial R^{pseudo}}{\partial \vec{\Sigma}}$ is a relative pseudo response sensitivity coefficient vector. Note that the pseudo response is defined as:

$$R^{pseudo} = \sum_{m=1}^{n_{mixture}} \sum_{g=1}^{n_{group}} \alpha_{m,g}\phi_{m,g} \tag{9.10}$$

where $\phi_{m,g}$ is a scalar flux for the mixture m and the energy group g and $\alpha_{m,g}$ is the flux weighted random number. The singular value spectrum of the matrix **S** for 1000 samples is shown in **Figure 9-13**. One can see that the singular value spectrum decreases very slowly which implies that the size of active subspace would be much larger than 1000.

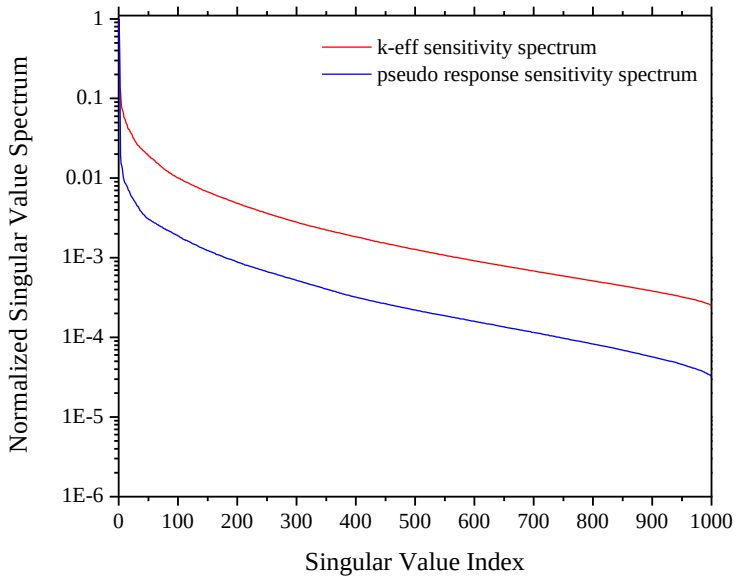

Figure 9-13. Singular Value Spectrum of Random Sensitivity Coefficient Matrix

www.manaraa.com

9.1.4. I-Subspace Construction

Now we have examined two active subspaces;

- V-active subspace of macroscopic cross section as outputs of BONAMI

(nuclide density and temperature perturbation and resonance self-shielding calculation)

- S-active subspace of macroscopic cross section as inputs of NEWT

(transport model sensitivity)

The previous result shows that the size of the S-active subspace of the macroscopic cross section as outputs of BONAMI would be 1000. This implies that the macroscopic variations can be accurately represented by 1000 basis vectors. On the other hand, the size of S-active subspace as inputs is expected to be large and it is unaffordable to conduct the GPT adjoint calculations very many times. However, it is obvious that the sensitivity information can be combined to macroscopic variations so that we can extract the components with ***large variations (V-Subspace)*** and ***high sensitivity (S-Subspace)***. The resulting size of intersection active subspace ***(I-Subspace)*** would be smaller than 1000. The intersection subspace is identified via the range finding algorithm with samples defined by:

$$\mathbf{Q}\mathbf{Q}^T \frac{\vec{\Sigma}}{k_{eff}} \frac{\partial k_{eff}}{\partial \vec{\Sigma}} \quad \text{or} \quad \mathbf{Q}\mathbf{Q}^T \frac{\vec{\Sigma}}{R^{pseudo}} \frac{\partial R^{pseudo}}{\partial \vec{\Sigma}} \tag{9.11}$$

where $\mathbf{Q}$ is the matrix of which columns are orthonormal basis vectors of macroscopic cross section variations. To estimate the size of the intersection subspace and error due to reduced order transformation, the singular value spectrum, portion of orthogonal component to active subspace and κ-metric are investigated.

www.manaraa.com

- **Singular Value Spectrum**

The singular value spectrum of intersection subspace is shown in **Figure 9-14**. Two spectrums of the intersection subspaces are compared to the subspace only of the macroscopic cross section variations. Note that the singular values of the intersection subspaces with k-eff sensitivity and flux sensitivity are calculated by singular value decomposition:

$$\mathbf{X}_{k_{eff}} = \mathbf{Q}\mathbf{Q}^T \left[\frac{\vec{\Sigma}}{k_{eff}} \frac{\partial k_{eff}}{\partial \vec{\Sigma}} \bigg|^{(1)} \quad \cdots \quad \frac{\vec{\Sigma}}{k_{eff}} \frac{\partial k_{eff}}{\partial \vec{\Sigma}} \bigg|^{(k)} \right] \tag{9.12}$$

$$\mathbf{X}_{flux} = \mathbf{Q}\mathbf{Q}^T \left[\frac{\vec{\Sigma}}{R^{pseudo}} \frac{\partial R^{pseudo}}{\partial \vec{\Sigma}} \bigg|^{(1)} \quad \cdots \quad \frac{\vec{\Sigma}}{R^{pseudo}} \frac{\partial R^{pseudo}}{\partial \vec{\Sigma}} \bigg|^{(k)} \right] \tag{9.13}$$

where $\mathbf{Q} \in \mathbb{R}^{44786 \times 1000}$ is the orthonormal basis of V-Subspace.

One can see that the singular value spectrums of the intersection subspaces decay faster than the one of V-Subspace. This implies that the further reduction would be achieved.

www.manaraa.com

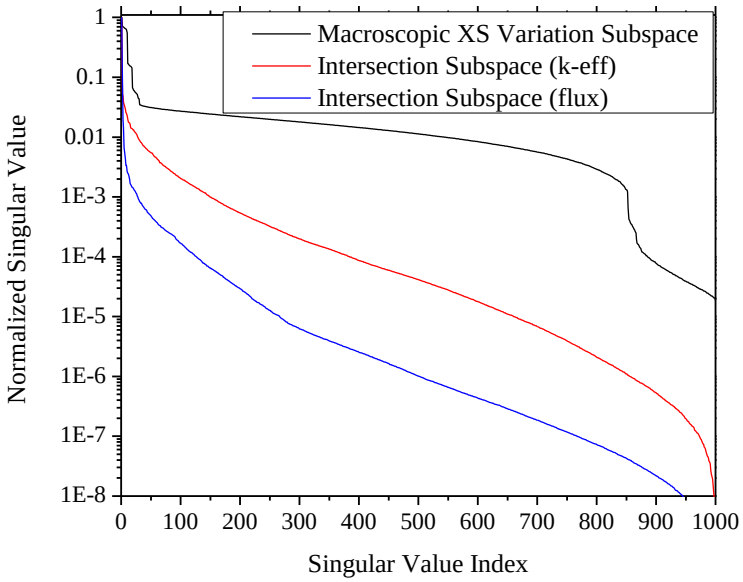

Figure 9-14. Singular Value Spectrum of Intersection Subspace

- **Portion of Orthogonal Component**

Given the basis of the macroscopic cross section variation and the sensitivity samples, the basis of the intersection subspace can be constructed by the range finding algorithm with:

$$\mathbf{Q}_{\text{intersection},k_{eff}} \leftarrow \mathbf{QQ}^T \left[\frac{\vec{\Sigma}}{k_{eff}} \frac{\partial k_{eff}}{\partial \vec{\Sigma}}\bigg|^{(1)} \quad \cdots \quad \frac{\vec{\Sigma}}{k_{eff}} \frac{\partial k_{eff}}{\partial \vec{\Sigma}}\bigg|^{(k)} \right] \tag{9.14}$$

$$\mathbf{Q}_{\text{intersection},\,flux} \leftarrow \mathbf{QQ}^T \left[\frac{\vec{\Sigma}}{R^{pseudo}} \frac{\partial R^{pseudo}}{\partial \vec{\Sigma}}\bigg|^{(1)} \quad \cdots \quad \frac{\vec{\Sigma}}{R^{pseudo}} \frac{\partial R^{pseudo}}{\partial \vec{\Sigma}}\bigg|^{(k)} \right] \tag{9.15}$$

In order to measure that discarded portion, the root mean square (RMS) error for random sample is calculated by:

www.manaraa.com

$$r.m.s = \sqrt{\frac{1}{n}\left[\left(\frac{\Delta\vec{\Sigma}}{\vec{\Sigma}^{(0)}}\right)^{\perp}\right]^{T}\left[\left(\frac{\Delta\vec{\Sigma}}{\vec{\Sigma}^{(0)}}\right)^{\perp}\right]} = \sqrt{\frac{1}{n}\sum_{i=1}^{n}\left\{\left(\frac{\Delta\Sigma_i}{\Sigma_i^{(0)}}\right)^{\perp}\right\}^2} \tag{9.16}$$

where $\left(\frac{\Delta\vec{\Sigma}}{\vec{\Sigma}^{(0)}}\right)^{\perp} = \left(\mathbf{I} - \mathbf{Q}_{\text{intersection}}\mathbf{Q}_{\text{intersection}}^{T}\right)\left(\frac{\Delta\vec{\Sigma}}{\vec{\Sigma}^{(0)}}\right)$.

In **Figure 9-15**, the results are compared. Note that with smaller sensitivity samples, the more components are discarded because those are considered as in-sensitive with respect to the response changes, i.e. k-eff or fluxes. As considering more sensitivity subspace, the intersection subspace would be closer to the macroscopic cross section variation subspace, i.e. the subspace spanned by $\mathbf{Q}$.

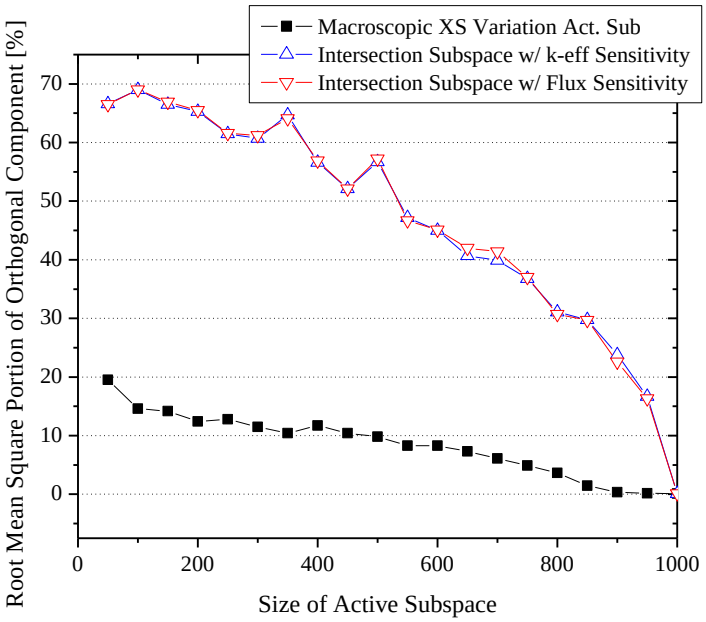

Figure 9-15. RMS Portion of Orthogonal Component of Intersection Subspace

www.manaraa.com

➢ κ-**metric**

First, the κ-metric test for the intersection subspace with k-eff sensitivity is conducted. For the intersection subspace construction, it is assumed that the V-Subspace is represented by 1000 basis, i.e. $\mathbf{Q} \in \mathbb{R}^{44786\times1000}$, and the intersection subspaces spanned by 400, 600 and 800 basis are compared to the case of V-Subspace.

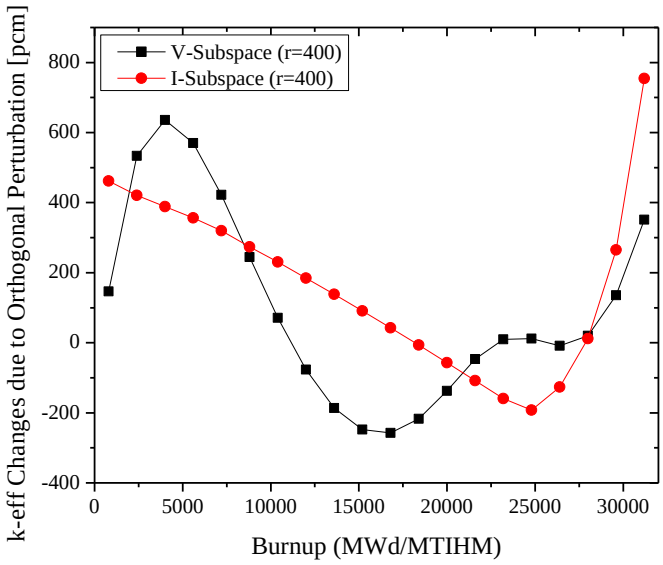

Figure 9-16. k-eff Changes due to Macroscopic Cross Section Orthogonal Perturbation (Intersection Subspace with k-eff Sensitivity, *r*=400)

www.manaraa.com

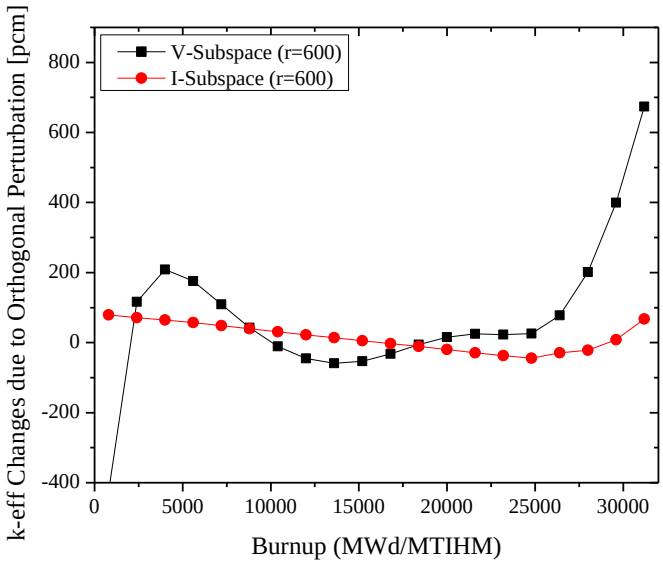

Figure 9-17. k-eff Changes due to Macroscopic Cross Section Orthogonal Perturbation (Intersection Subspace with k-eff Sensitivity, *r*=600)

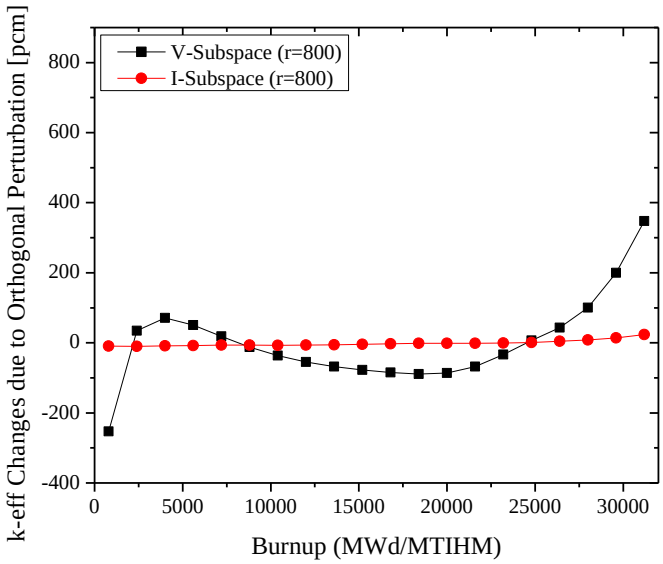

Figure 9-18. k-eff Changes due to Macroscopic Cross Section Orthogonal Perturbation (Intersection Subspace with k-eff Sensitivity, *r*=800)

www.manaraa.com

Second, the κ-metric test for the intersection subspace with flux sensitivity is conducted. For the intersection subspace construction, the macroscopic cross section variation is represented by 1000 basis, i.e. $\mathbf{Q} \in \mathbb{R}^{44786\times1000}$, and the intersection subspaces spanned by 400, 600 and 800 basis are compared to the case of V-Subspace. In **Figure 9-19 ~ 21**, the κ-metric test on the flux changes are conducted for fuel pin. In **Figure 9-22 ~ 24**, the κ-metric test on the flux changes are conducted for fuel pin with Gadolinium. Note that as the subspace size increases, the flux changes decrease which means the effects by the in-active components are diminished. Also, compared to the case of considering V-Subspace, the intersection subspace approach requires a smaller number of subspace basis vectors. Therefore, with the same number of basis vectors, the intersection subspace approach would product more accurate reduced order transformation. Or with the same error tolerance criteria, the intersection subspace approach requires a smaller number of basis vectors (i.e. more reduction).

www.manaraa.com

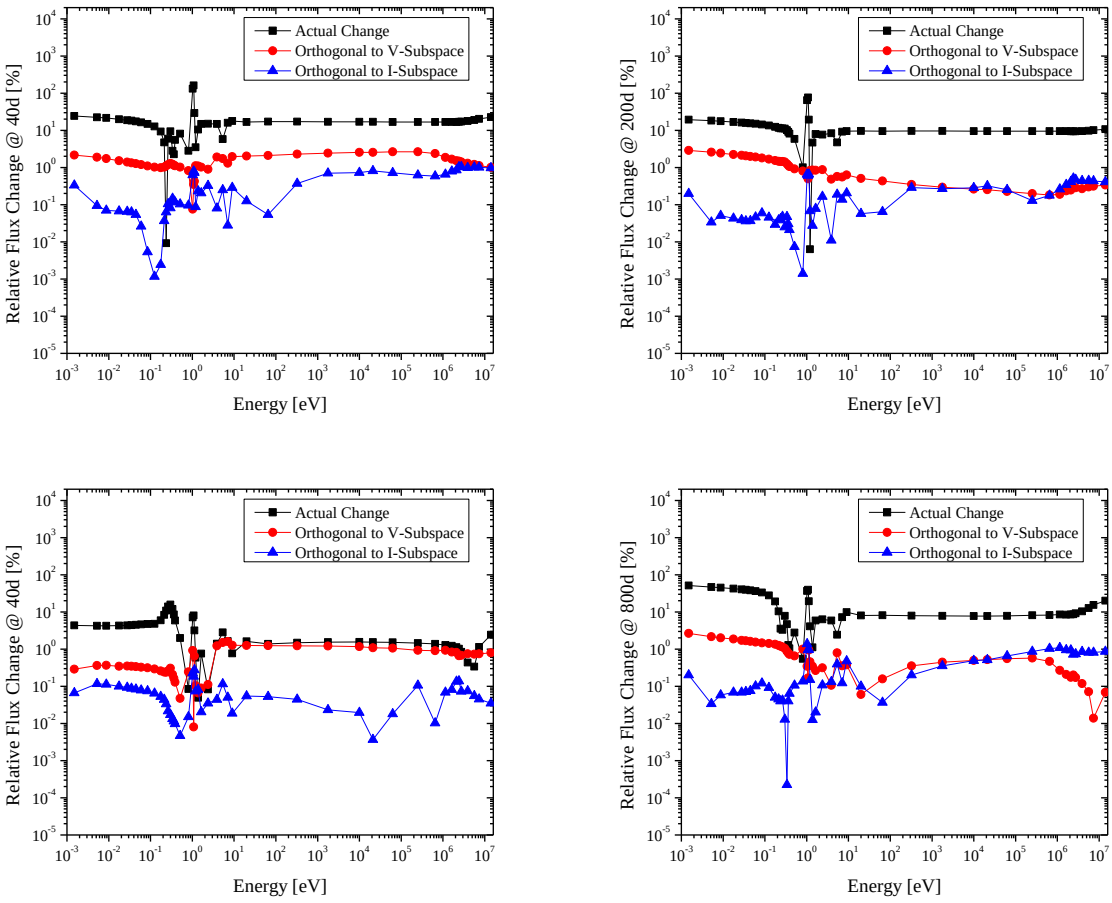

Figure 9-19. Flux Changes due to Macroscopic Cross Section Orthogonal Perturbation (Fuel Pin, Intersection Subspace with Flux Sensitivity, *r*=400)

www.manaraa.com

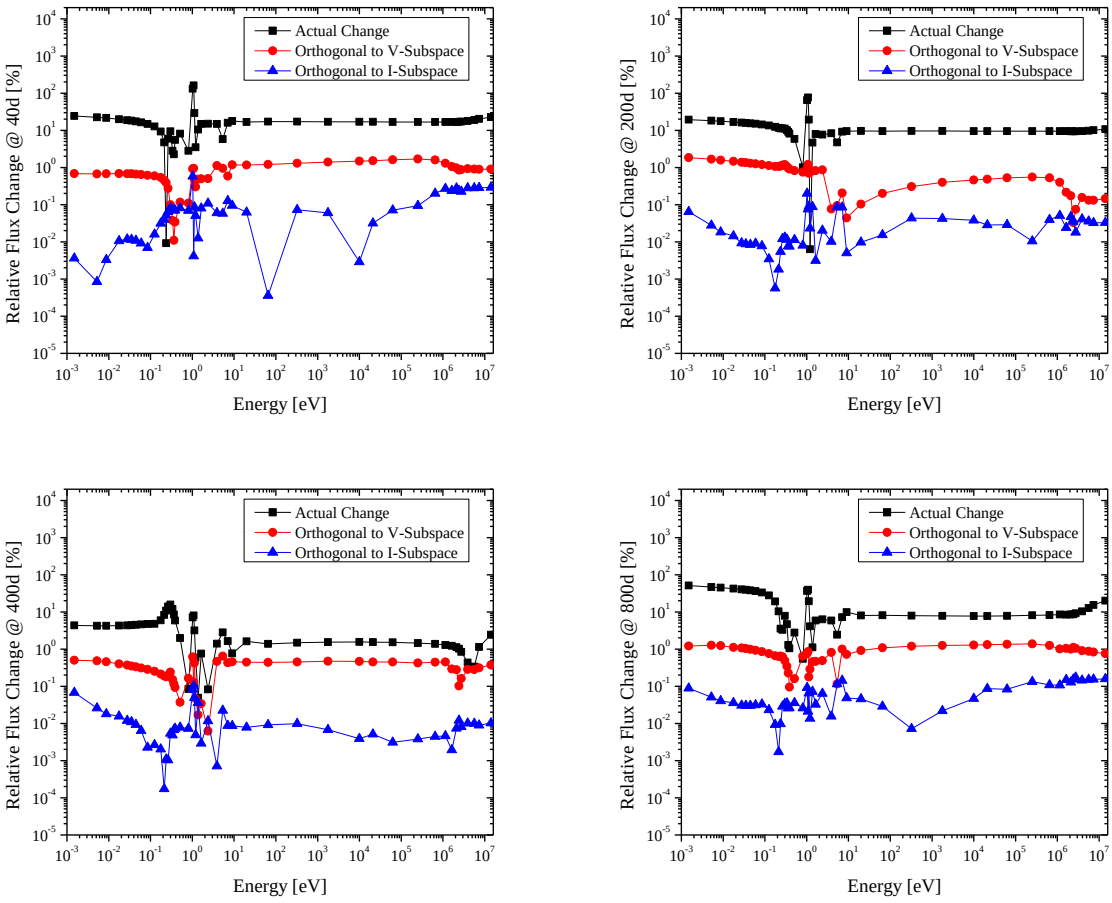

Figure 9-20. Flux Changes due to Macroscopic Cross Section Orthogonal Perturbation (Fuel Pin, Intersection Subspace with Flux Sensitivity, *r*=600)

www.manaraa.com

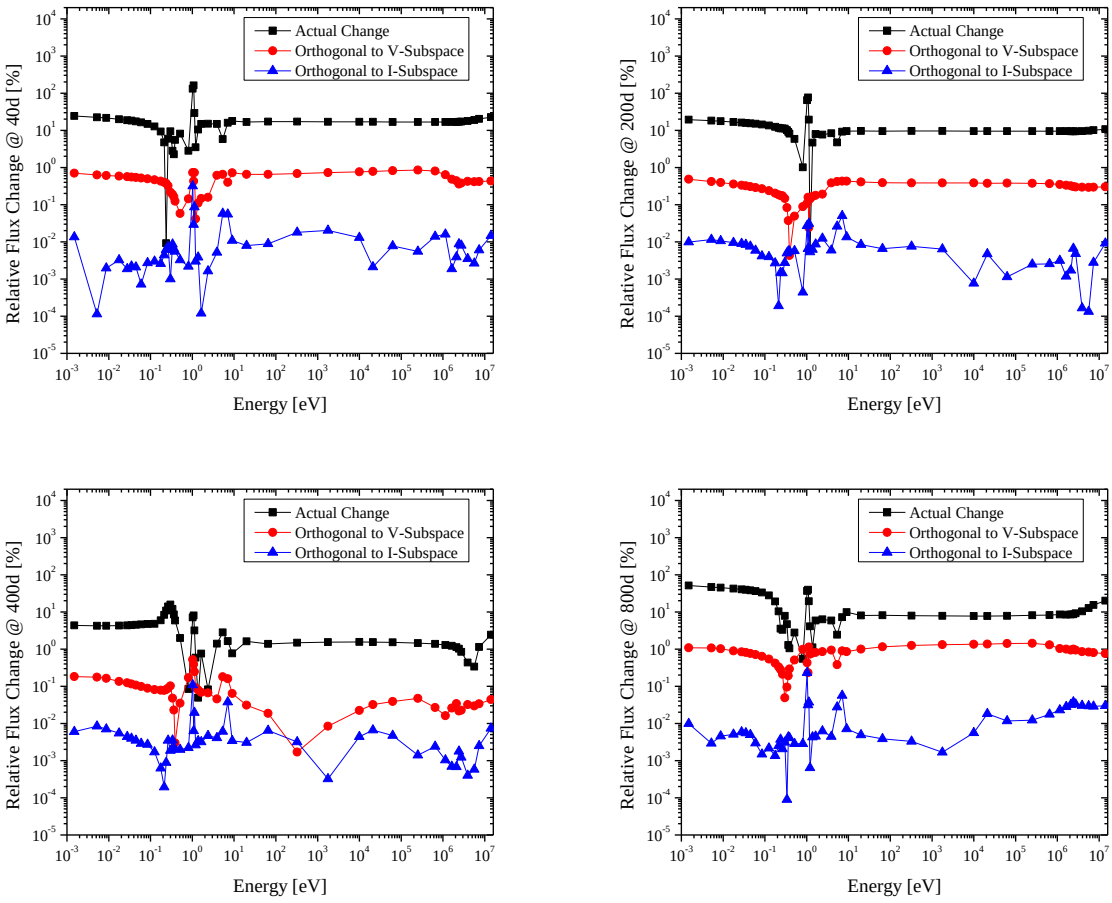

Figure 9-21. Flux Changes due to Macroscopic Cross Section Orthogonal Perturbation (Fuel Pin, Intersection Subspace with Flux Sensitivity, *r*=800)

www.manaraa.com

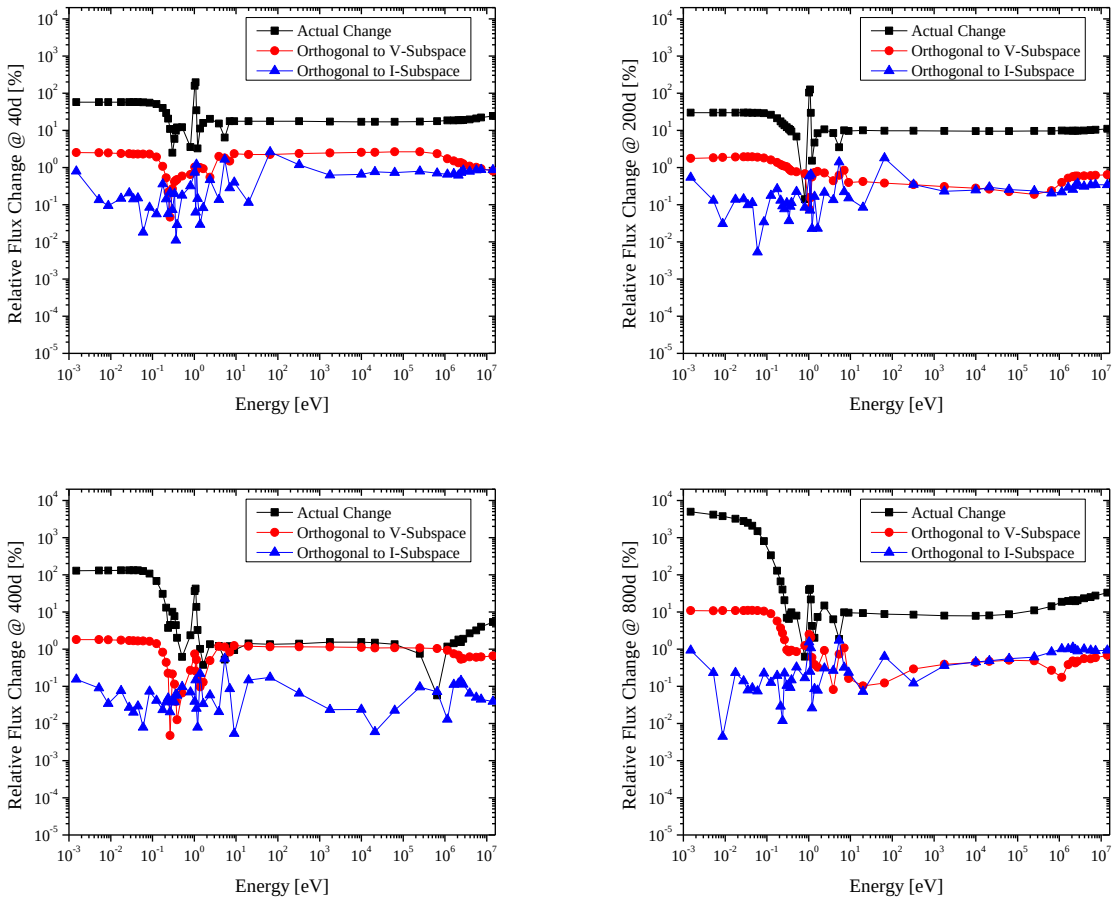

Figure 9-22. Flux Changes due to Macroscopic Cross Section Orthogonal Perturbation (Fuel + Gadolinium Pin, Intersection Subspace with Flux Sensitivity, *r*=400)

www.manaraa.com

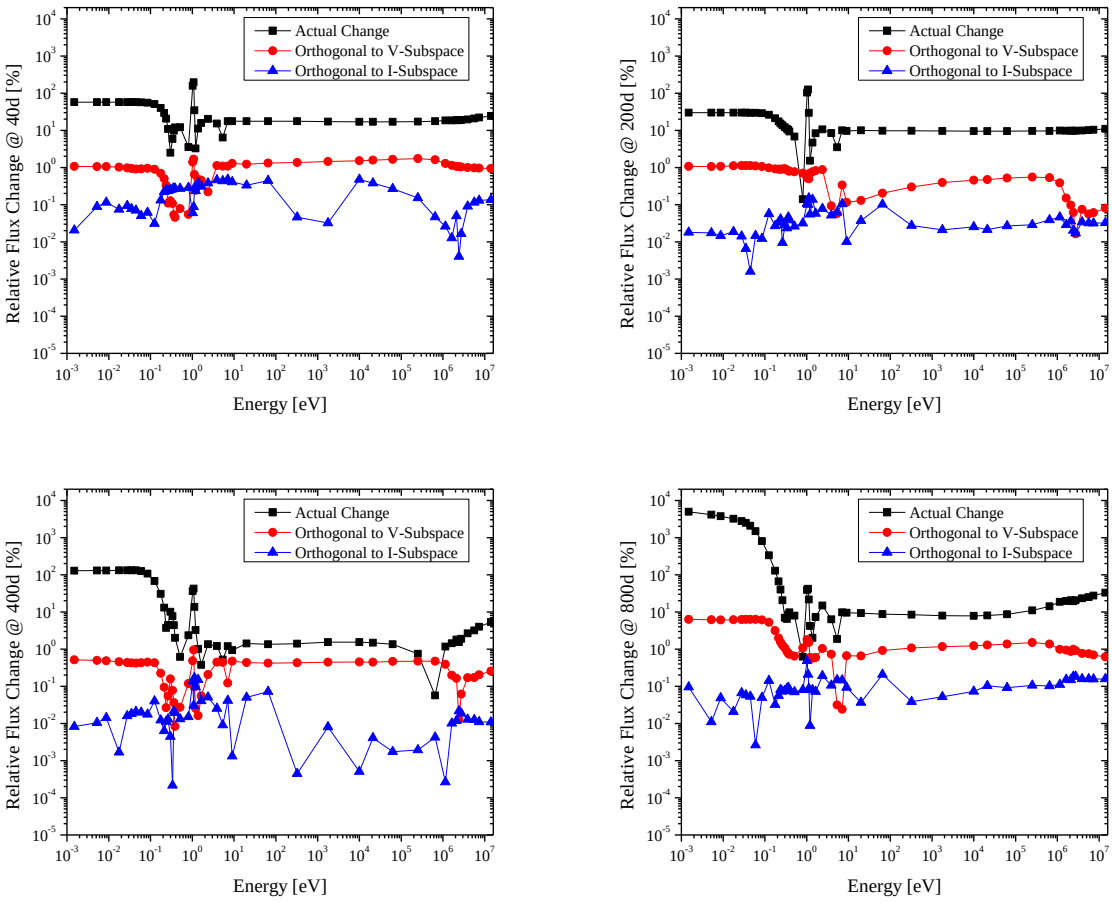

Figure 9-23. Flux Changes due to Macroscopic Cross Section Orthogonal Perturbation (Fuel + Gadolinium Pin, Intersection Subspace with Flux Sensitivity, *r*=600)

www.manaraa.com

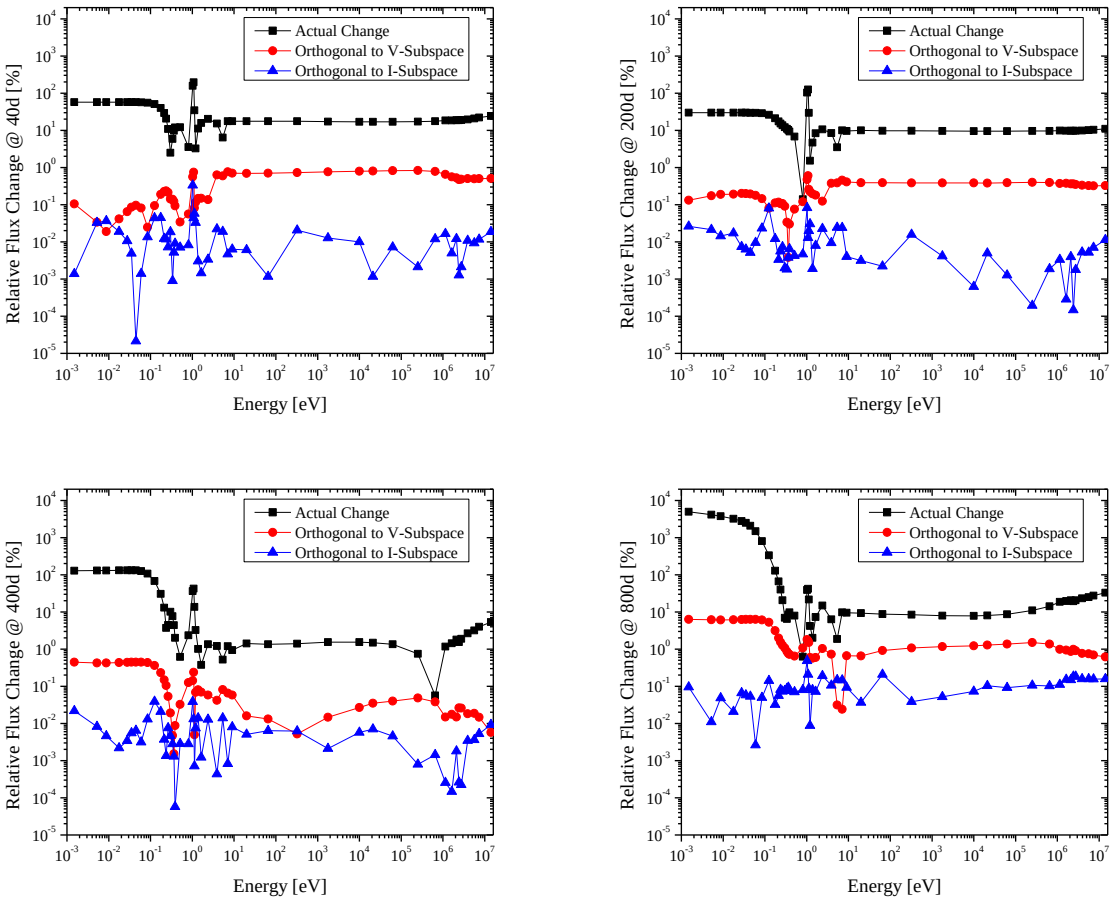

Figure 9-24. Flux Changes due to Macroscopic Cross Section Orthogonal Perturbation (Fuel + Gadolinium Pin, Intersection Subspace with Flux Sensitivity, *r*=800)

www.manaraa.com

Third, the κ-metric test for the intersection subspace with flux sensitivity is conducted. For the intersection subspace construction, the macroscopic cross section variation is represented by 1000 basis, i.e. $\mathbf{Q} \in \mathbb{R}^{44786\times1000}$, and the intersection subspaces spanned by 400, 600 and 800 basis are compared to the case of V-Subspace. In **Figure 9-25 ~ 27**, the κ-metric test results for few-group constants are shown and the same behavior with the previous tests can be observed, which implies that the intersection subspace approach can achieve the further reduction.

www.manaraa.com

Figure 9-25. Few Group Cross Section Changes due to Macroscopic Cross Section Orthogonal Perturbation (r=400)

www.manaraa.com

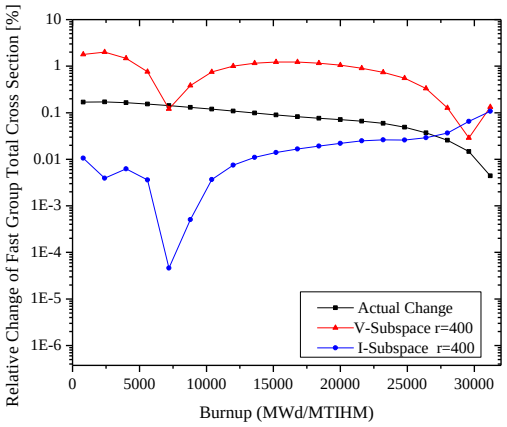

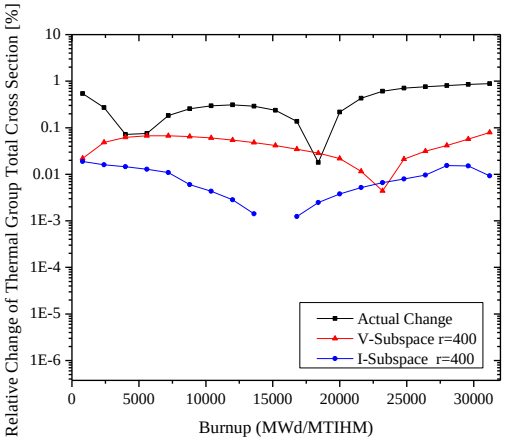

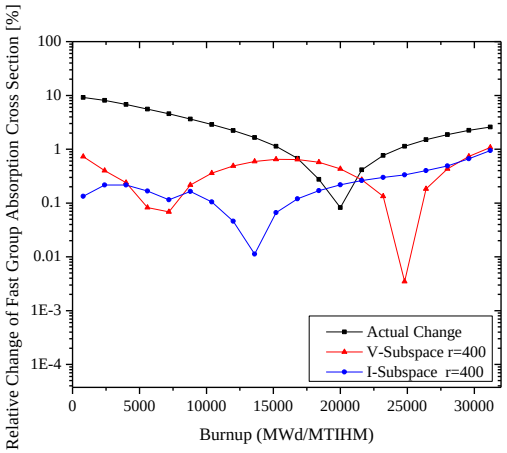

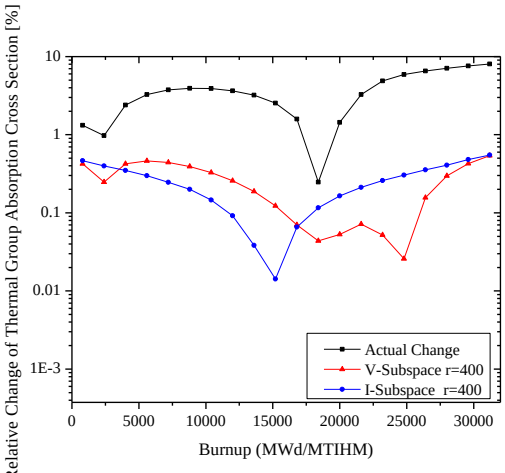

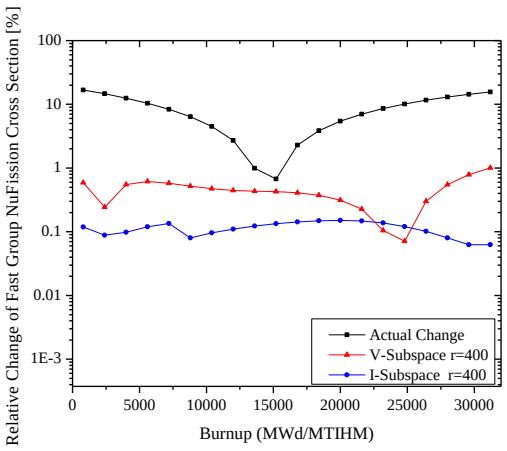

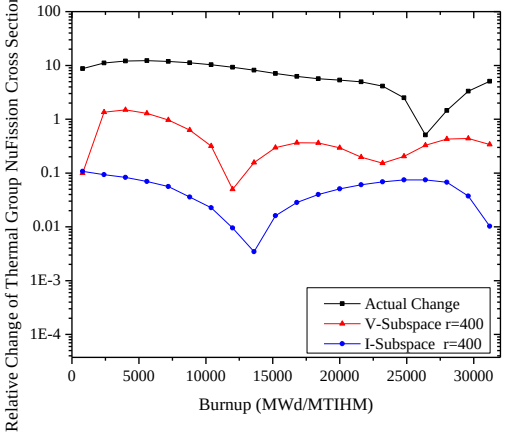

www.manaraa.com

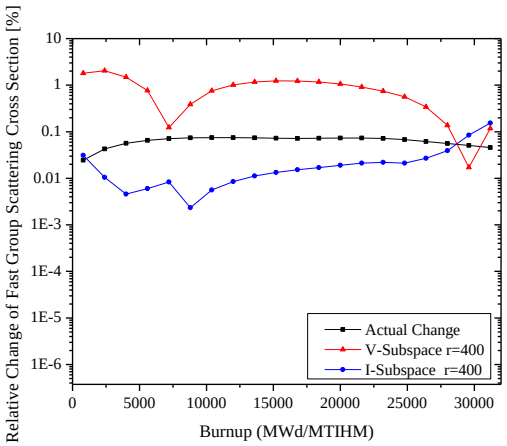

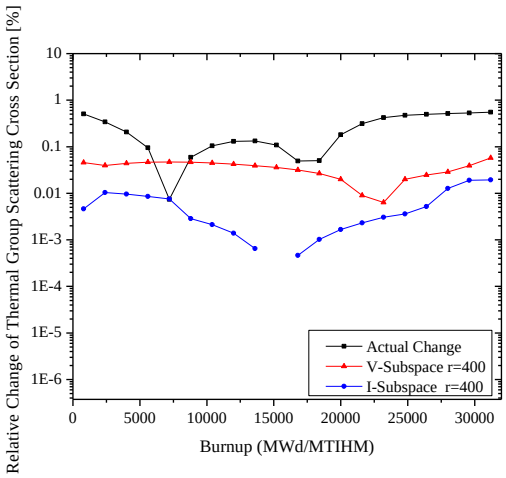

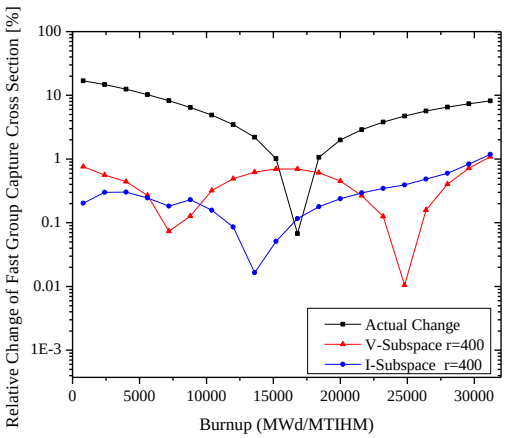

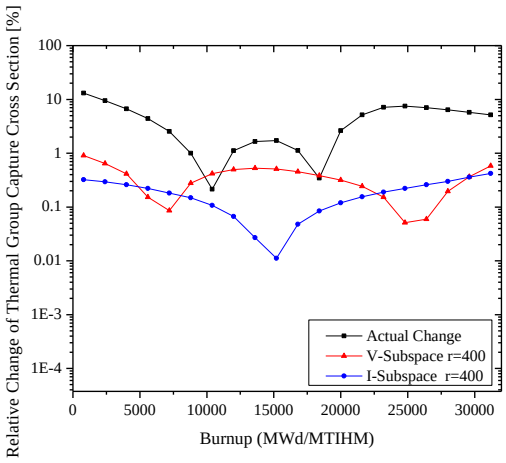

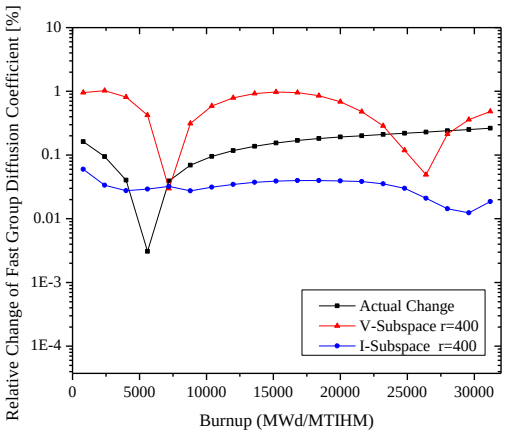

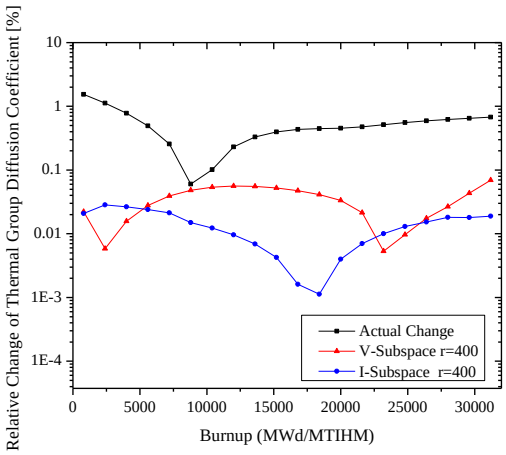

www.manaraa.com

Figure 9-26. Few Group Cross Section Changes due to Macroscopic Cross Section Orthogonal Perturbation (r=600)

www.manaraa.com

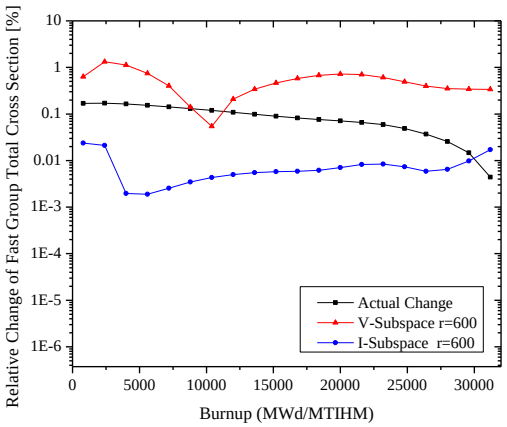

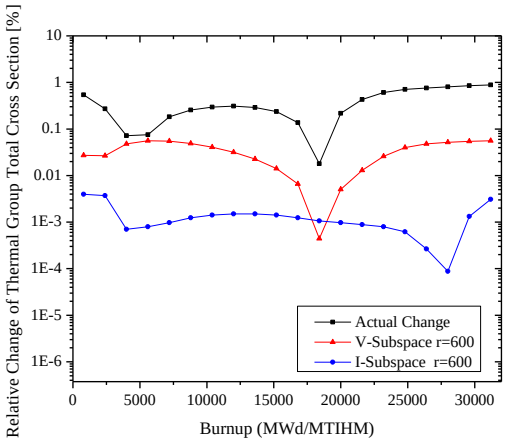

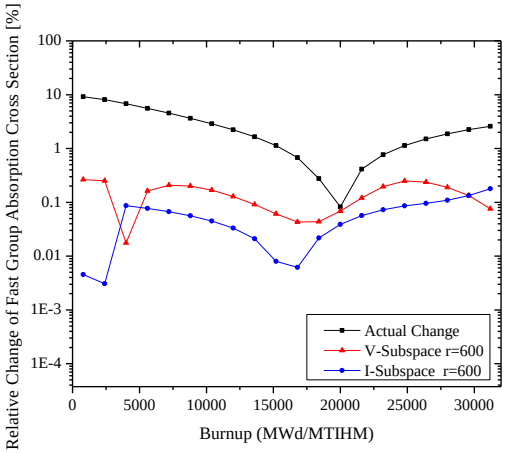

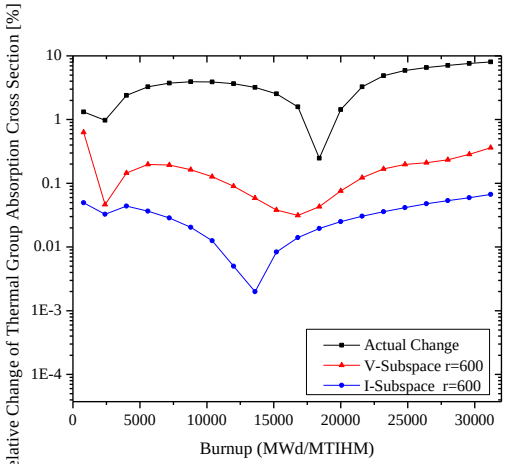

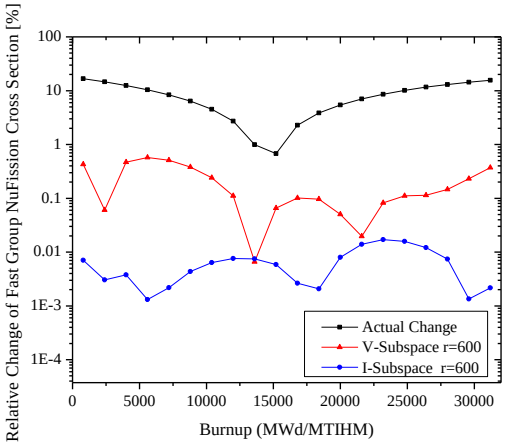

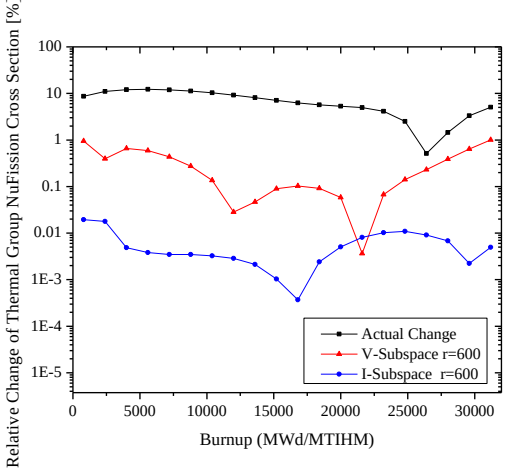

www.manaraa.com

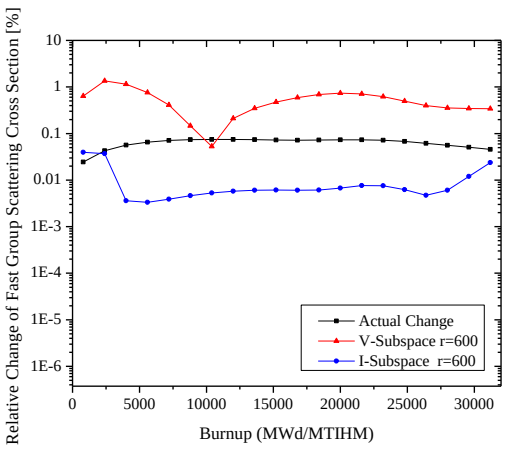

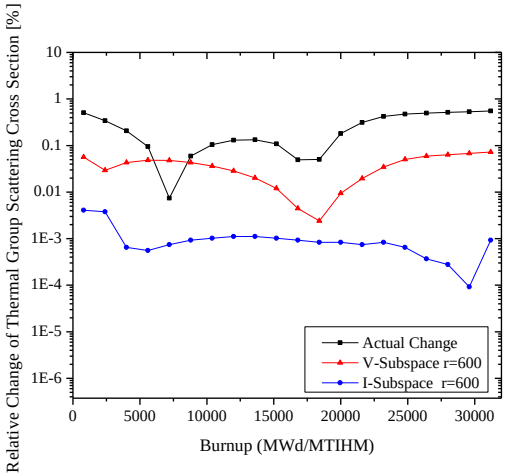

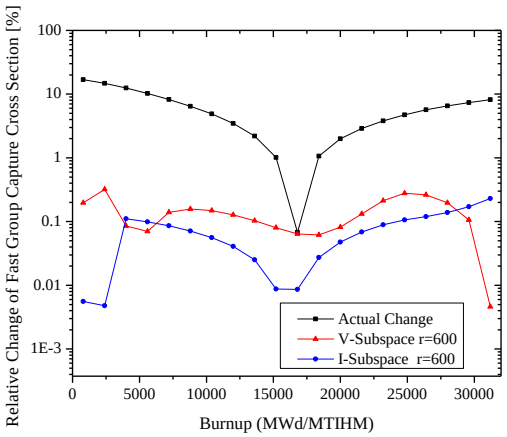

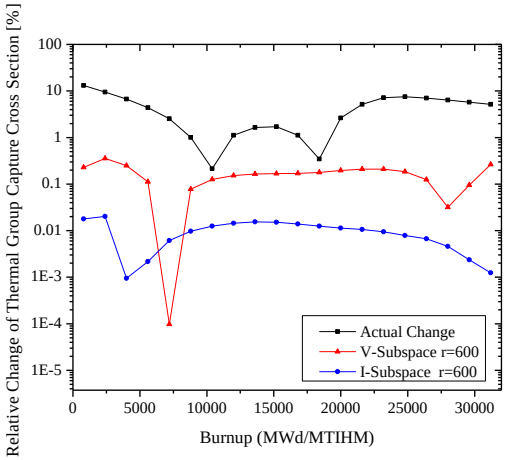

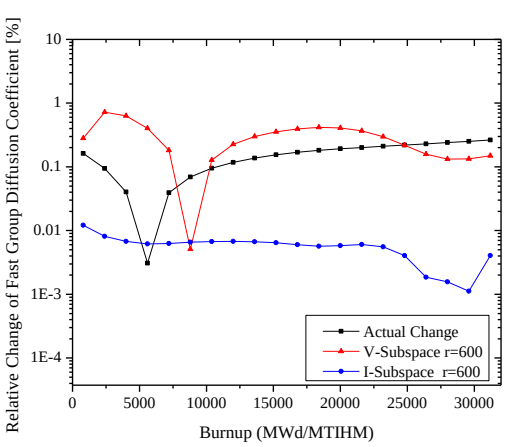

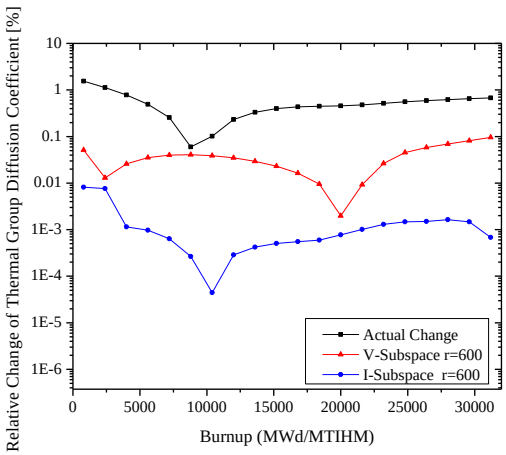

www.manaraa.com

Figure 9-27. Few Group Cross Section Changes due to Macroscopic Cross Section Orthogonal Perturbation (r=800)

www.manaraa.com

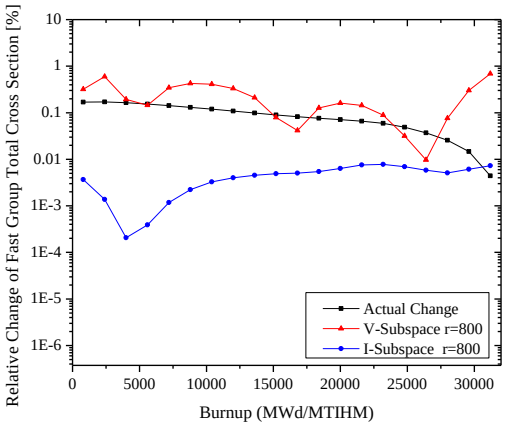

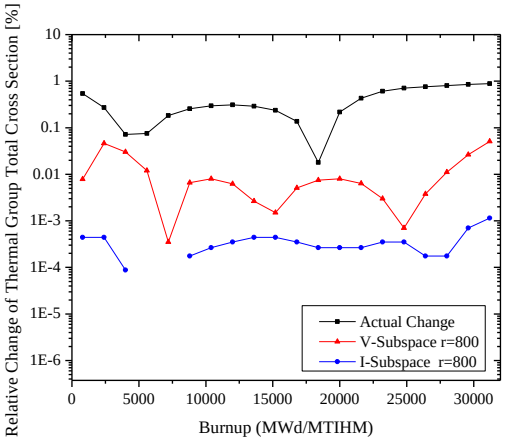

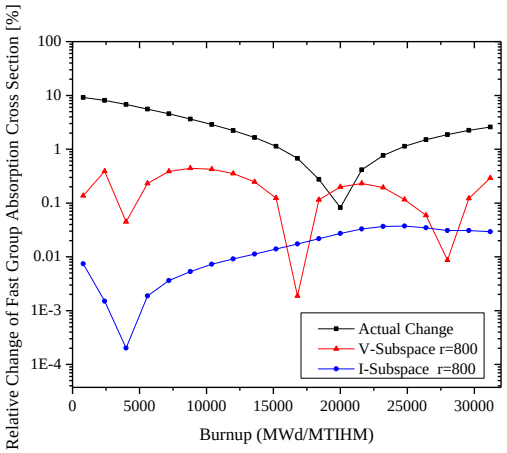

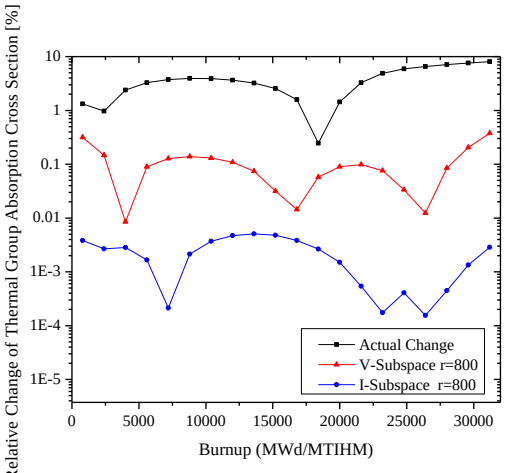

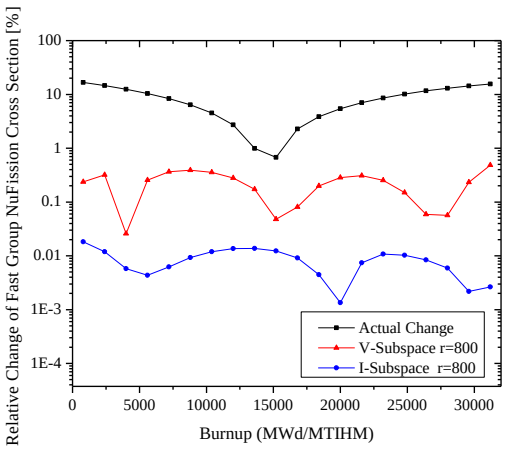

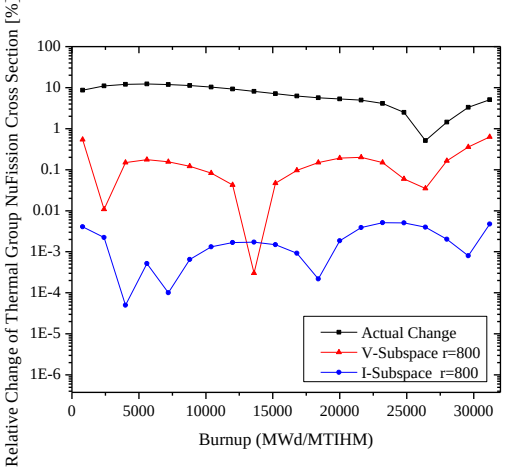

www.manaraa.com

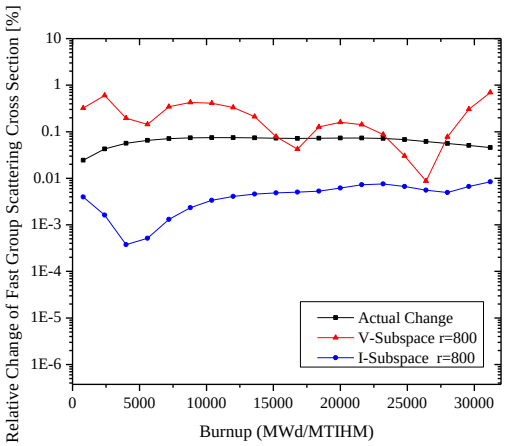

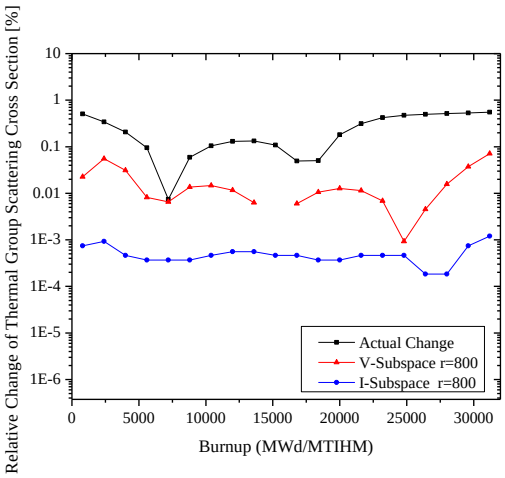

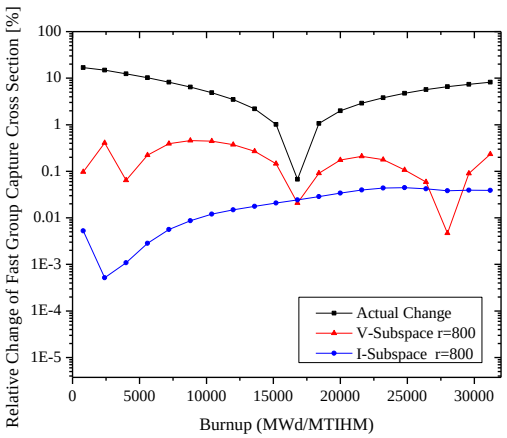

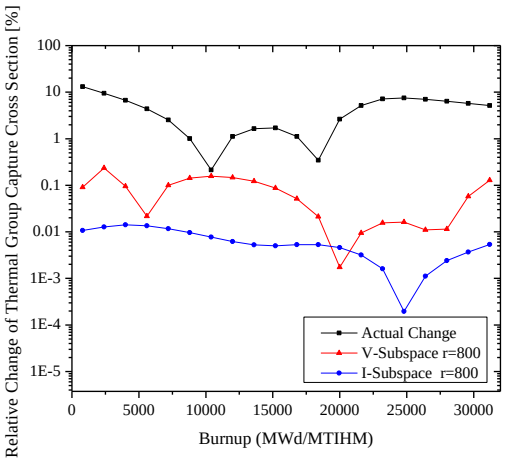

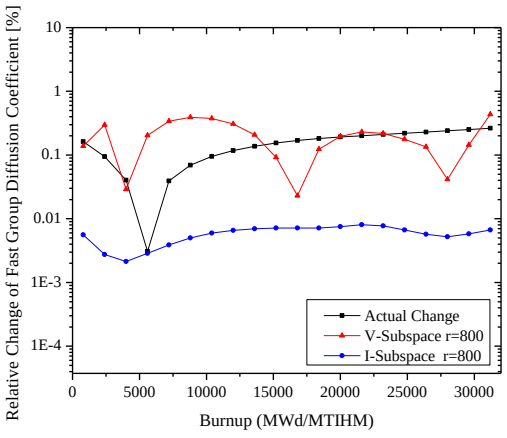

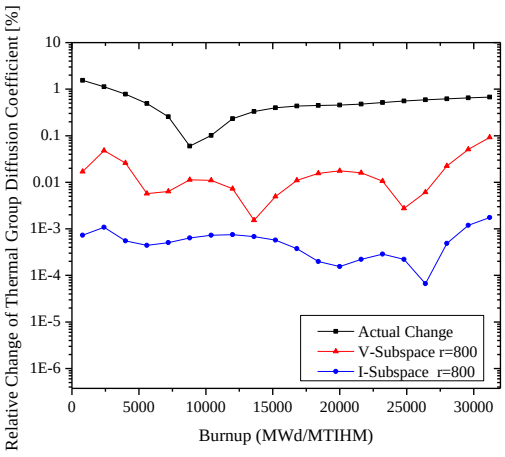

www.manaraa.com

In addition to κ-metric test in which the output response change due to in-active subspace components is examined, one more test is conducted to verify the constructed basis. The test procedure is the following:

Step 1) Generate 100 random cases with perturbing number densities and temperatures

Step 2) Calculate the k-eff changes due to perturbed parameters: $\left(\frac{\Delta\vec{\Sigma}^{(i)}}{\vec{\Sigma}^{(0)}}, \Delta k_{eff}^{(i)} \right)$ for $i = 1,...,100$

Step 3) Project the macroscopic cross section variations onto the intersection subspace and Calculate the k-eff changes: $\left(\mathbf{Q}_{\text{intersection}} \mathbf{Q}_{\text{intersection}}^{T} \frac{\Delta\vec{\Sigma}^{(i)}}{\vec{\Sigma}^{(0)}}, \Delta k_{eff,i-sub}^{(i)} \right)$ for $i = 1,...,100$

Step 4) Compare the two k_{eff} changes, i.e. $\Delta k_{eff}^{(i)}$ and $\Delta k_{eff,i-sub}^{(i)}$ for $i = 1,...,100$

The test is conducted with BWR assembly model (PB-2) and as the intersection subspace basis, 800 I-Subspace basis with 1000 V-Subspace basis is used, i.e. $\mathbf{Q}_{\text{intersection}} \in \mathbb{R}^{44786\times 800}$. In **Figure 9-28**, the comparison for k-eff changes for 10 random cases is presented. As can be seen, the k-eff changes due to macroscopic cross section perturbed along the intersection subspace are not much different with the actual k-eff changes. In **Table 9-4**, the frequency distribution table for 100 test cases is shown. Overall, two k-eff changes show similar distributions: 0.405 [pcm] average discrepancy and 51.923 [pcm] standard deviation. One can notice that there is a difference in range of 0~5000 (-5000~0) which is due to the sign of

www.manaraa.com

the k-eff changes are different though the magnitude of the discrepancy is small (Δk_{eff} =43.476 [pcm] and $\Delta k_{eff,i-sub}$ =-1.279 [pcm]).

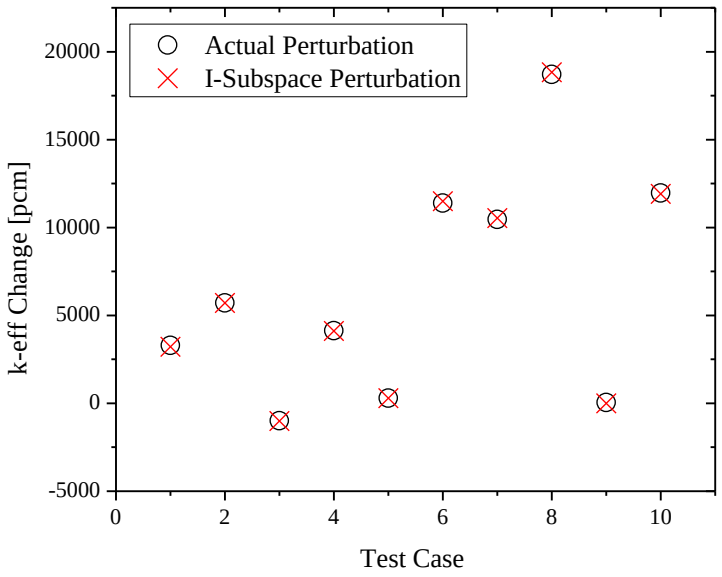

Figure 9-28. Comparison of k-eff Changes

Table 9-4. Comparison of k-eff Changes

Range [pcm]	**Actual Perturbation** (Δk_{eff})	**I-Subspace Perturbation** ($\Delta k_{eff,i-sub}$)
-10000 ~ -5000	7	7
-5000 ~ 0	13	14
0 ~ 5000	27	26
5000 ~ 10000	25	25
10000 ~ 15000	21	21
15000 ~ 20000	5	5
25000 ~ 30000	1	1
30000 ~ 35000	1	1

www.manaraa.com

9.2 PWR Assembly Model

9.2.1 Overview of Model

The Watts Bar Unit 1&2 reactor core is the typical four-loop Westinghouse pressurized water reactor (PWR) which is comprised of 193 assemblies arranged in core loading configuration shown in **Figure 9-29**. The general specifications can be found in Wagner and Parks (2003) and Godfrey (2011). In **Figure 9-30**, the original SCALE model originally provided by Godfrey is shown.

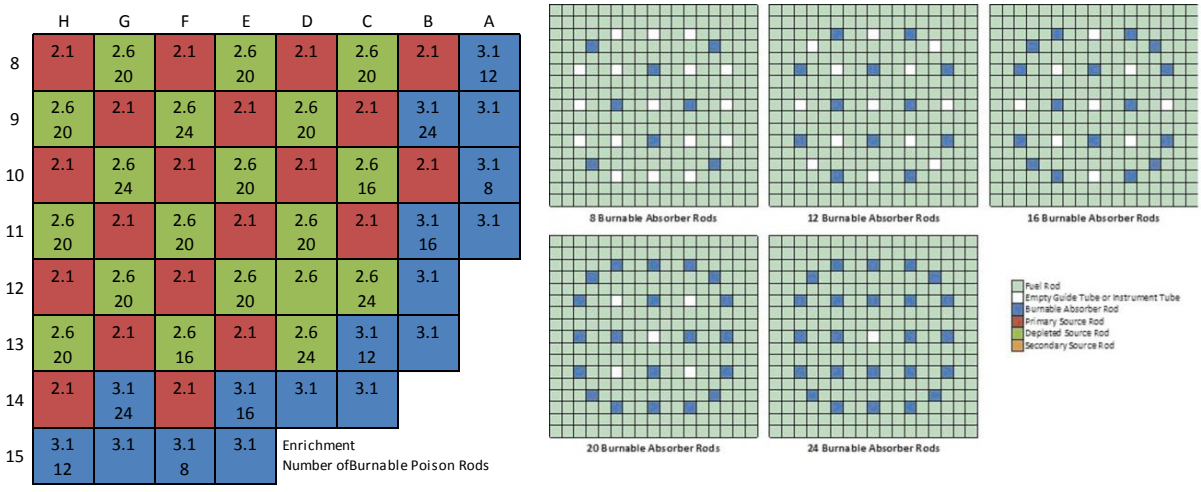

Figure 9-29. Loading Pattern & Burnable Poison Patterns – Quarter Core without Source Location

www.manaraa.com

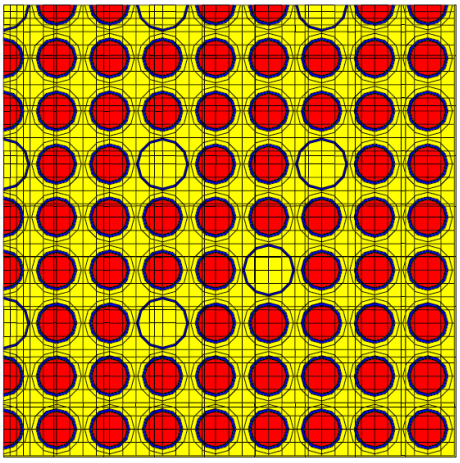

Figure 9-30. Watts-Bar Unit 2 SCALE Model for Criticality Calculation

9.2.2 Model Modification

The original SCALE model by Godfrey (2011) is for criticality calculation. For the purpose of this study, the model is modified:

- ✓ Modification 1): for depletion calculation, each fuel pin-cell is assigned unique material identification number to capture the burn-up effects.
- ✓ Modification 2): to model the different assembly types only by changing material compositions, burnable poison rods (BPRs) are modeled in homogeneous manner.
- ✓ Modification 3): to keep the execution time manageable, the diagonally symmetric properties of the assembly are considered so that the number of mixture numbers are reduced.
- ✓ Modification 4): to keep the execution time manageable, BONAMI is used for resonance calculation instead of default resonance calculation option (i.e. CENTRM).

www.manaraa.com

For Modification2), the burnable poison rods data is additionally collected and summarized below. According to Wagner and Parks (2003), there are two types of BPRs designs for Westinghouse fuel assembly

- Pyrex Burnable Absorber Assemblies (BAAs)
- Wet Annular Burnable Absorbers (WABAs)

In this study, only BAA is considered (no WABA, no source). The specification of BAA is summarized in **Table 9-5** and **Table 9-6**.

It is observed that compared to CENTRM (default option of TRITON module), BONAMI is much faster but shows unphysical criticality result (more than 4000 pcm difference). For Modification 4), the problem specific library is generated by collapsing 238 group library to 49 groups, i.e. 5 more groups are added into resonance region to 44 energy group library.

Considering the fuel enrichments and BPR insertions, the 10 assembly models are shown in **Figure 9-31**. The red circles show the location of guide tube in which the BPR is inserted. To model the rod insertion by perturbing the material density, the inside of the guide tube is modeled as one mixture (homogenized). With this model, one can model the poison rod insertion by increasing poison material densities.

www.manaraa.com

Table 9-5. Burnable Absorber Assembly Geometry Specification

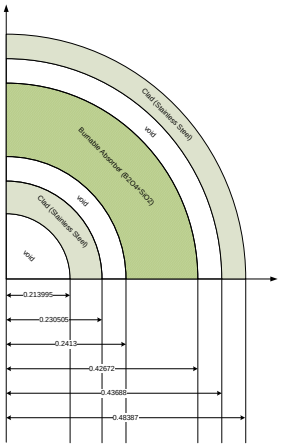

Description	BAA
BP material	B2O3-SiO2
Boron Loading	12.5 wt% B2O3 0.00624g B10/cm
BP density (g/cm3)	2.299
BP outer diameter(OD) (cm)	0.85344
BP inner diameter (ID) (cm)	0.48260
BPR clad material	Stainless Steel (Type 304)
BPR outer clad OD (cm)	0.96774
BPR outer clad ID (cm)	0.87376
BPR inner clad OD (cm)	0.46101
BPR inner clad ID (cm)	0.42799

Table 9-6. Burnable Absorber Assembly Material Specification

Description	Material ID	Nuclide Number Density
Clad	ss304	Standard Material Property
BAA	o	0.04497
	na	0.00165
	al	0.00058
	si	0.01799
	k	0.00011
	b-10	9.595E-4
	b-11	3.863E-3
Gap	n	5.000E-5

www.manaraa.com

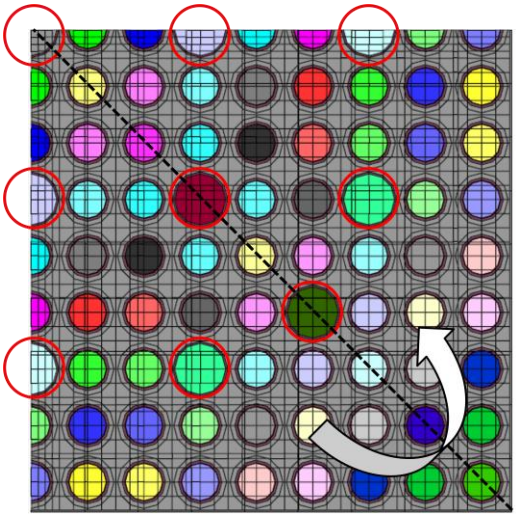

No.	Region	Enrich	No. BPRs	File Name
1	1	2.1	0	triton_R1_P0.inp
2	2	2.6	0	triton_R2_P0.inp
3	2	2.6	16	triton_R2_P16.inp
4	2	2.6	20	triton_R2_P20.inp
5	2	2.6	24	triton_R2_P24.inp
6	3	3.1	0	triton_R3_P0.inp
7	3	3.1	12	triton_R3_P12.inp
8	3	3.1	16	triton_R3_P16.inp
9	3	3.1	24	triton_R3_P24.inp
10	3	3.1	8	triton_R3_P8.inp

Figure 9-31. Modified Assembly Model

9.2.3 V-Subspace Construction

The macroscopic cross section changes due to material composition changes and fuel/moderator temperature change. The basis construction for the macroscopic cross section variations can be interpreted as capturing the pattern in macroscopic cross section changes. The range finding algorithm (RFA) can be used to construct the orthogonal basis, which is running the resonance model with perturbed material composition and temperatures and Gram-Schmidt orthonormalization-process to resulting macroscopic cross section vectors.

Sampling Scheme

To get the ranges of nuclide densities to be considered (we don't need to consider the number density from zero to infinity), the depletion calculations for each assembly model are conducted with varying fuel/moderator temperature. For every assembly types, the fuel

www.manaraa.com

temperature is perturbed by ±40% uniform distribution and the moderator temperature and moderator density are perturbed simply by ±10% uniform distribution. The nominal number density for each mixture is determined as the median value. In **Figure 9-32**, the number density of U-235 in a pin-cell is plotted and how to determine the nominal value N_0 and range of variation ΔN is illustrated.

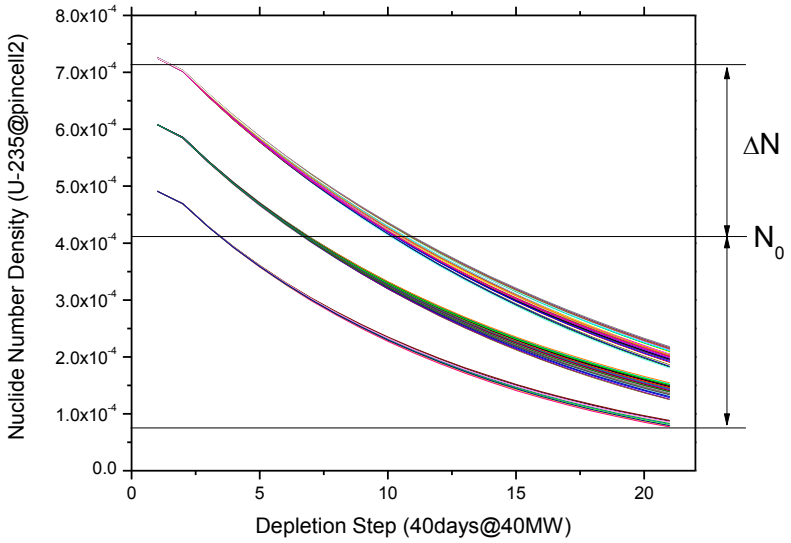

Figure 9-32. Determination of Number Density Variation Range

In this study, the randomized approach is adopted to generate the samples for subspace construction. To eliminate the unphysical condition (e.g. high uranium enrichment and high plutonium concentration) and make the sample configuration physically reasonable, the special sampling scheme is used. As illustrated in **Figure 9-33**, the number densities are perturbed by;

www.manaraa.com

1. the maximum (and minimum) number densities at each depletion step are collected and fitted by 5^{th} order polynomial regression analysis.
2. randomly sample the depletion step and calculate the max and min number densities by fitted functions.
3. sample the perturbed number density between the max and the min number densities.

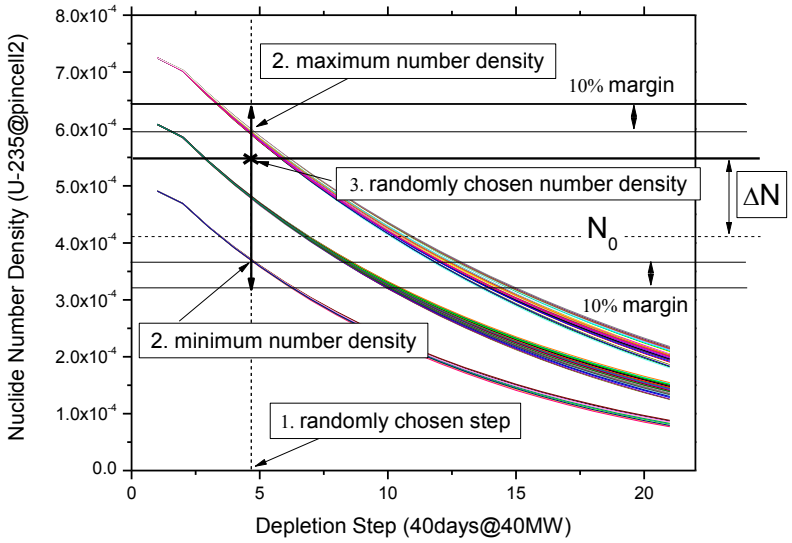

Figure 9-33. Determination of Perturbed Number Density

Basis Verification

To verify the basis, three methods are considered; singular value spectrum, portion of orthogonal component to active subspace and κ-metric. The first two approaches are almost

www.manaraa.com

free but only have mathematical meaning, while the κ-metric approach shows the actual error due to reduced order transformation but requires extra model executions.

- **Singular Value Spectrum**

Consider the matrix $\mathbf{X}$ of which the columns are the vectors of macroscopic cross sections calculated from resonance calculations with perturbed number densities and temperatures:

$$\mathbf{X} = \left[\Delta\vec{\Sigma}^{(1)} \quad \Delta\vec{\Sigma}^{(2)} \quad \cdots \right] \tag{9.17}$$

The singular value decomposition of the matrix $\mathbf{X}$ is given by:

$$\mathbf{X} = \mathbf{USV} = \sum_{i=1} \sigma_i \vec{u}_i \vec{v}_i^T \tag{9.18}$$

where $\vec{u}_i$ and $\vec{v}_i$ are the orthonormal vectors. Thus, the σ_i can be considered as the importance of the subspace spanned by $\vec{u}_i$ or $\vec{v}_i$.

In **Figure 9-34**, the singular value spectrum of the matrix $\mathbf{X}$ is presented. Note **that the original input parameter (i.e. macroscopic self-shielded cross section) dimension is 184,240** and there are 3,760 nuclides in 45 mixtures. It is important to note that around 3,800 index, the singular value drops rapidly. That is because there are 3,760 nuclides and macroscopic cross sections are highly correlated by number density. In other words, if the number density of a nuclide is changed, the 49 macroscopic cross sections (49 energy group) of the nuclide are changed mostly together. Due to the resonance effect depending on the

www.manaraa.com

temperature, those 49 values are not completely correlated so after 3,800, the singular value spectrum is still decaying gradually.

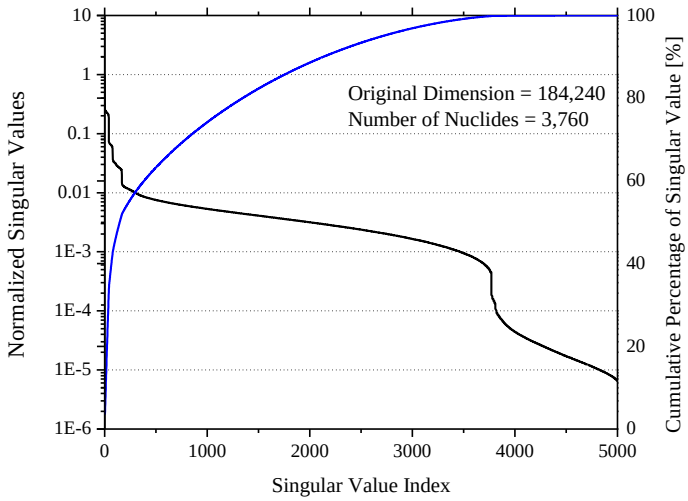

Figure 9-34. Singular Value Spectrum of Macroscopic Cross Sections

- **Portion of Orthogonal Component**

Given the basis $\mathbf{Q}$, the macroscopic cross section variations can be represented by:

$$\frac{\Delta\vec{\Sigma}}{\vec{\Sigma}^{(0)}} = \left(\frac{\Delta\vec{\Sigma}}{\vec{\Sigma}^{(0)}}\right)^{\|} + \left(\frac{\Delta\vec{\Sigma}}{\vec{\Sigma}^{(0)}}\right)^{\perp} = \mathbf{Q}\mathbf{Q}^{T}\frac{\Delta\vec{\Sigma}}{\vec{\Sigma}^{(0)}} + \left(\mathbf{I}-\mathbf{Q}\mathbf{Q}^{T}\right)\frac{\Delta\vec{\Sigma}}{\vec{\Sigma}^{(0)}} \tag{9.19}$$

where $\Delta\vec{\Sigma}^{\|}$ is the component in the active subspace and $\Delta\vec{\Sigma}^{\perp}$ is the component in the in-active subspace which is orthogonal to the active subspace. The main idea of the reduced order modeling is taking only the active subspace component and discarding the in-active subspace component. Thus, the discarded in-active subspace component can be considered as

www.manaraa.com

error due to reduced order transformation. In order to measure that discarded portion, the root mean square (RMS) error for random sample is calculated:

$$r.m.s = \sqrt{\frac{1}{n}\left[\left(\frac{\Delta\vec{\Sigma}}{\vec{\Sigma}^{(0)}}\right)^{\perp}\right]^{T}\left[\left(\frac{\Delta\vec{\Sigma}}{\vec{\Sigma}^{(0)}}\right)^{\perp}\right]} = \sqrt{\frac{1}{n}\sum_{i=1}^{n}\left\{\left(\frac{\Delta\Sigma_i}{\Sigma_i^{(0)}}\right)^{\perp}\right\}^{2}} \tag{9.20}$$

Test is conducted by following way:

Step 1) Choose the size of the active subspace ($r = 100, 200, 300, ..., 5000$)

Step 2) Calculate the basis

Step 3) For additional 10 random samples, calculate the RMS error metric

Step 4) Take the maximum among all RMS error metrics

In **Figure 9-35**, the error metric spectrum is presented. Like the singular value spectrum, around 3,800, the large drop is observed.

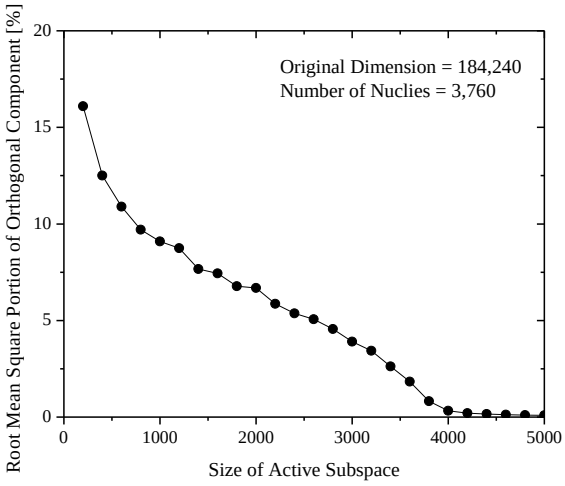

Figure 9-35. RMS Portion of Orthogonal Component of V-Subspace

www.manaraa.com

- **κ-metric**

The previous two approaches are based on completely mathematical sense. However, we need to consider the physical meaning of the subspace. Only considering the mathematical sense, the subspace construction algorithm tends to discard the directions with small variations but physically those directions may have large importance. For example, the macroscopic cross section change of moderator material may be small but the output responses are very sensitive to them. To ensure the constructed basis capture the physics properly, the extra simulation can be used. κ-metric method is examining the effect of the component not included in the active subspace. Simply, one can execute the code with input parameters perturbed along the direction orthogonal to the active subspace:

$$y = f\left(\Delta\vec{\Sigma}^{\perp}\right) = f\left(\left(\mathbf{I} - \mathbf{Q}\mathbf{Q}^{T}\right)\Delta\vec{\Sigma}\right) \tag{9.21}$$

where f can be considered as transport solver and y can be any response, e.g. k-eigenvalue or fluxes. The expected output response change would be small if the basis is constructed correctly.

The test is conducted by following procedure:

1. the test case is chosen (No. 5 assembly type (2.6% enrichment with 24 BPRs) and No. 6 assembly type (3.1% enrichment without BPR))
2. complete the depletion calculation and prepare the actual macroscopic cross section data
3. project the actual macroscopic cross section data onto the in-active subspace

www.manaraa.com

4. execute the simulation code (NEWT in SCALE6.1) with the projected cross section data
5. check the change of response interested

In **Figure 9-36**, the k-eigenvalue changes are plotted. The k-eigenvalues are changed from 5224 pcm to -10927 pcm with respect to the nominal status (0.88233491). The macroscopic cross sections are collected at each depletion step and projected onto the in-active subspace. In **Figure 9-37**, the k-eigenvalue changes are presented according to the size of active subspace, i.e. 1000, 2000, 3000, 4000 and 5000. As can be seen, the response changes due to in-active subspace components are getting smaller, which means the basis can capture the behavior of the macroscopic cross section changes more accurately. After 4,000, the results seem saturated as expected with consideration of the convergence criteria of k-eigenvalue, inner&outer iterations and mesh size for pincell calculations. In **Figure 9-38** and **Figure 9-39**, the κ-metric tests are conducted to the fluxes in a fuel pincell for No. 6 Assembly Type and No. 5 Assembly type, respectively. Same with before, as the size of active subspace increases, the effects from the in-active subspace decreases. Note that due to mesh sizing and resonance effects, some energy groups have inferior behavior. In **Figure 9-40** and **Figure 9-41**, the κ-metric tests are conducted for Few-group constants.

In this study, considering the convergence criteria of the transport solver and precision of cross section library, the active subspace size is assumed to 5,000 for intersection subspace construction.

www.manaraa.com

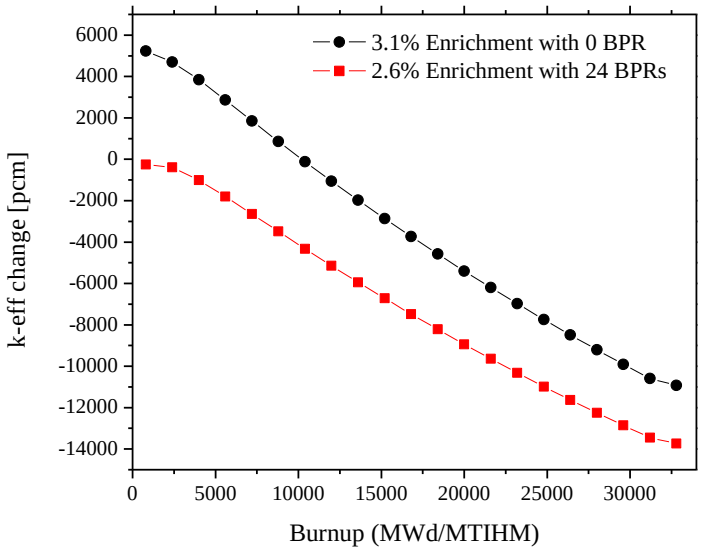

Figure 9-36. k-eff change due to fuel material depletion

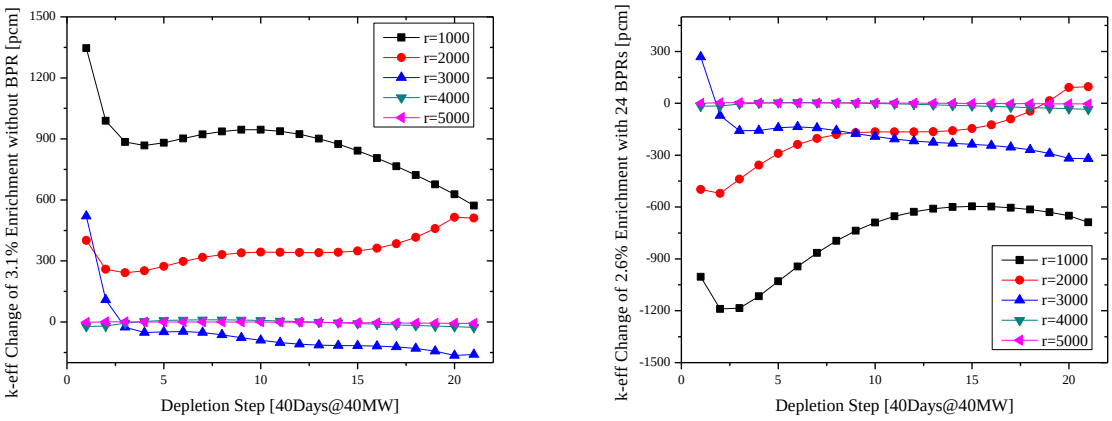

Figure 9-37. κ-metric test for k-eff with V-Subspace

www.manaraa.com

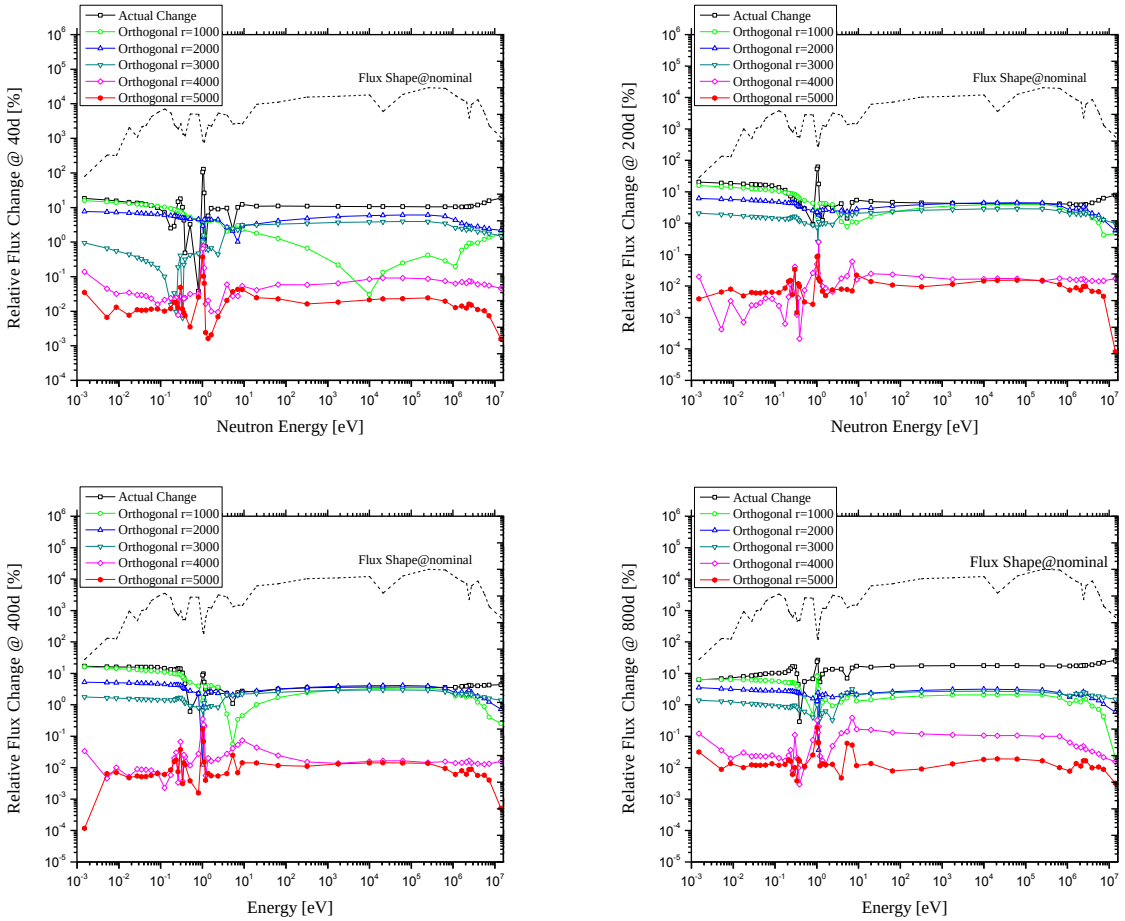

Figure 9-38. κ-metric test for fluxes with V-subspace (3.1% enrichment without BPR)

www.manaraa.com

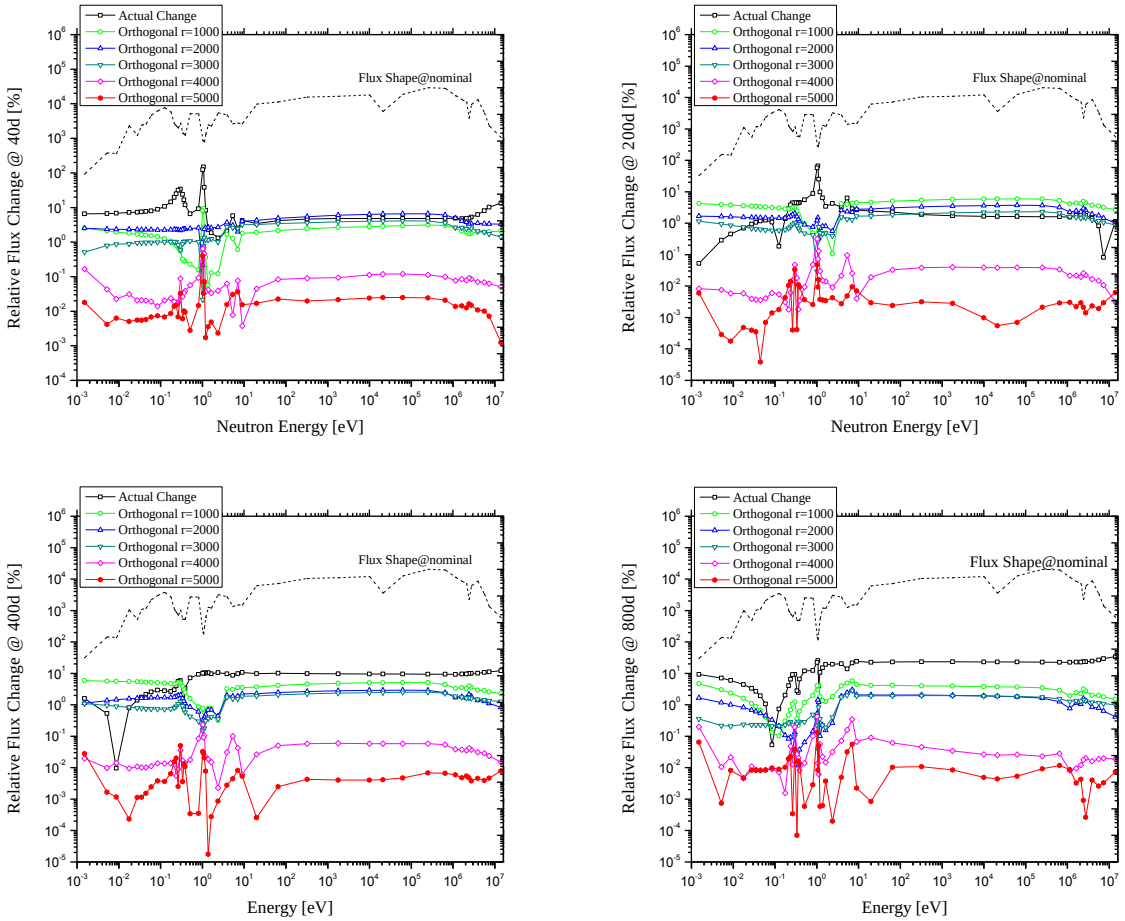

Figure 9-39. κ-metric test for fluxes with V-subspace (2.6% enrichment with 24 BPRs)

www.manaraa.com

Figure 9-40. κ -metric test for Few-Group Constants with V-subspace

(3.1% enrichment without BPR)

www.manaraa.com

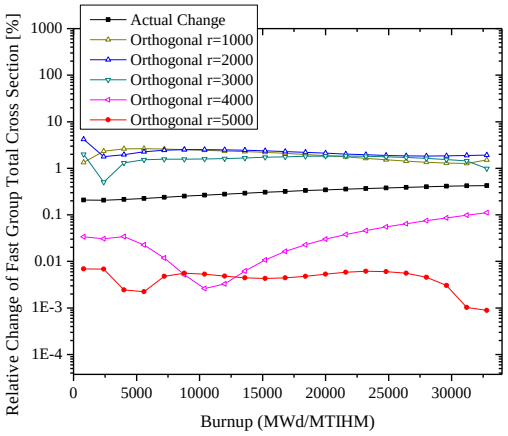

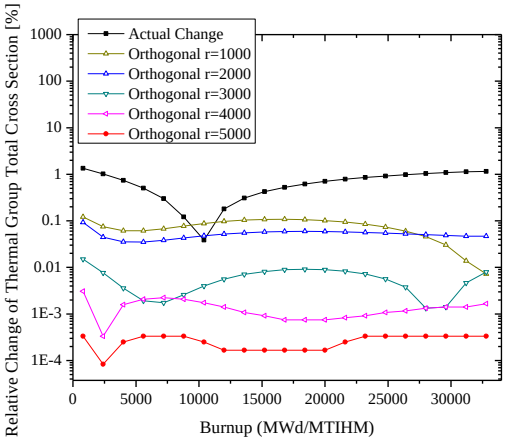

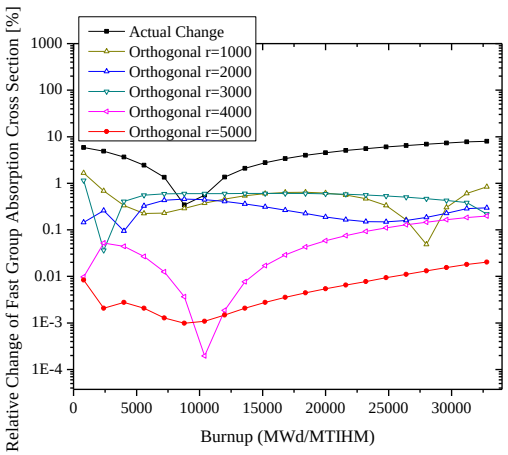

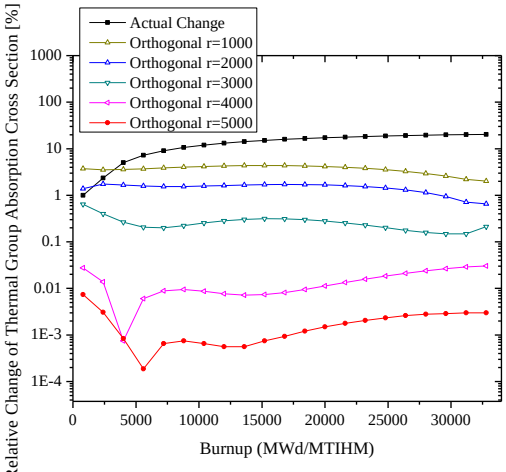

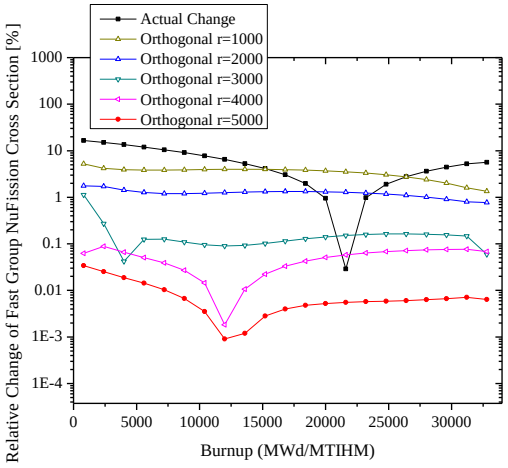

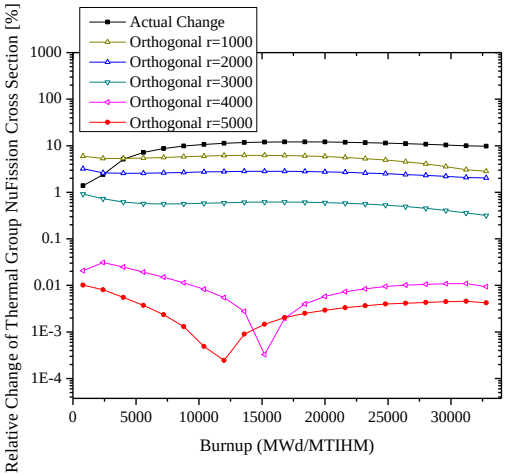

www.manaraa.com

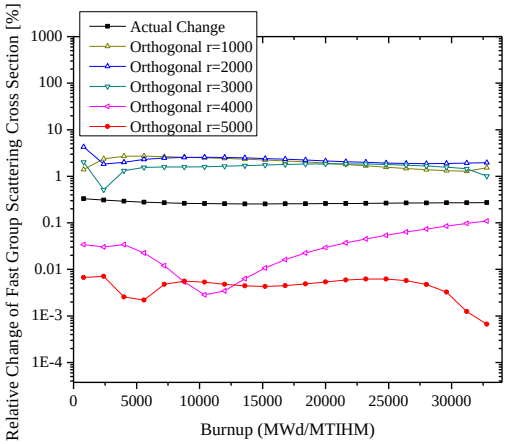

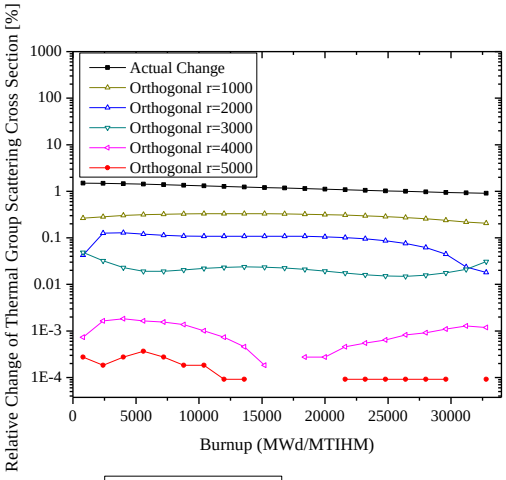

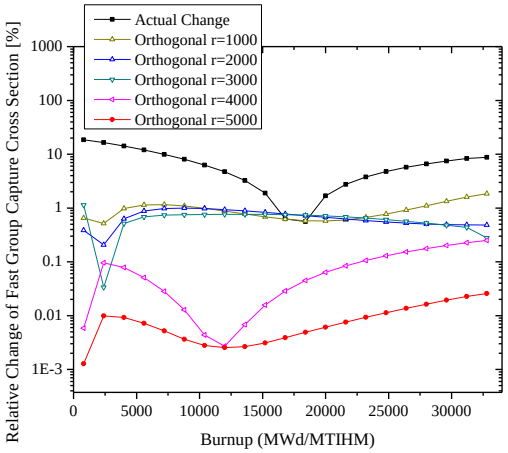

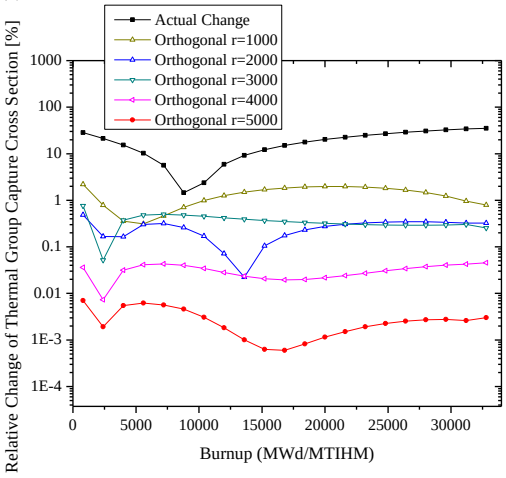

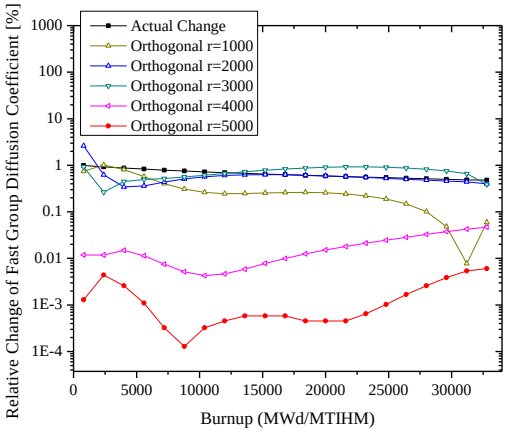

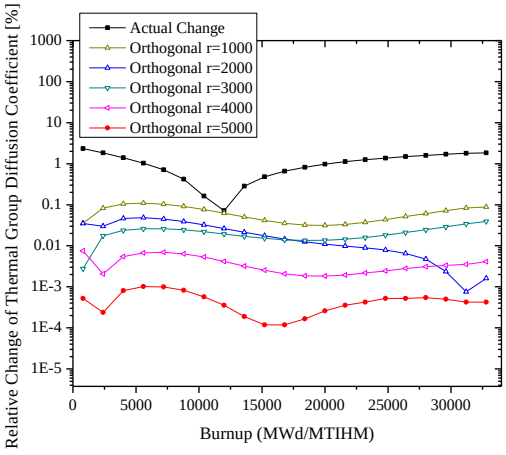

www.manaraa.com

Figure 9-41. κ-metric test for Few-Group Constants with V-subspace

(2.6% enrichment with 24 BPRs)

www.manaraa.com

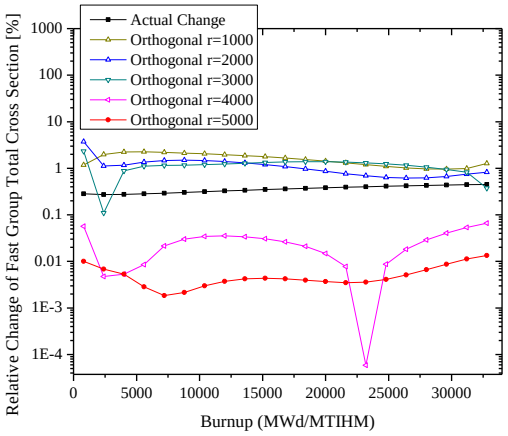

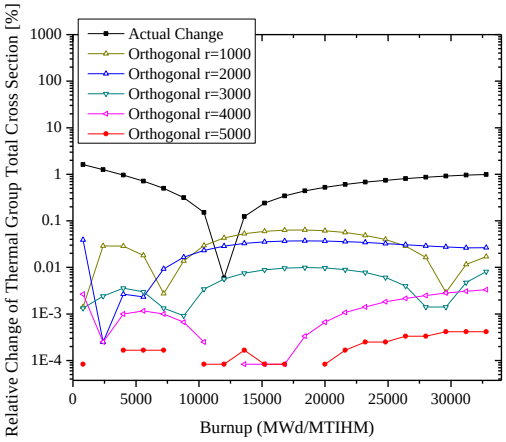

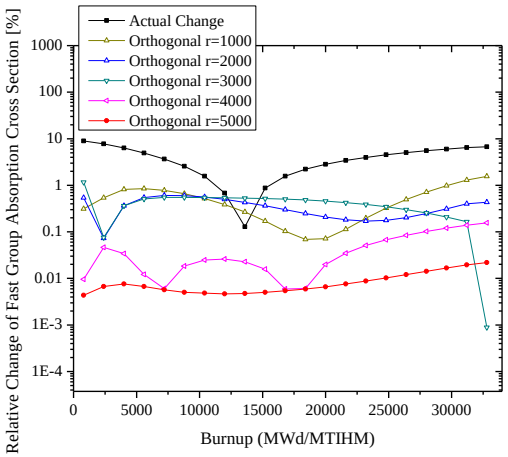

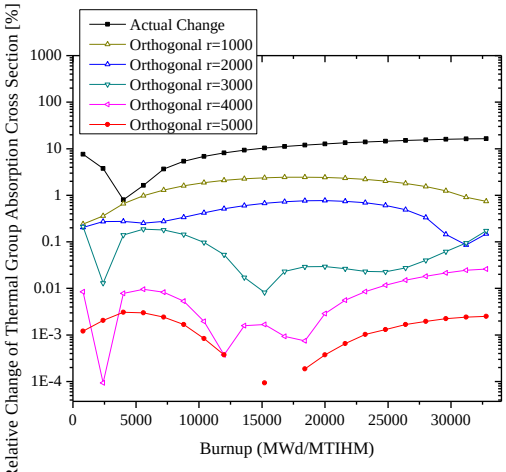

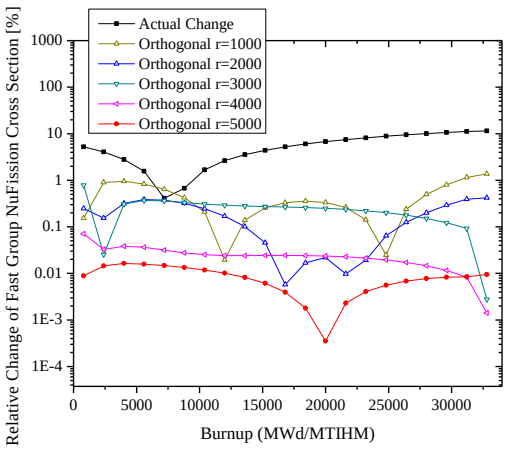

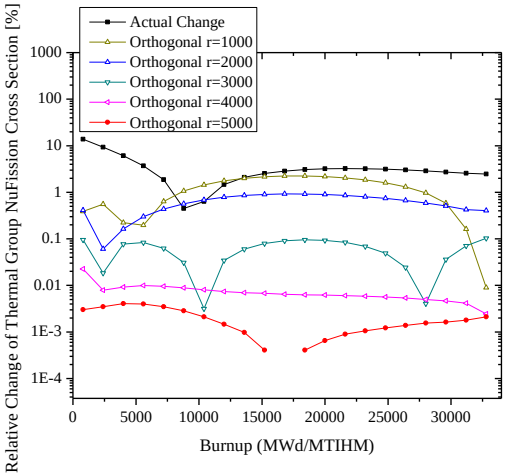

www.manaraa.com

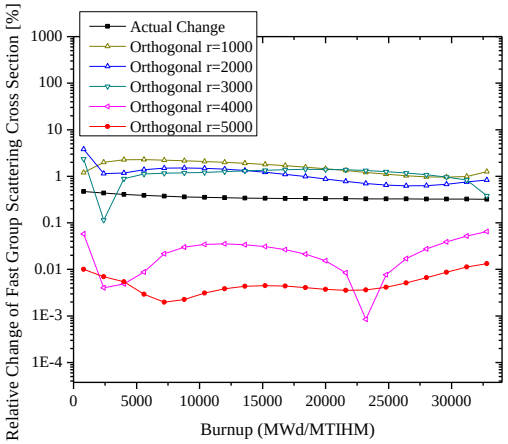

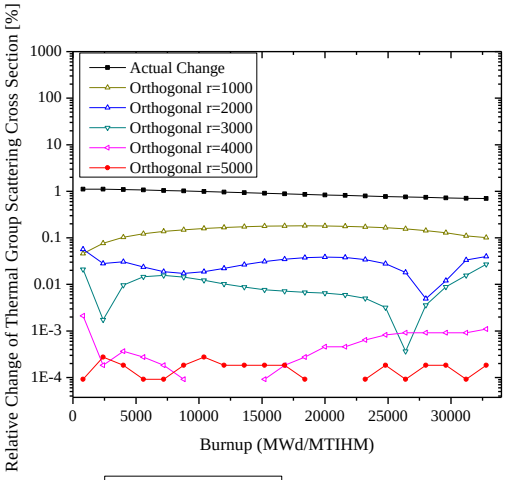

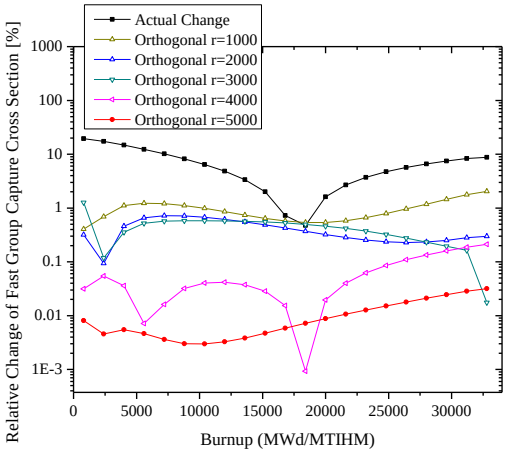

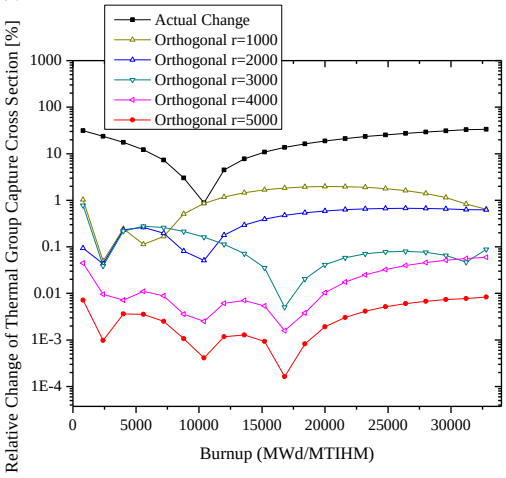

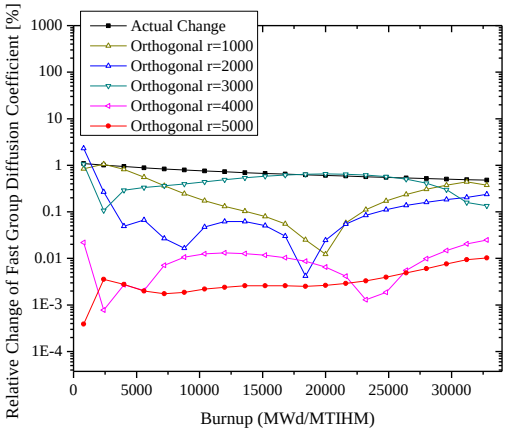

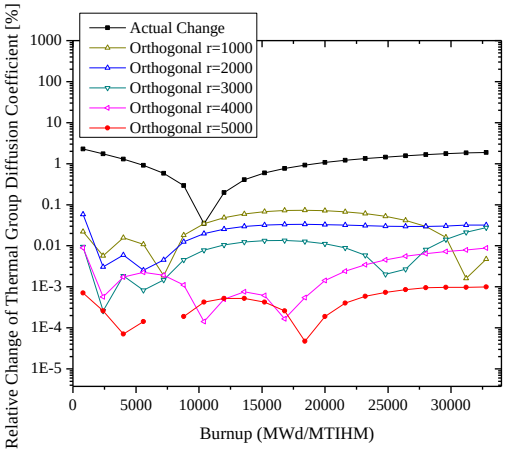

www.manaraa.com

9.2.4 I-Subspace Construction

The components of large variations extracted previously with resonance active subspace can be reduced by considering only components with high sensitivity. The sensitive components can be captured by examining the sensitivity profiles by adjoint sensitivity analysis and by projecting them onto the V-Subspace, one can finally identify the components in large variation and high sensitivity:

$$\mathbf{QQ}^T \left[\frac{\vec{\Sigma}}{k_{eff}} \frac{\partial k_{eff}}{\partial \vec{\Sigma}} \Big|^{(1)} \quad \cdots \quad \frac{\vec{\Sigma}}{k_{eff}} \frac{\partial k_{eff}}{\partial \vec{\Sigma}} \Big|^{(k)} \right] \tag{9.22}$$

$$\mathbf{QQ}^T \left[\frac{\vec{\Sigma}}{R^{pseudo}} \frac{\partial R^{pseudo}}{\partial \vec{\Sigma}} \Big|^{(1)} \quad \cdots \quad \frac{\vec{\Sigma}}{R^{pseudo}} \frac{\partial R^{pseudo}}{\partial \vec{\Sigma}} \Big|^{(k)} \right] \tag{9.23}$$

where $\mathbf{Q} \in \mathbb{R}^{184240 \times 5000}$ is the orthonormal basis of V-Subspace.

In **Figure 9-42** and **Figure 9-43**, the normalized singular value spectrum is compared. As can be seen, the spectrum of intersection is decaying faster than the case of V-active subspace. It means that 1) with same size of active subspace, intersection approach would be more accurate (capture the influential subspace more efficiently), 2) with same error tolerance criteria, intersection approach would produce the smaller size of basis (further reduction). In **Figure 9-44**, the κ-metric test with intersection subspace is presented. One can see that the error in transformation to 2,000 dimension would result in only a few tenth of pcm changes out of several thousands of k-eff actual changes. Also, in **Figure 9-45** ~ **Figure 9-48**, the κ-metric test results are shown. One can notice that 2000 intersection basis can represent the macroscopic cross section variations and sensitivities pretty accurately.

www.manaraa.com

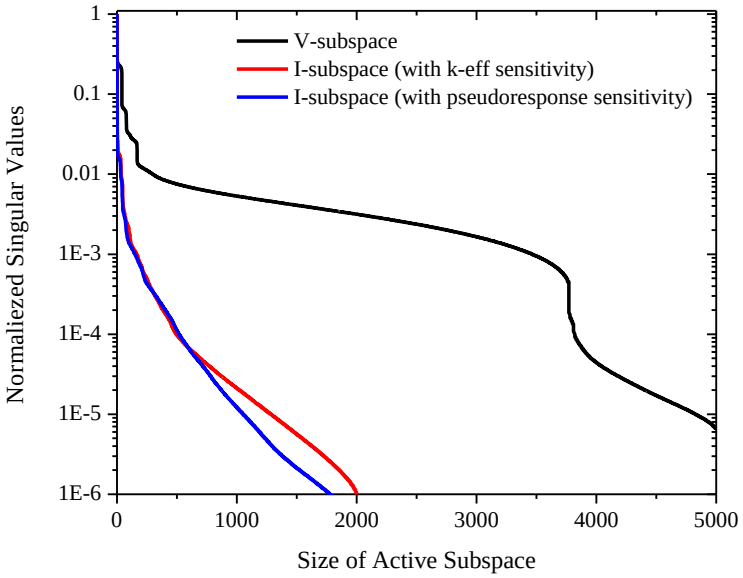

Figure 9-42. Comparison of Singular Value Spectrum

www.manaraa.com

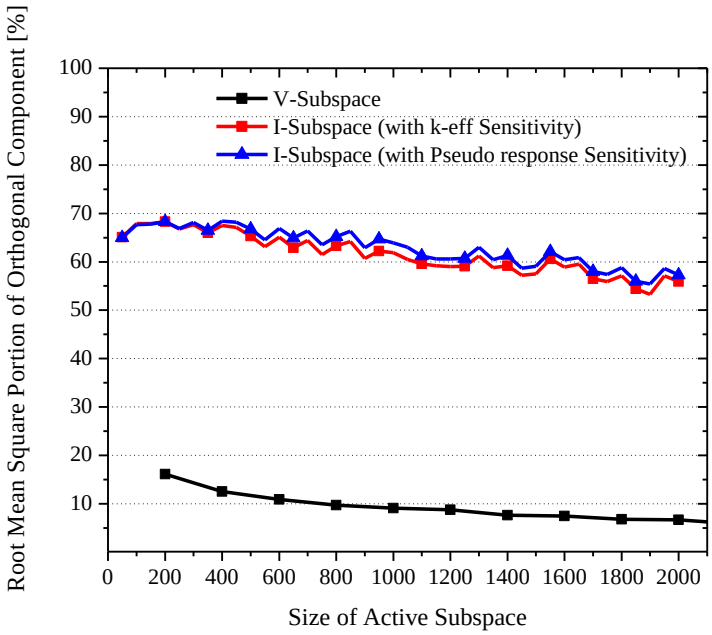

Figure 9-43. RMS Portion of Orthogonal Component of I-Subspace

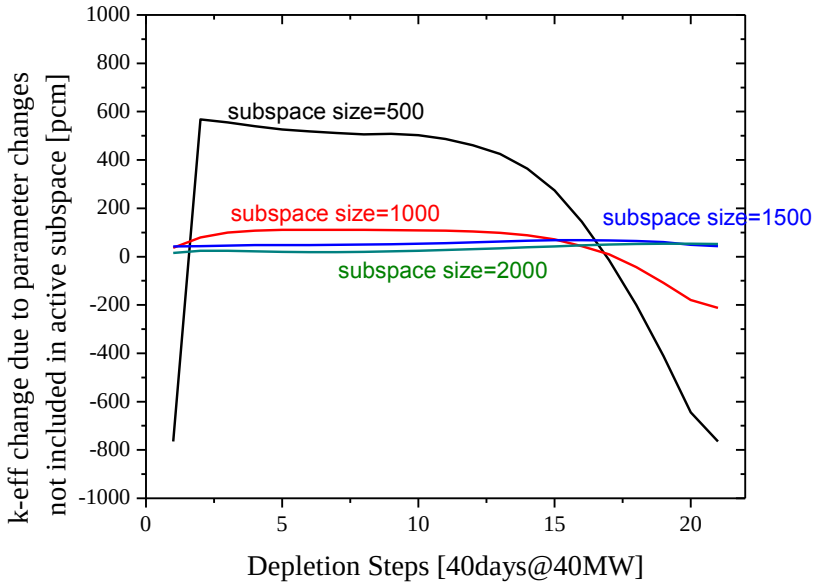

Figure 9-44. κ-metric test for k-eff with intersection active subspace

www.manaraa.com

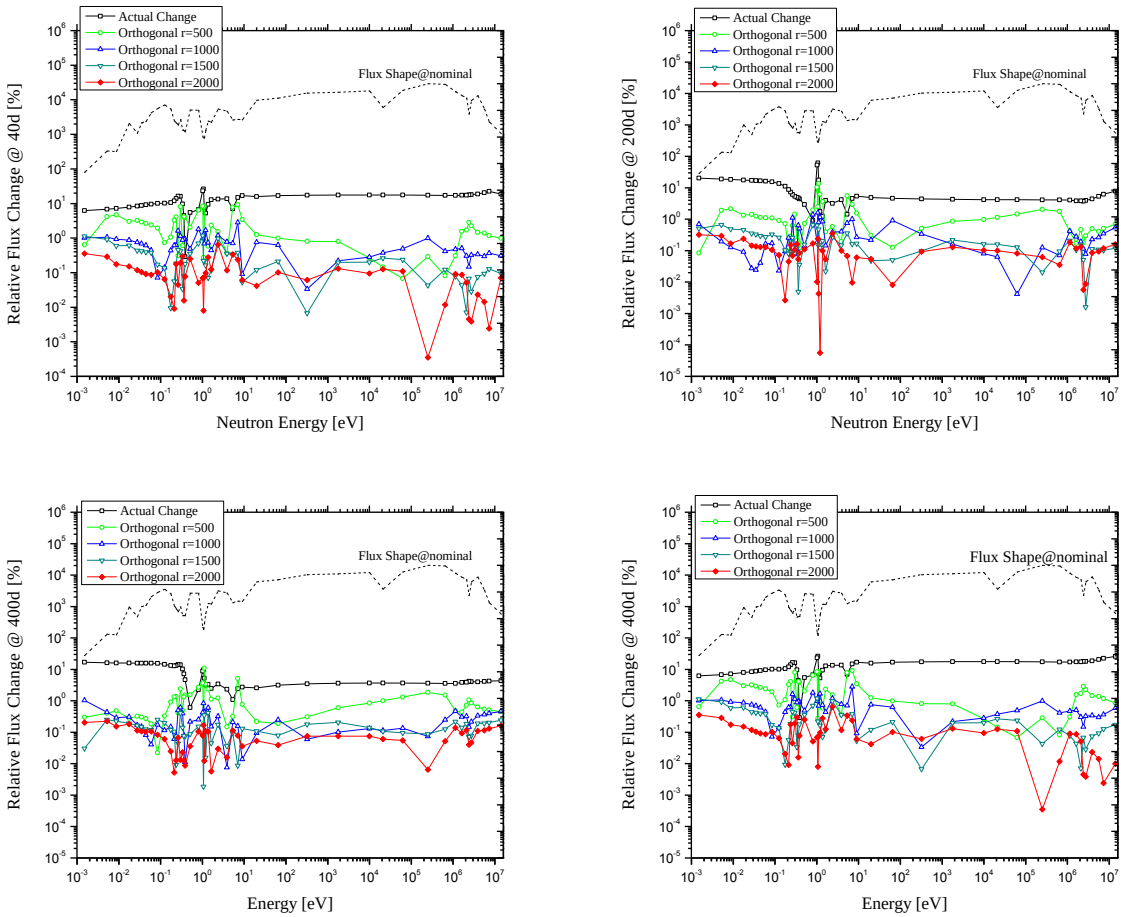

Figure 9-45. κ-metric test for fluxes with intersection active subspace (3.1% Enrichment without BPR)

www.manaraa.com

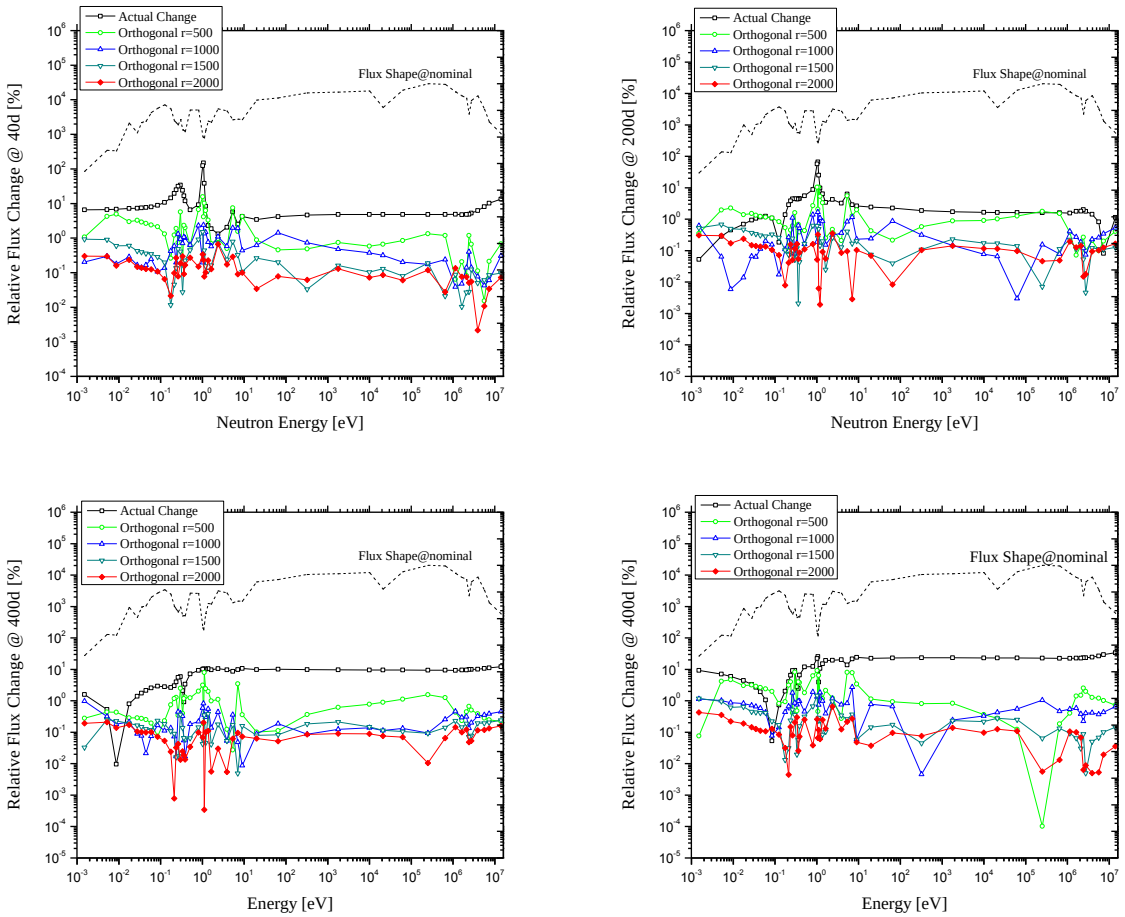

Figure 9-46. κ-metric test for fluxes with intersection active subspace (2.6% Enrichment without 24 BPRs)

www.manaraa.com

Figure 9-47. κ -metric test for Few-Group Constants with I-Subspace

(3.1% enrichment without BPR)

www.manaraa.com

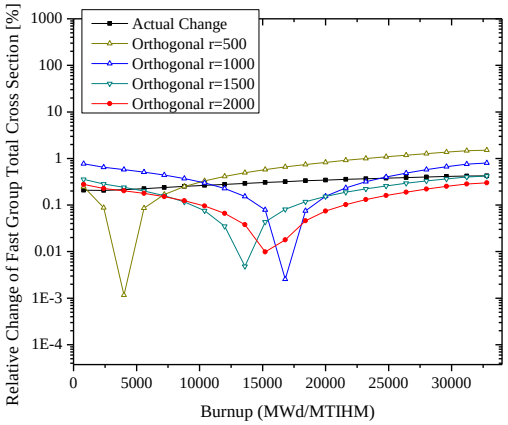

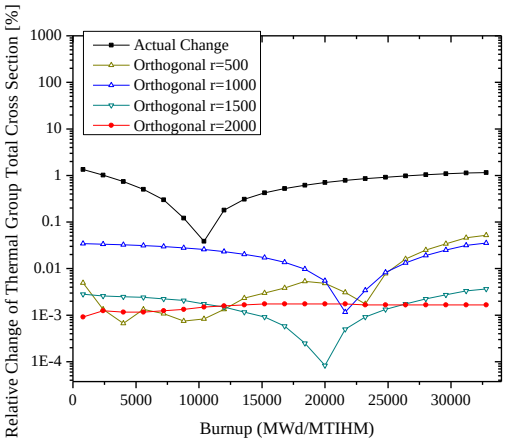

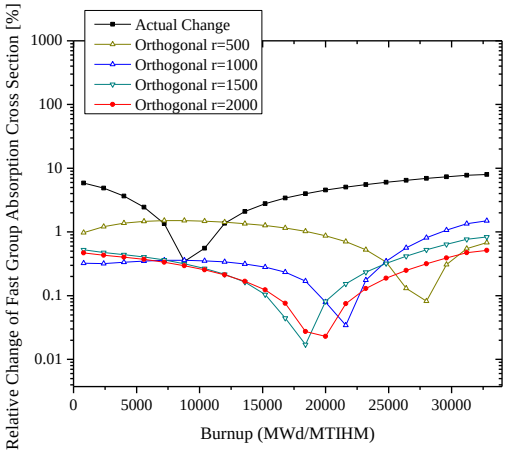

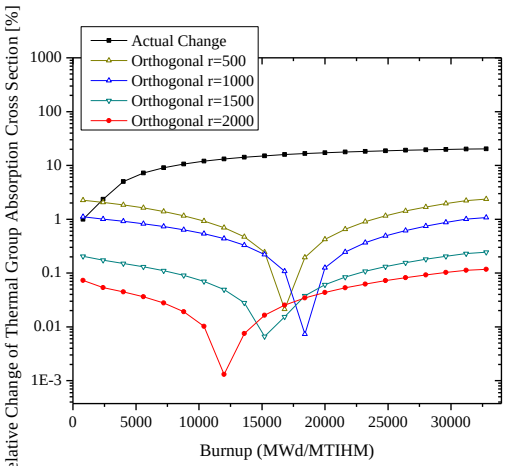

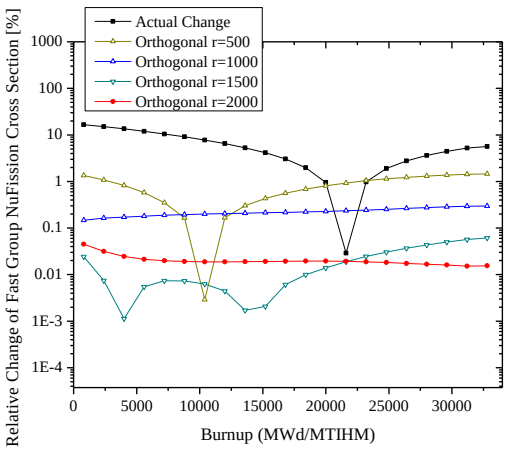

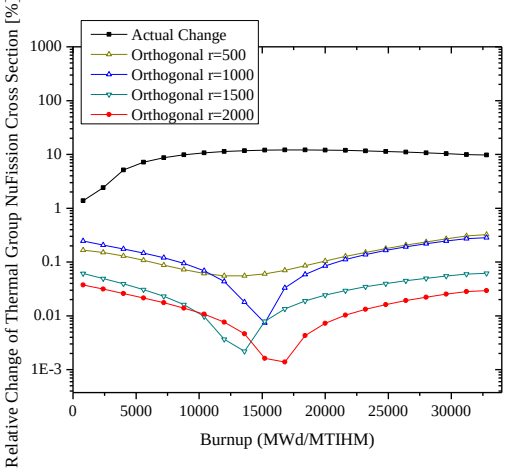

www.manaraa.com

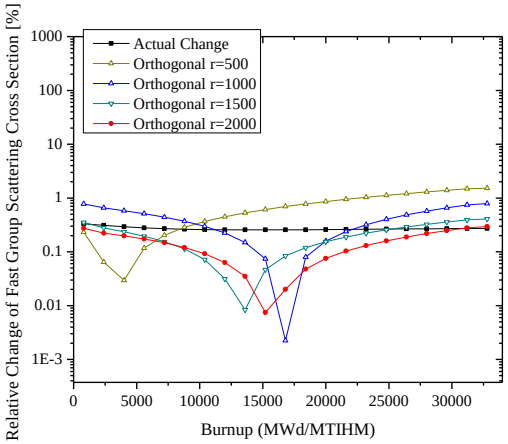

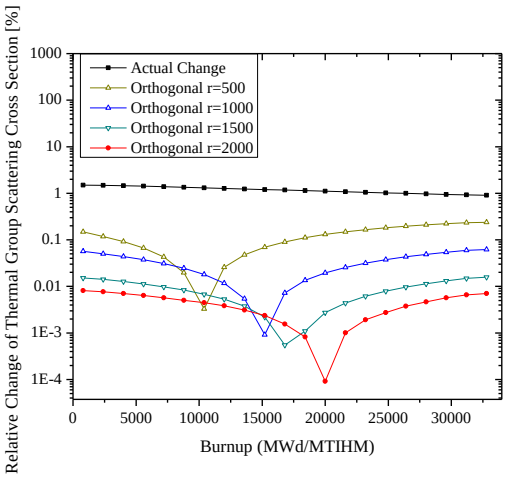

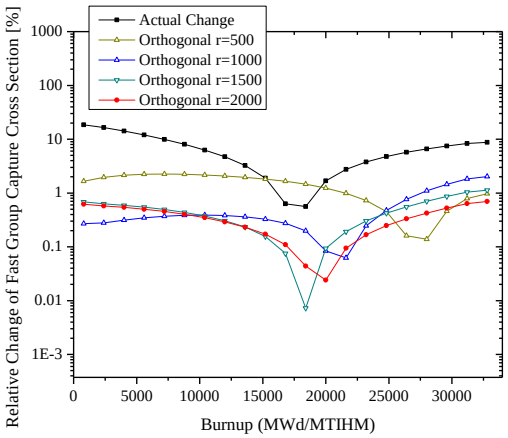

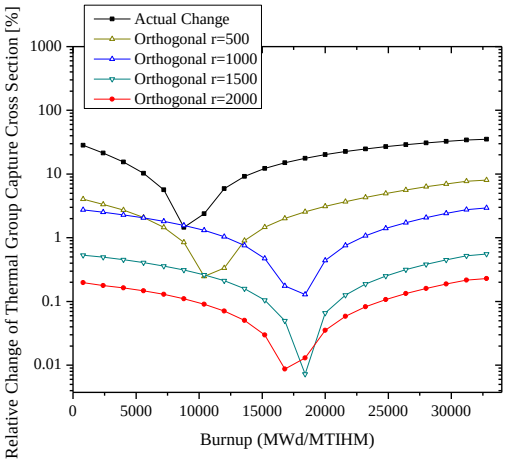

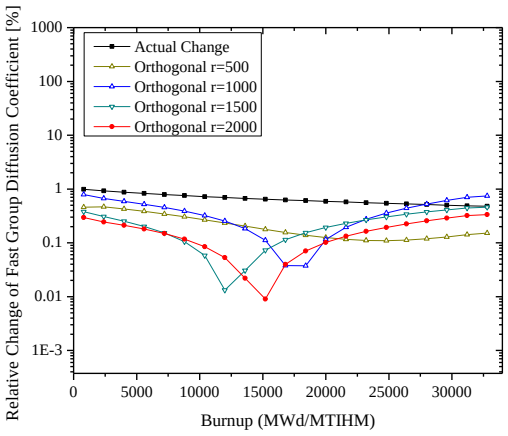

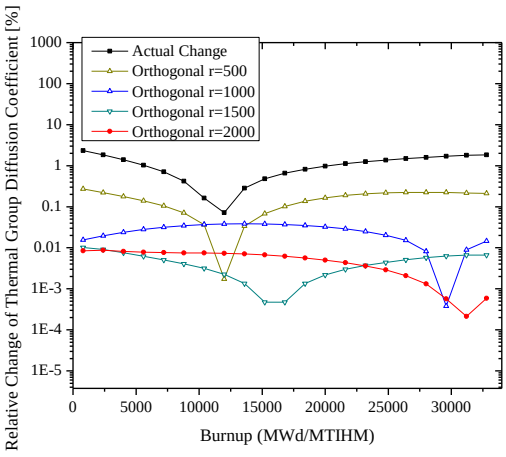

www.manaraa.com

Figure 9-48. κ -metric test for Few-Group Constants with I-Subspace

(2.6% enrichment with 24 BPRs)

www.manaraa.com

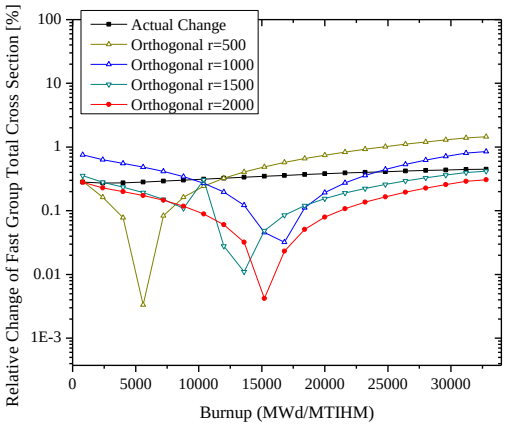

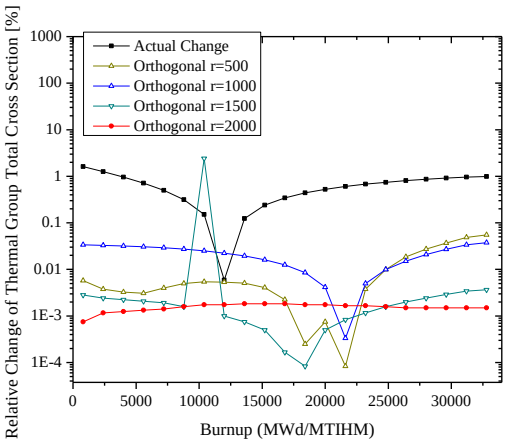

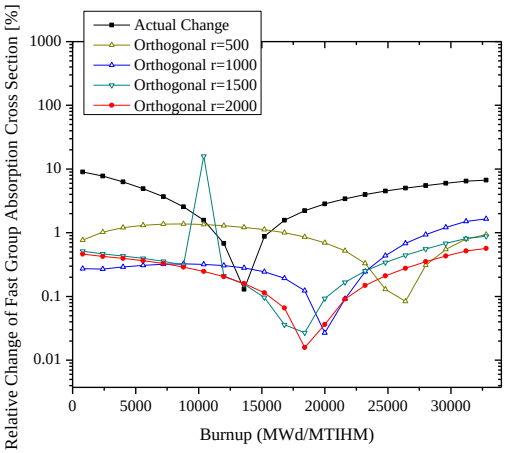

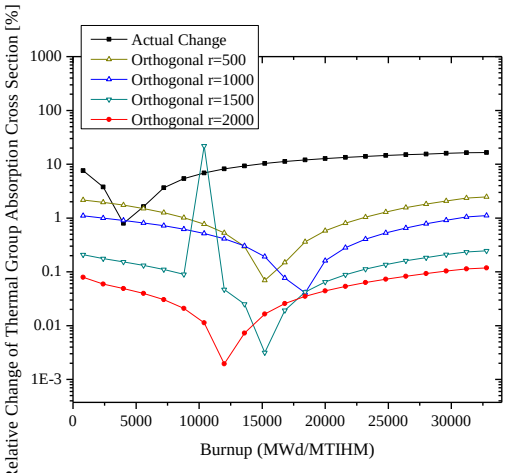

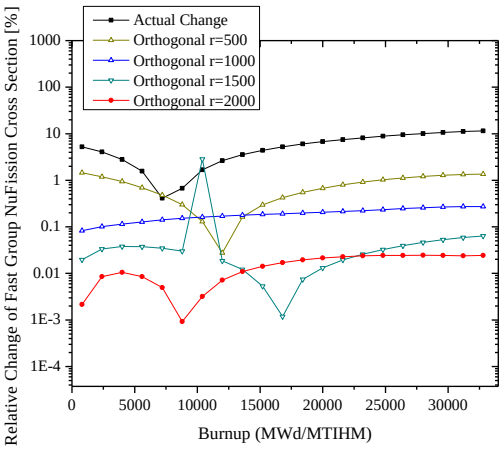

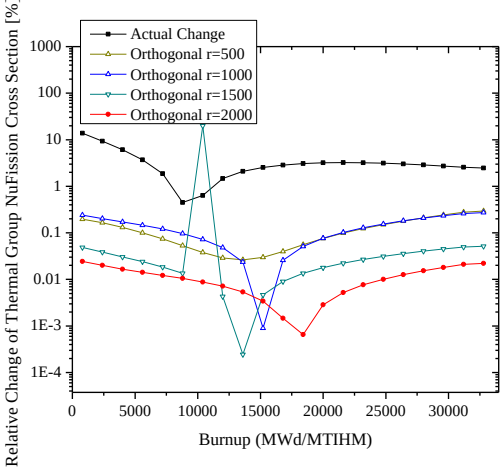

www.manaraa.com

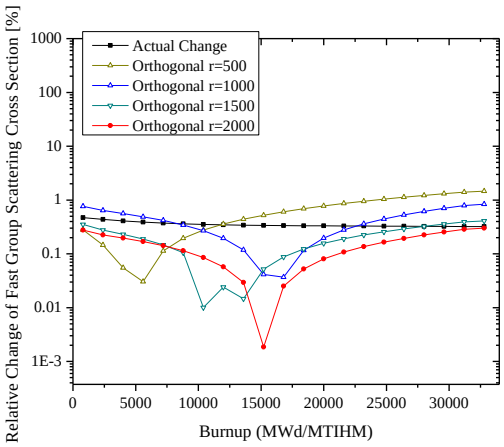

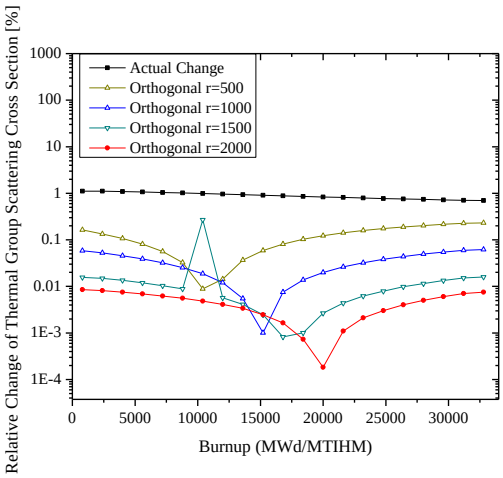

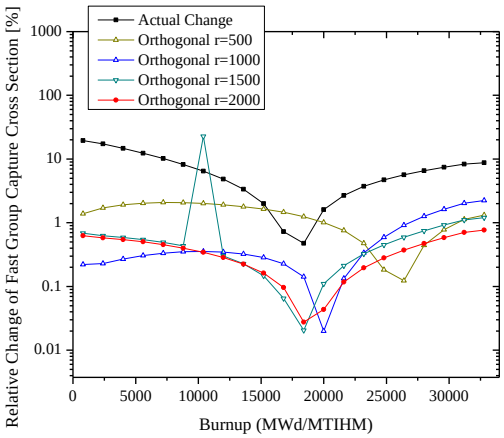

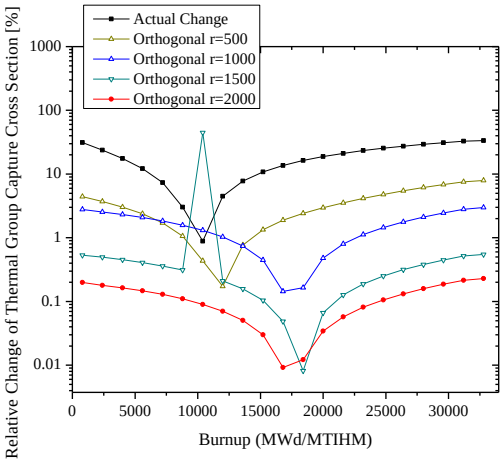

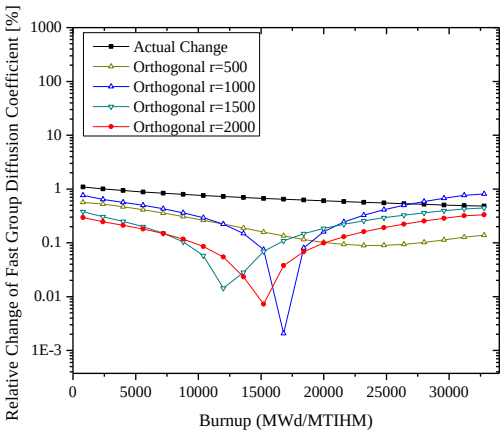

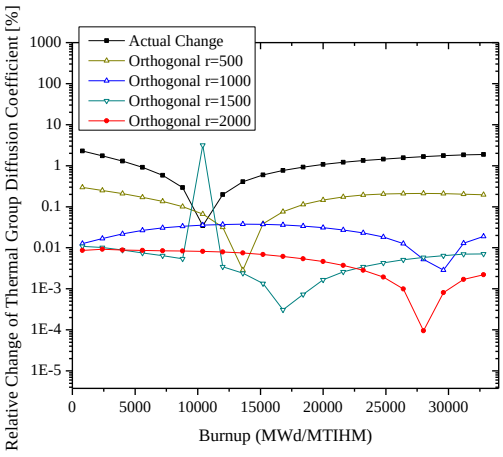

www.manaraa.com

9.3 Discussion

In this chapter, the proposed reduced order modeling with the intersection subspace approach via the range finding algorithm is implemented to examine the its performance for highly nonlinear and very large scale problems, i.e. PB-2 BWR assembly and WB-2 PWR assembly model. The assembly calculation is considered as a serially coupled model and relationships between two models, i.e. BONAMI and NEWT, are investigated. Overall, it is shown that the intersection approach can achieve the further reduction compared to only considering the macroscopic cross section variations due to perturbation of nuclide number densities and temperatures and resonance self-shielding calculation (V-subspace) with respect to the calculation precision:

- single precision (6 significant digits for ENDF cross section library)
- Transport solver convergence criteria (10^{-5} for BWR model, 10^{-4} for PWR model)

In **Table 9-7**, the summary of the dimensionality reduction is presented. One can notice that by using subspace methods, one can construct the orthogonormal basis for the dimensionally reduced representation of the macroscopic cross section while minimizing the reduced order transformation error. Note that one can construct more accurate reduced order representation by increasing the size of the subspace.

www.manaraa.com

Table 9-7. Summary of Reduced Order Modeling

	PB-2 BWR	**WB-2 PWR**
Original Dimension	44,786	184,240
Reduced Dimension (V-Subspace)	1,000 (2.23% of original dim.)	5,000 (2.71% of original dim.)
Reduced Dimension (I-Subspace)	600 (1.34% of original dim.)	2,000 (1.09% of original dim.)

Note that the error in the surrogate modeling with reduced order transformed input parameters can have two sources of error:

- Error from Reduced Order Modeling (ε_{ROM})
- Error from Surrogate Modeling (ε_{SM})

It is important to estimate the error due to reduced order modeling because it will propagate to the surrogate modeling step and may determine the surrogate modeling accuracy. To get a rough estimate of the error tolerance, a simple test is conducted in which all few group constants are perturbed randomly by 5% and 10% and check the k-eff changes calculated by core simulator (NESTLE) due to those perturbations. The reference k-eff is 1.003451 and 100 random cases are generated. Note that all few group constants' 5% perturbation results in only a few tenth of pcm difference. With regard to the κ-metric tests in the previous sections, the error due to reduced order transformation was less than 1% (mostly less than 0.1% for BWR case). Thus, the reduced order modeling conducted in this study can be considered reasonably accurate with respect to final core simulator calculation results.

www.manaraa.com

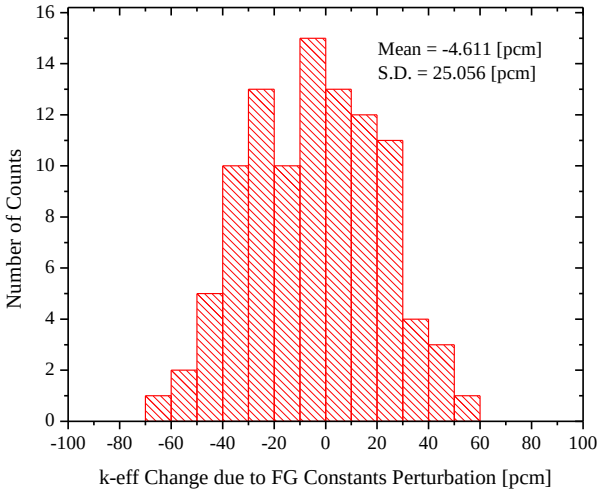

Figure 9-49. k-eff changes due to Random 5% FG constants Perturbation

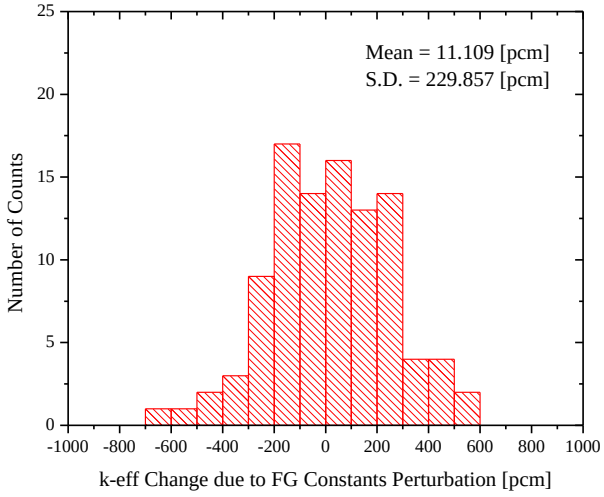

Figure 9-50. k-eff changes due to Random 10% FG constants Perturbation

www.manaraa.com

To estimate the surrogate model form, a simple linearity test is conducted. This is important because, as the model is highly nonlinear, the surrogate model should be the high order form. Test is conducted in the following way:

Step 1) the each macroscopic cross section's maximum value and minimum value for entire depletion range are collected: $\Sigma_{i,g}^{\max}$ and $\Sigma_{i,g}^{\min}$ for isotope i and energy g

Step 2) the reference perturbation is generated by perturbing within those maximum and minimum values:

$\Delta\Sigma_{i,g}^{(0)} = \left(\Sigma_{i,g}^{\max} - \Sigma_{i,g}^{\min}\right) \times \alpha$ where α is randomly generated number $-0.05 \le \alpha \le +0.05$

Step 3) the reference perturbation is increased by multiplying integer numbers:

$\Delta\Sigma_{i,g}^{(k)} = \Delta\Sigma_{i,g}^{(0)} \times k$ where $k = 1, ..., 20$

Step 4) NEWT is executed with the perturbed macroscopic cross section library.

With this perturbation scheme, one can perturb only in one direction so that it makes easier to analyze the nonlinearity. In **Figure 9-51**, the k-eff changes of PB-2 BWR assembly model due to macroscopic cross section perturbation is presented. Those k-eff values are fitted by polynomial regression analysis with several different orders and the goodness-of-fit (R^2) is compared in **Table 9-8**. One can notice that the k-eff change is from -101 pcm to -1699 pcm which is relatively smaller than the one considered in depletion calculation but

www.manaraa.com

second and third order polynomial regression analysis show pretty large discrepancy. This proves that the output response change would be nonlinear and more than fourth order would be required to accurately predict the response changes. Note that though the original inputs are reduced much, the reduced inputs are still too large to build a surrogate model with existing conventional surrogate modeling methods. Building a surrogate model for such a high dimensional model would be left for future works.

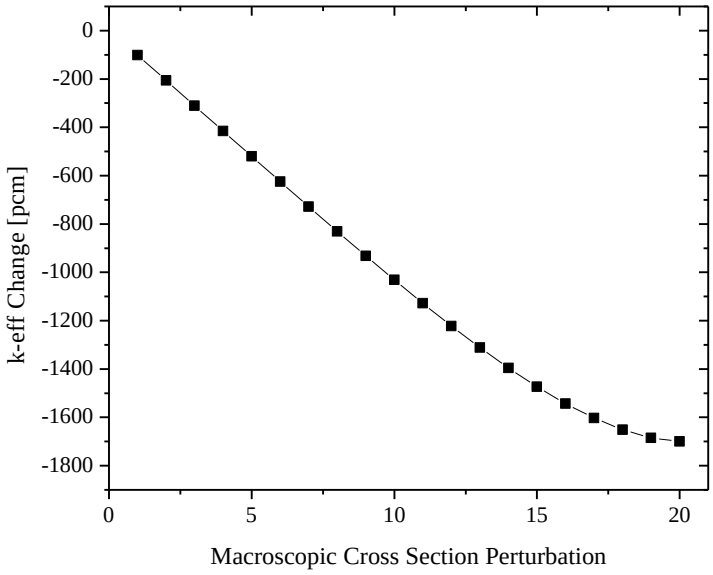

Figure 9-51. k-eff Changes due to One Direction Perturbation

www.manaraa.com

Table 9-8. Goodness-of-Fit Comparison of Different Polynomial Regression Order

Perturbation	Polynomial Regression Analysis Estimation Discrepancy [pcm]			
	Second Order	**Third Order**	**Fourth Order**	**Fifth Order**
1	34.9563	-7.3629	1.2979	-0.2123
2	15.4043	-0.1869	-0.6431	0.2324
3	0.1152	3.8276	-1.1871	0.2185
4	-11.1121	5.3528	-0.9132	0.0402
5	-18.5216	5.0184	-0.2868	-0.1403
6	-22.3573	3.4537	0.3831	-0.2173
7	-22.9461	1.2053	0.8608	-0.1918
8	-20.6032	-1.1685	1.0791	-0.0436
9	-15.8924	-3.3581	0.8783	0.0401
10	-9.1328	-4.8091	0.4999	0.1919
11	-1.0515	-5.3750	-0.0660	0.2435
12	7.6118	-4.9223	-0.6859	0.1537
13	16.1278	-3.3066	-1.0590	0.0652
14	23.3306	-0.8205	-1.1649	-0.1109
15	28.0052	2.1946	-0.8760	-0.2742
16	28.6957	5.1560	-0.1491	-0.2942
17	23.5910	7.1263	0.8603	-0.0917
18	10.4110	6.6990	1.6843	0.2801
19	-13.8201	1.7714	1.3152	0.4412
20	-52.8124	-10.4930	-1.8321	-0.3204
Goodness-of-Fit (R^2)	9.981487E-01	9.999102E-01	9.999964E-01	1.000000E+00

www.manaraa.com

CHAPTER 10. CONCLUSION

Thanks to the startling increase in computer power, much more complex nuclear reactor models can now be simulated. In addition, the accuracy of the simulation has been greatly improved with detailed physical models, sophisticated numerical scheme with better stability and less discretization errors and reduced uncertainty in model parameters. Over the past decades, a number of initiatives were proposed to improve further the accuracy of the simulation via the use of detailed first-principles type models to eliminate the underlying assumptions and approximations. Furthermore, it has become essential to defend the simulation results in a rigorous manner, i.e. via the use of a comprehensive uncertainty analysis. To realize the benefits of these initiatives in real engineering design where day-to-day decisions need to be made swiftly based on simulation results, the efficiency of the simulation has become an important consideration.

The objective of this dissertation is ***to reduce the computational cost in utilizing the high-fidelity computer simulation tools for sensitivity analysis, uncertainty quantification and design optimization***. To achieve that, the ***reduced order modeling*** was introduced. The premise is that by reducing the number of input parameters or state variables (output responses), the original problem can be solved more efficiently with reduced cost, i.e. less memory requirement or smaller number of floating point operations or code runs and

www.manaraa.com

ultimately current analysis methods which are unaffordable due to computational cost can be implemented for routine engineering analysis.

First contribution of this dissertation is to devise the efficient active-subspace identification algorithm based on the subspace methodology. We adopted the randomized range finder algorithm which mainly proposed and studied by mathematicians in numerical linear algebra community to accelerating matrix decomposition methods for low-rank approximation and incorporated into the reduced order modeling algorithms. Different with mathematicians' objective for randomized algorithm which is reducing the number of floating point operations of decomposition algorithms for given matrix, our primary concern is reducing the number of code executions to identify the range of active subspace while the explicit form of matrix or model is not given. Because our range finder algorithm is non-intrusive, there is no necessity for accessing and modifying source codes of legacy simulation programs. Thanks to randomness, the process for constructing orthonormal basis can make best of the cluster computing platform; thus, reduced order modeling itself can be efficiently performed in (semi-) parallel.

In that the reduced order modeling is an approximate of the original model, there must be errors introduced. It is obvious that the error should be quantified and controlled. Three methods are considered and examined for that purpose: singular value spectrum of random samples, magnitude in-active components and output response change due to in-active components. The numerical tests show that all three indicate the similar results while each method emphasizes on the specific physical or mathematical meaning.

www.manaraa.com

With the randomized range finding algorithm as the main engine, we could achieve the dimensionality reduction in two levels: state-level and input-level. State-level reduction is algorithmically straightforward and its physical meaning is easy and simple to understand. On the other hand, input-level reduction requires mathematical knowledge on subspace methodologies and first order derivatives should be provided to extract the sensitive components of input parameters. This dissertation put more efforts on the latter, input-level reduction, and tried to explain and illustrate the background theory, idea and algorithms concisely but in details as much as possible. To demonstrate the applicability, we have shown that the reduced order modeling can be successfully combined to other analysis methods:

- Reduced Order Initial Condition Perturbation Theory (state-level reduction)
- Reduced Order Hessian Construction (input-level reduction)
- Reduced Order Regression Analysis (input-level reduction)

With numerical tests, we could convince that the our hybrid reduced order modeling methods can be used to identify the influential components reliably and efficiently. Especially, the limit of parameter reduction, i.e. how much reducible, within an error tolerance was intensively investigated. The observations conclude that there are two factors to determine the reduction: model nonlinearity and magnitude of perturbation. It is obvious that if a model is more nonlinear, the larger size of subspace basis would be required due to nonlinear terms. As the input parameter perturbation increases, the effect from higher order terms becomes significant and cannot be neglected any more; thus, the larger size of subspace basis would be required to capture higher order effects. This implies that there is no

www.manaraa.com

a priori estimation of error due to reduced order modeling or active subspace size unless the model is investigated intrusively. Therefore, our adaptive basis construction approach can be rationalized.

Deliberating the incorporation of the reduced order modeling approach to the uncertainty quantification methods, we could come up with the idea of intersection subspace between two different active subspaces and could have shown that the further reduction can be achieved. Numerical tests were conducted to show that the number of code executions for uncertainty propagation be reducible without compromising the accuracy of analysis:

- Reduced Order Uncertainty Propagation with Linear Assumption
- Reduced Order Uncertainty Propagation via Nonlinear Surrogate Modeling

The input parameter perturbations due to uncertainty should be small in nuclear engineering, thus one can expect exceeding reduction in real reactor calculations. For very highly nonlinear problem which should not the case in nuclear engineering for safety reasons, nonlinear surrogate based uncertainty propagation was also examined. It drew an important finding that the linear assumption in uncertainty propagation could underestimate the output uncertainty, which could be an issue in case that the propagated uncertainty value would be used to critical decision making regarding to safety.

It was natural to consider the problem with multiple subspaces and move onto the multi-physics problems, which has been a common topic in computational science and engineering communities. We could generalize the intersection subspace approach to the coupled codes

www.manaraa.com

problems and numerically demonstrated in a problem that two codes are serially coupled but through another code, the latter code feedbacks to the former code in chain:

- Reduced Order Modeling for Multi-Physics Problems

Compared to uncertainty quantification, in general engineering applications, e.g. design optimization, the large variation of input parameters should be considered. We show that the feasibility of our reduced order modeling would be still applicable to very large scale problems with large variations. Also, we expect that as the more codes are coupled, the more reduction could be achieved, which is very promising because not only we can conduct the routine engineering calculation more efficiently but also we can deal with more complex problems.

In conclusion, we have proposed the efficient method for reduced order modeling and explored the applicability to nuclear reactor physics problems through numerical demonstrations. With the randomized algorithm, we make the best of the multi-core computing environments to perform the reduced order modeling. By combining the existing methods for surrogate modeling, e.g. perturbation theory, response surface modeling, we have shown that computationally expensive engineering analysis, e.g. sensitivity analysis or uncertainty quantification, can be conducted efficiently.

Though we were focusing on exercising the reduced order modeling on nuclear engineering problems and examining the applicability, the proposed methods and algorithms are general so it would be straightforward to extend to other engineering problems. Therefore, there are a lot of possiblily for future works in and out of reactor physics

www.manaraa.com

applications. First of all, the capability of the reduced order modeling for the assembly macroscopic cross-sections can be incorporated to core simulator for fuel loading pattern optimization. As mentioned in Chapter 2, the assembly model should be calculated very many time to capture the effects of different operating conditions. Core simulator gathers the few-group constants and interpolates to generate the input parameters for core-wise calculations. Once the surrogate model for few-group constants is constructed accurately with reduced order modeling and incorporate the surrogate to core simulator, repeating the assembly models and the interpolation of few-group constants would not be necessary and additional approximations could be avoided. Second, the intersection subspace approach can be applied to other coupled code problems, i.e. thermal-hydraulic and neutronics coupling. Because both codes are computationally intense, coupling them would require enormous computing resources. With aid of the reduced order modeling with intersection subspace approach, the computational cost can be effectively managed, e.g. determine the optimum mesh size or mesh structure or filter out the dominant physical process and parameters for subsequent analysis. In addition, the proposed reduced order modeling method is basically non-intrusive approach; thus, it can be easily applicable to any other problems if conducted properly. Near term goals include the application to licensing level reactor physics design calculations and nuclear power plant accident analysis for probabilistic risk analysis (PRA). In addition, the reduced order modeling can be useful for not only accelerating the simulations but also enhance the capability on dealing with more complex problems that may improve the accuracy of the simulation and broaden the application range. In the sense, we

www.manaraa.com

can think of incorporating the proposed reduced order modeling to under-developing codes as a built-in model.

www.manaraa.com

REFERENCES

Abdel-Khalik, H.S., "On Nonlinear Reduced Order Modeling", *International Conference on Mathematical and Computational Methods Applied to Nuclear Science and Engineering* (M&C 2011), Rio de Janeiro, RJ, Brazil, May 8-12, (2011).

Abdel-Khalik, H.S., "Adaptive Core Simulation", Ph.D dissertation, North Carolina State University, (2004).

Abdel-Khalik, H.S. and Hite, J.M., "Reduced Order Modeling: Tensor-Free Expansion for Nonlinear Features Identification", *Transactions of the American Nuclear Society*, Hollywood FL, June, (2011).

Abdel-Khalik, H.S., Turinsky, P.J. and Jessee, M.A. "Efficient Subspace Methods-based Algorithms for Performing Sensitivity, Uncertainty, and Adaptive Simulation of Large-Scale Computational Models", *Nuclear Science and Engineering* **159**, (2008); pp. 256-272.

Acharjee, S., Zabaras, N., "A concurrent model reduction approach on spatial and random domains for the solution of stochastic PDEs", *Int. J. Numer. Meth. Engng* **66**, (2006); pp. 1934-1954.

Acharjee, S., Zabaras, N., "A non-intrusive stochastic Galerkin approach for modeling uncertainty propagation in deformation processes", *Computers and Structures* **85**, (2007); pp. 244-254.

www.manaraa.com

Anile, A.M., Spinella, S. and Rinaudo, S., "Stochastic response surface method and tolerance analysis in microelectronics", *The International Journal for Computation and Mathematics in Electrical and Electronic Engineering*, Vol. **22**, No. 2, (2003); pp. 314-327.

Antoulas, A.C., Sorensen, D.C. and Gugercin, S., "A survey of model reduction methods for large-scale systems", *Structured Matrices in Operator Theory, Numerical Analysis, Control, Signal and Image Processing*, Contemporary Mathematics, AMS publications, **280**, (2001); pp. 193-219.

Astrid, P., "Reduction of Process Simulation Models: a proper orthogonal decomposition approach", Ph.D dissertation, Technishe Universiteit Eindhoven, (2004).

Astrid, P., Weiland, S., Willcox, K. and Backx, T., "Missing point estimation in models described by proper orthogonal decomposition", *IEEE Transactions on Automatic Control*, Vol. **53**, No. 10, (2008); pp. 2237-2251.

Astrid, P. and Verhoeven, A., "Application of least squares MPE technique in the reduced order modeling of electrical circuits", *Proceedings of 17th Int. Symposium on Mathematical Theory of Networks and Systems*, (2006); pp. 1980-1986.

Bai, Z., "Krylov subspace techniques for reduced-order modeling of large-scale dynamical systems", *Applied Numerical Mathematics* **43**, (2002); pp. 9-44.

Bang, Y.S., Abdel-Khalik, H.S. and Hite, J.M., "Hybrid Reduced Order Modeling Applied to Nonlinear Models", *International Journal for Numerical Methods in Engineering*, Vol. **91**, Issue 9, (2012a); pp. 929–949.

www.manaraa.com

Bang, Y.S., Wang, C.J. and Abdel-Khalik, H.S., "State-based Adjoint Method for Reduced Order Modeling", *Transport Theory and Statistical Physics*, Vol. **41**, (2012b); pp. 101-132.

Bang, Y.S. and Abdel-Khalik, H.S., "Projection-based Second Order Perturbation Theory", *Annals of Nuclear Energy*, (2012c).

Bang, Y.S. and Abdel-Khalik, H.S., "Multi-Surrogate Modeling for Computational Cost Reduction", *Transactions of the Korean Nuclear Society Spring Meeting*, Jeju, Korea, May 17-18, (2012d).

Bang, Y.S. and Abdel-Khalik, H.S., "Reduced Order Modeling for Multi-Physics Problems", *Transactions of the American Nuclear Society*, San Diego CA, (2012e).

Bang, Y.S. and Abdel-Khalik, H.S., "A Pseudo Generalized Perturbation Theory Approach for Sensitivity Analysis", *Transactions of the American Nuclear Society*, Hollywood FL, (2011a).

Bang, Y.S. and Abdel-Khalik, H.S., "ESM-based Regularized Hessian Construction Algorithm", *Transactions of the American Nuclear Society*, Hollywood FL, (2011b).

Bang, Y.S. and Abdel-Khalik, H.S., "Verification Tests for Uncertainty Quantification and Sensitivity Analysis Studies", *Transactions of the American Nuclear Society*, Washington DC, (2011c).

Banks, H.T., Beeler, S.C., Kepler, G.M. and Tran, H.T., "Reduced order modeling and control of thin film growth in an HPCVD reactor", *SIAM J. Appl. Math.*, Vol. **62**, No. 4, (2002); pp. 1251-1280.

www.manaraa.com

Barton, R.R., "Simulation optimization using metamodels", *Proceedings of the 2009 Winter Simulation Conference*, (2009); pp.230-238.

Bashir, K. Willcox, O. Ghattas, B. van Bloemen Waanders, J. Hill, "Hessian-based model reduction for large-scale systems with initial condition inputs", *International Journal for Numerical Methods in Engineering*, Vol. **73**, (2008); pp. 844–868

Benner, P., Quintana-Orti, E.S. and Quintana-Orti, G., "State-space truncation methods for parallel model reduction of large-scale systems", *Parallel Computing* **29**, (2003); pp. 1701-1722.

Berkooz, G., Holmes, P. and Lumley, J.L., "The Proper Orthogonal Decomposition in the Analysis of Turbulent Flows", *Annu. Rev. Fluid Mech.* **25**, (1993); pp. 539-575.

Booker, A.J., Dennis, Jr., J.E., Frank, P.D., Serafini, D.B., Torczon V. and Trosset, M.W., "A rigorous framework for optimization of expensive functions by surrogates", NASA/CR-1998-208735, ICASE Report No. 98-47, (1998).

Boraval, S., Le Bris, C., Lelièvre, T., Maday, Y., Nguyen, N.C. and Patera, A.T., "Reduced basis techniques for stochastic problems", *Archives of Computational Methods in Engineering*, Volume **17**, Number 4, (2010); pp. 435-454,

Boroushaki, M., Ghofrani, M.B., Lucas, C., Yazdanpanah, M.J. and Sadati, N., "Axial Offset Control of PWR Nuclear Reactor Core using Intelligent Techniques", *Nuclear Engineering and Design*, Vol. **227**, (2004); pp. 285-300

www.manaraa.com

Boroushaki, M., Ghofrani, M.B., Lucas, C., Yazdanpanah, M.J., "An Intelligent Nuclear Reactor Core Controller for Load Following Operations, using Recurrent Neural Networks and Fuzzy Systems", *Annals of Nuclear Energy*, Vol. **30**, (2003); pp. 63-80

Bui-Thanh, T., Willcox, K., Ghattas, O. and Waanders, B.V.B., "Goal-oriented, model-constrained optimization for reduction of large-scale systems", *Journal of Computational Physics* **224**, (2007); pp. 880-896.

Bui-Thanh, T. and Willcox, K., "Parametric reduced-order models for probabilistic analysis of unsteady aerodynamic applications", *AIAA Journal*, Vol. **46**, No. 10, (2008); pp. 2520-2529.

Cacuci, D.G., *Sensitivity and uncertainty analysis: theory*, CRC press, (2003).

Charturantabut, S., Sorensen, D.C., "Discrete empirical interpolation for nonlinear model reduction", Tech. Rep. 09-05, Department of Computational and Applied Mathematics, Rice University, (2009).

Chen, W., Jin, R., Sudjianto, A., "Analytical global sensitivity analysis and uncertainty propagation for robust design", *Journal of Quality Technology*, vol. **38**, no. 4, (2006); pp. 333-348.

Cho, B.H. and No. H.C., "Design of Stability and Performance Robust Fuzzy Logic Gain Scheduler for Nuclear Steam Generators", *IEEE Transactions on Nuclear Science*, Vol. **44**, No. 3, (1997).

www.manaraa.com

Choi, Y.J., Kim, H.K., Baek, W.P. and Chang, S.H., "Hybrid Accident Simulation Methodology using Artificial Neural Networks for Nuclear Power Plants", *Information Sciences*, Vol. **160**, (2004); pp. 207-224

Crestaux, T., Le Maitre, O. and Martinez, J.M., "Polynomial chaos expansion for sensitivity analysis", *Reliability Engineering and System Safety* **94**, (2009); pp. 1161-1172.

Daescu, D.N. and Navon, I.M., "Efficiency of a POD-based reduced second-order adjoint model in 4D-var data assimilation", *Int. J. Numer. Meth. Fluids* **53**, (2007); pp. 985-1004.

Dubey, B.P. and Jagannathan, V. and Kataria, S.K., "Quick and Reliable Estimation of Power Distribution in a PHWR by ANN", *Annals of Nuclear Energy*, Vol. **25**, No. 8, (1998); pp. 567-579

Doebling, S.W., Hemez, F.M., Schultze, J.F. and Cundy, A.L., "A metamodel-based approach to model validation for nonlinear finite element simulations", *Proceedings of IMAC XX*, (2002).

Duderstadt, J.J. and Hamilton, L.J., *Nuclear Reactor Analysis*, John Wiler & Sons, Inc., (1976).

Eldred, M.S., "Recent advances in non-intrusive polynomial chaos and stochastic collocation methods for uncertainty analysis and design", *50th AIAA/ASME/ASCE/AHS/ASC Structures, Structural Dynamics, and Materials Conference*, (2009).

www.manaraa.com

Eldred, M.S., Giunta, A.A., Collis, S.S., Alexandrov, N.A., and Lewis, R.M., "Second-Order Corrections for Surrogate-Based Optimization with Model Hierarchies", *Proceedings of the 11th AIAA/ISSMO Multidisplinary Analysis & Optimization Conference*, AIAA, Albany, NY, August 30-September 1, (2004); pp. 2004-4457.

Entzinger, J.O. and Ruan, D., "Optimizing Nuclear Reactor Operation using Soft Computing Techniques", In C. Kahraman (Ed.), *Fuzzy Applications in Industrial Engineering*, volume 201 of Studies in Fuzziness and Soft Computing, chapter 2.4. Springer Verlag, Heidelberg, Germany (ISBN 978-3-540-33516-0), (2006).

Erdogan, A. and Geckinli, M., "A PWR Reload Optimisation Code (XCore) using Artificial Neural Networks and Genetic Algorithms", *Annals of Nuclear Energy*, Vol. **30**, (2003); pp. 35-53

Faghihi, F., Khalafi, H. and Mirvakili, S. M., "A Literature Survey of Neutronics and Thermal-Hydraulics Codes for Investigating Reactor Core Parameters; Artificial Neural Networks as the VVER-1000 Core Predictor", *Nuclear Power - System Simulations and Operation*, Pavel Tsvetkov (Ed.), ISBN: 978-953-307-506-8, InTech, (2011): Available from: http://www.intechopen.com/books/nuclear-power-system-simulations-and-operation/a-literature-survey-of-neutronics-and-thermal-hydraulics-codes-for-investigating-reactor-core-parame

Feldmann, P. and Freund, R.W., "Efficient linear circuit analysis by Pade approximation via the Lanczos process", *IEEE Transactions on Computer-Aided Design of Integrated Circuits and Systems* **14**, (1995); pp. 639-649.

www.manaraa.com

Field, R.V., "Numerical methods to estimate the coefficients of the polynomial chaos expansion", *15th ASCE Engineering Mechanics Conference*, (2002).

Fodor, I.K., "A survey of dimension reduction techniques", LLNL technical report, UCRL-ID-148494, (2002).

Forrester, A.I.J. and Keane, A.J., "Recent advances in surrogate-based optimization", *Progress in Aerospace Sciences*, Vol. **45**, Issues 1-3, (2009); pp.50-79.

Franke, T. and Nielson, G., "Smooth interpolation of large sets of scattered data", *International Journal for Numerical Methods in Engineering*, Vol. **15**, No. 11, (1980); pp.1691-1704.

Freund, R.W., "Krylov-subspace methods for reduced-order modeling in circuit simulation", *J. Comput. Appl. Math*. **123**, (2000); pp. 395-521.

Friedman, J. and Stuetzel, W., "Projection pursuit regression", *JASA:Theory and Methods*, **76**, (1981); pp. 817-823.

Friedman, J. H., "Multivariate Adaptive Regression Splines", *The Annals of Statistics*, **19**(1), (1991); pp.1-141.

Galbally, D., Fidkowski, K., Willcox, K. and Ghattas, O., "Non-linear model reduction for uncertainty quantification in large-scale inverse problems", *Int. J. Numer. Meth. Engng*, (2009).

Gandini, A., "Higher Order Time-Dependent Generalized Perturbation Theory", *Nuclear Science and Engineering*, **67**, (1978a); pp. 91-106.

www.manaraa.com

Gandini, A., "Implicit and Explicit Higher Order Perturbation Methods for Nuclear Reactor Analysis", *Nuclear Science and Engineering*, **67**, (1978b); pp. 347-355.

Ghanem, R. and Spanos, P., *Stochastic Finite Elements: A Spectral Approach*, Springer-Verlag, (1991).

Ghanmi, S., Bouhaddi, N. and Bouazizi, M.L., "Stochastic response surface method for robust design", *IMAC-XXIV: Conference & Exposition on Structural Dynamics*, (2006).

Giunta, A.A. and Watson, L.T., "A comparison of approximation modeling techniques: Polynomial versus Interpolating models", *AIAA-98-4758*, (1998).

Giunta, A.A., Eldred, M.S., Castro, J.P., "Uncertainty quantification using response surface approximations", *9th ASCE specialty Conference on Probabilistic Mechanics and Structural Reliability*, (2004).

Glaz, B., Goel, T., Liu, L., Friedmann, P.P. and Haftka, R.T., "Multi-surrogate approach to helicopter rotor blade vibration reduction", *AIAA Journal*, Vol. **47**, No. 1, (2009); pp. 271-282.

Godfrey, A., *Physical Reactor Specification*, CASL-U-2011-0132-000, ORNL, September, (2011).

Goel, T., Haftka, R.T., Shyy, W. and Queipo, N.V., "Ensemble of surrogates", *Structural and Multidisciplinary Optimization Journal*, (2006).

Goel, T., "Multiple surrogates and error modeling in optimization of liquid rocket propulsion components", Ph.D dissertation, University of Florida, (2007).

Golub, G. H., Van Loan, C. F., *Matrix Computations (3rd ed.)*, John Hopkins, (1996).

www.manaraa.com

Greenspan, E., Karni, Y. and Gilai, D., "Higher Order Effects in Cross Section Sensitivity Analysis", *Workshop on Theory and Application of Sensitivity and Uncertainty Analysis*, Oak Ridge, TN, (1978).

Greenspan, E. and Gilai, D., "Second-Order Generalized Perturbation Theory for Source-Driven Systems', *Nuclear Science and Engineering*, **68**, (1978); pp. 1-9.

Grepl, M.A. and Patera, A.T., "A posteriori error bounds for reduced-basis approximations of parameterized parabolic partial differential equations", *ESAIM: Mathematical Modeling and Numerical Analysis*, Vol. **39**, No. 1, (2005); pp. 157-181.

Gugercin, S. and Antoulas, A.C., "A Survey of Model Reduction by Balanced Truncation and Some New Results", *Int. J. Control*, Vol. **77**, No. 8, (2004); pp. 748-766.

Guo, Y., Gong, C., Zeng, H.Y, "The Appliocation of Artificial Neural Network in Nuclear Energy", *Proceedings of the Ninth International Conference on Machine Learning and Cybernetics*, Qingdao, 11-14 July, (2010).

Haasdonk, B. and Ohlberger, M., "Reduced basis method for finite volume approximations of parametrized evolution equations", *M2AN, Math. Model. Numer. Anal.*, **42**(2), (2008).

Halko, N., Martinsson, P.G., and Tropp, J., "Finding structure with randomness: Probabilistic algorithms for constructing approximate matrix decompositions", *SIAM Review*, **53**(2), (2011).

Hardy, R.L., "Multiquadratic equations of topography and other irregular surfaces", *J. Geophys. Res.*, **76**, (1971); pp.1905-1915.

www.manaraa.com

Hedayat, A., Davilu, H., Barfrosh, A.A. and Sepanloo, K., "Optimization of the Core Configuration Design using a Hybrid Artificial Intelligence Algorithm for Research Reactors", *Nuclear Engineering and Design*, Vol. **239**, (2009); pp. 2786-2799

Hines, J.W. and Uhrig, R.E., "Trends in Computational Intelligence in Nuclear Engineering", *Progress in Nuclear Energy*, Vol. **46**, No. 3-4, (2005); pp. 167-175

Homescu, C., Petzold, L.R. and Serban, R., "Error Estimation for Reduced-Order Models of Dynamical Systems", *SIAM Review*, Vol. **49**, No. 2, (2007); pp. 277-299.

Holmes, P., Lumley, J. and Berkooz, G., *Turbulence, Coherent Structures, Dynamical Systems and Symmetry*, Cambridge University Press, Cambridge, UK, (1996).

Hwang, B.C., "Fault Detection and Diagnosis of a Nuclear Power Plant using Artificial Neural Networks", Thesis for the Degree of Master, Simon Fraser University, (1993).

Isukapalli, S.S., Roy, A., Georgopoulos, P.G., "Stochastic response surface methods (SRSMs) for uncertainty propagation: application to environmental and biological systems", *Risk Analysis*, Vol **18**, No.3 (1998); pp. 351-363.

Ivanov, K.N., Beam, T.M. and Baratta, A.J., *Pressurised Water Reactor Main Steam Line Break (MSLB) Benchmark, Volume I: Final Specifications*, US Nuclear Regulatory Commission/OECD Nuclear Energy Agency, NEA/NSC/DOC(99)8, (1999).

Jang, C.S., Shim, H.J. and Kim, C.H., "Optimization Layer by Layer Networks for In-Core Fuel Management Optimization Computations in PWRs", *Annals of Nuclear Energy*, Vol. **28**, (2001); pp.1115-1132

www.manaraa.com

Jin, R., Chen, W., Simpson, T.W., "Comparative studies of meta-modeling techniques under multiple modeling criteria", *Structural and Multi-disciplinary Optimization*, **23**(1), (2001); pp. 1-13.

Johnson, M., Moore L., Ylvisaker, D., "Minimax and Maximin Distance Designs", *J Stat Plann Inference*, **26**, pp.131-48, (1990).

Jones, D.R., Schonlau, M. and Welch, W.J., "Efficient global optimization of expensive black-box functions", *Journal of Global Optimization*, **13**, (1998); 455-492.

Joucla, J. and Probst, P., "Sensitivity analysis by the use of a surrogate model in LB-LOCA: LOFT L2-5 with CATHARE-2 V.2.5 code", *The 12th International Topical Meeting on Nuclear*, (2007).

Karhunen, K., "Zur spectral ehtorie stochastischer prozesse", *Ann. Acad. Sci. Fennicae. Ser. A.***134**, (1946).

Kennedy, C., Rabiti, C. and Abdel-Khalik, H.S., "On Rank Determination for Subspace Methods", *Transactions of the American Nuclear Society*, Washington DC, October 30-November 3, (2011).

Kewlani, G. and Iagnemma, K., "A stochastic response surface approach to statistical prediction of mobile robot mobility", *Intelligent Robots and Systems*, (2008); pp. 2234-2239.

Khalafi, H. and Terman, M.S., "Development of a Neural Simulator for Research Reactor Dynamics", *Progress in Nuclear Energy*, Vol. **51**, (2009); pp. 135-140

www.manaraa.com

Khorramabadi, S.S., Boroushaki, M. and Lucas, C., "Emotional Learning based Intelligent Controller for a PWR Nuclear Reactor Core during Load Following Operation", *Annals of Nuclear Energy*, Vol. **35**, (2008); pp. 2051-2058

Kim, K.H. and Bartlett, E.B., "Nuclear Power Plant Fault Diagnosis using Neural Networks with Error Estimation by Series Association", *IEEE Transactions on Nuclear Science*, Vol. **43**, No. 4, (1996); pp. 2373-2388

Klindworth, D., Grepl, M.A. and Vossen, G., "Certified reduced basis methods for parametrized parabolic partial differential equations with non-affine source terms", *Computer Methods in Applied Mechanics and Engineering*, (2011).

Kosambi, D.D., "Statistics in Function Space", *J. Indian Math. Soc.* **7**, (1943); pp. 45-62.

Lall, S., Marsden, J.E. and Glavaski, S., "A subspace approach to balanced truncation for model reduction of nonlinear control systems", *Int. J. Robust Nonlinear Control* **12**, (2002); pp. 519-535.

Kupka, K. and Meloun, M., "Neural Network Time Series Classification of Changes in Nuclear Power Plant Processes", *Joint Statistical Meeting Proceedings*, American Statistical Association, (2009).

Ku, C.C., Lee, K.Y. and Edwards, R.M., "Improved Nuclear Reactor Temperature Control Using Diagonal Recurrent Neural Networks", *IEEE Transactions on Nuclear Science*, Vol. **39**, No. 6, (1992).

www.manaraa.com

Lall, S. and Beck, C., "Error-Bounds for Balanced Model-Reduction of Linear Time-Varying Systems", *IEEE Transaction on Automatic Control*, Vol. **48**, No. 6, (2003); pp. 946-956.

Lamarsh, J.R. and Baratta, A.J., *Introduction to Nuclear Engineering (3rd Edition)*, Prentice Hall, Upper Saddle River, New Jersey, (2001).

Laslett, G., "Kriging and Splines: an empirical comparison of their predictive performance in some applications", *JASA: Applications and Case Studies*, **89**, (1994); pp. 391-400.

Laurenceau, J. and Meaux, M., "Comparison of gradient and response surface based optimization frameworks using adjoint method", *49th AIAA/ASME/ASCE/AHS/ASC Structures, Structural Dynamics, and Materials Conference & 16th AIAA/ASME/AHS Adaptive Structures Conference*, (2008).

Lee, D.J., Rhodes, J. and Smith, K., "Quadratic Depletion Model for Gadolinium Isopotes in CASMO-5", *Advances in Nuclear Fuel Management IV* (ANFM 2009), Hilton Head Island, South Carolina, USA, April 12-15, (2009).

Lee, S.J. and Seong, P.H., "A Dynamic Neural Network based Accident Diagnosis Advisory System for Nuclear Power Plants", *Progress in Nuclear Energy*, Vol. **46**, No. 3-4, (2005); pp. 268-281

Lewis, E.E. and Miller, Jr., W.F., *Computational Methods of Neutron Transport*, Wiley-Interscience, (1984).

Lewis, E.E., *Fundamentals of Nuclear Reactor Physics*, Academic Press, (2008).

www.manaraa.com

Liberman, C., Willcox, K. and Ghattas, O., "Parameter and state model reduction for large-scale statistical inverse problems", *SIAM journal on scientific computing*, **32**(5), (2010).

Liem, R.P., "Surrogate Modeling for large-scale black-box systems", Ph.D dissertation, MIT, (2007).

Liberty, E., Woolfe, F. F., Martinsson, P.G., Rokhlin, V., and Tygert, M., "Randomized Algorithms for the Low-Rank Approximation of Matrices", *Proceedings of the National Academy of Science* **104**, (2007).

Lockwood, B.A. and Anitescu, M., "Gradient-enhanced universal kriging for uncertainty propagation", Reprint ANL/MCS-P1808-1110, (2010).

Loève, M., "Functions aleatoire de second ordre", *C.R.acad. Sci. Paris*, **220**, (1945).

Lophaven, S.N., Nielsen, H.B. and Søndergaard, J., "DACE - a MATLAB kriging toolbox", Tech. Rep. IMM-TR-2002-12, Informatics and Mathematical Modeling, Technical University of Denmark, Denmark, (2002), available at http://www2.imm.dtu.dk/~hbn/dace/.

Lumley, J. L., "The structure of inhomogeneous turbulence", *In Atmospheric Turbulence and Wave Propagation*, (1967); pp. 166-78.

Macdonald, I.A., "Comparison of sampling techniques on the performance of Monte-Carlo based sensitivity analysis", *Eleventh International IBPSA Conference*, (2009).

Mackay, D.J.C., "Bayesian methods for adaptive models", Ph.D dissertation, California Institute of Technology, (1991).

www.manaraa.com

Mahoney, M.W., "Randomized Algorithms for Matrices and Data", *Foundations and Trends in Machine Learning*, NOW Publishers, Boston, (2011).

Malik, A.H., Memon, A.A. and Khan, "Identification of Nonlinear Dynamics of Nuclear Power Reactor using Adaptive Feedforward Neural Network", *Proceedings of Pakistan Academy of Science*, Vol. **47**, No. 2, (2010); pp. 111-120

Mathelin, L., Hussaini, M.Y., Zang, T.A. and Bataille, F., "Uncertainty propagation for turbulent, compressible flow in a quasi-1d nozzle using stochastic methods", *167th AIAA Computational Fluid Dynamics Conference*, (2003).

Maute, K., Weickum, G. and Eldred, M., "A reduced-order stochastic finite element approach for design optimization under uncertainty", *Structural Safety* **31**, (2009); pp. 450-459.

Mazrou, H. and Hamadouche, M., "Application of Artificial Neural Network for Safety Core Parameters Prediction in LWRRS", *Progress in Nuclear Energy*, Vol. **44**, No. 3, (2004); pp. 263-275

McKay, M.D., Conover, W.J., and Beckman, R.J., "A Comparison of Three Methods for Selecting Values of Input Variables in the Analysis of Output from a Computer Code", *Technometrics*, **21**, pp.239-245, (1979).

Mckinley, M.S. and Rahnema, F., "Higher-Order Boundary Condition Perturbation Theory for the Neutron Transport Equation", Nuclear Science and Engineering, Vol. **140**, (2002); pp. 285-294.

www.manaraa.com

Mckinley, M.S. and Rahnema, F., "Higher-Order Boundary Condition Perturbation Theory for the Diffusion Approximation", Nuclear Science and Engineering, Vol. **136**, (2000); pp. 15-33.

Mitani, H., "Higher Order Perturbation Method in Reactor Calculations", *Nuclear Science and Engineering*, **51**, (1973); pp. 180-188.

Montes, J.L., Francois, J.L., Ortiz, J.J., Martin-del-Campo, C. and Perusquia, R., "Local Power Peaking Factor Estimation in Nuclear Fuel by Artificial Neural Networks", *Annals of Nuclear Energy*, Vol. **36**, (2009); pp. 121-130

Moore, B.E., Principal component analysis in linear systems: Controllability, Observability, and Model Reduction", *IEEE Transactions on Automatic Control*, Vol. **AC-26**, No.1, (1981); pp. 17-32.

Moore, B.R., Turinsky, P.J. and Karve, A.A., "FORMOSA-B: A Boiling Water Reactor In-Core Fuel Management Optimization Package", Nuclear Technology **126**, 153, (1999).

Mullis, C.T. and Roberts, R.A., "Synthesis of Minimum Roundoff Noise Fixed Point Digital Filters", *IEEE Transactions on Circuits and Systems*, CAS-23, (1976); pp. 551-562.

Myers, R.H., Montgomery, D.C., and Anderson-Cook, C.M., *Response surface methodology: process and product optimization using designed experiments – 3rd ed.*, John Wiley & Sons, Inc., (2008).

www.manaraa.com

Na, M.G., Jung, D.W. and Shin, S.H., "Estimation of the Nuclear Power Peaking Factor using In-core Sensor Signals", *Journal of the Korean Nuclear Society*, Vol. **36**, No. 5, (2004); pp. 420-429

Na, M.G., Sim, Y.R., Park, K.H., Lee, S.M., Jung, D.W., Shin, S.H., Upadhyaya, B.R., Zhao, K. and Lu, B., "Sensor Monitoring Using a Fuzzy Neural Network with an Automatic Structure Constructor", *IEEE Transaction on Nuclear Science*, Vol. **50**, No. 2, (2003).

Nadaraya, E. A., "On Estimating Regression", *Theory of Probability and its Applications* **9** (1), (1964); pp.141–142.

Nair, P.B. and Keane, A.J., "New Developments in Computational Stochastic Mechanics, Part I: Theory", *Proceedings of the 41st AIAA/ASME/ASCE/AHS/ASC Structures, Structural Dynamics and Materials Conference*, (2000a).

Nair, P.B. and Keane, A.J., "New Developments in Computational Stochastic Mechanics, Part II: Applications", *Proceedings of the 41st AIAA/ASME/ASCE/AHS/ASC Structures, Structural Dynamics and Materials Conference*, (2000b).

Nair, P.B., "On the Theoretical Foundations of Stochastic Reduced Basis Methods", *Proceedings of the 42nd AIAA/ASME/ASCE/AHS/ASC Structures, Structural Dynamics and Materials Conference*, (2001).

Nair, P.B. and Keane, A.J., "Stochastic Reduced Basis Methods", *AIAA Journal* **40**, (2003); pp. 1653-1664.

www.manaraa.com

Obukhov, A.M., "Statistical Description of Continuous Fields", *Re. Geophys. Int. Akad. Nauk. SSSR* **24**, (1954); pp. 3-42.

Ortiz, J.J. and Requena, I., "Using a Multi-State Recurrent Neural Network to Optimize Loading Patterns in BWRs", *Annals of Nuclear Energy*, Vol. **31**, (2004); pp. 789-803

Owen, A.B., "Orthogonal arrays for computer experiments, integration and visualization", *Statistical Sinica*, **2**(2), pp.439-452, (1992).

Park, H.M. and Jung, W.S., "A recursive algorithm for multidimensional inverse heat conduction problems by means of mode reduction", *Chemical Engineering Science* **55**, (2000); pp. 5155-5124.

Patra, S.R., Jehadeesan, R., Rajeswari, S. and Satyamurthy, S.A.V., "Artificial Neural Network Model for Intermediate Heat Exchange of Nuclear Reactor", International *Journal of Computer Applications*, Vol. **1**, No. 26, (2010); pp. 63-69

Pazsit, I. and Kitamura, M., "The Role of Neural Networks in Reactor Diagnostics and Control", *Advances in Nuclear Science and Technology*, Vol. **24**, (1996); pp. 95-130

Penzl, T., "Algorithms for Model Reduction of Large Dynamical Systems", *Linear Algebra and its Applications*, **415**, (2006); pp. 322-343.

Perez-Cruz, J.H. and Poznyak, A., "Identification of Measurable Dynamics of a Nuclear Research Reactor Using Differential Neural Networks", *16th IEEE International Conference on Control Applications*, Part of IEEE Multi-conference on Systems and Control, Singapore, 1-3 October, (2007).

www.manaraa.com

Phillips, J.R., "Projection-based approaches for model reduction of weakly nonlinear, time-varying systems", *IEEE Transactions on Computer-aided Design of Integrated Circuits and Systems*, Vol. **22**, No. 2, (2003); pp. 171-187.

Pougachev, V.S., "General Theory of the Correlations of Random Functions", *Izv. Akad. Nauk. SSSR, Ser. Mat.* **17**, (1953).

Qian, Z, Seepersad, C.C., Joseph, V.R., Allen, J.K. and Wu, C.F.J., "Building surrogate models based on detailed and approximate simulations", *Journal of Mechanical Design*, Vol. **128**, Issue. 4, (2006); pp. 668-678.

Queipo, N.V., Haftka, R.T., Shyy, W., Goel, T., Vaidyanathan, R. and Tucker, P.K., "Surrogate-based analysis and optimization", *Progress in Aerospace Sciences* **41**, (2005); pp.1-28.

Radiation Safety Information Computational Center (RSICC), "SCALE: A Comprehensive Modeling and Simulation Suite for Nuclear Safety Analysis and Design", ORNL/TM-2005/39, Version 6.1., (2011).

Ramu, M., Raja, V.P., Thyla, P.R. and Gunaseelan, M., "Design optimization of complex structures using metamodels", *Jordan Journal of Mechanical and Industrial Engineering*, Vol. **4**, No. 5, (2010); pp. 653-664.

Rathinam, M. and Petzold, L.R., "An iterative method for simulation of large scale modular systems using reduced order models", *Proceedings of the 39th IEEE Conference on Decision and Control*, (2000); pp. 4630-4635.

www.manaraa.com

Rathinam, M. and Petzold, L.R., "A new look at proper orthogonal decomposition", *SIAM J. Numer. Anal.*, Vol. **41**, No. 5, (2003); pp. 1893-1925.

Reis, T. and Stykel, T., "Stability analysis and model order reduction for coupled systems", DFG-Forschungszentrum Matheon, Technical Report 241-2005, (2005).

Rewienski, M. and White, J., "Model order reduction for nonlinear dynamical systems based on trajectory piecewise-linear approximations", *Linear Algebra and its Applications* **415**, (2006); pp. 426-454.

Ridluan, A., Manic, M. and Tokuhiro, A., "EBaLM-THP – A Neural Network Thermohydraulic Prediction Model of Advanced Nuclear System Components", *Nuclear Engineering and Design*, Vol. **239**, (2009); pp. 308-319

Roderick, O., Anitescu, M. and Fischer, P., "Polynomial Regression Approaches using Derivative Information for Uncertainty Quantification", *Nuclear Science and Engineering*: **164**, (2010); pp. 122-139.

Roh, M.S., Cheon, S.W. and Chang, S.H., "Thermal Power Prediction of Nuclear Power Plant using Neural Network and Parity Space Model", *IEEE Transaction of Nuclear Science*, Vol. **38**, No. 2, (1991); pp. 866-872

Rutherford, A.C., Maupin, R.D., and Hemez, F.M., "Latin Hypercube Sampling vs. Metamodel Monte Carlo for propagating uncertainty through transient dynamics simulations", *IMAC-XXIV: Conference & Exposition on Structural Dynamics*, (2006).

www.manaraa.com

Sachdeva, S.K., Nair, P.B. and Keane, A.J., "Comparative study of projection schemes for stochastic finite element analysis", *Comput. Methods Appl. Mech. Engrg* **195**, (2006); pp. 2371-2392.

Sachdeva, S.K., Nair, P.B. and Keane, A.J., "Hybridization of stochastic reduced basis methods with polynomial chaos expansions", *Probabilistic Engineering Mechanics* **21**, (2006); pp. 182-192.

Sacks, J., Welch, W. J., Mitchell, T. J. and Wynn, H. P, "Design and analysis of computer experiments", *Statistical Science*, **4**(4), pp.409-435, (1989a).

Sacks J., Schiller, S. and Welch, W., "Designs for computer experiments", *Technometrics*, **31**, (1989b); pp. 41-47.

Sadighi, M., Setayeshi, S. and Salehi, A.A., "PWR Fuel Management Optimization using Neural Networks", *Annals of Nuclear Energy*, Vol. **29**, (2002); pp. 41-51

Santosh, T.V., Srivastava, A., Sanyasi Rao, V.V.S., Ghosh, A.K. and Kushwaha, H.S., "Diagnostic System for Identification of Accident Scenarios in Nuclear Power Plants using Artificial Neural Networks", *Reliability Engineering and System Safety*, Vol. **94**, (2009); pp. 759-762

Santosh, T.V., Vinod, G., Saraf, R.K., Ghosh, A.K. and Kushwaha, H.S., "Application of Artificial Neural Networks to Nuclear Power Plant Transient Diagnosis", *Reliability Engineering and System Safety*, Vol. **92**, (2007); pp. 1468-1472

www.manaraa.com

Sapp, B.J., "Randomized Algorithms for Low-Rank Matrix Decomposition", *Written Preliminary Examination II Report*, Computer and Information Science, University of Pennsylvania, (2011).

Scherpen, J.M.A., "Balancing for Nonlinear Systems", *Systems & Control Letters*, **21** (2), (1993); pp. 143-153.

Shepard, D., "A two-dimensional interpolation function for irregularly spaced data", *23rd ACM National Conference*, (1968); pp.517-523.

Schirru, R., Martines, A.S., Pereira, C.M.N.A., Domingos, R.P., Cachado, M.D. and Machado, L., "Intelligent Soft Computing in Nuclear Engineering in Brazil", *Progress in Nuclear Energy*, Vol. **35**, No. 3-4, (1999); pp. 367-391

Simpson, T.W., Peplinski, J.D., Koch, P.N. and Allen, J.K., "Meta-models for computer based engineering design: Survey and recommendations", *Engineering with Computers*, **17**(2), (2001); pp. 129-150.

Smith, M., *Neural Networks for Statistical Modeling*, Von Nostrand Reinhold, New York: (1993).

Stacey, W.M., *Variational Methods in Nuclear Reactor Physics*, New York: Academic Press., (1974).

Stamm'ler, R. J.J. and Abbate, M.J., *Methods of Steady-State Reactor Physics in Nuclear Design*, Academic Press, Inc., (1983).

Sudret, B., "Global sensitivity analysis using polynomial chaos expansion", *Reliab. Eng. Sys. Safety* **93** (2008); pp. 964–979.

www.manaraa.com

Tanabe, A. and Yamamoto, T., "Development of Neural Network for Analysis of Local Power Distributions in BWR Fuel Bundles", *Journal of Nuclear Science and Technology*, Vol. **30**, Issue. 8, (1993); pp. 804-812

Tang, B., "Orthogonal Array-based Latin Hypercubes", *J Am Stat Assoc*, **88**, pp.1324-1348, (1984).

Tatang, M.A., Pan, W., Prinn, R.G., McRae, G.J., "An efficient method for parametric uncertainty analysis of numerical geophysical models", *Journal of Geophysical Research*, Vol. **102**, No. D18, (1997); pp.21,925-21,932.

Thacker, W.I., Zhang, J., Watson, L.T., Birch, J.B., Iyer, M.A., and Berry, M.W., "Algorithm XXX: SHEPPACK: modified Shepard algorithm for interpolation of scattered multivariate data", Tech. Rep. TR-09-13, Computer Science, Virginia Polytechnic Institute & State University, USA, (2009).

Uhrig, R.E and Tsoukalas, L.H., "Soft Computing Technologies in Nuclear Engineering Applications", *Progress in Nuclear Energy*, Vol. **34**, No. 1, (1998); pp. 13-75

Varshney, A. and Armaou, A., "Nonlinear control of dissipative PDE systems employing adaptive model reduction", *Proceedings of the American Control Conference*, (2008); pp. 940-947.

Viana, F.A.C., "Multiple surrogates for prediction and optimization", Ph.D dissertation, University of Florida, (2011).

Villemagne, C.D., and Skelton, R.E., "Model reductions using a projection formulation", *Int. J. Control*, vol. **46**, no. 6, (1987); pp. 2141-2169.

www.manaraa.com

Vinod, S.G., Babar, A.K., Kushwaha, H.S. and Raj, V.V., "Symptom based Diagnostic System for Nuclear Power Plant Operations using Artificial Neural Networks", *Reliability Engineering and System Safety*, Vol. **82**, (2003); pp. 33-40

Wagner, J.C. and Parks, C.V., *Parametric Study of the Effect of Burnable Poison Rods for PWR Burnup Credit*, NUREG/CR-6761 (ORNL-TM-2000/373), ORNL, March, (2002).

Webster, C.G., "Sparse grid stochastic collocation techniques for the numerical solution of partial differential equations with random input data", Ph.D dissertation, The Florida State University, (2007).

Wei, H.M., Su, G.H., Tian, W.X., Qiu, S.Z. and Ni, W.G., "Study on the Characteristic Points of Boiling Curve by using Wavelet Analysis and Genetic Neural Network", *Nuclear Engineering and Design*, Vol. **239**, (2009); pp. 2317-2325

Wigner, E., "Effect of Small Perturbations on Pile Period". Manhattan Project Report CP-G-3048 (1945).

Wilks, S., "Determination of Sample Sizes for Setting Tolerance Limits", *Annals of Math. Statistics*, **12**, 91, (1941).

Williams, M.L., *Perturbation Theory for Reactor Analysis*, CRC Handbook of Nuclear Reactor Calculations, pp. 63-188, CRC Press, 1986.

Xu, C., Luo, L. and Schuster, E., "On Recursive Proper Orthogonal Decomposition via Perturbation Theory with Applications to Disctributed Sensing in Cyber-Physical Systems", *American Control Conference*, (2010).

www.manaraa.com

Yakowitz, S., Szidarovsky, F., "A comparison of Kriging with non-parametric regression", *Journal of Multivariate Analysis*, **16**, (1985); pp. 21-53

Yamamoto, A., "Application of Neural Network for Loading Pattern Screening of In-Core Optimization Calculations", *Nuclear Technology*, Vol. **144**, (2003); pp. 63-75

Zhao, D. and Xue, D., "Performance comparison of metamodeling methods from the perspective of sample quality metirs", *Proceedings of the ASME 2009 international design engineering technical conferences & computers and information in engineering conference*, San Diego, California, USA, (2009)

Zhou, Z., Ong, Y.S., Lim, M.H. and Lee, B.S., "Memetic algorithm using multi-surrogates for computationally expensive optimization problems", *Soft Computing*, Vol. **11**, Issue, 10, (2007); pp. 957-971.

Zerpa, L., Queipo, N.V., Pintos, S. and Salager, J., "An optimization methodology of alkaline-surfactant-polymer flooding processes using field scale numerical simulation and multiple surrogates", *Journal of Petroleum Science and Engineering*, **47**, (2005); pp. 197-208.

www.manaraa.com

APPENDICES

www.manaraa.com

Appendix A

We wish to show that $\prod_{i=-1}^{k}\left(\vec{\beta}_i^T\vec{x}\right)$ is a polynomial of the same form as the k^{th} term of the Taylor series. First, we must introduce some notation. Throughout, we take $\vec{x},\vec{\beta}_i\in\mathbb{R}^n$ for $i=1,...,k$. Let $a\circ b$ denote the Schur product (also known as the Hadamard product) of a and b and $a\otimes b$ denote the Kronecker product. Also, denote:

$$\mathbf{B}=\vec{\beta}_1\otimes\vec{\beta}_2\otimes\cdots\otimes\vec{\beta}_k$$

$$\mathbf{X}=\vec{x}\otimes\vec{x}\otimes\cdots\otimes\vec{x}\ \ (k\text{ times})$$

We will adopt a notation common in the analysis community and define a multi-index, α, as an n-tuple of natural numbers. For a vector $\vec{x}\in\mathbb{R}^n$, we define multi-index operations as follows:

$$|\alpha|=\alpha_1+\alpha_2+\cdots+\alpha_n$$

$$\vec{x}^{\alpha}=x_1^{\alpha_1}x_2^{\alpha_2}\cdots x_n^{\alpha_n}$$

$$\alpha!=\alpha_1!\alpha_2!\cdots\alpha_n!$$

$$D^{\alpha}=\left(\frac{\partial}{\partial x_1}\right)^{\alpha_1}\left(\frac{\partial}{\partial x_2}\right)^{\alpha_2}\cdots\left(\frac{\partial}{\partial x_n}\right)^{\alpha_n}$$

Using this notation, we can express Taylor's theorem for a single-valued function about a point $\vec{x}_0$ compactly:

www.manaraa.com

$$f\left(\vec{x}\right)=\sum_{|x|\geq 0}\frac{D^{\alpha}f\left(\vec{x}_0\right)\left(\vec{x}-\vec{x}_0\right)^{\alpha}}{\alpha!} \tag{A.1}$$

where the kth term of (A.1) is:

$$f\left(\vec{x}\right)=\sum_{|\alpha|=k}\frac{D^{\alpha}f\left(\vec{x}_0\right)\left(\vec{x}-\vec{x}_0\right)^{\alpha}}{\alpha!} \tag{A.2}$$

The multinomial theorem can also be expressed as follows:

$$\left(x_1+x_2+\cdots+x_k\right)^m=\sum_{|\alpha|=m}\frac{m!}{\alpha!}\vec{x}^{\alpha} \tag{A.3}$$

Note that $\left(\vec{\beta}_i^T\vec{x}\right)=\vec{1}_n^T\left(\vec{\beta}_i\circ\vec{x}\right)$, where $\vec{1}_n$ is a vector of dimension n where all entries are equal to 1. Applying the associative property of scalar multiplication, we can rewrite as follows:

$$\begin{aligned}\prod_{i=1}^{k}\left(\vec{\beta}_i^T\vec{x}\right)&=\left\{\vec{1}_n^T\left(\vec{\beta}_1\circ\vec{x}\right)\right\}\left\{\vec{1}_n^T\left(\vec{\beta}_2\circ\vec{x}\right)\right\}\cdots\left\{\vec{1}_n^T\left(\vec{\beta}_n\circ\vec{x}\right)\right\}\\&=\vec{1}_n\left(\mathbf{B}\circ\mathbf{X}\right)\vec{1}_{n^{k-1}}\end{aligned} \tag{A.4}$$

where $\mathbf{X}$ and $\mathbf{B}$ are $n^{k-1}\times n$ matrices that contain every combination of the entries in $\vec{x}$ and $\vec{\beta}_i$ such that the total order is n. Note that (A.3) implies that (A.2) is a polynomial with terms that are all possible combinations of entries in $\vec{x}$ that have total order n multiplied by constants and (A.4) is simply the sum of entries in $\left(\mathbf{B}\circ\mathbf{X}\right)$, thus we see that (A.2) and (A.4) are polynomials of the same form.

www.manaraa.com